TRANSVERSE VIBRATIONS
OF BELLOWS EXPANSION JOINTS

by

VAIDUTIS FELIKSAS JAKUBAUSKAS, B.Sc., M.Sc., M. Eng.

A Thesis
Submitted to the School of Graduate Studies
In Partial Fulfillment of the Requirements
For the Degree
Doctor of Philosophy

McMaster University

TRANSVERSE VIBRATIONS
OF BELLOWS EXPANSION JOINTS

DOCTOR OF PHILOSOPHY (1995)
(Mechanical Engineering)

McMaster University
Hamilton, Ontario

TITLE: Investigations of Transverse Vibrations of Bellows Expansion Joints

AUTHOR: Vaidutis Feliksas Jakubauskas,
B.Sc. (Kaunas Politechnical Institute, Lithuania)
M.Sc. (Odessa Civil Engineering Institute, Ukraine)
M.Eng. (McMaster University, Canada)

SUPERVISOR: Professor D.S. Weaver

NUMBER OF PAGES: xv, 245

ABSTRACT

Bellows expansion joints are used in piping systems to absorb significant axial and/or transverse motions. Unfortunately, their flexibility also makes them susceptible to vibration. This thesis presents a detailed analysis of the transverse vibrations of single and double bellows expansion joints, including the effects of internal fluid.

A differential equation of motion is developed which treats transverse bellows vibrations including the effects of fluid added mass, rotary inertia and internal pressure. The added mass is determined from potential flow theory and provided in the form of a mode dependent added mass coefficient. The equation of motion is solved for the first four transverse modes and comparison with experiments shows excellent agreement. The neglect of rotary inertia and the effect of convolution distortion on fluid added mass in the EJMA Standard makes the latter's predictions for natural frequency significantly higher than those measured , especially for transverse modes above the fundamental.

The equation of motion is also solved approximately to provide an analytical expression for transverse natural frequencies. The results are presented in a form which makes hand calculations possible for the first four modes of single and double bellows expansion joints. Experiments in still fluid as well as flow-induced motion show excellent agreement with predicted frequencies.

ACKNOWLEDGEMENTS

I would like to express my sincere gratitude to my supervisor Dr. D.S. Weaver for suggesting the problem. His constant encouragement and advice, often extending beyond the scope of this work, are greatly appreciated.

I am grateful to the late Dr. F.A. Mirza for the use of his computer software.

I also am grateful to Dr. M.A. Dokainish for making it possible to use his computing facility.

I am thankful for the assistance offered by Mr. L.Baksys in the preparation of drawings and the final copy of the manuscript.

I acknowledge the financial support of the Natural Sciences and Engineering Research Council of Canada.

Lastly, I would like to thank my parents for their unending support and encouragement.

TABLE OF CONTENTS

LIST OF FIGURES

LIST OF TABLES

NOMENCLATURE

A	area of cross-section
a	connecting pipe length
E	modulus of elasticity
F_{sp}	spring force
f	frequency
h	convolution hight
I	second moment of cross-section
J	mass moment of inertia of cross-section per unit length
k	half-convolution axial spring rate of bellows
m	mass per unit bellows length
M	local bending moment
N	number of half-convolutions
p	convolution pitch
Q	shear force
R_m	mean radius of bellows
R_1	radius of convolution root
R_2	radius of convolution crown
S	convolution surface
t	nominal thickness of bellows material
$T(t)$	time harmonic function
U	convolution displacement
V	potential energy
W, T	kinetic energy
w_k	dynamic displacement of bellows axis
$X(x)$	mode shape function
x, y, z	coordinates
α_{f2k}	coefficient

δ_i	half-convolution root relative displacement
ε	axial strain
Φ	velocity potential
λ	half-convolution added fluid mass
μ	half-convolution added mass coefficient
ρ_f	density of fluid
ν	Poisson's ratio

CHAPTER 1

INTRODUCTION

Any piping system or a part of it is more or less flexible. In many cases, as in oil or gas pipe lines, for example, which are buried under the ground, the elongations or contractions are very small due to almost constant inside and outside pipe temperature. In these cases the natural flexibility of the piping system itself is completely sufficient to accept small elongations. However, in many other cases, such as the piping systems of modern fossil or nuclear power plants or in aircraft and space technology, the elongations and contractions of the piping system can be very significant and frequent due to changes in temperature or to mechanical motions of the separate sections of the structure with respect to each other. Therefore, where the natural flexibility of the piping system itself is not adequate, artificial flexible elements, such as expansion loops or expansion joints are used. Reciprocating machines, such as compressors, are usually connected to the piping system through flexible elements in order to prevent noise and stress propagation over the whole piping system.

As a flexible element, the metallic bellows has been in use in engineering practice since the end of the last century. At first it was applied as a pressure gauge in barometers and later, in the piping systems of the modern thermal power plants, where the corrugated pipe expansion joints (bellows) began to replace the expansion loops, which were loosing too much head and becoming too bulky.

The most important part of the expansion joint is the bellows, which consists of a number of uniform convolutions. The bellows convolutions have appeared in practice in a variety of shapes, the most popular of which consists of flat circular rings connected to two toroidal half-rings, forming the root and the tip of a convolution. These are called U-convolutions. This particular shape of convolution is most widely used because it permits formation of the complete bellows either mechanically or hydraulically from a single piece of light gage cylinder. Practically all other convolution shape bellows are assembled by the welding of separately stamped convolution elements, which makes them much more costly. Therefore, throughout this thesis only U-shaped bellows are referred to, although all the derived formulae or calculation methods used can be equally well applied to the other covolution shape bellows.

Today bellows-type expansion joints have become so widely used in various piping systems, that the production of them has developed into a new branch of industry. As a result, the Expansion Joints Manufacturers Association (EJMA) was founded in 1955 by a group of companies, experienced in the design, fabrication, and application of bellows expansion joints.

On one hand, bellows expansion joints are very compact and very flexible devices for accommodation of large axial or transverse displacements, while on the other they are very susceptable to vibrations which can be easily excited either structurally, through the fixed ends of the expansion joint, or by the fluid flowing inside the bellows. Practice shows that the latter type of excitation is most common and most dangerous. When the flow velocity is sufficiently high, significant flow-induced vibrations can develop which usually lead to premature fatigue related failure of the bellows. This has been demonstrated by the failure of numerous bellows used in the Joint European Torus (JET) fusion energy project, Weaver and Aisworth (1989), for example.

Despite a wide variety of universal expansion joint designs, from the structural standpoint, practically all of them fall into two categories: expansion joints with and without lateral supports. Therefore, in addition to the single bellows expansion joint, these two types of universal expansion joints are extensively analyzed throughout this thesis.

From the beginning, researchers were naturally interested in investigating the static strength and, of course, the stability of bellows. Just some twenty five years ago, with the increased use of bellows in high technology, the investigations of the dynamical behaviour of bellows began. Since the most important and obvious excitation source for the bellows expansion joint installed in a straight section of a pipeline is the inside flow, which is nearly axisymmetric, researchers paid primary attention to axial vibration of the expansion joints. Comparison of numerical and experimental results for axial natural frequencies of bellows expansion joints confirm sufficiently high precision of corresponding formulae recommended by the EJMA Standard (1980).

According to the EJMA Standard, an expansion joint can be installed in proximity to elbows or any other piece of the fitting. In this case, the flow is no longer subjected to the ideal axisymmetric conditions typical of bellows in a straight pipe section. Therefore, significant lateral vibrations could be excited in such cases. Comparison of the present experimental investigations of lateral vibrations of single and double bellows expansion joints with theoretical calculations using EJMA Standard formulae demonstrated up to 400% difference with respect to experimental data for higher vibration modes. For the dynamic evaluation of an expansion joint, the natural frequencies must be known more precisely than recommended by the EJMA Standard. This is the primary purpose of this thesis.

In principle, the dynamic calculation of an expansion joint may be divided into the following four steps:

1. Determination of the excitation load, which is probably caused by free shear layer instability over the periodic cavities created by the bellows convolutions,

2. Determination of the frequencies of natural vibrations of the expansion joint with fluid inside,

3. Determination of the maximum dynamic displacements and stresses in the bellows material,

4. Comparison with the allowable values of the displacements and stresses at the given conditions.

The science of hydrodynamics is concerned with the solution of the first step problem. The methods of hydrodynamics and theory of vibrations are to be used for a solution of the second step problem. The last two steps are problems addressed by the theory of vibration and strength of materials. It is not difficult to understand, that the these four steps taken together create a very complex scientific problem, not least because the prediction of the excitation force amplitude is extremely difficult. In such cases the most reliable method of solving the problem is through experimentation. However, frequently it is sufficient to provide a simplified dynamical solution for the system, which consists of the first and second steps mentioned above, i.e. by predicting the forcing and natural frequencies, and ensuring that frequency coincidence never occurs. This thesis develops the theoretical tools to allow the designer to do just that.

Chapter 2 is a literature review. The history of the problem of hydroelasticity is briefly elucidated. Currently existing approaches, methods, and some results of the theoretical, numerical, and experimental investigations of transverse vibrations of bellows are reviewed. It was found that little attention has been paid up to now to the investigation of transverse vibrations of bellows. Moreover, the investigations are very scattered and in some cases their results contradictory. On the one hand, this can be explained by the complexity of the bellows as an elastic system, the investigation of which different authors have undertaken with different combinations of simplified assumptions in mind. On the other hand, this uncertainty demonstrates that the investigations of transverse vibrations in bellows is still in the initial phase.

In Chapter 3, the general formulation of the problem of hydroelasticity is given. Two methods for solving the problem are presented, and the peculiarities related to the transverse bellows vibration problem are discussed in detail. The bending stiffness of bellows is expressed through the axial bellows spring rate, which can be calculated using already existing formulae. For more precise calculations of the axial spring rate, the shell and the solid of revolution finite element algorithms are provided. Also, the inertial properties of fluid in bellows are thoroughly discussed. The original approach of calculation of added mass is elaborated in this chapter.

The bellows is a complex, periodic kind of shell. In the case of transverse vibration of bellows, the problem turns into tri-dimensional eigenvalue problem with hundreds or even thousands of elements. Such problems must be solved using powerful computers. Therefore, previous studies of the transverse vibration of bellows usually reduced the tri-dimensional shell problem to a beam transverse vibration problem with mixed success. The approach taken in this thesis is a similar beam approach. It should be noted, that in order to reduce the general bellows shell problem to the beam transverse vibration problem, a number of important assumptions have to be made prior to the derivation of the differential equation. All the assumptions are extensively discussed, and the differential equation is derived in Chapter 4.

Practicing designers usually prefer to use short explicit formulae rather than complex computer codes and numerical simulations. Keeping this in mind, the Rayleigh quotient method was chosen to obtain the natural frequency expressions for expansion joints. It should be noted that much higher precision than usual was achieved using as admissible functions, not some static deflection curves satisfying given boundary conditions as recommended in the vibration textbooks, but the mode functions of the simply Bernoulli-Euler differential equation, assuming that the inertia of rotation of the cross-section and the pressure inside the bellows affect the modeshape very little. The correctness of this assumption was confirmed by the natural frequency results, obtained from the experiment.

In Chapter 5 the natural frequency solution for a single bellows expansion joint is given. As an approximate mode function the Bernoulli-Euler differential equation solution for fixed-fixed end conditions is taken. Comparison with the exact solution is provided, which demonstrates very high precision of the frequency expression obtained from the Rayleigh quotient.

The double bellows expansion joint possesses two distinct vibration mode families: so called lateral and rocking. The first attempts to solve this problem showed that the solution resulted in very long and complex mathematical expressions. Therefore, the double bellows expansion joint natural vibration problem was divided into two separate problems, one for lateral, the other for rocking modes. These two problems are governed by the same differential equation, but have two different sets of boundary conditions. Such division of one problem into two made possible the essential simplification of the solution procedure of the general problem from the mathematical standpoint. For both lateral and rocking mode boundary conditions, the Bernoulli-Euler differential equation was solved to obtain the approximate mode shapes for substitution into the Rayleigh quotient expression of the real double bellows expansion joint system. The exact solutions of the frequency equations of these two separate problems compared with the results calculated from the Rayleigh quotient expressions exhibited very little error. In Chapters 6 and 7 these two separate lateral and rocking mode problems are solved.

Chapter 8 is devoted to the experimental investigation of the natural vibrations in bellows expansion joints. The experiments were conducted with empty bellows to test the main assumption of reduction of the bellows as a shell to the bellows as a beam and the assumption of the negligibility of the shear. The experiments with stagnant water inside the bellows were performed to test the added mass formula, derived in Chapter 3. The effect of inside pressure on the frequency was checked by means of experiments. Finally, the natural vibration experiments were conducted with the bellows installed in a flow loop to test all assumptions combined, including the assumptions about the negligibility of the influence of the Coriolis and the centrifugal forces exerted on the bellows by the flowing fluid.

Chapter 9 is concerned with flow-induced vibrations in bellows. The experiments were conducted with single and double bellows specimens installed in various locations of the loop to test the influence of a change in the hydrodynamical exciting force on the modes and vibration amplitudes of the bellows. The experiments were set up to allow a velocity range from zero up to 10 m/s bulk flow velocity.

Chapter 10 summarizes the results of the entire investigation and examines the capability and limitations of the formulae developed for design purposes.

CHAPTER 2

REVIEW OF INVESTIGATIONS OF TRANSVERSE VIBRATIONS IN CORRUGATED PIPE EXPANSION JOINTS

2.1. General Information about Flow-Induced Vibrations

Flow-induced vibrations of elastic bodies involve the interaction between the elastic and inertial forces of the elastic body and the fluid. The vibration excitation mechanisms are often not well understood, since flow-induced vibration phenomena are usually very complex and diverse. The exact determination of the nature of the interaction between the structure and fluid and the magnitude of force of the interaction is extremely difficult. The flow-induced vibrations appear in tubes, in heat exchangers, and steam generators, International Symposium on Vibration Problems in Industry (1973), Paidoussis (1979), Shin and Wambsganss (1975); in nuclear fuel assemblies, Oldaker et al. (1973); in hydrotechnical components and structures, Weaver (1976), IUTAM/IAHR (1974); in naval and space industry, Sainsbury and King (1971), Symposium on Solid-fluid Interaction (1963). The wind excitation of buildings and other overground structures is another area where the Flow-Induced Vibration science can be applied, Sainsbury and King (1971).

The list of the published papers in the field of Flow-Induced Vibrations is growing rapidly and these publications are spread over a large number of journals because of the diversity of the flow-induced vibration phenomena. Naudascher (1967), Toebes (1965) and others attempted to classify the flow induced vibration phenomena. However, most of the flow-induced vibrations according to Weaver (1989) can be characterized as:

a) Forced vibrations,

b) Self-controlled vibrations,

c) Self-excited vibrations.

Forced vibrations problems stem from variety of sources. These include the vibrations induced by turbulent flow, vibrations as a response of tall buildings or aircraft structures to wind gusts, the vibration of ship propeller blades excited by the periodical flow caused by the proximity of the ship hull, the response of a pipe conducting some fluid, or of a marine vehicle operating at the surface of the water. When the excitation is random, a statistical technique is usually used for determining of the exciting force distribution over the surface of the structure. Whether these excitations are random or periodic, the necessary feature for this class of response problems is that the motion of the structure has no "feed-back" effect on the fluid forces. Therefore, the excitation force can be studied separately from the vibration problem using a rigid model. This separation of the whole response problem into two independent ones greatly simplifies the solution.

In self-controlled vibration problems some periodicity exists in the flow even in the case of the completely stationary structure. When this periodicity coincides with some natural frequency of the structure, resonance takes place. The vibration amplitude increases until the structural motion starts to control the fluid excitation force by the developed feed-back mechanism. Under these conditions, over some fluid velocity range, the vibration response of the system is controlled not by flow velocity, but by the vibrating structure. This fluid velocity range is called the "lock-in" region. A common source of periodicity in the flow is vortex shedding. Examples of this class of flow-induced vibrations can be the vibrations of smokestacks, high towers, turbine blade vibrations, etc.. Such vibrations can be prevented by changing either the stiffness or the mass of the structure to alter the natural frequency or, more effectively, by changing the geometry to alter the fluid excitation.

Self-excited vibrations appear in such systems when the motion of the structure itself creates the periodic fluid force which in turn amplifies the vibration of the structure. The periodic fluid force doesn't exist in the absence of structural motion, as in the case of self-controlled vibrations. This is the main distinction between these two types of flow-induced vibrations. Examples of self-excited vibrations are bending-torsion vibrations of aircraft wings, the oscillation of gate seals, the galloping of frosted wires, and the vibration of vertical lift gates. Because of the interaction between fluid and elastic forces, both self-controlled and self-excited vibrations are called fluid-elastic vibrations.

Since it is possible to obtain exact solutions only for a limited number of simplified and usually idealized problems, it is often necessary to employ experimental methods to determine the solution of fluid-elastic phenomena encountered in todays modern designs. Dimensional analysis and similitude theory are often used to analyze very complex phenomena. The experimental information needed is usually in the form of fluid-dynamic coefficients, stability thresholds, pressure distribution, velocity profiles, amplitude, and frequency of oscillation. To study the response of such models wind tunnels and water loops are usually used.

In flow-induced vibration problems related to liquid flows it is very important to take into account the inertia of the fluid because this is usually great enough to change vibration frequencies considerably or sometimes even the modes of vibration of a system. The motion of any rigid or elastic body in a fluid is accompanied by a flow of fluid around the body. Considering the fluid to be perfect and incompressible and its flow as steady and irrotational, both drag and lift forces for the body possessing central symmetry, according to the paradox of D'Alambert, are equal to zero. The viscosity of the fluid must be taken into account to obtain the real drag force. However, if the motion of the body is nonuniform, the flow initiated in the perfect fluid is not steady anymore. In this case the flow generates a drag force on the body and this force appears as if the inertia of the body had been increased. Since the vibrational motion is nonuniform, the mass of the vibrating body appears as if increased by some amount of "additional mass" in comparison with its mass in vacuum. This phenomenon may be accompanied by a significant drop in the natural frequency of the vibrating body if the fluid density is sufficiently high. It should be noted that the term "additional mass" doesn't mean that a certain amount of the fluid really has the same acceleration as the vibrating body.

The British scientist Green (1833) in the nineteenth century understood the phenomena of additional mass. It was encountered in practice during the investigations of the influence of water on the vibration of dams in seismic regions. The first theoretical solution of this problem for a solid dam was accomplished by Westergaard (1932). It was determined by him, and later by other authors, that in most cases, the compressibility and viscosity of the fluid can be neglected completely. The first attempts to take into account the inertial properties of the fluid in the shipbuilding industry were made by Lewis (1929) and Koch (1933). Various theoretical investigations of the vibration of vertical and horizontal rectangular plates were performed by Sheinin (1967). The first attempts to evaluate theoretically the additional mass in bellows were made by Gerlach (1969).

2.2. The Survey of Flow-Induced Vibrations of Corrugated Pipe Expansion Joints

Corrugated pipes have been used in engineering practice for more than one hundred years. At first they were used mostly as sensitive pressure gauges. After World War II, with accelerating technological advance, especially in the piping systems of the modern thermal power plants, corrugated pipe expansion joints (bellows) began to replace the loop type expansion joints, which were losing too much head and which became too bulky in very dense piping systems. Later, bellows found an application in modern airplanes, rockets, and space technology. The geometry of a bellows is shown in Fig.2.1. As seen in Fig.2.2a and b, two types of expansion joints are being used in engineering practice: single and double bellows expansion joints. To reduce the susceptibility to buckling, lateral supports may be provided as shown in Fig.2.2c.

From the beginning, researchers were interested in investigation of the static strength and stability of bellows. Only some twenty five years ago, with the increased use of bellows in high technology, investigations of the dynamical behaviour of bellows began.

As seen from Fig.2.1a, a bellows is an extremely complex kind of shell. Gerlach (1969) distinguishes three types of axial vibration modes of a bellows which are shown in Fig.2.3a, b, c. In addition to these, in the case of longer bellows, the transverse vibration modes (see Fig.2.3 d) are likely to occur.

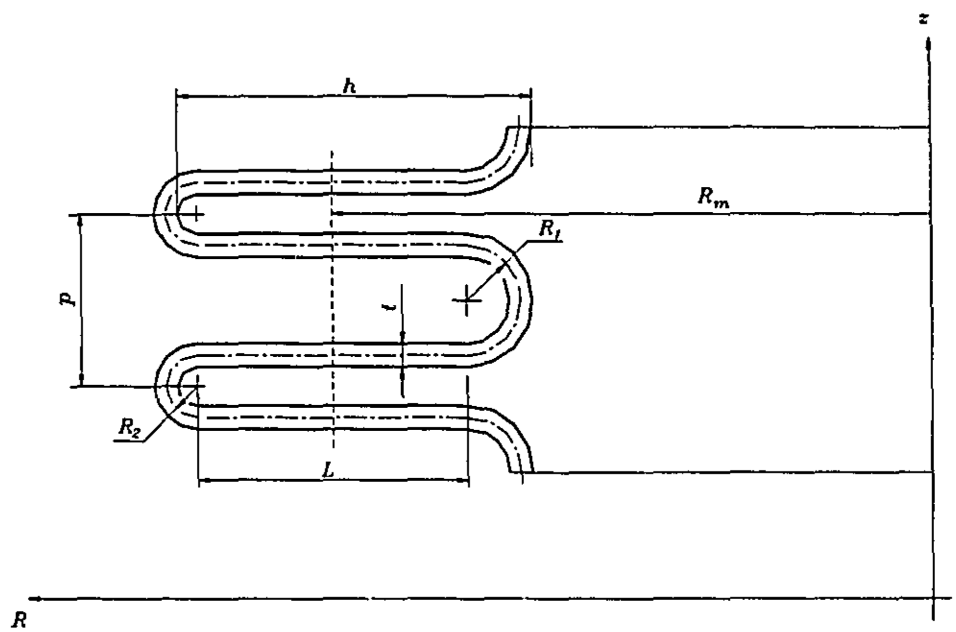

Fig.2.1. The geometry of bellows

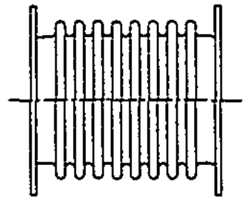

a) Single bellows expansion joint

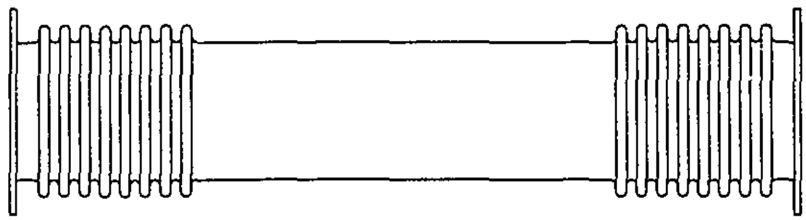

b) Double bellows universal expansion joint

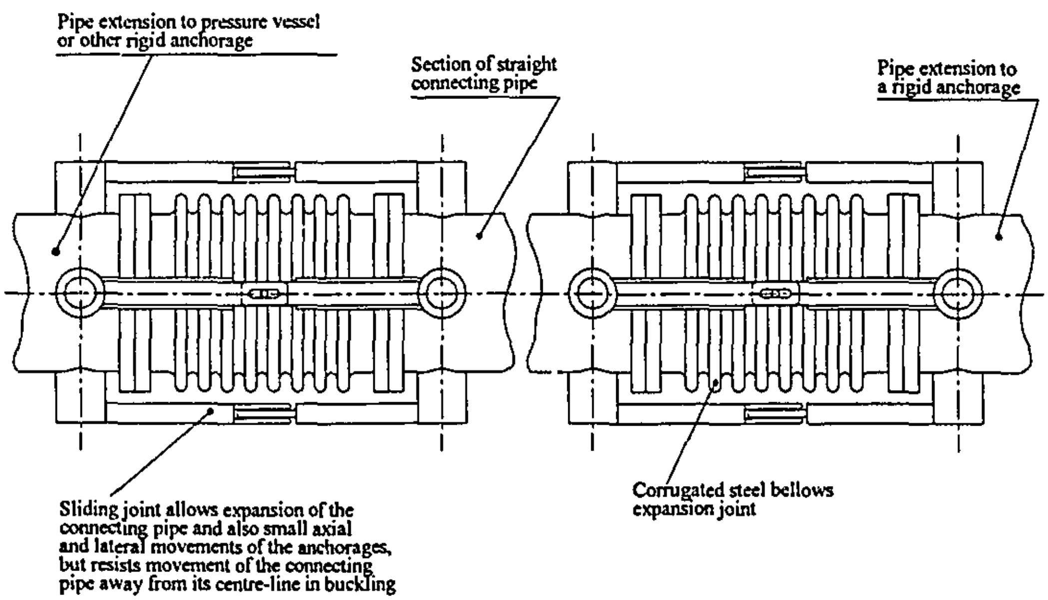

c) Double bellows universal expansion joint with lateral supports

Fig.2.2. Various types of expansion joints

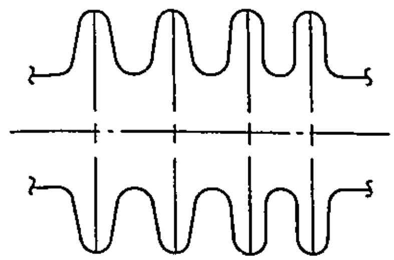

a) Axisymmetric longitudinal mode

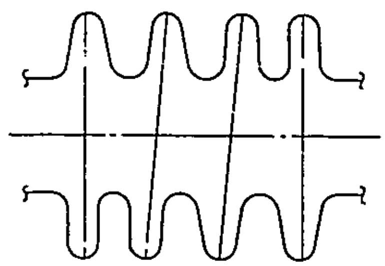

b) Nonsymmetric longitudinal mode

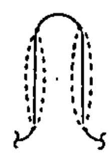

c) Local convolute bending mode

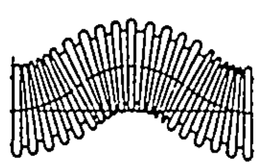

d) Bellows bending mode

Fig.2.3. The kinds of bellows vibration modes

Since the most important and obvious excitation source for bellows installed in a straight section of a pipeline is the inside flow which is nearly axisymmetric, researchers naturally paid attention primarily to axial vibrations of expansion joints.

The first detailed study of flow induced vibrations in bellows seems to have been conducted by Gerlach (1969), who concluded that the source of fluid excitation was vortex shedding from the convolution tips. In a subsequent paper (1972), Gerlach noted from the flow visualization studies that the flow structure over the bellows remained turbulent in the absence of bellows vibration.Thus, he recognized the fundamental fluid-elastic nature of the phenomenon, but maintained his view that vortex shedding was the excitation mechanism. He developed a "stress indicator", based on the assumptions of linear forced vibration theory, to provide an index of the severity of vibrations. Bass and Holster (1972) extended the work of Gerlach to bellows with internal cryogenic flows. They found that internal cavitation or boiling due to heat transfer and the formation of frost or condensation on the outside of the bellows convolutions – all had the effect of damping the vibrations.

Rockwell and Naudascher (1978) suggested that the excitation mechanism was probably free shear layer instability over the periodic cavities created by the bellows convolutions. These authors also noted that the Strouhal number reported for bellows was less than one half of that for a rectangular cavity and speculated that the effect of rounded corners in the case of bellows was to reduce the predominant oscillation frequency.

It has been shown by Franke and Carr (1975) that ramping the upstream and downstream corners of rectangular cavities is very effective in reducing the free shear layer oscillations.

Weaver and Ainsworth (1989) conducted experimental investigations of the flow induced vibrations of 20 mm diameter Inconel 600 bellows and found large amplitude flow-excited vibrations at velocities exceeding 4.5 m/s under ideal upstream flow conditions. These vibrations were clearly adequate to explain the service failures because of fatigue of the bellows during the test program. They found that the effect of service upstream flow conditions is to produce a high velocity jet across a portion of the bellows circumference. The result is a reduction in the mean flow velocity through the bellows required to excite resonance. According to these authors, it is desirable to avoid such flow geometry singularities such as abrupt transitions and elbows immediately upstream of bellows. Weaver and Ainsworth agree with the suggestion of Rockwell and Naudascher (1978) that the vibration excitation mechanism would appear to be free shear layer instability. A succession of bellows modes are excited with increasing flow velocity. The authors found the Strouhal number corresponding to the peak vibration amplitude in each mode based on a convolution pitch equal 0.45. This agrees with the Strouhal number for free shear layer instability over a deep cavity.

The experimental results obtained using flow visualization by Gidi (1993) demonstrated that the vibration of the convolution and the vortex shedding process are due to an instability in the free shear layer. This instability is, in turn, triggered by the motion of a convolution. This process leads to a resonant vibrational motion. Therefore, according to this author, the vibrations of bellows should be attributed to the class of self-excited vibrations.

2.3. The Survey of Investigations of Axial Stiffness of Bellows

Considering a bellows shell with its prolonged periodic geometry as a fixed-fixed beam, it is necessary to know the effective bending stiffness, *EI*. Calculation of *EI* for a classical beam is a simple problem, but this is not the case for bellows. It is rather impossible to calculate the first moment of inertia, *I*, taking into account just the geometry of the cross-section of bellows, as it is usually done in the case of a simple beam. Therefore, it seems that the bending stiffness of bellows, *EI*, can be calculated either numerically (using, for example, FEA) or from experiment. An experiment is time consuming and frequently very expensive. On the other hand, FEA is readily accessible, but in the case of the calculation of *EI* for bellows, the calculation becomes difficult for two reasons. First, bellows convolution is a very complex shell. Second, despite bellows axial symmetry, the problem becomes three-dimensional because of lateral deformation. Just the preparation of the input data file for such problem becomes a complex task for designers. Therefore, instead of a direct calculation of the transverse stiffness, EI, it is much easier for bellows expansion joints to calculate at first the axial stiffness, EA, and then, from the well known relationship, $EI = EAr^2$, to determine the transverse stiffness. Since this approach was used throughout this thesis, the existing methods for calculation of axial stiffness of bellows are briefly reviewed in the section below.

According to the EJMA Std. (1980), one convolution axial spring rate of bellows is:

$$f_i = 1.7\frac{d_p E_b t_p^3 n}{w^3 C_f}, \tag{2.1}$$

where

d_p is the mean diameter of bellows ($2R_m$ in Fig.2.1),

E_b is the modulus of elasticity,

t_p is the bellows material thickness factor, to correct for thinning during forming,

$$t_p = t\sqrt{\frac{d}{d_p}},$$

t is the nominal material thickness,

w is the convolution depth (h in Fig.2.1),

q is the bellows pitch (p in Fig.2.1)

C_f is the factor from the graph in Fig.2.4.

All parameters in formula (2.1) must be in lb-in-sec system.

Gerlach and Schroeder (1969) give another formula for calculation of the axial stiffness of bellows. Since these authors treat the bellows as an N degree of freedom in series connected spring-mass system, they use a so called elemental spring rate for one half-convolution,

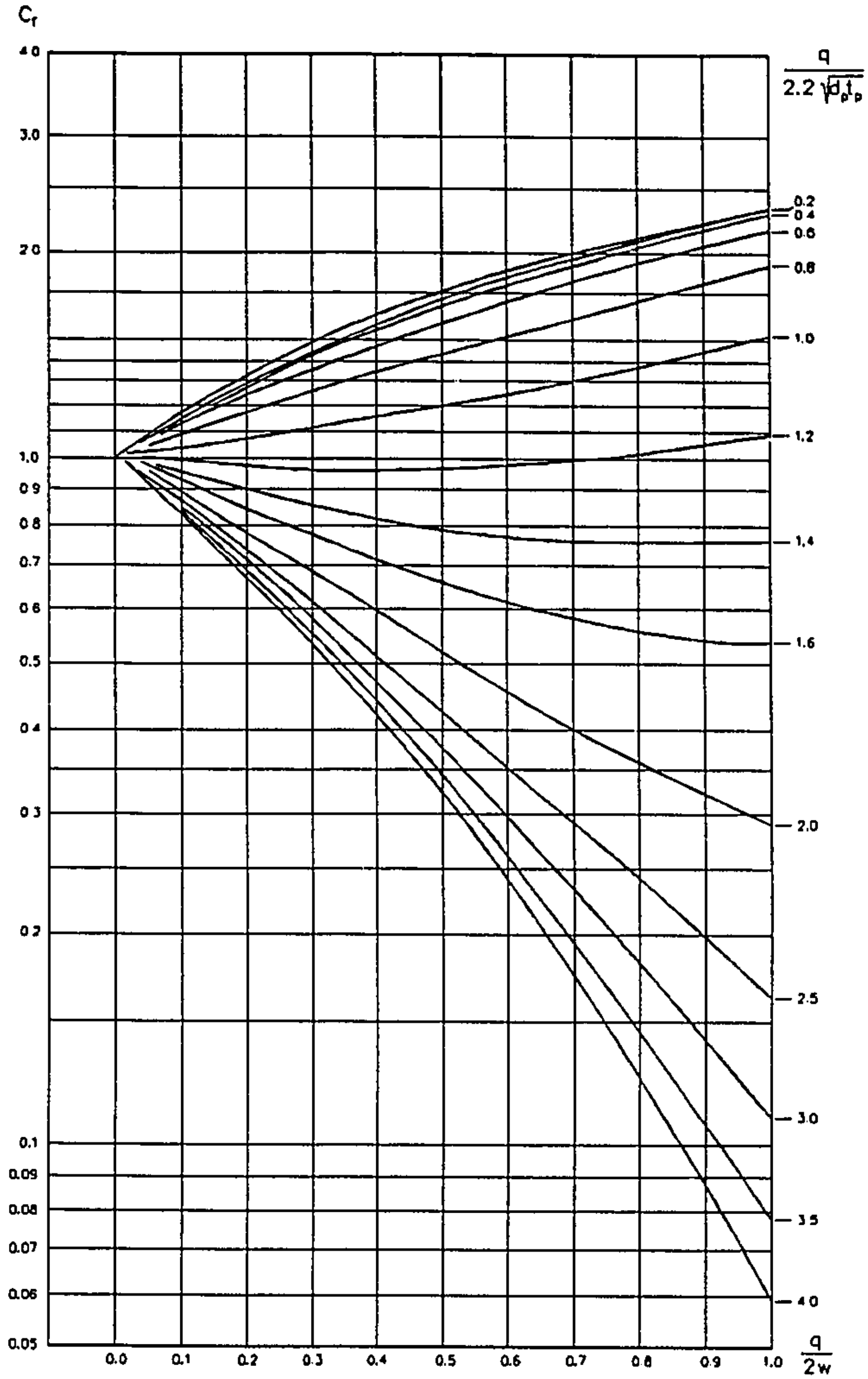

Fig.2.4. C_f for convoluted bellows, EJMA Std. (1980)

$$k = 2D_m E N_p \left(\frac{t}{h}\right)^3, \tag{2.2}$$

where

D_m is the mean diameter of bellows,

E is the modulus of elasticity,

N_p is the number of plies,

t is the thickness of the bellows wall,

h is the convolution height.

All parameters in formula (2.1) must be in lb-in-sec unit system.

Andreeva (1975) submits the following formula for axial stiffness of one half-convolution of bellows:

$$k = \frac{Eh^3}{AR_{out}^2}, \tag{2.3}$$

where

E is the modulus of elasticity,

h is the thickness of the bellows wall,

R_{out} is the outer radius of bellows,

A is the coefficient, dependent on ratio, $r = \frac{R_{out}}{R_{in}}$, as follows:

$$A = \frac{3\left(1-\mu^2\right)}{\pi}\left[\frac{r^2-1}{4r^2} - \frac{\ln^2 r}{r^2-1}\right],$$

R_{in} is the inner radius of bellows,

μ is the Poisson's coefficient.

According to Haringx (1952), the axial stiffness of bellows per one convolution is:

$$k = \frac{\pi \varepsilon E h^2 r_u^3}{\left(1-\nu^2\right) b^3 R_m^2}, \tag{2.4}$$

where,

E is the modulus of elasticity,

h is the thickness of bellows,

r_u is the outer radius of bellows,

r_i is the inner radius of bellows,

ν is the Poisson's coefficient,

b is the convolution depth,

R_m is the mean radius of bellows,

$$\varepsilon = -\frac{1}{3}\,\frac{\left(1+\rho^2\right)\left(1-\rho\right)^3}{1-\rho^2+\left(1+\rho^2\right)\ln\rho},$$

$$\rho = \frac{r_i}{r_u}.$$

Although the derivation of formulas (2.1), (2.2), (2.3) and (2.4) are based on the same flat ring approach, the numerical results of the axial bellows spring rate obtained from these formulas are quite different. This can be explained by the different methods used for evaluating of the influence of the rounded roots and tips of the convolutions adopted in these four formulas. Therefore, for more precise calculations of the axial stiffness of bellows expansion joints, it is necessary to resort to either experiment or Finite Element Analysis. This problem is analyzed in the next chapter in detail.

2.4. Investigations of Axial Vibrations in Bellows

Most earlier investigations of natural vibrations in bellows were conducted by Gerlach and Schroeder (1969). They found from experiments that three different kinds of structural modes can be excited by the flow: axisymmetric, cocking, and convolution bending modes. The last ones are the modes of higher order, where the order of the mode becomes equal or even higher than the number of convolutions.

The bellows are treated by these authors as an N degree of freedom in series connected spring-mass system, where $N = 2N_c - 1$, N_c being the number of convolutions. The elemental spring rate was given in a previous section by eq. (2.2):

$$k = 2D_m E N_p \left(\frac{t}{h}\right)^3, \tag{2.5}$$

The expression for the elemental mass is

$$m_m = \pi \rho_m D_m t N_p \left[\pi R_1 + \left(h - 2R_1\right)\right], \tag{2.6}$$

where

ρ_m is the density of the bellows material,

R_1 is the radius of the convolution tip.

The elemental added mass for the lower frequencies, caused by translational motion of a convolution is

$$m_{f1} = \frac{1}{2} \pi \rho_f D_m h \left(2R_1 - t\right) \tag{2.7}$$

and the elemental added mass for the higher frequencies is

$$m_{f2} = \pi \rho_f D_m h^3 \frac{1}{3\left(2R_1 - t\right)}. \tag{2.8}$$

Using (2.5), (2.6), and (2.7), the so called reference frequency with fluid inside is calculated from

$$f = \frac{1}{2\pi}\sqrt{\frac{k}{m_m + m_f}}. \tag{2.9}$$

The true modal frequency is then determined by multiplying the reference frequency value by the dimensionless frequency taken from Table 2.1, corresponding to the desired mode number, n, and the system degree of freedom, N, as follows:

$$f_n = k_n f, \tag{2.10}$$

where

f_n is the true modal frequency for the nth mode,

f is the reference frequency,

k_n is the dimensionless frequency parameter for the nth mode.

Table 2.1. Dimensionless frequencies parameters for bellows mechanical model, k_n, Gerlach and Shroeder (1969)

N	Mode number, n				
	1	2	3	4	5
1	1.414				
2	1.000	1.732			
3	0.765	1.414	1.845		
4	0.620	1.175	1.620	1.900	
5	0.520	1.000	1.414	1.732	1.930
6	0.445	0.862	1.247	1.564	1.802
7	0.390	0.765	1.111	1.414	1.663
8	0.347	0.684	1.000	1.286	1.532
9	0.314	0.618	0.908	1.176	1.414
10	0.285	0.563	0.831	1.082	1.310
11	0.264	0.518	0.765	1.000	1.217
12	0.245	0.479	0.709	0.929	1.136
13	0.226	0.445	0.661	0.868	1.064
14	0.213	0.416	0.618	0.814	1.000
15	0.199	0.390	0.583	0.765	0.942
16	0.185	0.367	0.547	0.722	0.891
17	0.174	0.347	0.518	0.684	0.845
18	0.165	0.329	0.491	0.649	0.803
19	0.157	0.313	0.467	0.618	0.765
20	0.149	0.298	0.445	0.590	0.731

It may be seen from the equation (2.5) that the given method of calculation of the frequencies of bellows doesn't take into account the double curvature of both the tip and the root of a convolution and the axisymmetry of bellows. In addition, the criteria for using formulas (2.7) and (2.8) is not clear. For some "transitional" mode, the formulas (2.7) and (2.8) should give equal or at least close results, i.e., the ratio $m_{f1}/m_{f2} \cong 1$. In reality, the ratio is $m_{f1}/m_{f2} = 3(2R_1 - t)^2/2h^2 \ll 1$ for reasonable dimensions of a, t, and h. Therefore, the use of the method explained above for higher ratios of R_1/D_m and h/D_m, for the modes of higher order as well as in the case of a low number of convolutions becomes questionable.

In another connection, the same authors offer to relate both kinds of added mass expressed by formulas (2.7) and (2.8) into the single formula as follows:

$$m_f = \frac{2N_c - 1 - n}{2N_c - 2} m_{f1} + \frac{n-1}{2N_c - 2} m_{f2}, \tag{2.11}$$

where

N_c is the number of convolutions,

n is the number of the mode.

Formula (2.11) is not applicable for $N_c = n = 1$.

The other similar approach for the calculation of natural frequencies in bellows is given in the EJMA Standard (1980):

$$f_n = C_n \sqrt{\frac{K_{SR}}{W}}, \tag{2.12}$$

where

$$K_{SR} = \frac{f_i}{N_c},$$

f_i is one convolution spring rate, given by eq.(2.1),

C_n is the coefficient given in the Table 2.2,

W is the total weight of the bellows.

Inch-pound-sec unit system must be used in both (2.12) and subsequent formulae. It should be noted that W includes the part of the additional mass of fluid which is trapped in the convolutions. The other part of the additional mass that is caused by the deformation of the convolution is not taken into account in W, which can lead to a significant error, especially for higher modes.

Table 2.2. Values of C_n for first 3 modes, EJMA Std. (1980)

N_c	C_1	C_2	C_3	C_4
1	8.84			
2	9.51	17.7	23.1	
3	9.75	18.8	26.5	32.5
4	9.75	19.1	27.8	35.4
5	9.81	19.3	28.4	36.8
6	9.81	19.4	28.7	37.5
7	9.81	19.5	28.9	38.0
8	9.81	19.5	29.1	38.2
9	9.81	19.5	29.1	38.5
10	9.81	19.6	29.2	38.6

Morishita, Ikahata, and Kitamura (1989) use the fixed-fixed uniform rod approach for the investigation of axial modes in bellows. Therefore, the formula for evaluating the natural frequencies of bellows is simple:

$$f_k = \frac{k}{2}\sqrt{\frac{K_{SR}\, g}{W}}, \tag{2.13}$$

where

g is the acceleration of gravity,

K_{SR} is the spring rate of bellows, given in EJMA Std.,

W is the total weight of bellows, as in EJMA Std.,

k is the mode number.

All the methods of calculation of axial vibrations of bellows considered in this section have one common insufficiency: they are simplified to an one-dimensional rod-beam system and are not reliable when the number of convolutions becomes comparatively small or the mode number becomes large. To get more precise results in such cases, the bellows must be treated as a shell of revolution. Just such an investigation of axisymmetric vibrations of bellows is presented by Jakubauskas (1991) and by Jakubauskas and Weaver (1992).

A finite element code was developed by these authors to solve the uncoupled hydroelasticity problem for axial bellows vibration. The bellows was modelled using two node, three degree of freedom per node axisymmetric constant meridional curvature shell elements as given by Ross (1983). As the in-plane displacement and rotation are negligible compared to the out-of-plane displacement of the shell, the stiffness and mass matrices were simplified using Irons' (1965) reduction process.

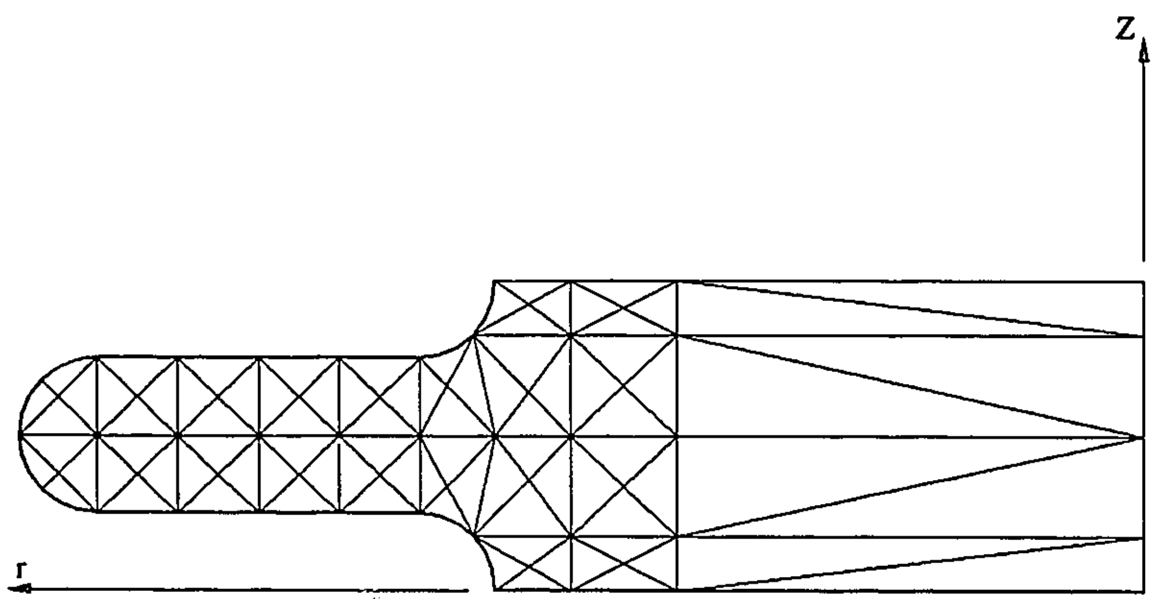

Fig.2.5. Finite element discretization of bellows and fluid domains

The fluid was modelled using three degree of freedom axisymmetric triangular elements. The shell and the fluid codes were tested against analytical solutions for some simple problems and found to give excellent predictions. They were then specialized for bellows vibration analysis as shown in Fig.2.5. It was found that 16 shell elements and 88 fluid elements per convolution were adequate for convergence of bellows natural frequencies up to mode numbers exceeding the number of bellows convolutions. The input data file for the code was very simple, requiring only the bellows geometry, the physical data for the bellows material and fluid, the number of bellows convolutions and the requisite number of natural frequencies.

The code was used to analyse the free vibrations of a five convolution stainless steel bellows with mean radius $R_m = 34.6$ mm, convolution radius $R_1=R_2=1.25$ mm, straight portion of convolution height $L = 3.21$mm, thickness $t = 0.28$ mm, modulus of elasticity $E = 2.07\times10^{11}$ Pa, Poisson's ratio $\nu = 0.3$, and density $\rho = 7860$ kg/m^3.

The predicted mode shapes are shown in Fig.2.7 in which vibration nodes are indicated by solid dots. Scrutiny of these mode shapes indicate at least two distinct types of convolution behaviour. The first involves nearly parallel motion of the sides of a convolution, i.e., in-phase translation with little shape distortion. For such motion, the added mass is expected to be reasonably approximated by the mass of fluid contained by a convolution as assumed by Gerlach (1969) and the EJMA Standard (1980). This behaviour is best illustrated by the first mode, especially the middle convolution.

The second type of convolution behaviour involves convolution shape distortion in which the sides of a convolution move out of phase with one another. In such a case, the fluid motion would be primarily in and out of the convolution and the added mass would not be reasonably represented by the mass of fluid contained by the convolution. This behaviour is particularly clear for the middle convolution in the second and sixth modes. However, convolution shape distortion tends to become dominant over convolution translation as the mode number increases. Thus, according to the authors, the added mass is expected to increase with mode number and not remain constant as assumed in the EJMA Standard analysis.

The computed added mass is plotted against mode number in Fig.2.6. The associated in-vacuo and fluid filled bellows natural frequencies are presented in the same figure. As anticipated by the authors, the added mass increases with mode number from the first to the fourth modes. However, the added mass for the fifth mode shows, rather unexpectedly, a sharp drop to a value slightly below that for the first mode.

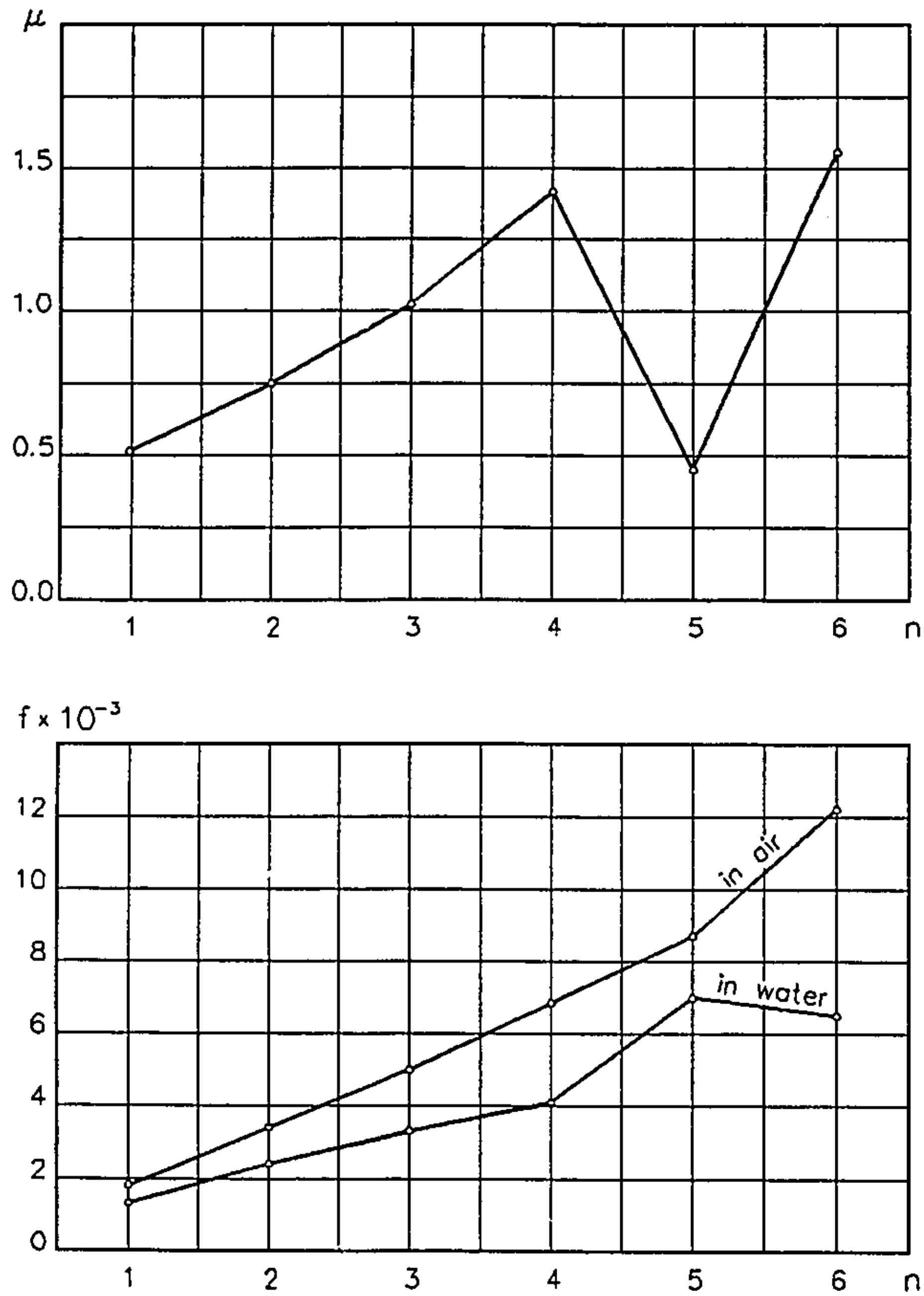

Fig.2.6. Bellows added mass coefficient μ and bellows frequency f (Hz) as functions of mode number for five convolution bellows, Jakubauskas and Weaver (1992)

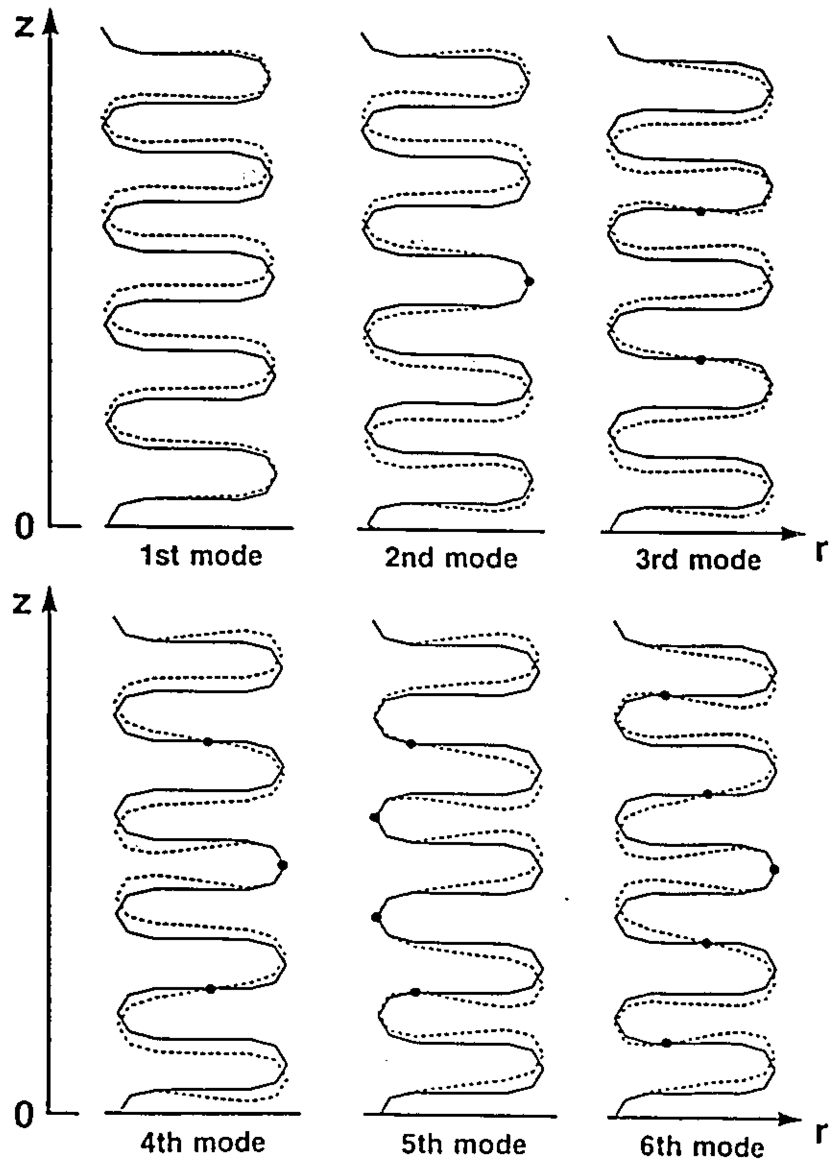

Fig.2.7. First 6 axisymmetric modes of five convolution bellows, Jakubauskas and Weaver (1992)

The authors explain this by examination of the mode shapes in Fig.2.7. The fifth mode has 4 internal vibration nodes at, or near, the convolution roots (internal tips).

these roots. This behaviour is clearest for the middle convolution. The fluid inertial effect for such a mode is expected to be less than that for a nearly pure translation of the convolution such as observed for the middle convolution in the first mode. It is noteworthy that this rocking behaviour and the resulting reduced added mass effect occured for the fifth mode of these 5 convolution bellows. Such behaviour is expected for any geometrically similar bellows when the mode number is equal to the number of convolutions. The sixth mode shape is more complex with some rocking of the end convolutions but considerable shape distortion of the middle three convolutions. Thus, there is a substantial increase in the added mass and a commensurate drop in the in-fluid natural frequency as compared with the fifth mode.

In order to verify the finite element code and check the above observations, the authors conducted experiments on a nine convolution and a five convolution bellows with the geometry and material data described above. The results of the experimental analysis are summarized in Tables 2.3. and 2.4. The comparison in Table 2.3 shows that the finite element predictions for both 5 and 9 convolution bellows in air are extremely good, probably within the experimental uncertainty limits. Note that the experimental frequencies in air are slightly below the predicted frequencies. The theoretical predictions for both bellows in water are also quite good, the largest error being less than 7%

Table 2.3. Comparison of experimental and FEA results for five convolution bellows, Jakubauskas (1991)

Mode shape #	in air		Error	in water		Error
	Exp.	FEA		Exp.	FEA	
	Hz	Hz	%	Hz	Hz	%
1	1600	1602	0.13	1300	1269	2.38
2	3175	3212	1.17	2400	2350	2.08
3	4800	4839	0.82	3550	3311	6.73
4	6400	6524	1.94	-	4227	-

Table 2.4. Comparison of experimental and FEA results for nine convolution bellows, Jakubauskas (1991)

Mode shape #	in air		Error	in water		Error
	Exp.	FEA		Exp.	FEA	
	Hz	Hz	%	Hz	Hz	%
1	887	891	0.45	737	722	2.04
2	1762	1793	1.76	1425	1386	2.74
3	2675	2692	0.64	2000	2010	0.50
4	3525	3591	1.87	-	2576	-

for the third mode of the shorter bellows. The experimental frequencies in water are all slightly above the predicted frequencies. These comparisons suggest that the fluid added mass may be slightly overpredicted by the finite element analysis.

2.5. The Survey of Investigations of Transverse Vibrations of Corrugated Pipe Expansion Joints

According to the EJMA Standard (1980), the expansion joint can be installed in proximity to elbows as shown in Fig.2.8. In this case the flow no longer corresponds to the ideal axisymmetric conditions, typical of bellows in straight pipes. Therefore, significant lateral vibrations of bellows may be excited in such cases. Probably, for this reason the EJMA Standard. cites just two types of vibration, axial and lateral bending, and provides corresponding formulas for the calculation of the natural frequencies. The formulas for lateral vibrations are:

a) Single bellows expansion joint,

$$f_n = C_n \frac{D_m}{l} \sqrt{\frac{K_{SR}}{W}}, \tag{2.14}$$

here

Mode #	1	2	3	4	5
C_n	24.8	68.2	133	221	330

b) Dual bellows expansion joint lateral mode,

$$f_1 = \frac{5.42\,D_m}{l}\sqrt{\frac{K_{SR}}{W}}\,. \tag{2.15}$$

c) Dual bellows expansion joint rocking mode,

$$f_2 = \frac{9.38\,D_m}{l}\sqrt{\frac{K_{SR}}{W}}\,. \tag{2.16}$$

In these formulas,

f_n is the natural frequency in the nth mode, (Hz),

K_{SR} is the overall bellows axial spring rate,

W is the overall weight of the bellows including the fluid mass if it is applicable,

D_m is the bellows mean diameter,

l is the bellows live length.

All parameters in the formulas above are in the lb-in-sec unit system. Comparative calculations by the author have shown, that these formulas have been derived from the Bernoulli-Euler differential equation for beam vibration and take into account only the mass and the bending stiffness of bellows. Therefore, they may not be very accurate, especially keeping in mind the extreme shortness and very complex geometry of bellows.

As in the EJMA Standard, Li Ting-Xin et al. (1986) suggest use of the simple fixed-fixed Bernoulli-Euler beam solution for the calculation of transverse vibrations of single bellows. Therefore, their method of calculation may be expected to lead to significant error as well, although the authors claim very good agreement with experiment.

For the investigation of lateral modes Morishita, Ikahata, and Kitamura (1989) used the Timoshenko differential equation for the beam fixed-fixed end conditions. They state that the shear effect is negligibly small for bellows and can be ignored. In their opinion, in addition to the Bernoulli-Euler conditions, it is necessary to take into account just the

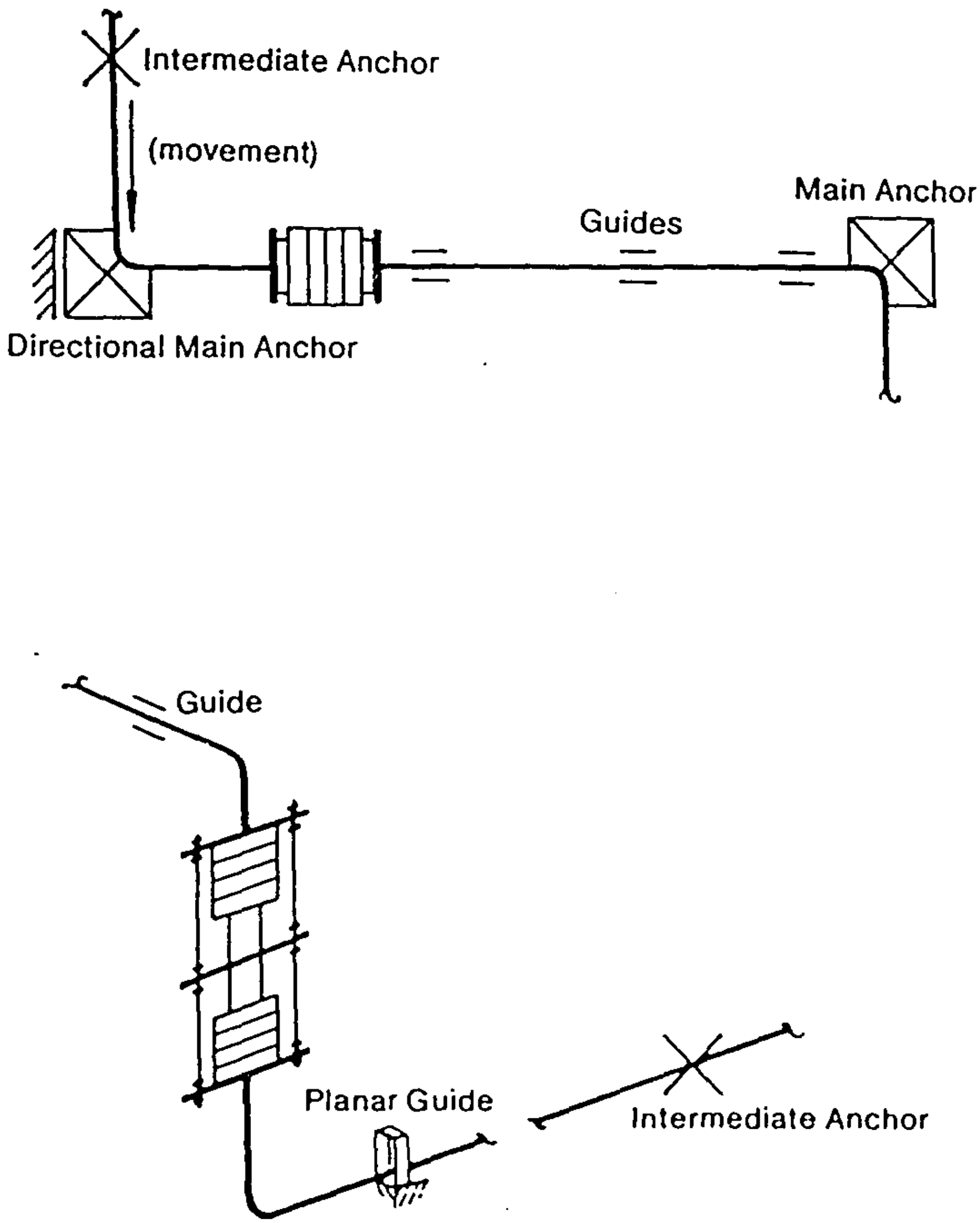

Fig.2.8. Installation examples of bellows

rotary inertia of the bellows cross-section, including the effect of the rotary inertia of the fluid trapped between the convolutions. The natural frequency formula for a single bellows expansion joint derived by these authors is

$$f_n = C_n \frac{D_m}{l} \sqrt{\frac{g K_{SR}}{W}}, \tag{2.17}$$

where,

$$C_n = \frac{b_k}{1 + \dfrac{D_m^2}{8\,l^2} \dfrac{(1 + h\gamma)}{1 + \dfrac{D_m}{2}\gamma} a_k},$$

$$\gamma = \frac{\rho_f}{\rho_b} \frac{p}{4\,t\,L_d},$$

$$L_d = h + \left(\frac{\pi}{2} - 1\right) \frac{p}{2}$$

Mode #	1	2	3	4	5
a_k	12.30	45.92	98.92	175.6	264.0
b_k	1.585	12.01	46.29	126.5	282.2

ρ_f, ρ_b are the densities of the fluid and the bellows material respectively,

t is the wall thickness of bellows,

D_m is the mean diameter of bellows,

h is the convolution depth,

l is the length of the bellows,

p is the bellows pitch,

g is the acceleration of gravity,

K_{SR} is the overall spring rate of bellows,

W is the overall weight of the bellows.

These authors suggest use of eq. (2.17) to calculate lateral frequencies of bellows with a sleeve inside, with slightly different C_n, and W:

$$C_n = \left(\frac{b_k}{1 + \dfrac{d_p^2 (1 + h\gamma)}{8 L_b^2 \left(1 + \dfrac{d_p}{2} \eta(\varepsilon) \gamma\right)} a_k} \right)^{\frac{1}{2}},$$

$$W = 2\pi g \left(\rho_m \frac{t L_d}{p} + \rho_f \frac{d_p}{8} \eta(\varepsilon) \right) d_p \, L_b,$$

where

$$\eta(\varepsilon) = \frac{1 + \varepsilon^2}{1 - \varepsilon^2},$$

$$\varepsilon = \frac{d_s}{d_p},$$

d_s is the outer diameter of the sleeve.

The same authors performed a FE analysis of the vibration of bellows using two-node six DOF beam elements and got fairly good agreement with experimental and theoretical results calculated from the simplified formula (2.17).

Comparative calculations of various natural frequencies using formulas (2.14) and (2.17) have shown that the frequency result obtained from formula (2.17) derived by Morashita et al. (1989) is approximately 20% lower than the result obtained using EJMA Standard (1980) formula (2.14). The significant difference between these two frequency results shows the importance of the rotary inertia of the cross-section of a bellows. Taking into account the pressurization and added mass related to convolution deformation effects, this difference should increase even more.

A review of the literature failed to turn up any numerical calculations for the transverse vibrations of bellows as a shell, perhaps because the eigenvalue problem for such complex shells as bellows require so much computational effort.

As seen from Fig.2.1, just a single convolution of a bellows is a very complex shell. Therefore, more precise finite element discretisation of a bellows requires a large number of finite elements for a single convolution only. In addition to this, as mentioned above, such eigenvalue problems require significant computational effort. On the other hand, while bellows are very complex as a shell, they possess very clear geometrical periodicity along the axis of symmetry, which makes a bellows similar to a deep beam at least. By happy coincidence, the longer bellows are, the more complex as a shell they become, but at the same time the more they resemble a beam. Therefore, it is convenient from the point of view of the transverse vibrations to treat a bellows expansion joint as a beam. In the following chapters, the beam approach to this problem will be founded in detail.

CHAPTER 3

STIFFNESS AND INERTIAL PROPERTIES IN CASE OF TRANSVERSE VIBRATION OF BELLOWS

3.1.The Bending Stiffness of Bellows

When considering a bellows as a fixed-fixed beam it is necessary to know the bending stiffness, EI. The calculation of EI for a classical beam is a simple problem, but this is not the case for a bellows. As was mentioned in the previous chapter, it is impossible to calculate the first moment of inertia, I, considering just the cross-section of a bellows as is usually done in the case of a beam. The derivation of the bending stiffness, EI, for bellows is given below.

Let the axial spring rate per one half convolution be k. On the other hand, the axial spring rate for a classical bar, according to Frocht (1951), is

$$k_b = \frac{EA}{l} \ ,$$

where

A is the area of the cross-section,

l is the length of a bar.

Now let $l = p/2$, i.e., the bar length is one half the convolution pitch, p. Then, equating k to k_b we can express the equivalent cross-sectional area of a bellows,

$$A_{eq} = \frac{kp}{2E},$$

where E is the real value of the Young's modulus of the bellows material. Geometrically, a bellows can be approximated by a thin cylinder of mean radius, R_m .Therefore, the radius of gyration of a bellows can be written, according to Beer and Johnston (1981), as

$$r^2 = \frac{R_m^2}{2}.$$

According to the well known formula from the strength of materials, $I = Ar^2$, the equivalent second moment of area then becomes

$$I_{eq} = A_{eq} r^2 = \frac{kpR_m^2}{4E}.$$

Then, the bending stiffness of bellows is,

$$EI_{eq} = \frac{1}{4} kpR_m^2. \tag{3.1}$$

This is the easiest way for obtaining the bending stiffness of a bellows if the axial bellows spring rate per one half convolution, k, is known in advance. The accuracy of this method depends completely on the accuracy of the available axial spring rate value, k. As was mentioned in Chapter 2, the various explicit formulas available in the literature for calculation of the axial stiffness of a bellows give scattered and therefore not very reliable results. For this reason, the following three sections of this chapter are devoted to calculation of the axial stiffness of a bellows using Finite Element Analysis.

3.2. Bellows as a Shell of Revolution

The wall thickness of a bellows in comparison with its other dimensions is usually a very small quantity. Therefore, a thin shell theory can be applied to describe the stiffness of bellows. It was found that, for the bellows under consideration, it was appropriate to use the two node axisymmetric constant meridional curvature shell element (ACMC), given by Ross (1983), reduced to the straight conical one.

The element has three degrees of freedom per nodal circle (u, w, and θ), making a total of six degrees of freedom per element, as shown in Fig. 3.1. The elemental stiffness matrix in local coordinates is

$$[k_i] = 2\pi \int_{-1}^{1} [B]^T [D][B] r l \, d\xi \, , \tag{3.2}$$

where

$$l = \frac{1}{2} \sqrt{(R_2 - R_1)^2 + (Z_2 - Z_1)^2} \, ,$$

$$r = \frac{R_2 + R_1}{2} + \frac{R_2 - R_1}{2} \, ,$$

$$[D] = \frac{Et}{(1-\nu^2)} \begin{bmatrix} 1 & \nu & 0 & 0 \\ \nu & 1 & 0 & 0 \\ 0 & 0 & t^2/12 & \nu t^2/12 \\ 0 & 0 & \nu t^2/12 & t^2/12 \end{bmatrix} ,$$

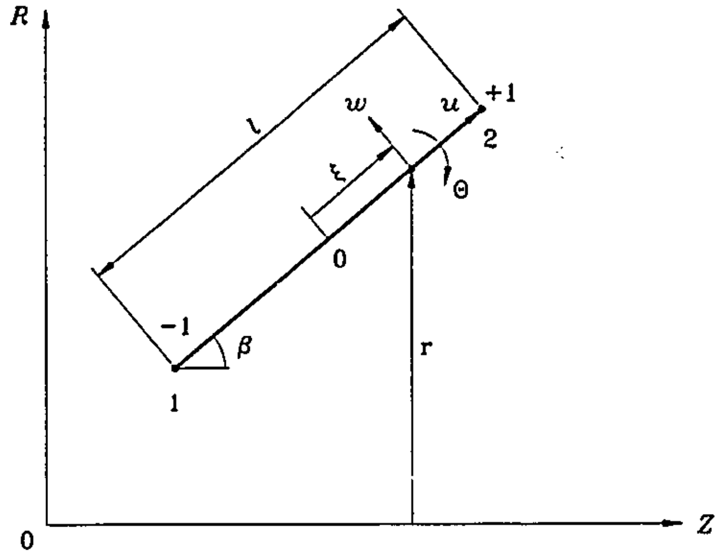

Fig.3.1. Two node 6 DOF axisymmetric element

$$
[B] = \left[\begin{array}{c:c:c:c:c:c}
\dfrac{-1}{l} & 0 & 0 & \dfrac{1}{l} & 0 & 0 \\
\hdashline
\dfrac{(1-\xi)\sin\beta}{2r} & \dfrac{(\xi^3-3\xi+2)\cos\beta}{4r} & \dfrac{(1+\xi)(1-\xi)^2 l\cos\beta}{8r} & \dfrac{(1+\xi)\sin\beta}{2r} & \dfrac{(-\xi^3+3\xi+2)\cos\beta}{4r} & \dfrac{(-1-\xi)(1+\xi)^2 l\cos\beta}{8r} \\
\hdashline
0 & \dfrac{-6\xi}{l^2} & \dfrac{-(3\xi-1)}{l} & 0 & \dfrac{6\xi}{l^2} & \dfrac{-(3\xi+1)}{l} \\
\hdashline
0 & \dfrac{-3(\xi^2-1)\sin\beta}{2rl} & \dfrac{(-1-2\xi+3\xi^2)\sin\beta}{4r} & 0 & \dfrac{-3(-\xi^2+1)\sin\beta}{2rl} & \dfrac{(1-2\xi-3\xi^3)\sin\beta}{4r}
\end{array} \right],
$$

$$\sin\beta = \frac{1}{l}(R_2 - R_1),$$
$$\cos\beta = \frac{1}{l}(Z_2 - Z_1),$$

$$[N] = \left[\begin{array}{c:c:c:c:c:c} \frac{1-\xi}{2} & 0 & 0 & \frac{1-\xi}{2} & 0 & 0 \\ \hdashline 0 & \frac{\xi^3 - 3\xi + 2}{4} & \frac{(1+\xi)(1-\xi)^2 l}{8} & 0 & \frac{-\xi^3 + 3\xi + 2}{4} & \frac{-(1-\xi)(1+\xi)^2 l}{8} \end{array}\right],$$

ξ is the normalised local coordinate,

t is the thickness of the shell,

ν is Poisson's ratio,

E is Young's modulus,

R, Z are nodal coordinates.

The elemental stiffness matrix in global coordinates is

$$\left[k_i^0\right] = [DC]^T [k_i][DC], \tag{3.3}$$

where,

$$[DC] = \left[\begin{array}{c:c} \varsigma & 0_3 \\ \hdashline 0_3 & \xi \end{array}\right],$$

$$\varsigma = \left[\begin{array}{c:c:c} C & S & 0 \\ \hdashline -S & C & 0 \\ \hdashline 0 & 0 & 1 \end{array}\right],$$

$C = \cos\beta, \qquad S = \sin\beta$.

The integration was carried out using four Gauss points. The half-convolution calculation domain is shown in Fig.3.2.

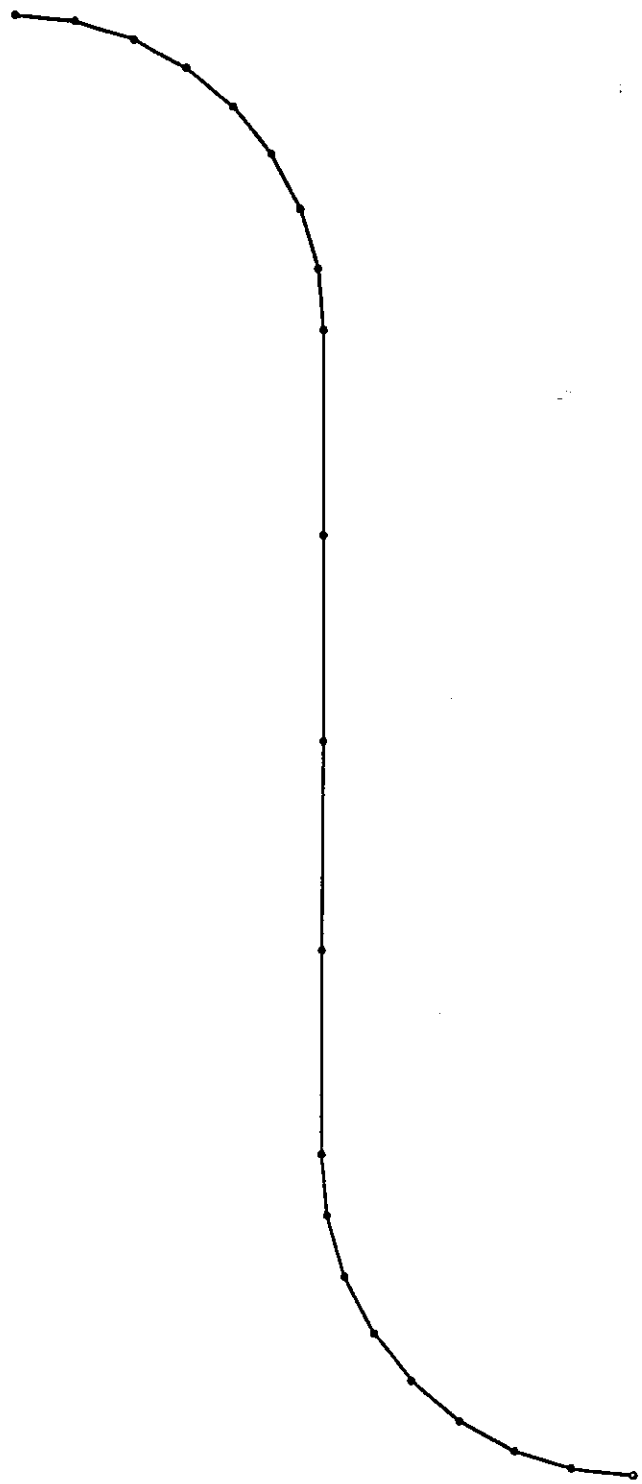

Fig.3.2. Half-convolution domain for shell element

3.3. Bellows as a Solid of Revolution

A bellows can be considered as a solid of revolution. Provided a load is axisymmetric as well, the circumferential displacement of a bellows becomes equal to zero and only a radial cross-section needs to be analyzed, subdivided into some typical elements. The cylindrical coordinate system is the most convenient, and when it is used, the element stiffness matrix, according to Smith and Griffiths (1988), is

$$[k_i] = \iiint_V [B]^T [D][B]\, r\, dr\, d\theta\, dz\,,$$

which, integrated over the entire circumferential length, becomes

$$[k] = 2\pi \iint_S [B]^T [D][B]\, r\, dr\, dz\,, \tag{3.4}$$

where

r, z are the axisymmetric coordinates,

$[B]$ is the matrix,

$[D]$ is the material property matrix,

S is the area of the finite element.

Since the radial cross-section domain of a bellows has curved boundaries, it is convenient to use a solid isoparametric element to describe this elasticity problem. The most suitable as a parent element for the bellows domain with curved bundaries is the eight-noded square element shown in Fig.3.3a, which can be mapped to the curved isoparametric one, Fig.3.3b, by means of the shape functions, N_i, of the parent element,

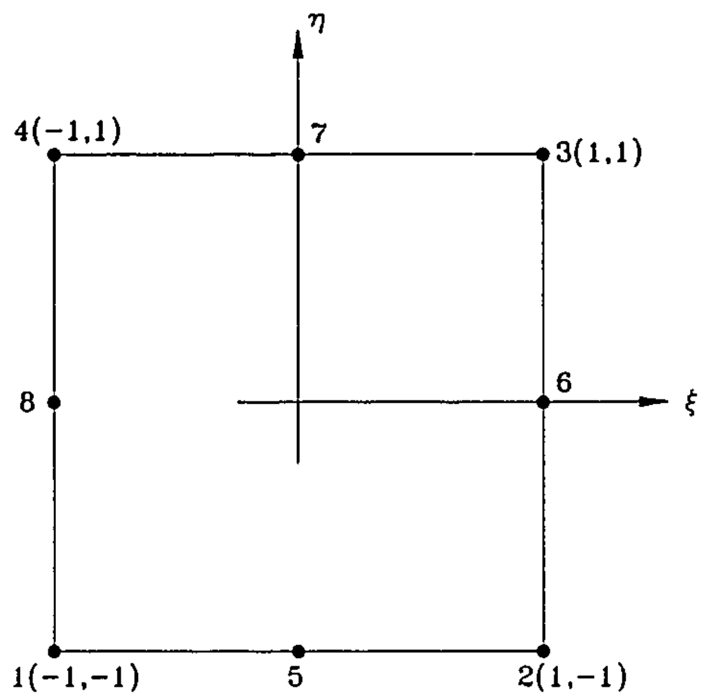

a) parent element

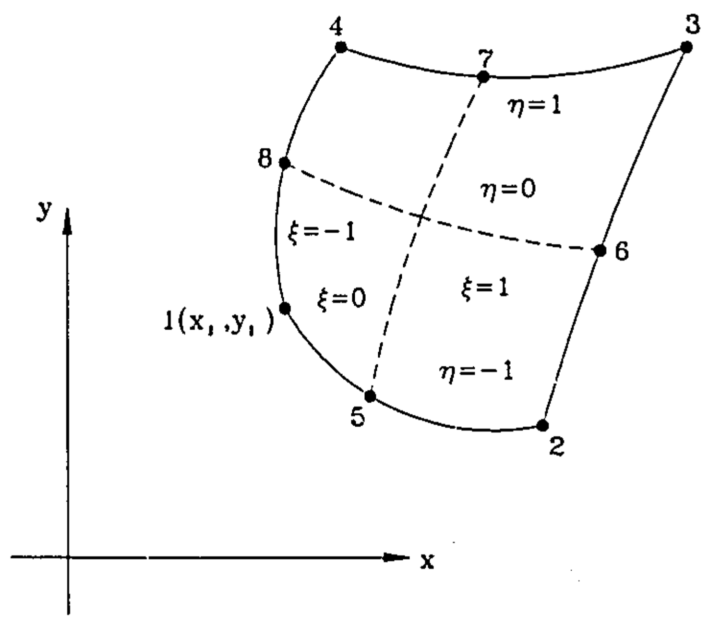

b) isoparametric element

Fig.3.3. 8-noded parent and isoparametric elements

$$r = \sum_{i=1}^{8} N_i r_i = \{N\}^T \{r\} \ ,$$
$$z = \sum_{i=1}^{8} N_i z_i = \{N\}^T \{z\} \ .$$

Here

$$\{N\}^T = \langle N_1, N_2, \ldots, N_8 \rangle ,$$
$$\{r\}^T = \langle r_1, r_2, \ldots, r_8 \rangle ,$$
$$\{z\}^T = \langle z_1, z_2, \ldots, z_8 \rangle ,$$

where, according to Tong and Rossetos (1977), for an element with C_0 continuity shown in Fig.3.3a,

$$N_i = \frac{1}{4}(1+\xi\xi_i)(1+\varsigma\varsigma_i)(\xi\xi_i+\varsigma\varsigma_i-1) , \qquad i = 1, 2, 3, 4 ,$$
$$N_i = \frac{1}{2}(1-\xi^2)(1+\varsigma\varsigma_i) , \qquad i = 5, 7 ,$$
$$N_i = \frac{1}{2}(1-\varsigma^2)(1+\xi\xi_i) , \qquad i = 6, 8 .$$

The displacements are approximated by

$$u = \sum_{i=1}^{8} N_i \, u_i \ ,$$

$$v = \sum_{i=1}^{8} N_i \, u_i \ ,$$

or

$$\begin{Bmatrix} u \\ v \end{Bmatrix} = [N] \{\delta\} \ , \tag{3.5}$$

where

$$[N]=\begin{bmatrix} N_1 & 0 & N_2 & 0 & N_3 & 0 & N_4 & 0 & N_5 & 0 & N_6 & 0 & N_7 & 0 & N_8 & 0 \\ 0 & N_1 & 0 & N_2 & 0 & N_3 & 0 & N_4 & 0 & N_5 & 0 & N_6 & 0 & N_7 & 0 & N_8 \end{bmatrix}.$$

According to Smith and Griffiths (1988), the strain-displacement relations for the axisymmetric case are:

$$\{\varepsilon\}=[L]\begin{Bmatrix} u \\ v \end{Bmatrix}, \tag{3.6}$$

where

$$[L]=\begin{bmatrix} \frac{\partial}{\partial r} & 0 \\ 0 & \frac{\partial}{\partial z} \\ \frac{\partial}{\partial z} & \frac{\partial}{\partial r} \\ \frac{1}{r} & 0 \end{bmatrix},$$

$$\{\varepsilon\} = \langle \varepsilon_r \; \varepsilon_z \; \varepsilon_{rz} \; \varepsilon_\theta \rangle .$$

Substitution of (3.5) into (3.6) gives

$$\{\varepsilon\}=[B]\{\delta\},$$

where

$$[B]=[L][N],$$

or

$$[B]=\begin{bmatrix} \frac{\partial N_1}{\partial r} & 0 & \frac{\partial N_2}{\partial r} & 0 & \cdots & \frac{\partial N_8}{\partial r} & 0 \\ 0 & \frac{\partial N_1}{\partial z} & 0 & \frac{\partial N_2}{\partial z} & \cdots & 0 & \frac{\partial N_8}{\partial z} \\ \frac{\partial N_1}{\partial z} & \frac{\partial N_1}{\partial r} & \frac{\partial N_2}{\partial z} & \frac{\partial N_2}{\partial r} & \cdots & \frac{\partial N_8}{\partial z} & \frac{\partial N_8}{\partial r} \\ \frac{N_1}{r} & 0 & \frac{N_2}{r} & 0 & \cdots & \frac{N_8}{r} & 0 \end{bmatrix}. \tag{3.7}$$

The derivatives of N_i with respect to r, z and ξ, ζ, needed in element matrix calculations, are related by

$$\begin{bmatrix} \dfrac{\partial N_i}{\partial r} \\ \dfrac{\partial N_i}{\partial z} \end{bmatrix} = [J]^{-1} \begin{bmatrix} \dfrac{\partial N_i}{\partial \xi} \\ \dfrac{\partial N_i}{\partial \varsigma} \end{bmatrix},$$

where $[J]$ is the so called Jacobian matrix:

$$[J] = \begin{bmatrix} \dfrac{\partial r}{\partial \xi} & \dfrac{\partial z}{\partial \xi} \\ \dfrac{\partial r}{\partial \varsigma} & \dfrac{\partial z}{\partial \varsigma} \end{bmatrix}.$$

Taking the inverted Jacobian matrix as

$$[J]^{-1} = \begin{bmatrix} I_{11} & I_{12} \\ I_{21} & I_{22} \end{bmatrix},$$

the matrix $[B]$, given by (3.7), can be rewritten as follows:

$$[B]=\begin{bmatrix} I_{11}N_{1}, \quad +I_{12}N_{1}, & 0 & \cdots & 0 \\ 0 & I_{21}N_{1}, \quad +I_{22}N_{1}, & \cdots & I_{21}N_{8}, \quad +I_{22}N_{8}, \\ I_{21}N_{1}, \quad +I_{22}N_{1}, & I_{11}N_{1}, \quad +I_{12}N_{1}, & \cdots & I_{11}N_{8}, \quad +I_{12}N_{8}, \\ \dfrac{N_1}{r} & 0 & \cdots & 0 \end{bmatrix}, \quad (3.8)$$

where

$$N_i = \frac{\partial N_i}{\partial \xi},$$

$$N_i = \frac{\partial N_i}{\partial \varsigma},$$

The differential area element required for stiffness matrix calculations can be given as follows:

$$dr\, dz = \det[J]\, d\xi\, d\varsigma. \quad (3.9)$$

As shown by Tong and Rossetos (1977), the material property matrix for the axi-symmetric case is:

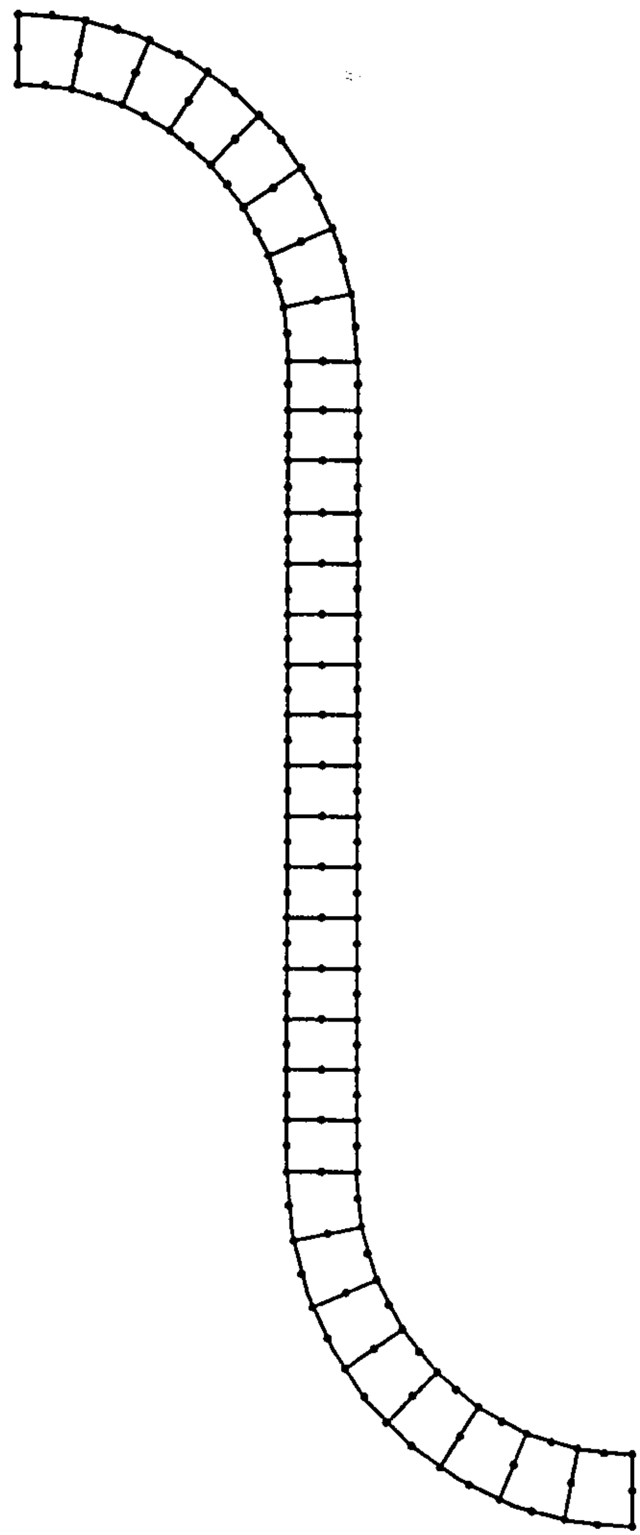

Fig.3.4. Half-convolution domain for solid element

$$[D]=\frac{E}{(1+\nu)(1-2\nu)}\begin{bmatrix} 1-\nu & \nu & 0 & \nu \\ \nu & 1-\nu & 0 & \nu \\ 0 & 0 & \frac{1-2\nu}{2} & 0 \\ \nu & \nu & 0 & 1-\nu \end{bmatrix}. \tag{3.10}$$

Substitution of (3.8), (3.9), and (3.10) into (3.4) gives the stiffness matrix for any axisymmetric element in the domain. Now the elemental stiffness expression can be programmed into some basic finite element program. The mesh of the half-convolution domain is shown in Fig.3.4.

3.4. Peculiarities and Comparison of Results for Calculation of Axial Stiffness of Bellows

Preliminary calculations showed that the longitudinal stiffness of bellows varies from one half-convolution to another, as shown in Table 3.1, where the first half-convolution is at the fixed end, and the sixth one is in the middle of the bellows. In this table, the axial spring rate for one half-convolution, k , was calculated for the bellows expansion joint with the following geometrical and physical parameters: number of convolutions, $N=6$, mean radius of bellows, $R_m=0.0844$ m, convolution radii, $R_1=0.003082$ m, $R_2=0.002682$ m, convolution height, $h=0.01575$ m, wall thickness, $t=0.0006$ m, Young's modulus, $E=2.0\times 10^{11}$ N/m^2, and Poisson's ratio, $\nu=0.3$. As seen from the table 3.1, the boundary half-convolution is the stiffest due to its fixed end.

Table 3.1. Distribution of stiffness in bellows

Number of half-convolutions	1	2	3	4	5	6
k (N/m)	4016064	3472222	3628447	3645643	3657644	3679175

The stiffness of the next-to-boundary half-convolution abruptly drops, then remains approximately constant to the middle of the bellows. Therefore, instead of calculating the stiffness for the expansion joint as a unit by creating a large input data file, it is sufficient to calculate the stiffness of two types of half-convolutions, one boundary and one inner half-convolution taken separately.

The mesh for one half-convolution as a shell of revolution is shown in Fig.3.2. Since conical elements were used in this case, significantly more elements were used in such areas, for a good geometrical approximation of the curved portions of the half-convolution. The boundary conditions for a boundary half-convolution are:

a) At the fixed end, both the axial and radial displacements, as well as the rotation, are set equal to zero.

b) At the other end, just the rotation is suppressed.

The boundary conditions for any inner half-convolution are:

a) At one end, the axial displacement and rotation are set equal to zero.

b) At the other end, just the rotation is suppressed.

A 1N axial force was used as a load applied at the free end of the half-convolution. Then the calculated axial displacement of the point of application of force, Δl, and the value of the force, F, were used to calculate the axial spring rate of the one half-convolution as follows:

$$k = \frac{F}{\Delta l} .$$

Then, in consideration of the bellows as a series of half-convolutions, the spring rate of the whole expansion joint can be calculated from the well known relationship

$$\frac{1}{k_{tot}} = \frac{2}{k_0} + \frac{n}{k_1} ,$$

where

k_{tot} is the total spring rate of the expansion joint,

k_0 is the spring rate of the boundary half-convolution,

k_I is the spring rate of the inner half-convolution,

n is the total number of inner half-convolutions.

Now the mean stiffness of one half-convolution is

$$k = \frac{k_{tot}}{2+n} \, .$$

In the case of relatively short bellows, when the number of convolutions is less than, say, 6, it is more convenient to calculate the spring rate for one half of the bellows, $k_{1/2}$,at once. Then, the total spring rate of the bellows,

$$k_{tot} = \frac{k_{1/2}}{2} \, .$$

The boundary conditions at both ends in this case stay the same as for the boundary half-convolution described above.

The mesh for one half-convolution as a solid of revolution is shown in Fig.3.4. The boundary conditions for boundary half-convolutions are:

a) At the fixed end nodes both axial and radial displacements are set equal to zero.

b) At the opposite end nodes just radial displacements are suppressed.

For any inner half-convolution, just axial displacements at the one of the end nodes have to be suppressed.

To draw some conclusions about the accuracy of the calculations of the bellows axial spring rate using different methods, the axial spring rate was calculated for the expansion joint with the following parameters: number of convolutions, N = 9, mean radius of bellows, R_m = 0.03465 m, bellows pich, p = 0.005 m, convolution depth, h = 0.0571 m, wall thickness, t = 0.00028 m, elastic modulus, $E = 2.07 \times 10^{11}$ N/m^2, and Poisson's ratio, $\nu = 0.3$. The results of the calculation are shown in Table 3.2. As seen from the table, both FEA methods give very close results. The result obtained from Gerlach's formula (2.2) in comparison with FEA is underestimated by about 8.5% The result obtained from EJMA formula (2.1) is overestimated by about 18%. The results of Haringx's and Andreeva's formulas, (2.4) and (2.3), are considerably overestimated (58%). Therefore, this author recommends use of the FEA for more precise calculations of the axial spring rate of bellows.

Table 3.2. Comparison of the calculation results of the axial stiffness of the expansion joint using different methods

	Gerlach f. (2.2)	FEA Shell	FEA Solid	EJMA St f. (2.1)	Haringx f. (2.4)	Andreeva f. (2.3)
k_{tot} (N/m)	188000	205384	206129	241931	325424	325721

3.5. Bellows Mass

The bellows mass per unit length is calculated taking into account the corrugated geometry of the bellows, Fig.2.1,

$$m_b = \frac{\pi R_m(\pi R_1 + \pi R_2 + 2L)}{R_1 + R_2} t\rho_b .$$

Here R_1 , R_2 , R_m , and L are geometrical parameters, explained in Section 2.1, Fig.2.1. The bellows mass per unit length expressed in terms of bellows pitch, p, convolution depth, h, and convolution thickness, t, becomes,

$$m_b = \frac{4\pi R_m}{p}(h + 0.285p)\, t\rho_b . \tag{3.12}$$

3.6. Additional Fluid Mass of Bellows

When the beam concept is being used for the solution of the bellows transverse vibration problem, it is necessary to know the added mass per unit length, m_f. If the bellows is filled with fluid, m_f becomes a complex quantity and can be considered as consisting of the following parts:

$$m_f = m_{f1} + m_{f2}\ , \tag{3.13}$$

where

- m_{f1} is the added fluid mass per unit length of bellows which appears as a result of transverse motion of fluid in bellows,
- m_{f2} is the equivalent added mass of fluid per unit length of bellows which appears as a consequence of convolution distortion during bending vibration. It is practically equal to zero in the case of a smooth pipe.

The additional mass, m_{f1}, is uniform if the geometry of the bellows is uniform along the whole axial length. It is equal to the amount of fluid contained in one unit of the bellows length:

$$m_{f1} = \pi R_m'^2 \rho_f\ , \tag{3.14}$$

where R_m' can be expressed through other geometrical parameters of the bellows as follows (see Fig.2.1):

$$R_m' = R_m - \frac{h}{2} + \frac{2hR_2}{p}\ .$$

However, the additional mass, m_{f2}, being dependent on deformation of the convolution, is not uniform despite a uniform geometry of the bellows. It is proportional to the absolute value of the curvature of the bellows axis during the bending deformation and, as usual, mass, $m_{f2}(x)$ is always positive, as shown in Fig.3.5, line 1. Therefore, the final expression for the total added mass of the bellows should be noted as follows:

$$m_f = m_{f1} + m_{f2}(x)\,. \tag{3.15}$$

Therefore, the differential equation for bending of a bellows

$$EI\frac{\partial^4 w}{\partial x^2} + \left[m_b + m_{f1} + m_{f2}(x)\right]\frac{\partial^2 w}{\partial t^2} = 0\,,$$

becomes nonlinear, because the coefficient of the time derivative depends on the coordinate x. Since the added mass $m_{f2}(x)$ is always a positive function, this bending differential equation can be linearized using the mean value of the $m_{f2}(x)$, m_{f2k} (see Fig. 3.5, line 2). Then the expression (3.15) becomes constant with respect to x:

$$m_f = m_{f1} + m_{f2k} \tag{3.16}$$

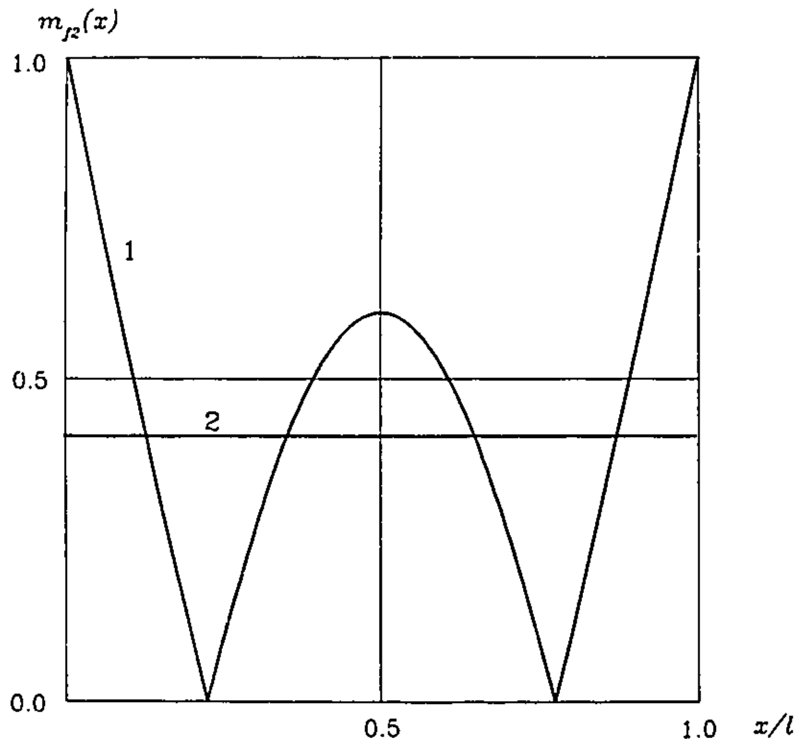

Fig.3.5. Distribution of added mass, $m_{f2}(x)$,
over the length of fixed-fixed bellows (first mode).

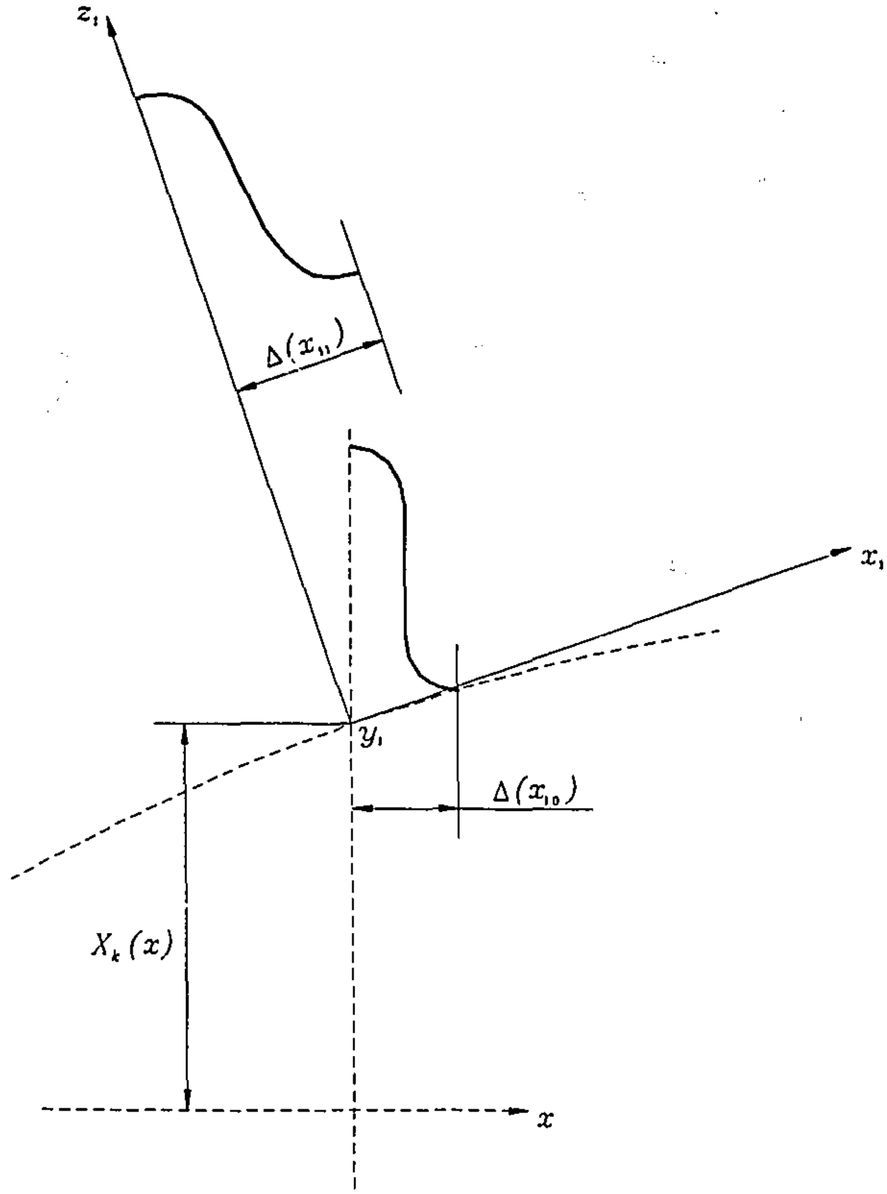

Fig.3.6. Initial and deformed shapes of bellows convolution

where m_{f2k} depends just on the mode number, k, and can be found from the equality of kinetic energies of the added masses as follows.

Let the relative bellows-fluid interface displacement with respect to x_1, y_1, z_1 be

$$U = \delta_i \; U_{norm1}(x_1, y_1, z_1)\, T(t)\,, \tag{3.17}$$

where,

δ_i is the axial deformation of the ith half-convolution at the convolution root, which can be found as $\delta_i = \Delta(x_{i1}) - \Delta(x_{i0})$, as shown in Fig. 3.6,

U_{norm1} is normalized to unity displacement of the convolution surface,

$T(t)$ is the time dependent function.

Now we will determine the relationship between $\delta_i(x)$ and the mode function of the bellows axis, $X_k(x)$. For a beam, the bending moment, M, at any cross-section is related to its stiffness, EI, according to

$$M = EI\,X_k''(x)\,. \tag{3.18}$$

The stress at any cross-section point is

$$\sigma = \frac{M}{I} z_1\,, \tag{3.19}$$

where z_1 is the distance of the point of interest from the neutral plane of the beam. According to the Hooke's law,

$$\sigma = E\varepsilon\,, \tag{3.20}$$

where ε is the strain. On the basis of the convolution half-pitch, $p/2$,

$$\varepsilon_i = \frac{2\delta_i}{p}\,.$$

Substitution of (3.18) into (3.19), then (3.19) into (3.20) and (3.20) into the ε_i expression above finally gives the convolution root elongation (or contraction) as a function of the second derivative of the mode function, $X_k''(x)$:

$$\delta_i = z_1 \frac{p}{2} X_k''(x_i)\,.$$

For the convolution root (see Fig.2.1),

$$z_1 = R_m - \frac{h}{2},$$

therefore, the expression for δ_i can be rewritten as

$$\delta_i = X_k''(x_i)\left(R_m - \frac{h}{2}\right)\frac{p}{2}.$$

This is the relationship between the ith convolution root half-pitch elongation, δ_i, and the bellows axis deflection, $X_k(x)$, at the particular cross-section of bellows. Substitution into (3.17) gives

$$U = X_k''(x_i)\left(R_m - \frac{h}{2}\right)\frac{p}{2}U_{norm1}(x_1, y_1, z_1)\,T(t). \tag{3.21}$$

This is the relationship between the bellows surface relative displacement, U, and the mode function, $X_k(x)$.

Let the one half-convolution added mass caused by convolution distortion be λ. Then, the kinetic energy of the excited cross fluid flow in one half-convolution space is:

$$W_{1/2} = \iint_S \frac{\lambda \dot{U}^2}{2S}\,dS.$$

Using (3.21), the above kinetic energy expression can be rewritten as follows:

$$W_{1/2} = \frac{\lambda \dot{T}^2(t)}{2S} X_k''^2(x_i)\left(R_m - \frac{h}{2}\right)^2 \frac{p^2}{4} \iint_S U_{norm1}^2(x_1, y_1, z_1)\,dS.$$

The total bellows kinetic energy becomes

$$W = \frac{\lambda \dot{T}^2(t)}{4}\left(R_m - \frac{h}{2}\right)^2 p \frac{1}{S} \iint_S U_{norm1}^2(x_1, y_1, z_1)\, dS \sum_1^{2N} X_k''^2(x_i) \frac{p}{2},$$

where N is the number of convolutions in the bellows.

According to the definition of the bounded integral, the sum residing in the above expression for the kinetic energy can be approximated as,

$$\sum_1^{2N} X_k''^2(x_i) \frac{p}{2} \cong \int_0^l X_k''^2(x)\, dx.$$

The calculations conducted within a practical range of bellows geometrical parameters (see Fig.2.1), $h = (0.19 \pm 0.04)\, R_m$ and $R_2 = (0.0316 \pm 0.0055)\, R_m + t/2$, showed that the ratio,

$$\frac{\iint_S U_{norm1}^2(x_1, y_1, z_1)\, dS}{S},$$

residing in expression for W above is nearly constant, varying between 0.1313-0.1327. This occurred because the loaded large mean radius bellows half-convolution behaves more like a fixed-fixed beam than a ring with fixed-fixed perimeters. For a real fixed-fixed beam, this ratio, regardless of the length of a beam, is constant. Therefore, for this comparatively narrow range of parameters h and R_2, the ratio was considered constant and equal to 0.132. Then the kinetic energy expression, W, becomes:

$$W = 0.132 \frac{\lambda \dot{T}^2(t)}{4}\left(R_m - \frac{h}{2}\right)^2 p \int_0^l X_k''^2(x)\, dx. \tag{3.22}$$

On the other hand, the total kinetic energy caused by convolution distortion is,

$$W = \int_0^l \frac{m_{f2k}\dot{w}_k^2}{2}\,dx.$$

If

$$w_k = X_k(x)\,T(t),$$

the kinetic energy expression above becomes

$$W = \frac{m_{f2k}}{2}\,\dot{T}^2(t)\int_0^l X_k^2(x)\,dx, \tag{3.23}$$

Equating equations (3.22) and (3.23) gives the uniform added mass along the axis of the bellows,

$$m_{f2k} = 0.066\frac{\int_0^l \left(\frac{d^2X_k}{dx^2}\right)^2 dx}{\int_0^l X_k^2(x)\,dx}\left(R_m - \frac{h}{2}\right)^2 p\lambda\,, \tag{3.24}$$

or

$$m_{f2k} = \alpha_{f2k}\,\lambda\,, \tag{3.25}$$

where,

$$\alpha_{f2k} = 0.066\frac{\int_0^l \left(\frac{d^2X_k}{dx^2}\right)^2 dx}{\int_0^l X_k^2(x)\,dx}\left(R_m - \frac{h}{2}\right)^2 p. \tag{3.26}$$

As seen from expression (3.24), the final calculations for m_{2fk} can be performed having the mode function expression and the added mass for one half-convolution, λ , only. The added mass, λ , can be calculated having solved the velocity-potential of the relative cross-flow caused by convolution deformation during the bending of the bellows.

Therefore, the following section is devoted to solution of the velocity-potential caused by this cross-flow inside of a convolution.

3.7. FE Formulation of Laplace Equation in 3D Domain with Mixed Boundary Conditions

It is not difficult to imagine that the volume of every convolution (Fig.3.7, volume between planes, p_1 and p_2) during the bending of the bellows remains constant since the volume increments above and bellow the neutral plane, p_3 , are equal and have opposite signs. Therefore, despite the nonuniform bending deformation of the bellows along its axis (as was shown in the previous section, proportional to $X_k''(x)$), this crossflow can be assumed to be locked inside of one convolution space. Therefore, the planes p_1 and p_2 can be modelled by imaginary impenetrable surfaces with boundary conditions,

$$\left.\frac{\partial \Phi_0}{\partial n}\right|_{p_1, p_2} = 0.$$

Considering the boundary condition at the convolution surface, let the convolution-fluid interface displacement normalized to unity be

$$U_{norm1} = U_{norm1}(x,y,z)\ T(t). \tag{3.27}$$

(Here and in later sections of this chapter, for simplicity, the indices will be dropped and the notation x, y, z instead of x_1, y_1, z_1 and U instead of U_{norm1} will be used). Let us examine the components of U, U_x, U_y, and U_z. It was shown by Jakubauskas (1991) that in the case of axial deformation of the bellows, the axial displacements are considerably larger than the radial ones. A similar relationship holds in the case of the bending deformation of the bellows as well, if the neutral plane is the x, y plane (see Fig.3.7).Here $|U_y| \ll |U_x|$ and $|U_z| \ll |U_x|$. Therefore, in further considerations of the boundary condition on the convolution surface, just U_x will be taken into account and U_z and U_y will be neglected. In general, the displacement U_x can be obtained by solving the bending eigenvalue problem for a fixed-fixed bellows. Since it is a tridimensional shell problem, it becomes very time consuming for both the designer and the computer. It is not difficult to understand that a single convolution wall is much stiffer than the whole bellows in the axial or transverse directions. Therefore, the convolution wall during the bellows vibration is almost under kinematic excitation, and for this reason its dynamic displacement field is very close to the static bellows bending displacement field. Furthermore, the static convolution wall bending displacement field can be approximated from the static axial displacement field using the relationship

$$U_x = U_{xst}\, z$$

where,

z is the distance of the point of the convolution under consideration from the neutral plane x, y, Fig.3.7,

U_{xst} is the axisymmetric static displacement field of a convolution wall.

Then the normal part of U can be written as

$$U_n = U_{xst}\,(x,y,z)\; z\; T(t).$$

The boundary condition for the fluid domain on the vibrating boundary becomes

$$\left.\frac{\partial \Phi}{\partial n}\right|_S = -\frac{\partial U_n}{\partial t} = -\,U_{xst}(x,y,z)\; z\; \dot{T}(t), \tag{3.28}$$

since the tangential part, U_τ, in the case of the ideal fluid doesn't affect the flow at all. It was shown by Sheinin (1967), provided the solution of the structural motion is (3.27), that the velocity potential function of the excited flow may be written as

$$\Phi = \Phi_0(x,y,z)\, \dot{T}(t), \tag{3.29}$$

where

Φ_0 is the amplitude of the velocity potential,

$T(t)$ is the time harmonic function.

Now the boundary condition at the convolution surface can be obtained by substitution of (3.29) into (3.28),

$$\left.\frac{\partial \Phi_0}{\partial n}\right|_S = -U_{xst}(x,y,z)\,z\,. \tag{3.30}$$

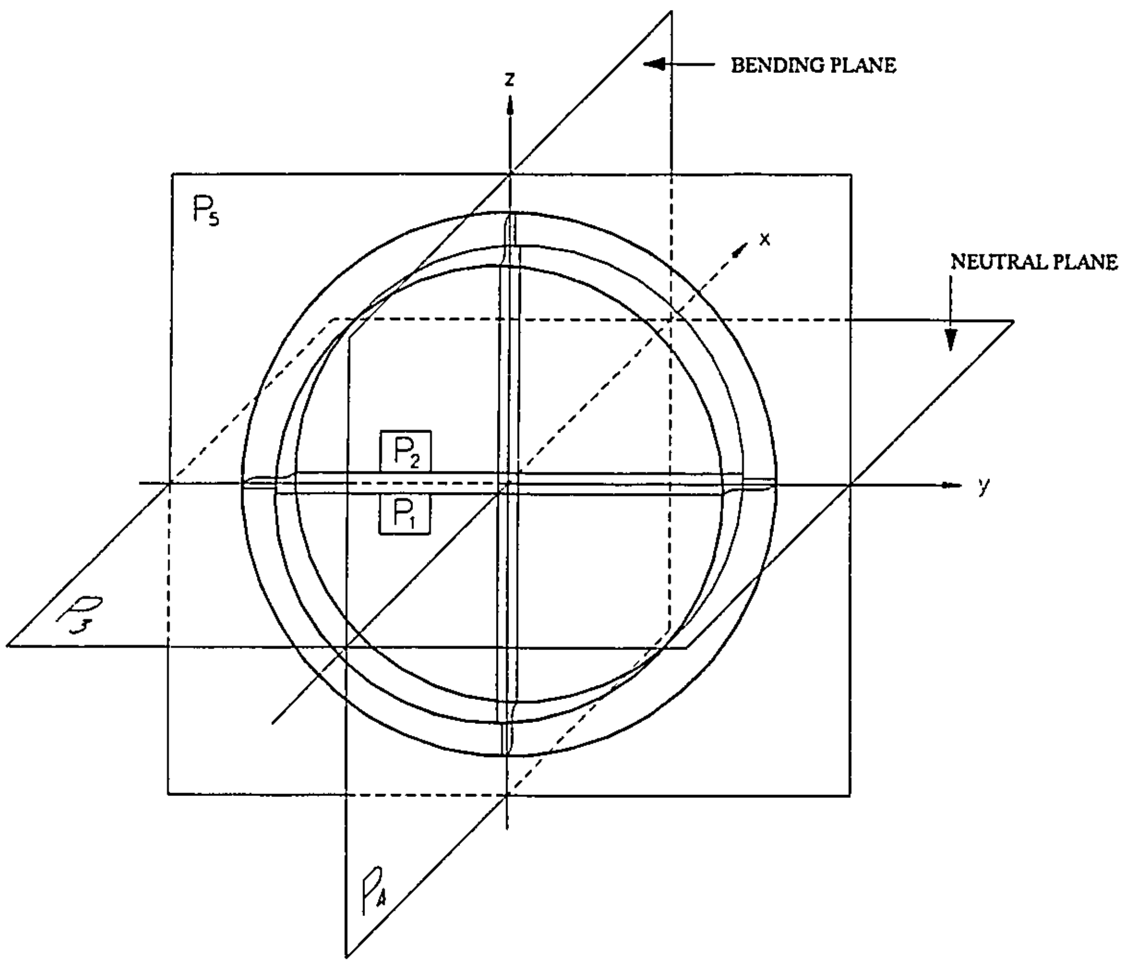

Fig.3.7. Division of the convolution by planes of symmetry

The areas of fluid above and below the plane, p_3 , are geometrically symmetrical with respect to this plane. In addition, the absolute values of the boundary condition (3.30) at the corresponding locations with respect to the same plane, p_3, are equal but have opposite signs. These facts lead to the conclusion that the excited crossflow has mirror image symmetry with respect to the plane, p_3, and therefore, the velocity potential on p_3 is equal to zero, $\Phi_0 = 0$.

Since a convolution deforms symmetrically with respect to the plane, p_4 , the boundary condition (3.30) is symmetric with respect to this plane. Therefore, the excited crossflow is symmetric with respect to this plane and cannot be crossed by the flow. For this reason the boundary condition on the plane, p_4, is known,

$$\left.\frac{\partial \Phi_0}{\partial n}\right|_{p_4} = 0.$$

Furthermore, the figure plane is the plane of symmetry of the crossflow, too, because of the symmetry of the boundary condition (3.30) with respect to the figure plane, p_5. Therefore, as explained above, the velocity potential boundary condition on this plane is,

$$\left.\frac{\partial \Phi_0}{\partial n}\right|_{p_5} = 0.$$

As seen from Fig.3.7, the three mutually orthogonal planes, p_3, p_4, and p_5 divide the whole space of the convolution into eight equal parts with identical boundary conditions. Therefore, the above mentioned velocity potential problem can be solved using just 1/8 part of the whole convolution with appropriate boundary conditions, as shown in Fig.3.8.

The fluid flow, excited by the convolution motion (and considered to be perfect and incompressible) can be described by the tridimensional Laplace equation,

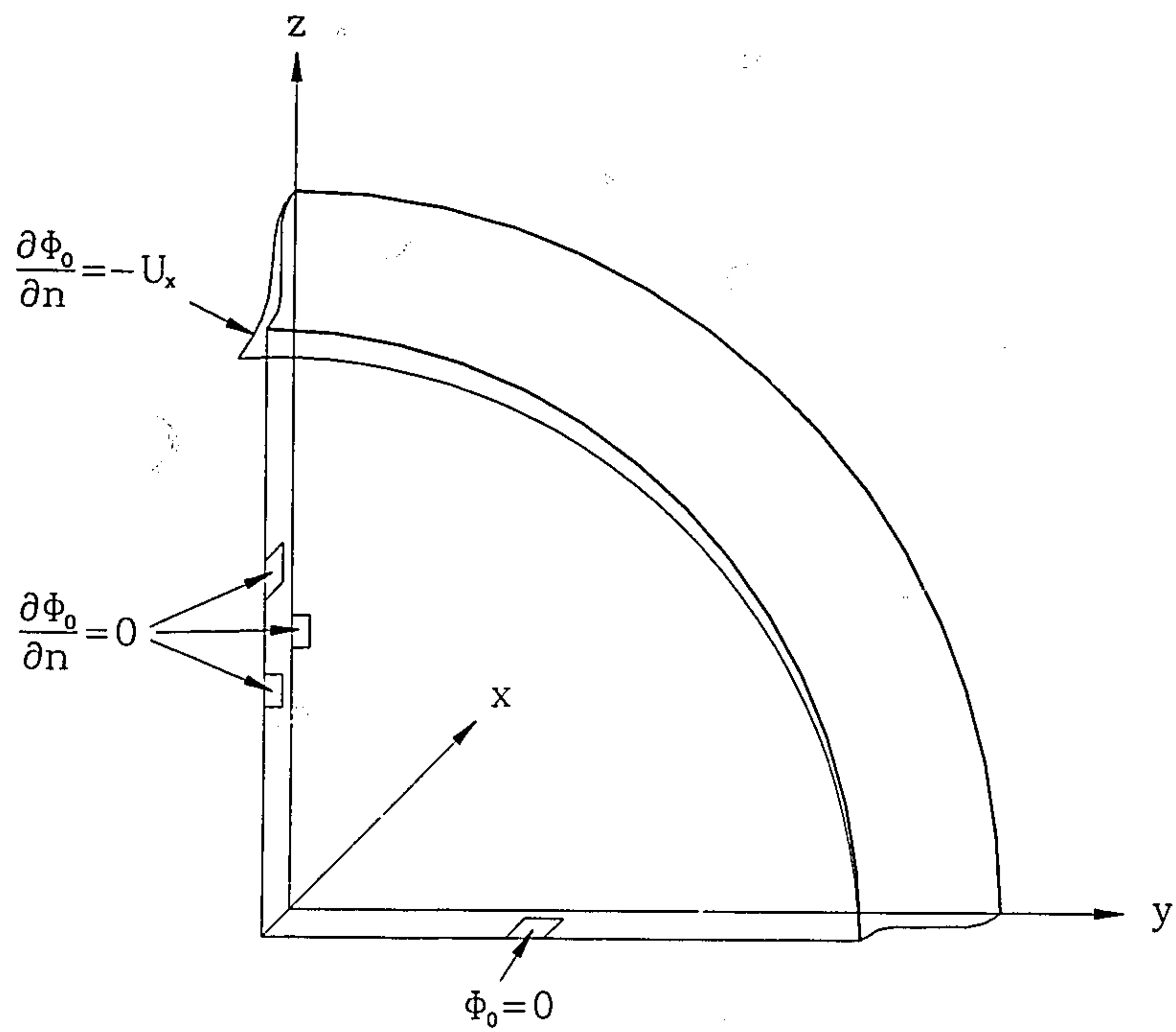

Fig.3.8. The solution domain with boundary conditions

$$\frac{\partial^2 \Phi_0}{\partial x^2} + \frac{\partial^2 \Phi_0}{\partial y^2} + \frac{\partial^2 \Phi_0}{\partial z^2} = 0. \tag{3.31}$$

The variational principle for equations (3.30) and (3.31) is given by

$$J(\Phi_0) = \int_V \frac{1}{2} \left[\left(\frac{\partial \Phi_0}{\partial x} \right)^2 + \left(\frac{\partial \Phi_0}{\partial y} \right)^2 + \left(\frac{\partial \Phi_0}{\partial z} \right)^2 \right] dV - \int_S U_n \Phi_0 \, dS. \tag{3.32}$$

Assume finite element approximation for Φ_0 as

$$\Phi_0 = \sum_{i=1}^{n} N_i \Phi_{0i} = \{N\}^T \{\Phi_0\}^T = \{\Phi_0\}^T \{N\}, \tag{3.33}$$

where

N_i are the shape functions,

Φ_0 are the nodal values of Φ_0,

n is the number of nodes (and DOF) per element.

Substitution of eq.(3.33) into (3.32) yields

$$J_e(\Phi_{0i}^e) = \int_V \frac{1}{2} \{\Phi_0^e\}^T \left[\frac{\partial\{N\}^T}{\partial x} \frac{\partial\{N\}}{\partial x} + \frac{\partial\{N\}^T}{\partial y} \frac{\partial\{N\}}{\partial y} + \frac{\partial\{N\}^T}{\partial z} \frac{\partial\{N\}}{\partial z} \right] \{\Phi_0^e\} \, dV$$

$$- \int_S U_n \{\Phi_0^e\}^T \{N\} \, dS. \tag{3.34}$$

Let

$$\int_V \left[\frac{\partial\{N\}^T}{\partial x} \frac{\partial\{N\}}{\partial x} + \frac{\partial\{N\}^T}{\partial y} \frac{\partial\{N\}}{\partial y} + \frac{\partial\{N\}^T}{\partial z} \frac{\partial\{N\}}{\partial z} \right] dV = [H^e], \tag{3.35}$$

$$\int_S U_n \{N\} \, dS = \{f^e\}. \tag{3.36}$$

Then eq.(3.34) can be rewritten as

$$J_e(\Phi_{0i}^e) = \frac{1}{2} \{\Phi_0^e\}^T [H^e] \{\Phi_0^e\} - \{\Phi_0^e\}^T \{f^e\}.$$

$\delta J(\Phi) = 0$ for stationarity then leads to

$$[H^e]\{\Phi_0^e\} - \{f^e\} = \{0\},$$

where

$$\{\Phi_0^e\} = \langle \Phi_{01}^e, \Phi_{02}^e, \cdots, \Phi_{0n}^e \rangle,$$

$$\{f^e\}^T = \langle f_1^e, f_2^e, \cdots, f_n^e \rangle.$$

The element matrix and the load vector expressions, (3.35) and (3.36), can be rewritten as follows,

$$[H^e] = \iiint_V \left[\frac{\partial \{N\}^T}{\partial x} \frac{\partial \{N\}}{\partial x} + \frac{\partial \{N\}^T}{\partial y} \frac{\partial \{N\}}{\partial y} + \frac{\partial \{N\}^T}{\partial z} \frac{\partial \{N\}}{\partial z} \right] dx\, dy\, dz, \qquad (3.37)$$

$$\{f^e\} = \iint_S U_n \{N\}\, dS,$$

the elements of which should be integrated over the curved surface of the bellows convolution. Therefore, it is desirable to use isoparametric elements with curved boundaries. The most suitable parent element for the domain shown in Fig.3.8 is the 20-noded cubic element, Fig.3.9a, which can be mapped to the curved isoparametric, Fig.3.9b, by means of shape functions, N_i, of the parent cubic element,

$$x = \sum_{i=1}^{20} N_i x_i = \{N\}^T \{x\},$$

$$y = \sum_{i=1}^{20} N_i y_i = \{N\}^T \{y\},$$

(3.39)

$$z = \sum_{i=1}^{20} N_i z_i = \{N\}^T \{z\},$$

here,

$$\{N\}^T = \langle N_1, N_2, \cdots, N_{20} \rangle,$$

$$\{x\}^T = \langle x_1, x_2, \cdots, x_{20} \rangle,$$

$$\{y\}^T = \langle y_1, y_2, \cdots, y_{20} \rangle,$$

$$\{z\}^T = \langle z_1, z_2, \cdots, z_{20} \rangle,$$

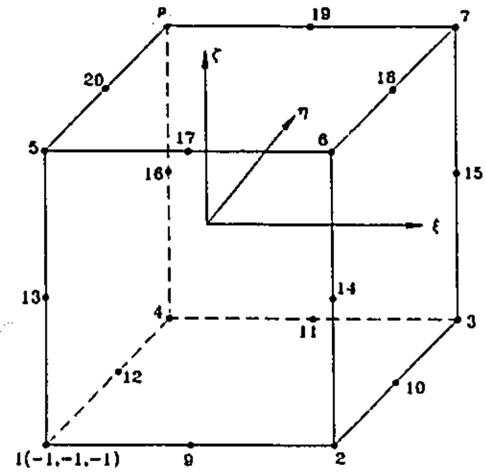

a) Parent element

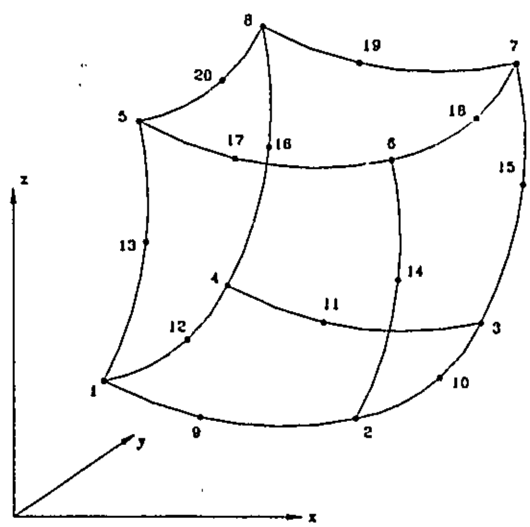

b) Isoparametric element

Fig.3.9. Parent and isoparametric elements

where, according to Tong and Rossetos (1977), for an element with C_0 continuity shown in Fig.3.9,

$$N_i = \frac{1}{8}(1+\xi\xi_i)(1+\eta\eta_i)(1+\varsigma\varsigma_i)(\xi\xi_1+\eta\eta_1+\varsigma\varsigma_1-2) \qquad i=1,2,\cdots,8,$$

$$N_i = \frac{1}{4}(1-\xi^2)(1+\eta\eta_i)(1+\varsigma\varsigma_i) \qquad i=9,11,17,19,$$

$$N_i = \frac{1}{4}(1-\eta^2)(1+\varsigma\varsigma_i)(1+\xi\xi_i) \qquad i=10,12,18,20,$$

$$N_i = \frac{1}{4}(1-\varsigma^2)(1+\xi\xi_i)(1+\varsigma\varsigma_i) \qquad i=13,14,15,16.$$

The derivatives of N_i with respect to x, y, z and ξ, η, ζ needed in the element formula are related by,

$$\begin{bmatrix} \dfrac{\partial N_i}{\partial x} \\ \dfrac{\partial N_i}{\partial y} \\ \dfrac{\partial N_i}{\partial z} \end{bmatrix} = [J]^{-1} \begin{bmatrix} \dfrac{\partial N_i}{\partial \xi} \\ \dfrac{\partial N_i}{\partial \eta} \\ \dfrac{\partial N_i}{\partial \varsigma} \end{bmatrix},$$

where $[J]$ is the familiar Jacobian,

$$[J] = \begin{bmatrix} \dfrac{\partial x}{\partial \xi} & \dfrac{\partial y}{\partial \xi} & \dfrac{\partial z}{\partial \xi} \\ \dfrac{\partial x}{\partial \eta} & \dfrac{\partial y}{\partial \eta} & \dfrac{\partial z}{\partial \eta} \\ \dfrac{\partial x}{\partial \varsigma} & \dfrac{\partial y}{\partial \varsigma} & \dfrac{\partial z}{\partial \varsigma} \end{bmatrix}.$$

The volume element $dx\,dy\,dz$ needed for this calculation can be given as

$$dx\,dy\,dz = \det[J]\,d\xi\,d\eta\,d\zeta,$$

so that (3.37) becomes

$$[H^e] = \int_{-1}^{+1}\int_{-1}^{+1}\int_{-1}^{+1}\left[\frac{\partial\{N\}^T}{\partial x}\frac{\partial\{N\}}{\partial x}+\frac{\partial\{N\}^T}{\partial y}\frac{\partial\{N\}}{\partial y}+\frac{\partial\{N\}^T}{\partial z}\frac{\partial\{N\}}{\partial z}\right]\det[J]\,d\xi\,d\eta\,d\varsigma \qquad (3.40)$$

The normal derivative, U_n , can be mapped to the parent element corresponding surface using the same shape functions:

$$U_n = \{N\}^T\{U_n\}.$$

Substitution of this expression into (3.38) gives

$$\{f^e\}^T = \iint_S \{N\}\{N\}^T\{U_n\}\,dS, \qquad (3.41)$$

where dS is the differential element of the tridimensional surface S of the same face of the curvilinear finite element shown in Fig.3.9b. To evaluate this surface integral we will use the parametrization of the surface S by shape functions $\{N\}$ using expressions for co-ordinates (3.39) which are functions of u and v. Then, according to Flanders (1985),

$$dS = \sqrt{\left(\begin{vmatrix}\frac{\partial y}{\partial u} & \frac{\partial z}{\partial u}\\ \frac{\partial y}{\partial v} & \frac{\partial z}{\partial v}\end{vmatrix}\right)^2+\left(\begin{vmatrix}\frac{\partial x}{\partial u} & \frac{\partial z}{\partial u}\\ \frac{\partial x}{\partial v} & \frac{\partial z}{\partial v}\end{vmatrix}\right)^2+\left(\begin{vmatrix}\frac{\partial x}{\partial u} & \frac{\partial y}{\partial u}\\ \frac{\partial x}{\partial v} & \frac{\partial y}{\partial v}\end{vmatrix}\right)^2}\;du\,dv. \qquad (3.42)$$

Here u and v denotes either η and ζ for the faces with $\xi = \pm 1$, or ξ and ζ for the faces $\eta = \pm 1$, or ξ and η for the faces $\zeta = \pm 1$ of the parent element, shown in Fig.3.9. Now we will express the normal derivative value, U_n , which is the x, y, z function in general. Since the displacement vector at the particular convolution location,

$$U = U_x i + U_y j + U_z k$$

and the unit normal vector is

$$\boldsymbol{n} = \frac{\begin{vmatrix} \boldsymbol{i} & \boldsymbol{j} & \boldsymbol{k} \\ \frac{\partial x}{\partial u} & \frac{\partial y}{\partial u} & \frac{\partial z}{\partial u} \\ \frac{\partial x}{\partial v} & \frac{\partial y}{\partial v} & \frac{\partial z}{\partial v} \end{vmatrix}}{\sqrt{\left(\begin{vmatrix} \frac{\partial y}{\partial u} & \frac{\partial z}{\partial u} \\ \frac{\partial y}{\partial v} & \frac{\partial z}{\partial v} \end{vmatrix}\right)^2 + \left(\begin{vmatrix} \frac{\partial x}{\partial u} & \frac{\partial z}{\partial u} \\ \frac{\partial x}{\partial v} & \frac{\partial z}{\partial v} \end{vmatrix}\right)^2 + \left(\begin{vmatrix} \frac{\partial x}{\partial u} & \frac{\partial y}{\partial u} \\ \frac{\partial x}{\partial v} & \frac{\partial y}{\partial v} \end{vmatrix}\right)^2}},$$

the normal U_n becomes

$$U_n = \boldsymbol{U} \cdot \boldsymbol{n} = \frac{\begin{vmatrix} U_x & U_y & U_z \\ \frac{\partial x}{\partial u} & \frac{\partial y}{\partial u} & \frac{\partial z}{\partial u} \\ \frac{\partial x}{\partial v} & \frac{\partial y}{\partial v} & \frac{\partial z}{\partial v} \end{vmatrix}}{\sqrt{\left(\begin{vmatrix} \frac{\partial y}{\partial u} & \frac{\partial z}{\partial u} \\ \frac{\partial y}{\partial v} & \frac{\partial z}{\partial v} \end{vmatrix}\right)^2 + \left(\begin{vmatrix} \frac{\partial x}{\partial u} & \frac{\partial z}{\partial u} \\ \frac{\partial x}{\partial v} & \frac{\partial z}{\partial v} \end{vmatrix}\right)^2 + \left(\begin{vmatrix} \frac{\partial x}{\partial u} & \frac{\partial y}{\partial u} \\ \frac{\partial x}{\partial v} & \frac{\partial y}{\partial v} \end{vmatrix}\right)^2}}, \tag{3.43}$$

Then the expression (3.41) becomes

$$\{f^{e}\}^T = \iint_S \{N\}\,\{N\}^T \begin{vmatrix} U_x & U_y & U_z \\ \frac{\partial x}{\partial u} & \frac{\partial y}{\partial u} & \frac{\partial z}{\partial u} \\ \frac{\partial x}{\partial v} & \frac{\partial y}{\partial v} & \frac{\partial z}{\partial v} \end{vmatrix} du\, dv. \tag{3.44}$$

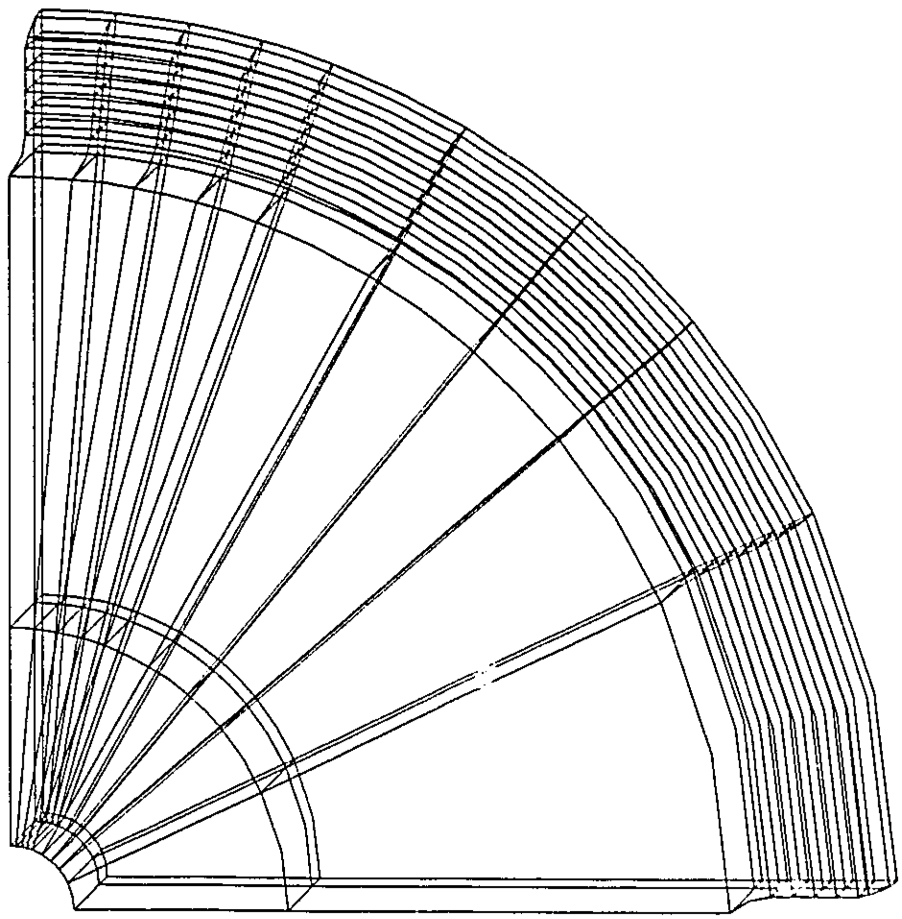

Fig.3.10. Spatial view of 3D mesh of 1/8 convolution space

Now the elemental stiffness and load expressions, (3.40) and (3.44), can be programmed into some basic finite element program to solve for the velocity potential, Φ_0, on the vibrating surface of the convolution.

It should be noted that the manual generation of the input data file for 3D finite element problems is very time consuming work and is very difficult to do without making mistakes. Therefore, it was decided to generate the input data file automatically, using a computer. The easiest way to implement this idea for an axisymmetric convolution space was by using a radially distributed mesh, as shown in Fig. 3.10.

3.8. Added Fluid Mass, λ

This type of added fluid mass is related to the crossflow acceleration of the fluid perpendicular to the axis of the bellows excited by the convolution deformation during vibration rather than to some discrete fluid mass.

According to Milne-Thompson (1968), the kinetic energy accumulated by the fluid and expressed through the velocity potential, Φ, on the vibrating boundary S is

$$W = -\frac{\rho_f}{2} \iint_S \Phi \frac{\partial \Phi}{\partial n}\bigg|_S dS. \tag{3.45}$$

Using (3.28) and (3.29), the expression (3.45) may be rewritten as follows:

$$W = \frac{\rho_f}{2} \dot{T}(t)^2 \iint_S \Phi_0(x,y,z) U_n(x,y,z)\, dS. \tag{3.46}$$

On the other hand, letting the distribution of the added fluid mass be uniform on the entire vibrating surface, S, the kinetic energy of the excited fluid flow becomes

$$W = \frac{\lambda \dot{T}^2(t)}{2S} \iint_S U^2(x,y,z)\, dS, \tag{3.47}$$

where S is the surface area of the convolution. Equating kinetic energies (3.46) and 3.47) gives the added mass expression for the three-dimensional flow:

$$\lambda = \rho S \frac{\iint_S \Phi_0(x,y,z) U_n(x,y,z)\, dS}{\iint_S U^2(x,y,z)\, dS}. \tag{3.48}$$

To use the expression for the added mass above it is necessary to know in advance the velocity potential, Φ_0, on the vibrating surface of the bellows convolution. Having the velocity potential, the formula (3.48) can be used to calculate the added fluid mass, λ.

The surface area of the 1/8 convolution is

$$S = \iint dS.$$

This surface area integral can be integrated in two steps. First, it can be integrated over the face of the element with boundary condition, U_n. The parametrization of S_i by

$$x = \sum_{i=1}^{8} N_i^{fc} x_i = \{N^{fc}\}^T \{x\},$$
$$y = \sum_{i=1}^{8} N_i^{fc} y_i = \{N^{fc}\}^T \{y\},$$
$$z = \sum_{i=1}^{8} N_i^{fc} z_i = \{N^{fc}\}^T \{z\},$$

is used here, as in the case of the calculation of the load vector, and runs over the appropriate face of the parent element shown in Fig.3.9 in the two-dimensional space (u,v). Here $\{N$ the shape function vector consisting of the functions of the nodes which belong to the face under the integration. Using parametrized dS expression (3.42), the surface area integral over element, i, can be expressed in a more convenient form for programming, as follows,

$$S_i = \iint_{D_i} \sqrt{ \left(\begin{vmatrix} \frac{\partial y}{\partial u} & \frac{\partial z}{\partial u} \\ \frac{\partial y}{\partial v} & \frac{\partial z}{\partial v} \end{vmatrix} \right)^2 + \left(\begin{vmatrix} \frac{\partial x}{\partial u} & \frac{\partial z}{\partial u} \\ \frac{\partial x}{\partial v} & \frac{\partial z}{\partial v} \end{vmatrix} \right)^2 + \left(\begin{vmatrix} \frac{\partial x}{\partial u} & \frac{\partial y}{\partial u} \\ \frac{\partial x}{\partial v} & \frac{\partial y}{\partial v} \end{vmatrix} \right)^2 } \, du \, dv,$$

where u, v, as was mentioned above, can be any combination of ξ, η, ζ. Now, for the second integration step, the simple summation over all the elements adjacent to the vibrating boundary gives the area of the whole vibrating surface of the domain, Fig.3.8,

$$S = S_1 + S_2 + \cdots + S_n. \tag{3.49}$$

The integral, $\iint\limits_S U^2(x,y,z)\,dS$, residing in formula (3.48), can be integrated the same way. Using expressions (3.42) and (3.43) we can write for the ith element:

$$\iint\limits_{S_i} U^2(x,y,z)\,dS =$$

$$= \iint\limits_{D_i} \left(U_x^2 + U_y^2 + U_z^2\right) \sqrt{\left(\begin{vmatrix} \frac{\partial y}{\partial u} & \frac{\partial z}{\partial u} \\ \frac{\partial y}{\partial v} & \frac{\partial z}{\partial v} \end{vmatrix}\right)^2 + \left(\begin{vmatrix} \frac{\partial x}{\partial u} & \frac{\partial z}{\partial u} \\ \frac{\partial x}{\partial v} & \frac{\partial z}{\partial v} \end{vmatrix}\right)^2 + \left(\begin{vmatrix} \frac{\partial x}{\partial u} & \frac{\partial y}{\partial u} \\ \frac{\partial x}{\partial v} & \frac{\partial y}{\partial v} \end{vmatrix}\right)^2}\; du\,dv.$$

Now the overall integral is

$$\iint\limits_S U^2(x,y,z)\,dS = \sum_{i=1}^{n} \iint\limits_{S_i} U^2(x,y,z)\,dS. \tag{3.50}$$

The last integral in formula (3.48) is

$$\iint\limits_S \Phi_0(x,y,z)\; U_n(x,y,z)\,dS,$$

and can be integrated similarly. The parametrization of the velocity potential over the particular face of the ith element is:

$$\Phi_0(x,y,z) = \sum_{i=1}^{8} N_i^{fc}\Phi_{0i} = \{N^{fc}\}^T\{\Phi_0\}. \tag{3.51}$$

Now, using expressions (3.43) and (3.51), we can write

$$\iint_{S_i} \Phi_0(x,y,z)\,U_n(x,y,z)\,dS = \iint_{D_i} \Phi_0(x,y,z) \begin{vmatrix} U_x & U_y & U_z \\ \dfrac{\partial x}{\partial u} & \dfrac{\partial y}{\partial u} & \dfrac{\partial z}{\partial u} \\ \dfrac{\partial x}{\partial v} & \dfrac{\partial y}{\partial v} & \dfrac{\partial z}{\partial v} \end{vmatrix} du\,dv$$

and the total integral,

$$\iint_{S} \Phi_0(x,y,z)\,U_n(x,y,z)\,dS = \sum_{i=1}^{n} \iint_{S_i} \Phi_0(x,y,z)\,U_n(x,y,z)\,dS. \tag{3.52}$$

Finally, substitution of the values of the integrals (3.49), (3.50) and (3.52) into formula (3.48) gives the added mass value for 1/8 of the convolution.

It is obvious, from explanations above, that the calculations of added mass λ according to formula (3.48) are practically impossible to perform manually, using a calculator. Therefore, those calculations were programmed as a Fortran subroutine into a single combined program together with calculations of the velocity potential as explained in the previous section.

The added fluid mass for one half-convolution, caused by distortion of the convolution walls, may be expressed symbolically as

$$\lambda = f\left(\rho_f, R_m, R_2, L\right), \tag{3.53}$$

where

ρ_f is the density of fluid (kg/m^3),

R_m, R_2, L are the geometrical parameters (m), see Fig.2.1.

The dimensional analysis of (3.53) gives

$$\frac{\lambda}{\rho_f R_m^3} = F\left(\frac{R_2}{R_m}, \frac{L}{R_m}\right). \quad (3.54)$$

The nondimensional expression on the left side of (3.54) can be called the coefficient of fluid added mass, μ, of a half-convolution, and is defined as

$$\mu = \frac{\lambda}{\rho_f R_m^3}. \quad (3.55)$$

As seen from (3.54), the coefficient μ for all geometrically similar convolutions is the same. However, the added masses are different because they depend on the mean radius of the bellows, R_m:

$$\lambda = \mu \rho_f R_m^3. \quad (3.56)$$

Coefficient μ was calculated using the algorithm described in Sections 3.7 and 3.8. The computation results for the most common geometrical parameters of a convolution are plotted in Fig. 3.11.

Finally, the total bellows mass per unit length using (3.12), (3.14), (3.16), (3.24), and (3.56) may be written as follows:

$$m_{tot} = \frac{4\pi R_m}{p}(h + 0.285\,p)\,t\rho_b + \left[\pi\left(R_m - \frac{h}{2} + \frac{2hR_2}{p}\right)^2 + \alpha_{f2k}\,\mu R_m^3\right]\rho_f. \quad (3.57)$$

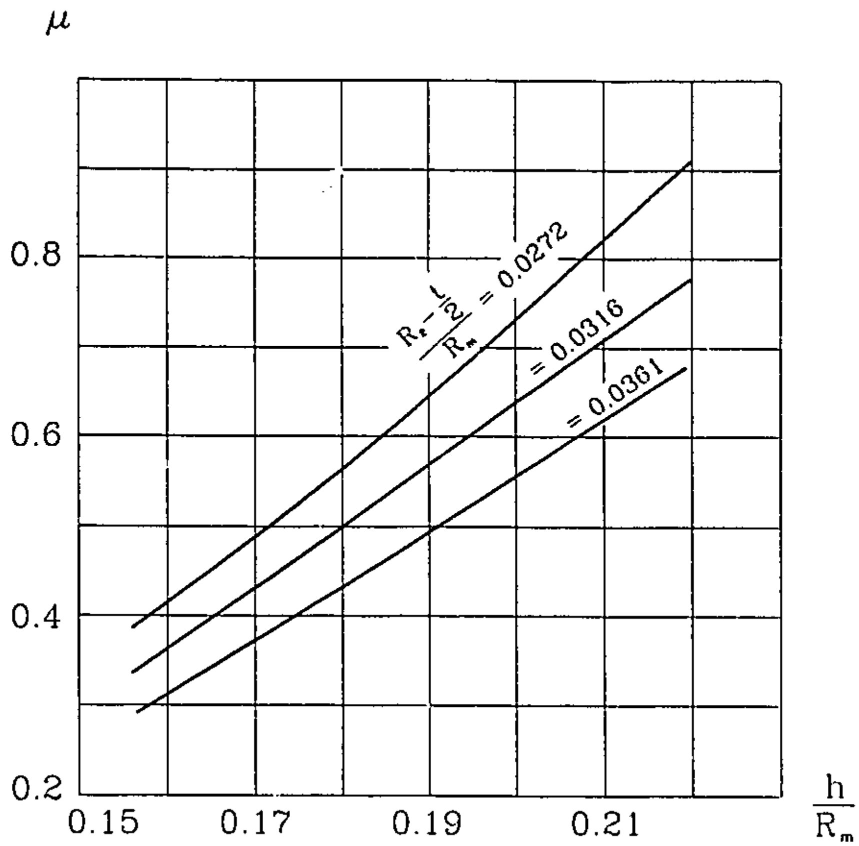

Fig. 3.11. Added mass μ versus $\dfrac{h}{R_m}$.

3.9. Mass Moment of Inertia of Bellows Cross-section

In terms of the classical beam parameters, the diameter of a bellows is usually large in comparison with its axial dimension. Therefore, the inertia of the cross-section about the axis of the bellows becomes an important factor in its transverse vibration. The total mass moment of inertia of the bellows per unit length can be considered as consisting of the following three parts. The first is the moment of inertia of dry bellows, J_b. The second part is the moment of inertia of the fluid trapped in the convolutions, J_{f1}. The third part is the moment of inertia of the fluid contained in the central portion of the bellows. This part of the total moment, at least for fluids with relatively low viscosity, such as water or light fuels, is very small and, according to some authors, Paidoussis et al. (1986), Pramila et al. (1991), can be ignored. Therefore,

$$J = J_b + J_{f1}.$$

It is known from beam theory, that

$$J = I\rho,$$

where

I is the second moment of area,

ρ is the density.

Using this we can rewrite the above equation as

$$J = I_b\rho_b + I_{f1}\rho_f. \tag{3.58}$$

The equivalent bellows thickness can be obtained geometrically as

$$t_b = t \times \frac{\pi R_1 + \pi R_2 + 2L}{p}. \tag{3.59}$$

Here t, p, L, R_2 and R_1 are the geometric parameters of the bellows as explained in Section 2.1. The equivalent area of the cross-section of the bellows is,

$$A_b = 2\pi R_m t_b, \tag{3.60}$$

the equivalent second moment of area,

$$I_b = r_{in}^2 A_b. \tag{3.61}$$

Since the radius of gyration for a thin circular cross section is

$$r_{in}^2 = \frac{R_m^2}{2}, \tag{3.62}$$

substitution of (3.59) into (3.60) and subsequently (3.60) and (3.62) into (3.61) finally gives

$$I_b = \frac{\pi R_m^3 t(\pi R_1 + \pi R_2 + 2L)}{2(R_1 + R_2)}. \tag{3.63}$$

It should be noted that this moment of inertia, I_b, is not the same as I_{eq} obtained in Section 3.1 and it can be used for calculation of the mass moment of inertia of the bellows according to formula (3.58) only.

Now we will calculate the equivalent fluid mass moment of inertia, I_{f1}. One convolution volume (see Fig.2.1) is given by:

$$V_{1con} = 2\pi R_m (L + R_1 + R_2)(2R_2 - t).$$

Since one convolution length is equal to $2R_1 + 2R_2$, the mean cross-sectional area of fluid trapped in a convolution is:

$$A_{f1} = \frac{\pi R_m (L + R_1 + R_2)(2R_2 - t)}{R_1 + R_2}. \quad (3.64$$

As before,

$$I_{f1} = r_{in}^2 A_{f1}.$$

Substitution of (3.62) and (3.64) into the above expression gives

$$I_{f1} = \frac{\pi R_m^3 (L + R_1 + R_2)(2R_2 - t)}{2(R_1 + R_2)}. \tag{3.65}$$

Substitution of(3.63) and (3.65) into (3.58) finally gives the expression for the total mass moment of inertia per unit bellows length:

$$J = \frac{\pi R_m^3 t\left(\pi R_1 + \pi R_2 + 2L\right)}{2(R_1 + R_2)}\rho_b + \frac{\pi R_m^3\left(L + R_1 + R_2\right)\left(2R_2 - t\right)}{2(R_1 + R_2)}\rho_f\,, \tag{3.66}$$

or

$$J = \pi R_m^3\left[\left(2\frac{h}{p} + 0.571\right)t\rho_b + \frac{h}{p}\left(2R_2 - t\right)\rho_f\right]. \tag{3.67}$$

3.10. Mass Moment of Inertia of Connecting Pipe of Universal Expansion Joint

In the case of vibration of universal expansion joints accompanied by any of the rocking modes (see Fig. 3.12), the connecting pipe AO rotates about the middle point of the expansion joint, O. Therefore, it is necessary to know the mass moment of inertia of the connecting pipe including fluid (if applicable) about the point of rotation, O. According to Paliunas (1982), the mass moment of inertia of a thin cylindrical shell is

$$J_{sh.(O)} = \frac{ma^2}{3} + \frac{mR^2}{2}\,,$$

where m is the mass of the cylinder OA. Letting m_p to be the mass per unit length of the pipe, the above formula becomes:

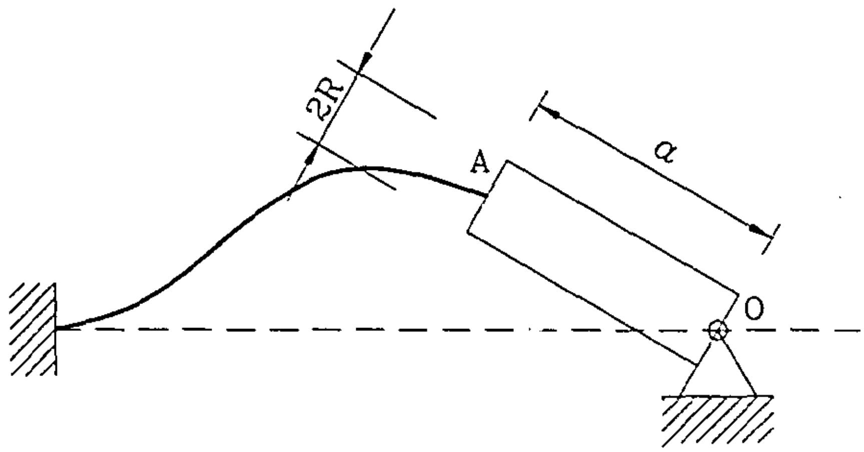

Fig. 3.12. Rocking mode of universal expansion joint

$$J_{sh.(O)} = \frac{m_p a^3}{3} + \frac{m_p a R^2}{2}.$$

For the fluid cylinder inside the pipe,

$$J_{f1.(O)} = \frac{m_{f1} a^2}{3} + \frac{m_{f1} R^2}{4}.$$

Defining the fluid mass per unit length of the connecting pipe as m_{f3}, the above formula can be rearranged as follows:

$$J_{f1.(O)} = \frac{m_{f3} a^3}{3} + \frac{m_{f3} a R^2}{4}.$$

The total mass moment of inertia of one half of the connecting pipe about the point of rotation, O, including the inertia of rotation of any lateral supports, M_h, (if applicable) changes to:

$$J_{tot} = J_{sh.(O)} + J_{fl.(O)} + J_{h(O)}$$

or

$$J_{tot} = \frac{\left(m_p + m_{f3}\right)a^3}{3} + \frac{\left(2m_p + m_{f3}\right)a R^2}{4} + M_h a^2 \,. \tag{3.68}$$

CHAPTER 4

ASSUMPTIONS AND
DIFFERENTIAL EQUATION OF TRANSVERSE VIBRATION OF BELLOWS

4.1. The Modes of Natural Transverse Vibration of Bellows Expansion Joints

As mentioned in Chapter 2, corrugated pipe expansion joints can vibrate according to longitudinal, shell, and beam modes. The rest of the Chapters of this thesis will be devoted to the last type of joint vibrations, beam vibration modes.

A bellows expansion joint is usually welded to pipe ends or flanges which are very stiff in comparison with the bellows itself. Therefore, it is very reasonable to assume that the expansion joint is perfectly fixed at both ends. For this reason, the modes of transverse vibration of a single bellows expansion joint (Fig.2.2a) almost exactly coincide with the fixed-fixed beam mode shapes.

A universal expansion joint (Fig.2.2b, c) has in between two bellows elements a smooth connecting pipe, which is generally many times stiffer than the bellows. It can be assumed, for the sake of simplicity, to be perfectly rigid. Therefore, the system under consideration can be represented as a fixed-fixed system of two elastic beams with a rigid section in the middle as shown in Fig.4.1. From the point of view of transverse vibrations,

Fig.4.1. Universal expansion joint as elastic system

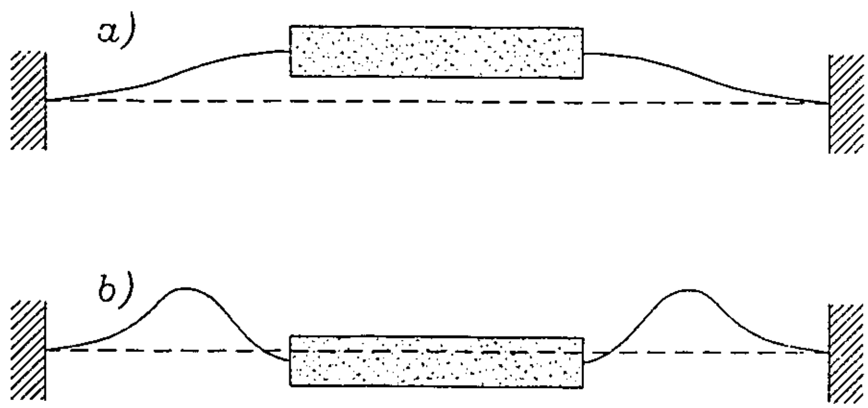

Fig.4.2. Lateral modes: a) first, b) second

two types of transverse vibration modes can be expected, so called "lateral" modes shown in Fig.4.2, and "rocking" modes shown in Fig.4.3.

a)

b)

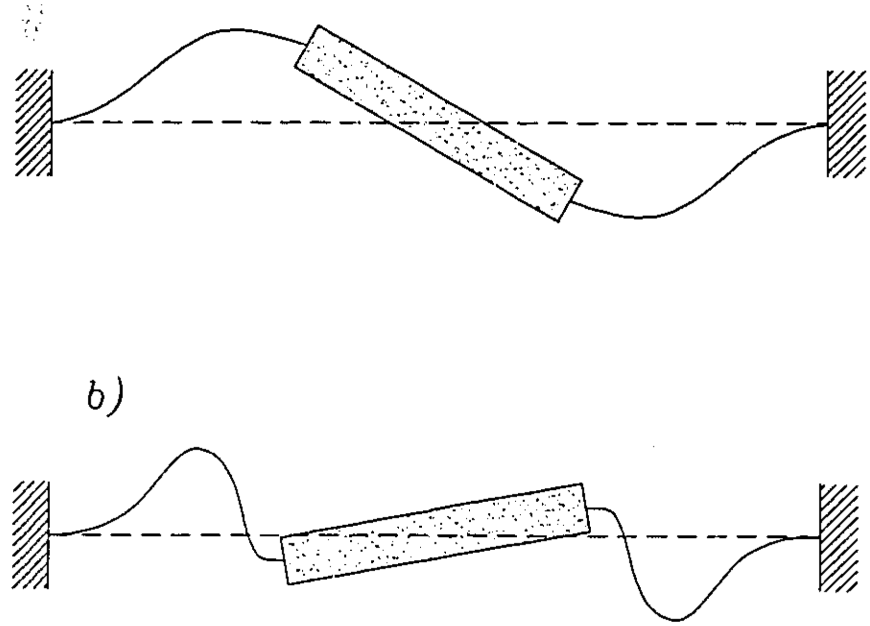

Fig.4.3. Rocking modes: a) first, b) second

Later calculations showed that the frequencies of the second mode shapes in both types of modes are much higher than the first mode frequencies. In the case of lateral modes (Fig.4.2), the ratio of first to second mode frequency is greater than 10. Perhaps for this reason, neither the EJMA Standard (1980) nor other authors mention higher modes at all.

In general, the universal expansion joint vibration problem can be modelled by the system of two bending differential equations together with eight boundary conditions. But if it is split into two separate problems according to the two types of bending modes, the solution can be simplified substantially by considering just one half, either left or right, of the whole system shown in Fig.4.1. These two problems are described in the following chapters in detail.

4.2. The Influence of Shear and Inertia of Rotation of Cross-section on Vibrating Bellows

The bellows is a comparatively short and bulky structure. Therefore, for the investigation of the transverse vibration of a bellows it seems necessary to use the Timoshenko differential equation which takes into account the influence of shear force and the rotary inertia of the cross section of the beam.

Let us look more closely at the ratio of shear to rotary inertia in the case of a bellows. The Timoshenko differential equation is:

$$EI\frac{\partial^4 w}{\partial x^4} + m_b\frac{\partial^2 w}{\partial t^2} - \left(\rho I + \frac{\rho EI}{Gk'}\right)\frac{\partial^4 w}{\partial x^2 \partial t^2} + \frac{\rho^2 I}{Gk'}\frac{\partial^4 w}{\partial t^4} = 0, \tag{4.1}$$

where

E is the modulus of elasticity of the material,

G is the shear modulus of the beam,

I is the second moment of area of the cross section,

m_b is the beam mass per unit length,

ρ is the density of the material,

k' is the cross-section correction coefficient,

w is the deflection,

x is the coordinate,

t is the time.

For the circular cross-section of a thin tubular beam, k' is approximately given by Paidoussis et al. (1986):

$$k' = \frac{6(1+\nu)(1+\alpha^2)^2}{(7+6\nu)(1+\alpha^2)^2 + (20+12\nu)\alpha^2}, \tag{4.2}$$

where

ν is the Poisson's ratio,

α is the ratio of internal to external radius of a tube.

Let's consider the tube of radius R_m = 0.03465 m, wall thickness t = 0.00028 m, and $\nu = 0.25$. Then $R_{int} = 0.03446$ m, $R_{out} = 0.03474$ m and

$$\alpha = \frac{R_{int}}{R_{out}} = 0.992.$$

For these data, according to formula (4.2), $k' = 0.53$. Since

$$G = \frac{E}{2(1+\nu)}, \tag{4.3}$$

the shear term coefficient in eq.(4.1) becomes

$$\frac{\rho EI}{Gk'} = \frac{2(1+\nu)I}{k'} = \frac{2(1+0.25)I\rho}{0.53} = 4.72\,\rho I.$$

Since the rotary inertia coefficient in eq (4.1) is equal to ρI, the ratio of shear to rotary inertia is

$$\frac{\rho EI}{Gk'} / \rho I = 4.72$$

which shows that for the ordinary beam (or tube) the influence of the rotary inertia is 4.72 time less than the influence of the shear. Therefore, sometimes, in short beam problems the rotary inertia can be neglected.

Now let us look at the bellows as a tube with convoluted surface as shown in Fig.2.1. Let us have the same mean radius, $R_m = 0.03465$ m, and wall thickness, $t = 0.00028$ m, as before in the smooth tube example and, in addition, $R_1 = R_2 = 0.00125$ m, and moderate convolution depth, $h = 0.00571$ m ($L = 0.00321$ m). The half convolution longitudinal stiffness of a bellows can be approximately calculated using, for example, formula (2.2):

$$k = 4R_m E\left(\frac{t}{h}\right)^3 = 4 \times 0.03465 \times 2.07 \times 10^{11}\left(\frac{0.00028}{0.00571}\right)^3 = 3.383 \times 10^6 \text{ N/m.}$$

It was shown in the previous chapter, that the bending stiffness of a bellows, EI, can be calculated from the axial spring rate, k, according to formula (3.1)

$$EI = \frac{1}{4}kpR_m^2 = \frac{1}{4} \times 3.383 \times 10^6 \times 0.005 \times 0.03465^2 = 5.078 \quad \text{Nm}^2.$$

Using formula (4.3) we calculate $G = 0.828 \times 10^{11}$ N/m^2. Therefore,

$$\frac{\rho EI}{Gk} = \rho\frac{5.078}{0.828 \times 10^{11} \times 0.53} = \rho \times 11.57 \times 10^{-11} \quad \text{kgm.}$$

According to (3.63), the equivalent second moment of area,

$$I_b = \frac{\pi R_m^3 t(2\pi R_1 + 2L)}{4R_1} = \frac{\pi\, 0.03465^3 \times 0.00028(2\pi \times 0.00125 + 2 \times 0.00321)}{4 \times 0.00125}$$
$$= 1.045 \times 10^{-7} \quad \text{m}^4$$

Now the ratio shear/rotary inertia becomes

$$\frac{\rho EI}{Gk'} / \rho I_b = \frac{\rho \times 11.57 \times 10^{-11}}{\rho \times 1.045 \times 10^{-7}} = 11.072 \times 10^{-4}.$$

This ratio shows that for a corrugated pipe (bellows) with moderate convolution depth, the influence of the shear coefficient consists of just a very small fraction, 0.00111, of the rotary inertia, without taking into account the additional fluid rotary inertia. Therefore, for the investigation of the transverse vibration of a bellows, the influence of shear can be ignored, and only the rotary inertia must be accounted for.

Let us now consider the coefficient of the last term in equation (4.1), $\frac{\rho^2 I}{Gk'}$. In the above example, $EI = 5.078$ Nm^2. Then $I = 5.078/E$. Substituting the I value into the coefficient expression gives:

$$\frac{\rho^2 I}{Gk'} = \frac{5.078\rho^2}{EGk'}.$$

The large value of the product EG in the denominator compared to the numerator makes this coefficient negligibly small in comparison with coefficients of other terms in the equation (4.1). Therefore, this term can be ignored too.

Now we will examine the influence of rotary inertia on the frequency of natural vibrations in a bellows. For the sake of simplicity, we will investigate the vibrations of a simply supported hypothetical bellows with length, $l = 0.0693$ m. The differential equation for this problem is the same Timoshenko differential equation (4.1), but without the shear terms:

$$EI\frac{\partial^4 w}{\partial x^4} - J\frac{\partial^4 w}{\partial x^2\,\partial t^2} + m_{tot}\frac{\partial^2 w}{\partial t^2} = 0, \qquad (4.4)$$

where

J is the bellows cross-section rotary inertia per unit length,

m_{tot} is the total mass of bellows per unit length.

For simply supported ends, the first mode may be assumed to be defined by

$$w = A\sin\pi\frac{x}{l}\cos\omega_1 t. \qquad (4.5)$$

Substitution of (4.5) into the differential equation (4.4) gives

$$EI\left(\frac{\pi}{l}\right)^4 - \omega_1^2 J\left(\frac{\pi}{l}\right)^2 - \omega_1^2 m_{tot} = 0,$$

which leads to the frequency expression:

$$\omega_1 = \left(\frac{\pi}{l}\right)^2 \left(\frac{EI}{m_{tot}}\right)^{\frac{1}{2}} \left(\frac{1}{1+\frac{J}{m_{tot}}\left(\frac{\pi}{l}\right)^2}\right)^{\frac{1}{2}}.$$

The coefficient

$$\left(\frac{1}{1+\frac{J}{m_{tot}}\left(\frac{\pi}{l}\right)^2}\right)^{\frac{1}{2}} = K$$

in the above expression takes into account the rotary inertia of the bellows. It is seen that for $J = 0$, $K = 1$ and the frequency expression ω_1 becomes the well known frequency solution for the Bernoulli-Euler equation. Let us look at the numerical value of K for the bellows dimensions, mentioned above. Using formula (3.66),

$$\begin{aligned} J &= \frac{\pi R_m^3 t\left(\pi R_1 + \pi R_2 + 2L\right)}{2\left(R_1 + R_2\right)}\rho_b + \frac{\pi R_m^3\left(L + R_1 + R_2\right)\left(2R_2 - t\right)}{2\left(R_1 + R_2\right)}\rho_f \\ &= \frac{\pi \times 0.003465^3 \times 0.00028\left(2\pi \times 0.00125 + 2 \times 0.00321\right)}{2\left(0.00125 + 0.00125\right)} \times 7560 \\ &+ \frac{\pi \times 0.003465^3\left(0.00321 + 2 \times 0.00125\right)\left(2 \times 0.00125 - 0.00028\right)}{2\left(0.00125 + 0.00125\right)} \times 1000 \\ &= 0.001153 \quad \text{kgm.} \end{aligned}$$

The total mass, according to (3.12), without taking into account the added mass caused by convolution deformation is,

$$m_{tot} = \frac{\pi R_m \left(\pi R_1 + \pi R_2 + 2L\right)}{R_1 + R_2} \rho_b + \pi R_m^2 \rho_f$$

$$= \frac{\pi \times 0.03465 \left(2\pi \times 0.00125 + 2 \times 0.00321\right) 0.00028}{0.00125 + 0.00125} \times 7860 + \pi \times 0.03465^2 \times 1000$$

$$= 5.139 \quad \text{kg/m.}$$

Substitution of numerical values for J and m_{tot} into the expression for K gives

$$K = \left(\frac{1}{1 + \frac{0.001153}{5.139} \left(\frac{\pi}{0.0693} \right)^2} \right)^{\frac{1}{2}} = 0.827.$$

This value is less than unity which means that the inertia of rotation of the cross-section lowers the natural frequency in comparison with the Bernoulli-Euler solution by 17.3% for the simply supported bellows.Something similar is expected fixed-fixed bellows end conditions.

4.3. The Influence of the Coriolis Force on Natural Vibrations of Bellows

The simplest differential equation describing the vibrations of a pipe conveying fluid is

$$EI \frac{\partial^4 w}{\partial x^2} + 2m_{f1} \mathrm{v} \frac{\partial^2 w}{\partial t \, \partial x} + m_{tot} \frac{\partial^2 w}{\partial t^2} = 0, \tag{4.6}$$

where

m_{f1} is the fluid mass per unit length,

v is the bulk fluid velocity.

The rest of the parameters used in the above equation are the same as in equation (4.1). The second term represents the inertia force associated with the Coriolis acceleration which arises because the fluid is flowing with velocity, v, relative to the pipe, while the pipe itself has an angular velocity $\partial^2 w / \partial t\, \partial x$ at any point along its length. It is shown in numerous works, for example, Housner (1952), that for pipes with both ends supported the influence of Coriolis forces is negligible. Now we will check the influence of this type of force on the vibrating cylinder which is as short as bellows. For the sake of simplicity, we will solve this equation for the hypothetical simply supported bellows and then extrapolate the obtained results for a fixed-fixed bellows by comparison of the magnitudes of moments exerted by Coriolis forces on a bellows in cases of simply supported and fixed-fixed end conditions.

A simply supported pipe has the normal modes w_i satisfying equation (4.6)

$$w_i = \sum_{n=1,3,\ldots} A_n \sin\frac{n\pi x}{l} \sin\omega_i t + \sum_{k=2,4,\ldots} A_k \sin\frac{k\pi x}{l} \cos\omega_i t. \tag{4.7}$$

The normal mode w_i is composed of terms which interact with one another through the mixed derivative term

$$2m_{f1} \mathrm{v} \frac{\partial^2 w}{\partial t\, \partial x}.$$

The coefficients, A, and the natural frequency, ω_i, can be determined as follows. When expression (4.7) for w_i is substituted in equation (4.6), the mixed derivative gives rise to terms containing $\cos\frac{n\pi x}{l}$ and $\cos\frac{k\pi x}{l}$. These terms may be expanded in Fourier series

$$\cos\frac{n\pi x}{l} = \sum_{k=2,4,\ldots} \frac{4}{\pi} \frac{n}{k^2 - n^2} \sin\frac{k\pi x}{l}$$

and

$$\cos\frac{k\pi x}{l} = \sum_{n=1,3,\ldots} \frac{4}{\pi} \frac{k}{k^2 - n^2} \sin\frac{n\pi x}{l}$$

With these substitutions, all the terms in equation (4.7) can be collected in two groups according to whether they contain

$$\sin\frac{n\pi x}{l}\sin\omega_i t,$$

or

$$\sin\frac{k\pi x}{l}\cos\omega_i t.$$

The coefficients of these terms must then be equated to zero in order to satisfy equation (4.6). This gives the following set of algebraic equations for $n = 1,3,5,\ldots$ and $k = 2,4,6,\ldots$:

$$A_n\left[EI\left(\frac{n\pi}{l}\right)^4 - m_{tot}\omega_i^2\right] = \frac{8m_{f1}\mathrm{v}\omega_i}{l}\sum_{k=2,4,\ldots} A_k \frac{k^2}{k^2 - n^2}$$

$$A_k\left[EI\left(\frac{k\pi}{l}\right)^4 - m_{tot}\omega_i^2\right] = \frac{8m_{f1}\mathrm{v}\omega_i}{l}\sum_{n=1,3,\ldots} A_n \frac{n^2}{n^2 - k^2}.$$

Assume, for example, only the first two terms, $n = 1$, $k = 2$. Then

$$\left[EI\left(\frac{\pi}{l}\right)^4 - m_{tot}\omega_i^2\right]A_1 - \frac{32m_{f1}\mathrm{v}\omega_i}{3l}A_2 = 0,$$

$$\frac{8m_{f1}\mathrm{v}\omega_i}{3l}A_1 + \left[EI\left(\frac{2\pi}{l}\right)^4 - m_{tot}\omega_i^2\right]A_2 = 0.$$

If A_1 and A_2 are eliminated from these two equations, we will obtain, as a result, the frequency equation whose roots determine the natural frequencies ω_i of the two normal modes:

$$\omega_i^4 + \left[256\left(\frac{m_{f1}\mathrm{v}}{3m_{tot}l}\right)^2 - \frac{17\pi^4 EI}{m_{tot}\, l^4}\right]\omega_i^2 + \frac{16\pi^8 (EI)^2}{m_{tot}^2\, l^8} = 0. \tag{4.8}$$

We will solve this diquadratic equation for bellows geometrical parameters given in the previous section. In addition to those, we have to know the bellows and fluid masses, m_b and m_f. Let the bellows (steel) and fluid (water) densities be $\rho_b = 7860$ kg/m^3 and $\rho_f = 1000$ kg/m^3. From the previous section, $m_{tot} = 5.139$ kg/m and

$$m_{f1} = \pi R_m^2 \rho_f = \pi\,(0.03465)^2\,(1000) = 3.772 \ \ \text{kg/m}.$$

For the given bellows parameters, the first two natural frequencies were determined from equation (4.8) for various v and l. The calculation results are compared in Table 4.1 to those obtained from the simple Bernoulli-Euler equation (eq.4.6 without the Coriolis term). The frequency solution of this simplified equation for a simply supported beam is:

$$\omega_i = \left(\frac{i\pi}{l}\right)^2 \sqrt{\frac{EI}{m_{tot}}}.$$

It is seen from Tables 4.1 and 4.2 that even for the extreme v and l values, the Coriolis forces increase the natural frequency for the first mode and decrease it for the second mode 0.57 %. Setting the first mode amplitude $A_1 = 1$, either of the two equations above determine the second mode amplitude, A_2, for each normal mode. For bellows with the above data and $l = 0.1039$ m, the first natural frequency, $\omega_1 = 913.286$ rad/s. Then $A_2 = 0.00433$. It is obvious that both the l and ω_1 values are not large enough to excite the unsymmetrical A_2 component appreciably and, therefore, A_2 has a negligible effect upon the first mode frequency. According to Housner (1952), the strength of the coupling between modes decreases rapidly, so if A_1, A_2, and A_3 are retained, the magnitude A_3 is small compared to that of A_2 in the lowest mode of vibration. In general, the dynamic coupling is such that in the ith mode of vibration the coefficient A_i is the largest and the coefficients A_{i+1}, A_{i+2}, ... and A_{i-1}, A_{i-2}, ... decrease in magnitude very quickly as the subscript value departs from i.

Table 4.1. Comparison of natural frequencies (1/s) of bellows calculated with and without Coriolis term with eq. (4.8) for first mode (without/with/error%)

l (m) / v (m/s)	0.03465 (R_m)	0.0693 ($2R_m$)	0.1039 ($3R_m$)
2	8172.30 8172.51 0.0026 %	2043.08 2043.28 0.0098 %	908.034 908.242 0.023 %
5	8172.30 8173.60 0.016 %	2043.08 2044.38 0.064 %	908.034 909.338 0.14 %
10	8172.30 8177.51 0.064 %	2043.08 2048.30 0.25 %	908.034 913.286 0.57 %

Table 4.2. Comparison of natural frequencies (1/s) of bellows calculated with and without Coriolis term with eq. (4.8) for second mode (without/with/error%)

l (m) / v (m/s)	0.03465 (R_m)	0.0693 ($2R_m$)	0.1039 ($3R_m$)
2	32689.22 32688.38 0.0026 %	8172.30 8171.47 0.0098 %	3632.136 3631.303 0.023 %
5	32689.22 32684.01 0.016 %	8172.30 8167.10 0.064 %	3632.136 3626.928 0.14 %
10	32689.22 32668.40 0.064 %	8172.30 8151.46 0.25 %	3632.136 3611.249 0.57 %

These results apply to simply supported bellows only.

The distribution of the Coriolis force per unit length along the bellows can be expressed as

$$CorF(x) = 2\omega v m_{f1} = 2\frac{\partial^2 w}{\partial x\,\partial t} v m_{f1} \tag{4.9}$$

or the elemental force

$$dCorF(x) = 2\frac{\partial^2 w}{\partial x\,\partial t} v m_{f1}\,dx. \tag{4.10}$$

Since the mode shape of a simply supported pipe conveying fluid can be approximately expressed by

$$w_{smp} = \sin\frac{\pi x}{l}\,T(t),$$

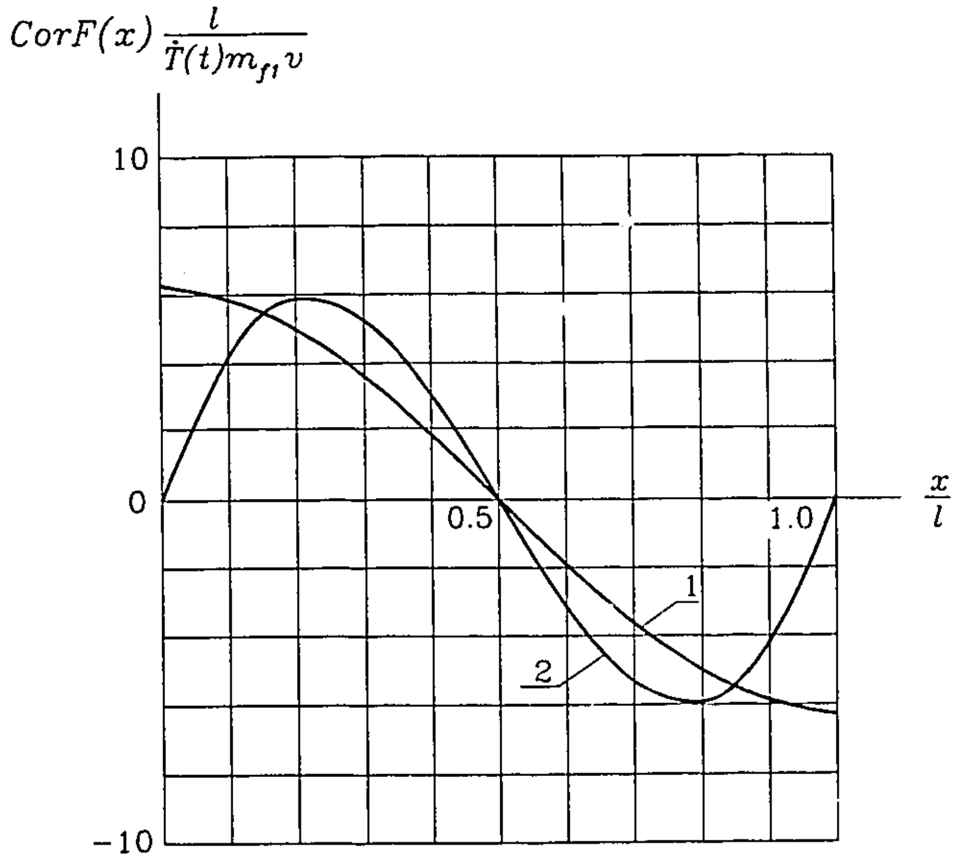

Fig.4.4. Distribution of Coriolis forces for simply supported ends – 1, and fixed-fixed ends – 2

then the distribution of the Coriolis force for the given mode shape,

$$CorF_{smp}(x) = 2v m_{f1}\frac{\pi}{l}\dot{T}(t)\cos\frac{\pi x}{l}$$

and elemental force

$$dCorF_{smp}(x) = 2\mathrm{v}m_{f1}\frac{\pi}{l}\dot{T}(t)\cos\frac{\pi x}{l}dx.$$

The distribution of the Coriolis force is shown in Fig.4.4. It appears that although the integral of the Coriolis force is equal to zero and doesn't perform any work, the integral moment of this force is:

$$\begin{aligned} CorM_{smp} &= \int_0^l x\, dCorF_{smp}(x) = \int_0^l x 2\mathrm{v}m_{f1}\frac{\pi}{l}\dot{T}(t)\cos\frac{\pi x}{l}dx \\ &= 2\mathrm{v}m_{f1}\frac{\pi}{l}\dot{T}(t)\int_0^l x\cos\frac{\pi x}{l}dx = -1.271\, m_{f1}\mathrm{v}\dot{T}(t). \end{aligned} \tag{4.11}$$

This moment becomes equal to zero at the extreme positions of the vibrating bellows and reaches its maximum at the position of equilibrium (depends on $\dot{T}(t)$). Therefore, under the influence of this moment, the mode shapes become non-classical, which then slightly affects the natural frequency of the pipe conveying fluid as was shown in the Tables 4.1 and 4.2.

Let us now calculate $CorM_{fix}$ for the fixed-fixed pipe. The approximate first vibration mode in this case is taken as the mode shape of the fixed-fixed beam, Filipov (1965):

$$\begin{aligned} w_{fix} = T(t)\Big[&0.62966\left(\cosh 4.73004\frac{x}{l} - \cos 4.73004\frac{x}{l}\right) \\ &- 0.61865\left(\sinh 4.73004\frac{x}{l} + \sin 4.73004\frac{x}{l}\right)\Big]. \end{aligned}$$

Substitution of this into (4.9) results in the following expression for the distribution of the Coriolis force

$$CorF_{fix}(x) = \frac{2m_{f1}v}{l}T(t)\left[2.97833\left(\sinh 4.73004\frac{x}{l} + \sin 4.73004\frac{x}{l}\right)\right.$$
$$\left. -2.92622\left(\cosh 4.73004\frac{x}{l} - \cos 4.73004\frac{x}{l}\right)\right]$$

and substitution of the same mode shape into (4.10) gives the elemental force

$$dCorF_{fix}(x) = \frac{2m_{f1}v}{l}T(t)\left[2.97833\left(\sinh 4.73004\frac{x}{l} + \sin 4.73004\frac{x}{l}\right)\right.$$
$$\left. -2.92622\left(\cosh 4.73004\frac{x}{l} - \cos 4.73004\frac{x}{l}\right)\right]dx.$$

Multiplying this elemental force by x and integrating over the length of the pipe results in the total moment of the Coriolis forces for the fixed-fixed bellows conveying fluid:

$$CorM_{fix} = \int_0^l x\, dCorF_{fix}$$
$$= \frac{2m_{f1}v}{l}T(t)\int_0^l x\left[2.97833\left(\sinh 4.73004\frac{x}{l} + \sin 4.73004\frac{x}{l}\right)\right.$$
$$\left. - 2.92622\left(\cosh 4.73004\frac{x}{l} - \cos 4.73004\frac{x}{l}\right)\right]dx = -1.041m_{f1}v\dot{T}(t). \quad (4.12)$$

The comparison of the Coriolis moments for simply supported, (4.11), and fixed-fixed, (4.12), bellows shows that the Coriolis moment $CorM_{fix}$ for the fixed-fixed case is only 82% of the moment $CorM_{smp}$ for the simply supported case. This fact can be readily seen from the comparison of the graphs for $CorF_{smp}$ and $CorF_{fix}$ in Fig.4.4. Therefore, we can conclude that the influence of the Coriolis forces on the natural frequencies of a bellows is even less than shown in Tables 4.1 and 4.2.

4.4. The Influence of Inside Pressure and the Centrifugal Force of the Flow on Transverse Vibration of Bellows

Let us derive the differential equation which, in addition to Bernoulli-Euler conditions, takes into account the static inside pressure and the centrifugal force of the inside flow. The differential element of such a pipe is shown in Fig.4.5. The moment equation with respect to point O is

$$\frac{\partial M}{\partial x}dx - Q\,dx + P\pi R_m^2\,dw = 0,$$

from where the shear force Q is

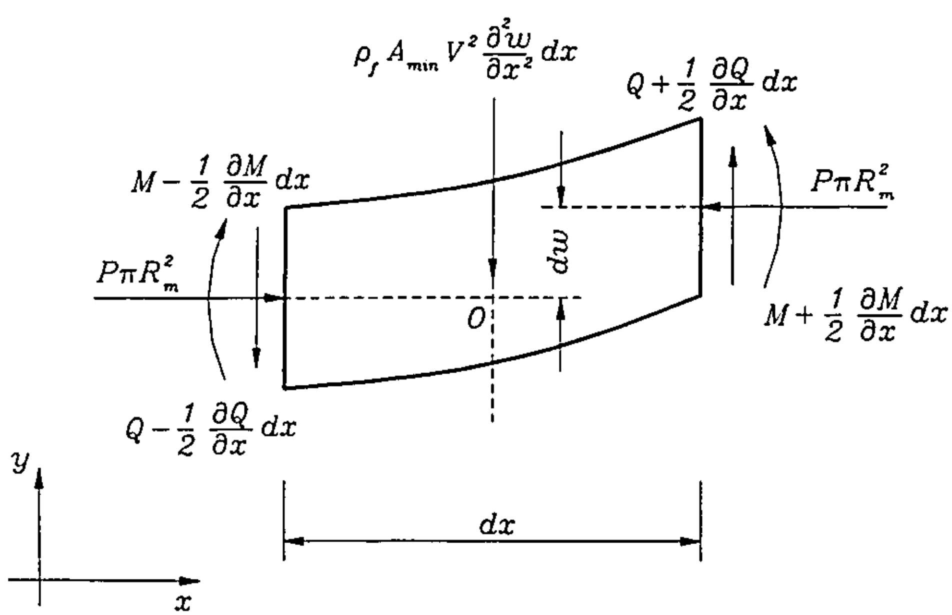

Fig.4.5. Differential element of bellows

$$Q = \frac{\partial M}{\partial x} + P\pi R_m^2\frac{\partial w}{\partial x}, \tag{4.13}$$

where

Q and M are the shear force and the moment in the bellows respectively,

P is the pressure in the bellows.

The translation differential equation with respect to the y direction is

$$m_b \frac{\partial^2 w}{\partial t^2} dx = -\rho_f A_{min} \mathrm{v}^2 \frac{\partial^2 w}{\partial x^2} dx - \frac{\partial Q}{\partial x} dx$$

or

$$m_b \frac{\partial^2 w}{\partial t^2} + \rho_f A_{min} \mathrm{v}^2 \frac{\partial^2 w}{\partial x^2} + \frac{\partial Q}{\partial x} = 0, \tag{4.14}$$

where A_{min} is the clear cross-section of the bellows (see Fig. 2.1):

$$A_{min} = \pi \left(R_m - \frac{L}{2} - R_1 - \frac{t}{2} \right)^2 .$$

From beam theory,

$$M = EI \frac{\partial^2 w}{\partial x^2} . \tag{4.15}$$

Substitution of (4.15) into (4.13), and subsequent substitution of (4.13) into 4.14) yields the desired differential equation for transverse vibration

$$EI \frac{\partial^4 w}{\partial x^4} + \left(P \pi R_m^2 + \rho_f A_{min} \mathrm{v}^2 \right) \frac{\partial^2 w}{\partial x^2} + m_b \frac{\partial^2 w}{\partial t^2} = 0. \tag{4.16}$$

It is seen from this equation that the effects of both pressurization and centrifugal force on the vibrating pipe are similar in that they are both coefficients of the curvature term, $\partial^2 w / \partial x^2$. Therefore, the differential equation which takes into account either or both of these two factors can be written in general as

$$EI\frac{\partial^4 w}{\partial x^4} + \eta\frac{\partial^2 w}{\partial x^2} + m_b\frac{\partial^2 w}{\partial t^2} = 0,$$

where η in this equation represents either the pressure coefficient, $P\pi R_m^2$, or the centrifugal force coefficient, $\rho_f A_{min} v^2$, or both of them taken together. The division of the above equation by *EI* gives

$$\frac{\partial^4 w}{\partial x^4} + \frac{\eta}{EI}\frac{\partial^2 w}{\partial x^2} + \frac{m_b}{EI}\frac{\partial^2 w}{\partial t^2} = 0. \qquad (4.17)$$

If

$$\sqrt{\frac{\eta}{2EI}} = c \qquad (4.18)$$

and

$$\sqrt[4]{\frac{m_b}{EI}} = a, \qquad (4.19)$$

then the differential equation (4.17) can be rewritten as

$$\frac{\partial^4 w}{\partial x^4} + 2c^2\frac{\partial^2 w}{\partial x^2} + a^4\frac{\partial^2 w}{\partial t^2} = 0. \qquad (4.20)$$

Let

$$w = X(x)\,T(t). \qquad (4.21)$$

Then, if *T(t)* is some harmonic function, the derivatives of (4.21) needed in eq.(4.20) are

$$\frac{\partial^4 w}{\partial x^4} = T\frac{dX^4}{dx^4}, \quad \frac{\partial^2 w}{\partial x^2} = T\frac{dX^2}{dx^2}, \quad \text{and} \quad \frac{\partial^2 w}{\partial t^2} = -\omega^2 XT.$$

Substitution of the above derivatives into (4.20) gives

$$\frac{dX^4}{dx^4} + 2c^2\frac{dX^2}{dx^2} - \lambda^4 X = 0, \tag{4.22}$$

where

$$\lambda^4 = a^4\omega^2. \tag{4.23}$$

Now let

$$X = Ce^{sx}.$$

Then

$$\frac{dX^4}{dx^4} = Cs^4e^{sx} \quad \text{and} \quad \frac{dX^2}{dx^2} = Cs^2e^{sx}.$$

Substitution of the above derivatives into (4.22) gives the quartic equation

$$s^4 + 2c^2s^2 - \lambda^4 = 0,$$

the roots of which are

$$s_{1,2} = \pm\alpha,$$

$$s_{3,4} = \pm i\beta,$$

where

$$\alpha = \sqrt{-c^2 + \sqrt{c^4 + \lambda^4}} \tag{4.24}$$

$$\beta = \sqrt{c^2 + \sqrt{c^4 + \lambda^4}}. \tag{4.25}$$

Solution of equation (4.22) can be written as

$$X = C_3e^{\alpha x} + C_4e^{-\alpha x} + C_5e^{i\beta x} + C_6e^{-i\beta x}. \tag{4.26}$$

By letting

$$C_3 = \frac{B+A}{2}, \quad C_4 = \frac{B-A}{2}, \quad C_5 = \frac{D-iC}{2}, \quad \text{and} \quad C_6 = \frac{D+iC}{2},$$

equation (4.26) can be rewritten as follows

$$X = A\sinh\alpha x + B\cosh\alpha x + C\sin\beta x + D\cos\beta x \tag{4.27}$$

and the derivative of which becomes

$$\frac{dX}{dx} = A\alpha\cosh\alpha x + B\alpha\sinh\alpha x + C\beta\cos\beta x - D\beta\sin\beta x. \tag{4.28}$$

Let's consider the fixed-fixed case of the pipe. Then the four required boundary conditions are:

$$X(0) = \frac{dX(0)}{dx} = X(l) = \frac{dX(l)}{dx} = 0.$$

Substitution of (4.27) and (4.28) into these four boundary conditions results in a system of linear simultaneous equations with respect to A, B, C, and D:

$$\begin{aligned}
&B + D = 0, \\
&A\alpha + C\beta = 0, \\
&A\sinh\alpha l + B\cosh\alpha l + C\sin\beta l + D\cos\beta l = 0, \\
&A\alpha\cosh\alpha l + B\alpha\sinh\alpha l + C\beta\cos\beta l - D\beta\sin\beta l = 0.
\end{aligned}$$

For a non-trivial solution, the determinant formed by the coefficients of this equation must be equal to zero:

$$\begin{vmatrix} 0 & 1 & 0 & 1 \\ \alpha & 0 & \beta & 0 \\ \sinh(\alpha l) & \cosh(\alpha l) & \sin(\beta l) & \cos(\beta l) \\ \alpha\cosh(\alpha l) & \alpha\sinh(\alpha l) & \beta\cos(\beta l) & -\beta\sin(\beta l) \end{vmatrix} = 0.$$

The expansion of the determinant results in the frequency equation for differential equation (4.20):

$$\left(\frac{\beta}{\alpha} - \frac{\alpha}{\beta}\right)\sinh(\alpha l)\ \sin(\beta l) + 2\cosh(\alpha l)\ \cos(\beta l) - 2 = 0. \tag{4.29}$$

Now we will investigate the influence of the inside pressure only. Then

$$\eta = P\pi R_m^2. \tag{4.30}$$

According to EJMA Standard (1980), the critical pressure for bellows,

$$P_{cr} = \frac{\pi k p}{l^2}$$

and the maximum allowed (design pressure) is just small fraction of it:

$$P_{max} = \frac{P_{cr}}{6.666} = \frac{\pi k p}{6.666\, l^2}. \tag{4.31}$$

According to (3.1),

$$EI = \frac{1}{4} k p R_m^2. \tag{4.32}$$

Substitution of (4.31) into (4.30) and subsequently (4.30) into (4.18) gives

$$c = 0.5477\frac{\pi}{l}.$$

For a real bellows length, say, $l = 2R_m = 0.0693$ m,

$$c = 24.831 \quad 1/\mathrm{m}^2 .$$

Now, using the numerical value of c and expressions for α ,(4.24), and β, (4.25), the frequency equation (4.29) can be solved numerically. The computerized solution for the first frequency gave $\lambda_1 = 65.61205$. From (4.23),

$$\omega = \frac{\lambda^2}{a^2}.$$

Substitution the expression (4.19) for a and the calculated λ_1 value into the above formula finally gives the first mode natural frequency of the 0.0693 m length fixed-fixed bellows:

$$\omega_1 = 4305.00\sqrt{\frac{EI}{m_b}}. \tag{4.33}$$

Let us express the natural frequency of the bellows when the inside-outside pressure difference is equal to zero. Then the second term in differential equation (4.20) and the solution of this simplified equation for the first mode of the fixed-fixed beam becomes the well known expression,

$$\omega = \frac{4.73^2}{l^2}\sqrt{\frac{EI}{m_b}}.$$

Substituting in the bellows length, $l = 0.0693$ m, gives

$$\omega = 4658.68\sqrt{\frac{EI}{m_b}}. \tag{4.34}$$

Comparison of the two frequencies (4.33) and (4.34) shows that taking into account the maximum pressure allowed by the EJMA Standard, the natural frequency becomes lower by 7.6%.

Now we will investigate the influence of the centrifugal fluid force on the natural frequencies of bellows. We can do this by comparing the two parts of the coefficient of the curvature term, $\partial w^2/\partial x^2$, in the differential equation (4.16), $P\pi R_m^2$ and $\rho_f A_{min} \mathrm{v}^2$. Using the same numerical values for geometrical and physical parameters, we can calculate the ratio,

$$\frac{\rho_f A_{min} \mathrm{v}^2}{P_{max} \pi R_m^2} = \frac{1000\left(0.003148\right)\left(10^2\right)}{6260.48} = 0.05 .$$

This ratio demonstrates that the influence of the centrifugal force is just 5% of the influence of the maximum allowed pressure, 7.6%. Thus, the natural frequency is lower by just $0.05 \times 7.6\% = 0.38\%$ even at such high fluid velocities as $\mathrm{v} = 10$ m/s.

4.5. Assumptions and Derivation of Differential Equation of Transverse Vibration of Bellows Using Newtonian Approach.

As shown in the previous sections, the influence of both Coriolis and centrifugal forces of flowing fluid on the natural frequency of bellows is smaller than 1% even for the highest possible fluid velocities in bellows. Furthermore, the effects of these two forces, at least for the odd number of vibration modes, oppose each other with respect to their effects on the natural frequency of bellows. Therefore, these two forces will be neglected in subsequent investigations of the vibration of bellows. As shown in Section 4.2, the influence of shear, due to the very high flexibility of bellows, is also negligibly small. Therefore, it can be ignored as well. The only remaining effects to be taken into account are the inertia of rotation, the pressurization effect, and two types of added fluid mass.

Considering the assumptions made, the derivation of the differential equation of the transverse vibration of the expansion joint is as follows.

In Fig.4.5 is shown the differential element of bellows with all the forces and moments acting on it. The moment differential equation about point O is:

$$J\frac{\partial^3 w}{\partial x\,\partial t^2}dx = \frac{\partial M}{\partial x}dx - Q\,dx + P\pi R_m^2\,dw\,,$$

where J is the total mass moment of bellows per bellows unit length. The transverse shear force is therefore:

$$Q = \frac{\partial M}{\partial x} + P\pi R_m^2\frac{dw}{dx} - J\frac{\partial^3 w}{\partial x\,\partial t^2}. \tag{4.33}$$

For a beam, the moment M is related to the lateral deflection by

$$M = EI\frac{\partial^2 w}{\partial x^2}.$$

Using this relationship, the shear force expression (4.33) can be rewritten as follows:

$$Q = EI\frac{\partial^3 w}{\partial x^3} + P\pi R_m^2\frac{dw}{dx} - J\frac{\partial^3 w}{\partial x\,\partial t^2}. \tag{4.34}$$

The differential equation for translation with respect to the y axis is:

$$m_{tot}\frac{\partial^2 w}{\partial t^2}dx = -\frac{\partial Q}{\partial x}dx$$

or

$$m_{tot}\frac{\partial^2 w}{\partial t^2} + \frac{\partial Q}{\partial x} = 0. \tag{4.35}$$

Differentiation of equation (4.34) with respect to coordinate x gives:

$$\frac{\partial Q}{\partial x} = \frac{\partial^4 w}{\partial x^4} + P\pi R_m^2\frac{\partial^2 w}{\partial x^2} - J\frac{\partial^4 w}{\partial x^2\,\partial t^2}.$$

Substitution of the last equation into (4.35) gives the differential equation of the transverse vibration of bellows:

$$EI\frac{\partial^4 w}{\partial x^4} + P\pi R_m^2\frac{\partial^2 w}{\partial x^2} - J\frac{\partial^4 w}{\partial x^2\,\partial t^2} + m_{tot}\frac{\partial^2 w}{\partial t^2} = 0, \tag{4.36}$$

where m_{tot} is given by (3.57),

$$m_{tot} = \frac{4\pi R_m}{p}\left(h + 0.285\,p\right)t\rho_b + \left[\pi\left(R_m - \frac{h}{2} + \frac{2hR_2}{p}\right)^2 + \alpha_{f2k}\,\mu R_m^3\right]\rho_f$$

and J is given by (3.67),

$$J = \pi R_m^3\left[\left(2\frac{h}{p} + 0.571\right)t\rho_b + \frac{h}{p}\left(2R_2 - t\right)\rho_f\right],$$

and the bending stiffness of bellows is given by (3.1):

$$EI = \frac{1}{4}kpR_m^2 .$$

CHAPTER 5

THEORETICAL INVESTIGATION OF NATURAL TRANSVERSE VIBRATIONS OF SINGLE BELLOWS EXPANSION JOINT

5.1. Solution of Differential Equation

The differential equation of the transverse vibration of bellows as derived in Chapter 4, eq.(4.36) is as follows:

$$EI\frac{\partial^4 w}{\partial x^4} + P\pi R_m^2 \frac{\partial^2 w}{\partial x^2} - J\frac{\partial^4 w}{\partial x^2 \partial t^2} + m_{tot}\frac{\partial^2 w}{\partial t^2} = 0. \qquad (5.1)$$

Bellows are usually fixed to much stiffer pipes in comparison with the bellows itself. Therefore, with a high degree of confidence, bellows may be considered as being fixed at both ends, as shown in Fig.5.1, where boundary conditions are just geometrical:

$$w(0,t) = \frac{\partial w(0,t)}{\partial x} = w(l,t) = \frac{\partial w(l,t)}{\partial x} = 0. \tag{5.2}$$

We employ a separation of variables approach by expressing w as the product of a function $X(x)$ and some harmonic function, $T(t)$. Thus,

$$w = X(x)\,T(t)\,. \tag{5.3}$$

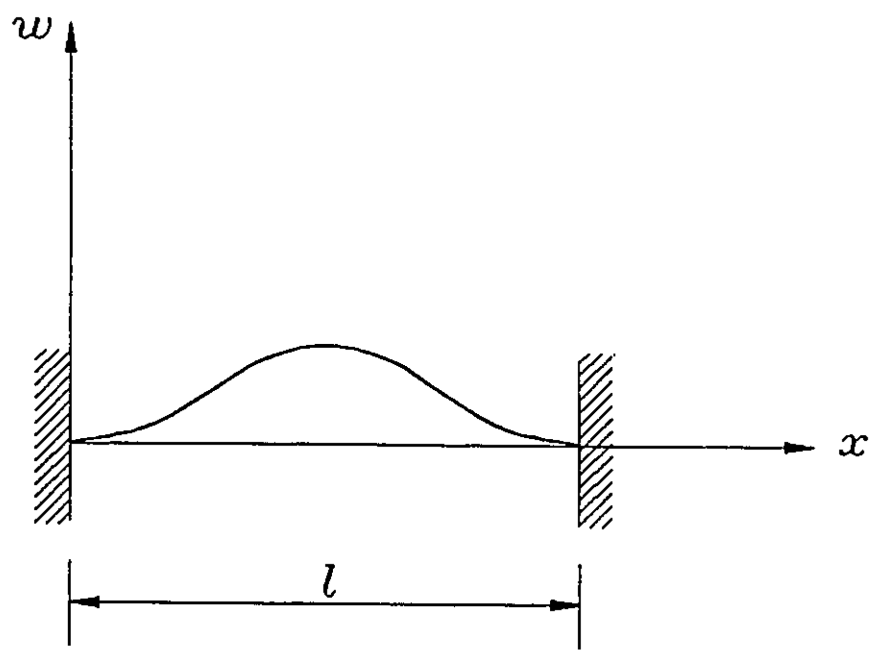

Fig.5.1. Mathematical model of the single bellows with fixed ends

Substitution of (5.3) into (5.1) and (5.2), and following division by $T(t)$ leads to the ordinary differential equation

$$EI\frac{d^4X}{dx^4} + P\pi R_m^2\frac{d^2X}{dx^2} + J\omega^2\frac{d^2X}{dx^2} - \omega^2 m_{tot}X = 0 \tag{5.4}$$

and boundary conditions

$$X(0) = \frac{dX(0)}{dx} = X(l) = \frac{dX(l)}{dx} = 0. \tag{5.5}$$

Now we multiply both sides of the differential equation (5.4) by X and integrate over the domain of the bellows, according to Voltera and Zachmanoglou (1965):

$$EI\int_0^l \frac{d^4X}{dx^4}Xdx + P\pi R_m^2\int_0^l \frac{d^2X}{dx^2}Xdx + J\omega^2\int_0^l \frac{d^2X}{dx^2}Xdx - \omega^2 m_{tot}\int_0^l X^2\,dx = 0.$$

Integrating the first integral by parts with respect to coordinate twice, and the second and third just once, we get:

$$EI\left[\frac{d^3X}{dx^3}X\Big|_0^l - \frac{d^2X}{dx^2}\frac{dX}{dx}\Big|_0^l + \int_0^l\left(\frac{d^2X}{dx^2}\right)^2 dx\right] + P\pi R_m^2\left[\frac{dX}{dx}X\Big|_0^l - \int_0^l\left(\frac{dX}{dx}\right)^2 dx\right]$$
$$+ J\omega^2\left[\frac{dX}{dx}X\Big|_0^l - \int_0^l\left(\frac{dX}{dx}\right)^2 dx - \omega^2 m_{tot}\int_0^l X^2dx\right] = 0,$$

or, after substitution of bounds:

$$EI\left[\frac{d^3X(l)}{dx^3}X(l) - \frac{d^3X(0)}{dx^3}X(0) - \frac{d^2X(l)}{dx^2}\frac{dX(l)}{dx} + \frac{d^2X(0)}{dx^2}\frac{dX(0)}{dx}\right.$$
$$\left.+ \int_0^l\left(\frac{d^2X}{dx^2}\right)^2 dx\right] + P\pi R_m^2\left[\frac{dX(l)}{dx}X(l) - \frac{dX(0)}{dx}X(0) - \int_0^l\left(\frac{dX}{dx}\right)^2 dx\right]$$
$$+ J\omega^2\left[\frac{dX(l)}{dx}X(l) - \frac{dX(0)}{dx}X(0) - \int_0^l\left(\frac{dX}{dx}\right)^2 dx\right] - \omega^2 m_{tot}\int_0^l X^2dx = 0.$$

Substitution of boundary conditions (5.5) into the above expression yields:

$$EI\int_0^l\left(\frac{d^2X}{dx^2}\right)^2dx - P\pi R_m^2\int_0^l\left(\frac{dX}{dx}\right)^2dx - J\omega^2\int_0^l\left(\frac{dX}{dx}\right)^2dx - \omega^2 m_{tot}\int_0^l X^2dx = 0.$$

Now the Rayleigh quotient for the fixed-fixed single bellows expansion joint can be expressed as follows:

$$\omega^2 = \frac{EI\int_0^l\left(\frac{d^2X}{dx^2}\right)^2dx - P\pi R_m^2\int_0^l\left(\frac{dX}{dx}\right)^2dx}{m_{tot}\int_0^l X^2dx + J\int_0^l\left(\frac{dX}{dx}\right)^2dx}. \tag{5.6}$$

The above expression is the so called "Rayleigh quotient" applied to the fixed-fixed bellows as a beam. With the exact eigenfunction X in the quotient, we clearly obtain the exact eigenvalue, ω. Often, the exact eigenfunction X is not known in advance. Therefore, the approximate function $\widetilde{X}$ is used, which reasonably resembles the particular mode shape and exactly satisfies given boundary conditions. Textbooks on vibrations usually advise use of the statical deflection curve caused, for example, by a uniformly distributed load, as the approximate eigenfunction $\widetilde{X}$. Thus, by using $\widetilde{X}_1$ in the Rayleigh quotient, we obtain an approximate eigenvalue, $\widetilde{\omega}_1^2$. It is shown in Beards (1983) that the Rayleigh quotient is a functional that has an extremum with respect to admissible functions, $\widetilde{X}_1$ satisfying the boundary conditions, the extremal function being the eigenfunction, X_1. This means that using a function, $\widetilde{X}_1$, in the Rayleigh quotient such that $\left(\widetilde{X}_1 - X_1\right)$ has a small average value over the beam, will result in an even smaller value for $\left(\widetilde{\omega}_1^2 - \omega_1^2\right)$, i.e. a good estimate of the mode shape gives an even better estimate of the natural frequency.

As an approximation for $\widetilde{X}_1$ in the Rayleigh quotient a static deflection curve satisfying the boundary conditions can be used. A better approximation can be obtained by using the solution of the simple Bernoulli-Euler differential equation. Then the precision of the eigenvalue, $\widetilde{\omega}_1^2$, calculated this way must be greater. Therefore, the next section of this chapter is concerned with the solution of the eigenfunction of the Bernoulli-Euler equation for the boundary conditions identical to those considered in this section.

5.2. Single Bellows Type Expansion Joint Natural Frequencies

The natural frequency formula for a universal expansion joint can be now easily derived from the Rayleigh quotient expression given in the previous section. Let ξ be the dimensionless coordinate:

$$\xi = \frac{x}{l}.$$

Upon substitution into (5.6), the natural frequency becomes:

$$f_k = \frac{1}{2\pi}\,\frac{A_1}{l^2}\sqrt{\frac{EI}{m_{tot}}}\sqrt{\frac{1 - A_2\dfrac{l^2}{EI}P\pi R_m^2}{1 + A_4\dfrac{J}{m_{tot}l^2}}}\,, \tag{5.7}$$

where

$$A_1 = \sqrt{\frac{\int_0^1 \left(\frac{d^2X}{d\xi^2}\right)^2 d\xi}{\int_0^1 X^2 d\xi}}, \quad A_2 = \frac{\int_0^1 \left(\frac{dX}{d\xi}\right)^2 d\xi}{\int_0^1 \left(\frac{d^2X}{d\xi^2}\right)^2 d\xi}, \quad A_4 = \frac{\int_0^1 \left(\frac{dX}{d\xi}\right)^2 d\xi}{\int_0^1 X^2 d\xi}, \tag{5.8}$$

Since, according to (3.1),

$$EI_{eq} = \frac{1}{4} kpR_m^2,$$

the final expression for the natural frequency of the transverse vibration of a single expansion joint becomes:

$$f_k = \frac{1}{4\pi} \frac{A_1 R_m}{l^2} \sqrt{\frac{kp}{m_{tot}}} \sqrt{\frac{1 - 4\pi A_2 \frac{l^2}{kp} P}{1 + A_4 \frac{J}{m_{tot} l^2}}}, \tag{5.9}$$

It follows from equation (5.9) that, in order to obtain the final expression for the frequency, f_k, it is necessary to calculate the nondimensional coefficients A_i, (5.8), in which the mode function, X, and its first and second derivatives are involved. The values of the integrals residing in the coefficients, A_i, may be calculated by integrating them algebraically or numerically.

It was explained above that the mode function for bellows (with a high degree of precision) can be approximated by the exact solution of the simpler Bernoulli-Euler equation with the same boundary conditions (5.5), (see, for example, Filipov (1965)):

$$X_k = (\sinh r_k - \sin r_k)(\cosh r_k\xi - \cos r_k\xi) - (\cosh r_k - \cos r_k)(\sinh r_k\xi - \sin r_k\xi).$$

For the first four modes,

$r_1 = 4.73004$, $r_2 = 7.8532045$, $r_3 = 10.9956075$, $r_4 = 14.1371669$.

Thus, the first mode function can be written as

$$X_1 = 1.01781(\cosh r_1\xi - \cos r_1\xi) - \sinh r_1\xi + \sin r_1\xi \ .$$

The first and the second derivatives of X_1 are

$$\frac{dX_1}{d\xi} = r_1\left[1.01781\left(\sinh r_1\xi + \sin r_1\xi\right) - \left(\cosh r_1\xi + \cos r_1\xi\right)\right],$$

$$\frac{d^2X_1}{d\xi^2} = r_1^2\left[1.01781\left(\cosh r_1\xi + \cos r_1\xi\right) - \left(\sinh r_1\xi - \sin r_1\xi\right)\right].$$

Using the mode functions and their derivatives, the coefficients A_i were calculated for the first four frequencies as shown in table 5.1.

Table 5.1. Coefficients A_i for the first four modes of single bellows expansion joint

Mode #	1	2	3	4
A_1	22.37	61.67	120.9	199.9
A_2	0.02458	0.01211	0.00677	0.00374
A_4	12.30	46.05	98.91	149.4

The total mass, required in equation (5.9), was derived in Chapter 3 and defined by equation (3.57):

$$m_{tot} = 4\pi R_m\left(\frac{h}{p} + 0.285\right)t\rho_b + \left[\pi\left(R_m - \frac{h}{2} + \frac{2hR_2}{p}\right)^2 + \alpha_{f2k}\,\mu R_m^3\right]\rho_f \ .$$

α_{f2k} has been calculated using formula (3.26),

$$\alpha_{f2k} = \frac{0.066}{l^4} \frac{\int_0^1 \left(\frac{d^2X}{d\xi^2}\right)^2 d\xi}{\int_0^1 X_k^2 \, d\xi} \left(R_m - \frac{h}{2}\right)^2 p \ ,$$

or

$$\alpha_{f2k} = 0.066 \frac{A_1^2}{l^4} \left(R_m - \frac{h}{2}\right)^2 p \ .$$

The total moment of inertia of the cross-section of a bellows was given by (3.67) as follows:

$$J = \pi R_m^3 \left[\left(2\frac{h}{p} + 0.571 \right) t\rho_b + \frac{h}{p}(2R_2 - t)\rho_f \right].$$

All geometrical and physical parameters residing in expressions for m_{tot} and J above are listed in Chapter 3 during their derivations.

5.3. The Exact Solution of Single Bellows Expansion Joint Natural Frequencies and its Comparison with Rayleigh Quotient Solution

The approximate natural frequency formula for a single bellows expansion joint was derived in the previous section using the Rayleigh method. Now we will solve the same problem exactly, in order to find the error present in the approximate solution (5.9).

The governing differential equation (5.4) from Section 5.1 is:

$$EI\frac{d^4X}{dx^4} + P\pi R_m^2 \frac{d^2X}{dx^2} + J\omega^2 \frac{d^2X}{dx^2} - \omega^2 m_{tot} X = 0 \, .$$

After division by *EI*,

$$\frac{d^4X}{dx^4} + \frac{P\pi R_m^2 + J\omega^2}{EI}\frac{d^2X}{dx^2} - \omega^2\frac{m_{tot}}{EI}X = 0. \tag{5.10}$$

Setting:

$$c = \sqrt{\frac{P\pi R_m^2 + J\omega^2}{2EI}} \tag{5.11}$$

and

$$\lambda = \sqrt{\frac{m_{tot}\omega^2}{EI}}, \tag{5.12}$$

eq.(5.10) becomes

$$\frac{d^4X}{dx^4} + 2c^2\frac{d^2X}{dx^2} - \lambda^4 X = 0\,.$$

This is the same equation as (4.22) in Section 4.4. Since the boundary conditions are the same as well, the characteristic equation is given by equation (4.29):

$$\left(\frac{\beta}{\alpha} - \frac{\alpha}{\beta}\right)\sinh\alpha l \sin\beta l + 2\cosh\alpha l \cos\beta l - 2 = 0\,, \tag{5.13}$$

where α and β are given by (4.24) and (4.25):

$$\alpha = \sqrt{-c^2 + \sqrt{c^4 + \lambda^4}}\,, \tag{5.14}$$

$$\beta = \sqrt{c^2 + \sqrt{c^4 + \lambda^4}}\,. \tag{5.15}$$

Taking the single bellows with geometrical and physical parameters, bellows length, l = 0.0693 m, mass moment of inertia per unit length, J = 0.001153 kgm,

EI = 5.078 Nm , and total mass, m_{tot} = 5.138 kg/m, according to (4.31), the maximum allowed pressure in the bellows is

$$P_{max} = \frac{\pi k p}{6.666 l^2} \quad (5.16)$$

As derived in Chapter 3, equation (3.1) gives:

$$EI = \frac{1}{4} k p R_m^2 . \quad (5.17)$$

Substitution of (5.16), (5.17) and the numerical values given above into (5.11) and (5.12) leads to

$$c = \sqrt{616.49 + 0.0001135\omega^2} \quad (5.18)$$

and

$$\lambda = 1.0029\sqrt{\omega} . \quad (5.19)$$

Now, using expressions (5.18), (5.19), (5.14) and (5.15), the frequency equation (5.13) can be solved with the computer's precision. The first three natural frequencies obtained from the computerized solution of (5.13) are given in Table 5.2 as the exact natural frequency, Exact ω.

Table 5.2. Comparison of the exact and approximate frequency solutions for the single bellows expansion joint

Mode #	Exact ω	Rayleigh ω	Error
	(rad/s)	(rad/s)	(%)
1	3400.334	3410.76	0.30
2	6490.355	6927.59	0.54
3	10401.470	10341.04	0.58

The first three natural frequencies were also calculated for the same bellows data using frequency formula (5.9) derived in the previous section from the Rayleigh quotient. Both results are compared in Table 5.1. The error of the frequency obtained from the Rayleigh quotient is about 0.5% or less at least for the first three modes. Therefore, the approximate Rayleigh quotient formula (5.9) is precise enough to use for the natural frequency estimation of single bellows expansion joints.

5.4. Instability Condition for Single Bellows Expansion Joint

It is obvious from eq.(5.9) that for a particular combination of the parameters P, p, k, and l, the numerator of the expression under the last root can become equal to zero:

$$1 - 4\pi A_2 \frac{l^2}{kp} P = 0 .$$

From this the instability pressure criteria becomes

$$P_{cr} = \frac{kp}{4\pi A_2 l^2} ,$$

or the first mode critical pressure,

$$P_{cr} = 3.238 \frac{kp}{l^2} . \tag{5.20}$$

This is the approximate P_{cr} solution, but it is quite close to the stability condition obtained from the exact solution, Chen and Lui (1987), of the Bernoulli-Euler equation (first mode):

$$P_{cr} = \frac{\pi k p}{l^2} .$$

CHAPTER 6

THEORETICAL INVESTIGATION OF NATURAL VIBRATIONS OF UNIVERSAL EXPANSION JOINT LATERAL MODE

6.1. Derivation of Boundary Conditions for Vibration of a Universal Expansion Joint in Lateral Mode

As seen from Fig.6.1, in the case of the vibration of bellows in lateral modes, the connecting pipe performs pure translational motion because of the geometrical and physical symmetry of the system, provided the Coriolis forces acting on the bellows from the fluid flowing inside are neglected. Therefore, as a mathematical approximation, one half of the physical system can be considered with its left end fixed and right end fixed to the vertical rollers, as shown in Fig.6.1.

Since at end A the bellows can be considered as fixed, the first two boundary conditions are simply geometrical,

$$w(0,t) = \frac{\partial w(0,t)}{\partial x} = 0. \tag{6.1}$$

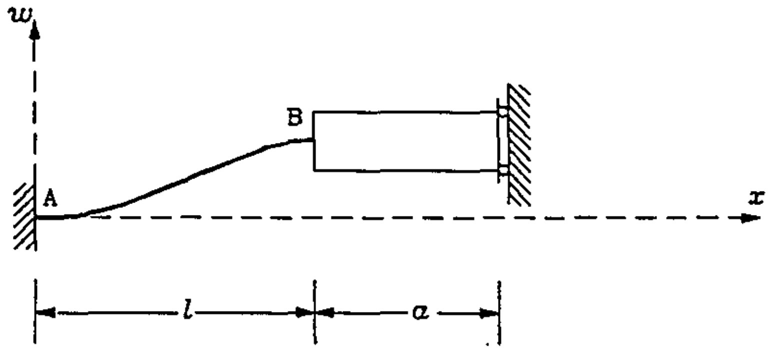

a) First mode shape

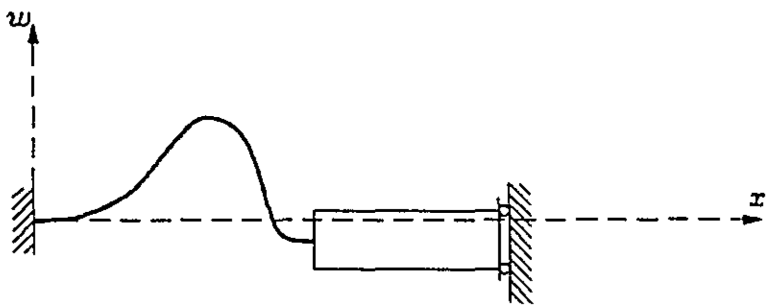

b) Second mode shape

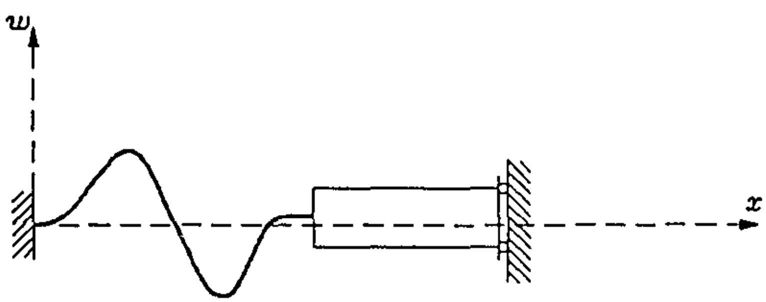

c) Third mode shape

Fig.6.1. Mathematical models of universal expansion joint for the lateral modes

It is not difficult to write the geometrical boundary condition at the end B. Since it doesn't rotate,

$$\frac{\partial w(l,t)}{\partial x} = 0. \tag{6.2}$$

The fourth boundary condition can be derived considering the translational motion of the left half of the connecting pipe. The differential equation of the connecting pipe together with lateral supports in this case is:

$$\left[M_h + \left(m_p + m_{f3}\right) a\right] \frac{\partial^2 w(l,t)}{\partial t^2} = Q(l,t) + F_{sp}. \tag{6.3}$$

where

a is the length of 1/2 of the connecting pipe,

m_p is the connecting pipe mass per unit length,

m_{f3} is the fluid mass per unit length in the connecting pipe,

$Q(l,t)$ is the shear force at the bellows end B,

M_h is the equivalent lateral support mass,

F_{sp} is the lateral support transverse stiffness force:

$$F_{sp} = -k_h\, w(l,t), \tag{6.4}$$

where k_h is the equivalent spring stiffness of the lateral support.

Substitution of (4.34) and (6.4) into the expression (6.3) gives

$$\left[M_h + \left(m_p + m_{f3}\right)a\right] \frac{\partial^2 w(l,t)}{\partial t^2} = -k_h w(l,t) + EI \frac{\partial^3 w(l,t)}{\partial x^3} + P\pi R_m^2 \frac{\partial w(l,t)}{\partial x} - J \frac{\partial^3 w(l,t)}{\partial x\, \partial t^2}.$$

Since the connecting pipe doesn't rotate, the last two terms in the above equation are zero, and the final expression of the fourth boundary condition becomes

$$\frac{\partial^3 w(l,t)}{\partial x^3} = \frac{1}{EI}\left[M_h + \left(m_p + m_{f3}\right)a\right]\frac{\partial^2 w(l,t)}{\partial t^2} + \frac{k_h}{EI}w(l,t). \tag{6.5}$$

6.2. Solution of Differential Equation

The differential equation for bellows was derived in Chapter 4 and is given by:

$$EI\frac{\partial^4 w}{\partial x^4} + P\pi R_m^2\frac{\partial^2 w}{\partial x^2} - J\frac{\partial^4 w}{\partial x^2\,\partial t^2} + m_{tot}\frac{\partial^2 w}{\partial t^2} = 0, \tag{6.6}$$

Using separation of variables by expressing w as the product of a function $X(x)$ and some harmonic function, $T(t)$,

$$w = X(x)\;T(t). \tag{6.7}$$

Substitution of (6.7) into (6.6), (6.5), (6.2), (6.1) and following division by $T(t)$ leads to the ordinary differential equation

$$EI\frac{d^4X}{dx^4} + P\pi R_m^2\frac{d^2X}{dx^2} + J\omega^2\frac{d^2X}{dx^2} - \omega^2 m_{tot}X = 0, \tag{6.8}$$

and boundary conditions:

$$X(0) = \frac{dX(0)}{dx} = 0, \tag{6.9}$$

$$\frac{dX(l)}{dx} = 0, \tag{6.10}$$

$$\frac{d^3X(l)}{dx^3} = -\frac{\omega^2}{EI}\left[M_h + \left(m_p + m_{f3}\right)a\right]X(l) + \frac{k_h}{EI}X(l). \qquad (6.11)$$

Now we multiply both sides of the differential equation (6.8) by X and integrate over the domain of the bellows, Voltera and Zachmanoglou (1965):

$$EI\int_0^l \frac{d^4X}{dx^4}X\,dx + P\pi R_m^2\int_0^l \frac{d^2X}{dx^2}X\,dx + J\omega^2\int_0^l \frac{d^2X}{dx^2}X\,dx - \omega^2 m_{tot}\int_0^l X^2\,dx = 0.$$

Integrating by parts the first integral with respect to the coordinate twice, and the second and third just once, we obtain:

$$EI\left[\frac{d^3X}{dx^3}X\Big|_0^l - \frac{d^2X}{dx^2}\frac{dX}{dx}\Big|_0^l + \int_0^l\left(\frac{d^2X}{dx^2}\right)^2 dx\right] + P\pi R_m^2\left[\frac{dX}{dx}X\Big|_0^l - \int_0^l\left(\frac{dX}{dx}\right)^2 dx\right]$$

$$+ J\omega^2\left[\frac{dX}{dx}X\Big|_0^l - \int_0^l\left(\frac{dX}{dx}\right)^2 dx - \omega^2 m_{tot}\int_0^l X^2\,dx\right] = 0,$$

or, after substitution of bounds:

$$EI\left[\frac{d^3X(l)}{dx^3}X(l) - \frac{d^3X(0)}{dx^3}X(0) - \frac{d^2X(l)}{dx^2}\frac{dX(l)}{dx} + \frac{d^2X(0)}{dx^2}\frac{dX(0)}{dx}\right.$$

$$\left. + \int_0^l\left(\frac{d^2X}{dx^2}\right)^2 dx\right] + P\pi R_m^2\left[\frac{dX(l)}{dx}X(l) - \frac{dX(0)}{dx}X(0) - \int_0^l\left(\frac{dX}{dx}\right)^2 dx\right]$$

$$+ J\omega^2\left[\frac{dX(l)}{dx}X(l) - \frac{dX(0)}{dx}X(0) - \int_0^l\left(\frac{dX}{dx}\right)^2 dx\right] - \omega^2 m_{tot}\int_0^l X^2\,dx = 0.$$

Substitution of boundary conditions (6.9), (6.10), and (6.11) into the above expression gives:

$$-\frac{\omega^2}{EI}\left[M_h+\left(m_p+m_{f3}\right)a\right]X^2+\frac{k_h}{EI}X^2+EI\int_0^l\left(\frac{d^2X}{dx^2}\right)^2dx-P\pi R_m^2\int_0^l\left(\frac{dX}{dx}\right)^2dx$$

$$-J\omega^2\int_0^l\left(\frac{dX}{dx}\right)^2dx-\omega^2 m_{tot}\int_0^l X^2dx=0.$$

Now the Rayleigh quotient for the differential equation (6.6) and boundary condition set (6.1), (6.2), and (6.5), expressed from the equation above is

$$\omega^2=\frac{EI\int_0^l\left(\frac{d^2X}{dx^2}\right)^2dx-P\pi R_m^2\int_0^l\left(\frac{dX}{dx}\right)^2dx+k_hX^2(l)}{m_{tot}\int_0^l X^2dx+J\int_0^l\left(\frac{dX}{dx}\right)^2dx+\left[M_h+\left(m_p+m_{f3}\right)a\right]X^2(l)}, \tag{6.12}$$

This can be solved assuming some admissible function, $X(x)$, as an approximate mode function. The natural frequency is therefore:

$$f_k=\frac{1}{2\pi}\sqrt{\frac{EI\int_0^l\left(\frac{d^2X}{dx^2}\right)^2dx-P\pi R_m^2\int_0^l\left(\frac{dX}{dx}\right)^2dx+k_hX^2(l)}{m_{tot}\int_0^l X^2dx+J\int_0^l\left(\frac{dX}{dx}\right)^2dx+\left[M_h+\left(m_p+m_{f3}\right)a\right]X^2(l)}}. \tag{6.13}$$

As explained in Chapter 5, the approximate mode function for bellows (with a high degree of precision) can be taken as the solution of the Bernoulli-Euler equation. Therefore, the next section is devoted to the solution of the Bernoulli-Euler equation for the system shown in Fig.6.1.

6.3. Solution of Bernoulli-Euler Equation

When simplified to the Bernoulli-Euler conditions for the bellows, equation (6.6) becomes:

$$EI\frac{\partial^4 w}{\partial x^4} + m_{tot}\frac{\partial^2 w}{\partial t^2} = 0. \tag{6.14}$$

The boundary conditions were derived in Section 5.1:

$$w(0) = \frac{\partial w(0)}{\partial x} = 0, \tag{6.15}$$

$$\frac{\partial w(l)}{\partial x} = 0, \tag{6.16}$$

and

$$\frac{\partial^3 w(l,t)}{\partial x^3} = \frac{M_h + (m_p + m_{f3})a}{EI}\frac{\partial^2 w(l,t)}{\partial t^2} + \frac{k_h}{EI}w(l,t). \tag{6.17}$$

As in the previous section, taking $w = X(x)\,T(t)$, the differential equation (6.14) becomes

$$EI\frac{d^4 X}{dx^4} - \omega^2 m_{tot} X = 0,$$

or

$$\frac{d^4 X}{dx^4} - k^4 X = 0, \tag{6.18}$$

if

$$k^4 = \frac{\omega^2 m_{tot}}{EI}. \tag{6.19}$$

Boundary condition (6.17) becomes:

$$\frac{d^3X(l)}{dx^3} = -\frac{\omega^2\left[M_h+\left(m_p+m_{f3}\right)a\right]}{EI}X(l) + \frac{k_h}{EI}X(l)$$

or

$$\frac{d^3X(l)}{dx^3} = -bX(l) \tag{6.20}$$

if

$$b = \frac{\omega^2\left[M_h+\left(m_p+m_{f3}\right)a\right]}{EI} - \frac{k_h}{EI}. \tag{6.21}$$

The remaining boundary conditions, (6.16) and (6.15), become

$$\frac{dX(l)}{dx} = 0, \tag{6.22}$$

$$X(0) = \frac{dX(0)}{dx} = 0. \tag{6.23}$$

For the case where EI and m_{tot} are constants, the general solution of the equation (6.18), according to Babakov (1968), can be taken as follows:

$$X = AS(x) + BT(x) + CU(x) + DV(x), \tag{6.24}$$

where,

A, B, C, D are integration constants,

$S = \frac{1}{2}(\cosh kx + \cos kx),$

(6.25)

$$T = \frac{1}{2}\left(\sinh kx + \sin kx\right),$$

$$U = \frac{1}{2}\left(\cosh kx - \cos kx\right),$$

$$V = \frac{1}{2}\left(\sinh kx - \sin kx\right).$$

The boundary conditions (6.23) give $A = B = 0$ and the general solution (6.24) may be simplified to

$$X = CU(x) + DV(x), \tag{6.26}$$

the first three derivatives of which are:

$$\frac{dX}{dx} = CkT(x) + DkU(x),$$

$$\frac{d^2X}{dx^2} = Ck^2S(x) + Dk^2T(x),$$

$$\frac{d^3X}{dx^3} = Ck^3V(x) + Dk^3S(x).$$

Substitution of (6.26) and its derivatives into (6.20) and (6.22) leads to the system of linear equations with respect to constants C and D:

$$C\left[k^3V(l) + bU(l)\right] + D\left[k^3S(l) + bV(l)\right] = 0,$$
$$CT(l) + DU(l) = 0. \tag{6.27}$$

For a nontrivial solution, the determinant formed by the coefficients C and D in the above equations must be equal to zero:

$$\left| \begin{array}{c:c} k^3V(l)+bU(l) & k^3S(l)+bV(l) \\ \hdashline T(l) & U(l) \end{array} \right| = 0 .$$

The expansion of this determinant gives

$$k^3U(l)V(l) + bU^2(l) - k^3S(l)T(l) - bV(l)T(l) = 0 .$$

Substitution of the expressions for S, T, U, V given by (6.25) results in the frequency equation,

$$\cosh kl \ \sin kl + \sinh kl \ \cos kl - \frac{b}{k^3}\left(1 - \cosh kl \ \cos kl\right) = 0$$

or, after substituting b from (6.21), the frequency equation becomes

$$\cosh kl \ \sin kl + \sinh kl \ \cos kl$$
$$- \left[\frac{M_h + a\left(m_p + m_{f3}\right)}{l m_{tot}} kl - \frac{k_h}{\frac{EI}{l^3}} \frac{1}{(kl)^3} \right] \left(1 - \cosh kl \ \cos kl\right) = 0 .$$

Since the transverse stiffness of a fixed-fixed bellows as a beam, according to Frocht (1951), is

$$k_b = \frac{12\,EI}{l^3} ,$$

the frequency equation can be rewritten as

$$\cosh kl \ \sin kl + \sinh kl \ \cos kl$$
$$- \left[\frac{M_h + a\left(m_p + m_{f3}\right)}{l m_{tot}} kl - \frac{12\,k_h}{k_b} \frac{1}{(kl)^3} \right] \left(1 - \cosh kl \ \cos kl\right) = 0 . \qquad (6.28)$$

This is the frequency equation for the system shown in Fig.6.1. In the next two sections this frequency equation will be applied to find the mode functions of the Bernoulli-Euler equation (6.14) which will be used as the approximate mode functions for the approximate frequency, (6.13).

6.4. General Expression for Universal Expansion Joint Lateral Modes Natural Frequencies

The natural frequency formula for a universal expansion joint without lateral supports can now be easily acquired from the frequency expression (6.13) which, after substitution of the dimensionless coordinate $\xi = x/l$ becomes:

$$f_k = \frac{1}{2\pi}\sqrt{\frac{\dfrac{EI}{l^3}\displaystyle\int_0^1\left(\frac{d^2X}{d\xi^2}\right)^2 d\xi - \frac{P\pi R_m^2}{l}\int_0^1\left(\frac{dX}{d\xi}\right)^2 d\xi + k_h X^2(1)}{l m_{tot}\displaystyle\int_0^1 X^2 d\xi + \frac{J}{l}\int_0^1\left(\frac{dX}{d\xi}\right)^2 d\xi + \left[M_h + \left(m_p + m_{f3}\right)a\right]X^2(1)}},$$

or

$$f_k = \frac{1}{2\pi}\frac{A_1}{l^2}\sqrt{\frac{EI}{m_{tot}}}\sqrt{\frac{1 - A_2\dfrac{l^2}{EI}P\pi R_m^2 + A_3\dfrac{k_h l^3}{EI}}{1 + A_4\dfrac{J}{m_{tot}l^2} + A_5\dfrac{M_h + \left(m_p + m_{f3}\right)a}{m_{tot}l}}}, \tag{6.29}$$

where,

$$A_1 = \sqrt{\frac{\displaystyle\int_0^1\left(\frac{d^2X}{d\xi^2}\right)^2 d\xi}{\displaystyle\int_0^1 X^2 d\xi}}, \quad A_2 = \frac{\displaystyle\int_0^1\left(\frac{dX}{d\xi}\right)^2 d\xi}{\displaystyle\int_0^1\left(\frac{d^2X}{d\xi^2}\right)^2 d\xi}, \quad A_3 = \frac{X^2(1)}{\displaystyle\int_0^1\left(\frac{d^2X}{d\xi^2}\right)^2 d\xi},$$

$$A_4 = \frac{\int_0^1 \left(\frac{dX}{d\xi}\right)^2 d\xi}{\int_0^1 X^2 d\xi}, \qquad A_5 = \frac{X^2(1)}{\int_0^1 X^2 d\xi}. \tag{6.30}$$

Since, according to (3.1),

$$EI = \frac{1}{4} kpR_m^2,$$

the final expression for the natural frequency of the transverse vibration of a universal expansion joint in its lateral modes become:

$$f_k = \frac{1}{4\pi} \frac{A_1 R_m}{l^2} \sqrt{\frac{kp}{m_{tot}}} \sqrt{\frac{1 - 4\pi A_2 \frac{l^2}{kp} P + 4A_3 \frac{k_h l^3}{kpR_m^2}}{1 + A_4 \frac{J}{m_{tot} l^2} + A_5 \frac{M_h + \left(m_p + m_{f3}\right) a}{m_{tot} l}}}, \tag{6.31}$$

As seen from (6.31), in order to obtain the final expression for the frequency, f, it is necessary to calculate the integrals, residing in (6.30), in which the mode function, X, and its first and second derivatives are involved.

6.5. First Lateral Mode Natural Frequency of a Universal Expansion Joint without Lateral Supports

If there are no supports, then $k_h = 0$, $M_h = 0$, and the general frequency equation (6.28) becomes

$$\cosh kl\ \sin kl + \sinh kl\ \cos kl - \frac{a\left(m_p + m_{f3}\right)}{l m_{tot}} kl\left(1 - \cosh kl\ \cos kl\right) = 0. \qquad (6.32)$$

It is seen from the Fig.2.1 that for moderate convolution depth,

$$m_p + m_{f3} \cong m_{tot}.$$

Assume for the moment that the central pipe length $a = l$. Then the frequency equation (6.32) can be simplified to:

$$\cosh kl\ \sin kl + \sinh kl\ \cos kl - kl\left(1 - \cosh kl\ \cos kl\right) = 0,$$

the first frequency solution from which is $k_1 l = 1.71888$. Equation (6.26) can be re-written as:

$$X = U(x) + \frac{D}{C} V(x). \qquad (6.33)$$

Substitution of the $k_1 l$ value into the second of equations (6.27), gives the ratio

$$\frac{D}{C} = -\frac{T(l)}{U(l)} = -\frac{\sinh k_1 l + \sin k_1 l}{\cosh k_1 l - \cos k_1 l} = -1.218828.$$

Substitution of expressions for $U(x)$ and $V(x)$ from (6.25) and the value of the ratio D/C into (6.33) gives the exact mode function for the differential equation (6.14) which can be used as the approximate mode function for the calculation of the coefficients, A, in (6.30). This mode function, normalized to unity, becomes:

$$X = \frac{1}{0.9416}\left[\cosh c\frac{x}{l} - \cos c\frac{x}{l} - 1.218828\left(\sinh c\frac{x}{l} - \sin c\frac{x}{l}\right)\right], \qquad (6.34)$$

where $c = 1.718882$. Let

$$\frac{x}{l} = \xi.$$

Then the mode function (6.34) can be rewritten as

$$X = \frac{1}{0.9416}\left[\cosh c\xi - \cos c\xi - 1.21883\left(\sinh c\xi - \sin c\xi\right)\right],$$

the first and the second derivatives of which are:

$$\frac{dX}{dx} = \frac{c}{0.9416}\left[\sinh c\xi + \sin c\xi - 1.21883\left(\cosh c\xi - \cos c\xi\right)\right],$$

and

$$\frac{d^2X}{dx^2} = \frac{c^2}{0.9416}\left[\cosh c\xi + \cos c\xi - 1.21883\left(\sinh c\xi + \sin c\xi\right)\right].$$

Now values of the integrals in (6.30) can be obtained integrating them, numerically, using the computer. The value of $X(\xi)$ at $\xi = 1$ was calculated as $X(1) = 1.0$. Substitution of these values into expressions (6.30) gives:

$A_1 = 5.5411$, $A_2 = 0.10$, $A_4 = 3.1838$, $A_5 = 2.646$.

Substitution of these numerical values into (6.29) gives:

$$f_1 = \frac{1}{2\pi}\frac{5.6411}{l^2}\sqrt{\frac{EI}{m_{tot}}}\sqrt{\frac{1 - 0.1000\dfrac{l^2}{EI}P\pi R_m^2}{1 + \dfrac{3.1838J}{l^2 m_{tot}} + 2.646\dfrac{\left(m_p + m_{f3}\right)a}{l m_{tot}}}}. \qquad (6.35)$$

Let us now consider the case where the connecting pipe is much longer, i.e. $a = 2l$ and, as before, $k_h = 0$ and $M_h = 0$. In this case the frequency equation (6.32) becomes

$$\cosh kl\ \sin kl + \sinh kl\ \cos kl - 2kl\left(1-\cosh kl\ \cos kl\right) = 0,$$

the first solution of which is $k_1 l = 1.49954$, and the mode function obtained in the same way is

$$X = \frac{1}{0.7303}\left[\cosh c\frac{x}{l} - \cos c\frac{x}{l} - 1.370763\left(\sinh c\frac{x}{l} - \sin c\frac{x}{l}\right)\right], \qquad (6.36)$$

where $c = 1.49954$. Calculation of coefficients, A, (6.30), and substitution of their values into (6.29) gives the frequency expression, similar to (6.35),

$$f_1 = \frac{1}{2\pi}\,\frac{5.658}{l^2}\sqrt{\frac{EI}{m_{tot}}}\sqrt{\frac{1-0.1000\dfrac{l^2}{EI}P\pi R_m^2}{1+\dfrac{3.203\,J}{l^2 m_{tot}}+2.665\dfrac{\left(m_p+m_{f3}\right)a}{l m_{tot}}}}\,. \qquad (6.37)$$

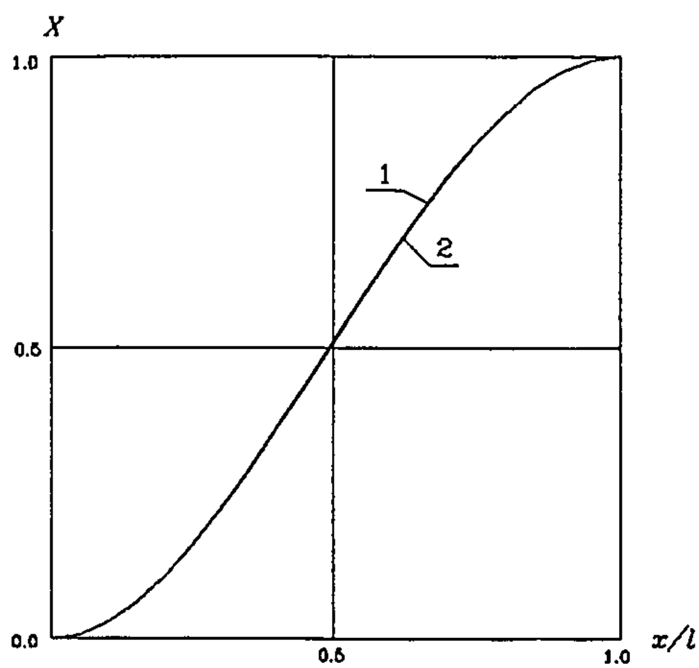

Fig.6.2. The first mode shapes: for $a = l$, (1) and for $a = 2l$, (2)

The mode shapes for $a = l$ and $a = 2l$ are compared in Fig.6.2. As seen from this figure, the difference between these two modes is negligible. Let us compare the two frequency expressions (6.35), (6.37) derived using these slightly different mode functions obtained for $a = l$ and $a = 2l$ respectively. For this we have to take the same typical bellows for which $EI = 5.0$ Nm^2, $J = 11.5\times10^{-4}$ kgm, $P\pi R_m^2 = 6000$ N, $m_{tot} = m_p + m_{f3} = 5.0$ kg/m, and $a = l = 0.075$ m. Substitution of these values into equations (6.35) and (6.37) gives $f = 46.83$ Hz and $f = 46.84$ Hz respectively. The frequencies for the same data as above, except that $a = 2l$, are found to be $f = 35.904$ Hz and $f = 35.905$ Hz. The comparison of these two pairs of frequencies shows that the differences between them are very small. Thus, while the first natural frequency of lateral motion of a universal expansion joint is dependent on the length of the connecting pipe, the frequency equations (6.35) and (6.37) give essentialy the same result over the practical range of connecting pipe lengths. Averaging the coefficients of equations (6.35) and (6.37) gives a practical design formula.

$$f_1 = \frac{1}{2\pi}\frac{5.650}{l^2}\sqrt{\frac{EI}{m_{tot}}}\sqrt{\frac{1 - 0.1\dfrac{l^2}{EI}P\pi R_m^2}{1 + \dfrac{3.193J}{l^2 m_{tot}} + 2.656\dfrac{(m_p + m_{f3})a}{l m_{tot}}}} .$$

The final expression (6.31) for the natural frequency of the transverse vibration of a universal expansion joint according to the first lateral mode without lateral supports becomes:

$$f_1 = \frac{1}{4\pi}\frac{5.650}{l^2}\sqrt{\frac{kpR_m^2}{m_{tot}}}\sqrt{\frac{1 - 0.4\pi\dfrac{l^2}{kp}P}{1 + \dfrac{3.193J}{m_{tot}l^2} + 2.656\dfrac{(m_p + m_{f3})a}{m_{tot}l}}} ,$$

or,

$$f_1 = \frac{1}{4\pi}\,\frac{A_1 R_m}{l^2}\,\sqrt{\frac{kp}{m_{tot}}}\,\sqrt{\frac{1-4\pi A_2 \frac{l^2}{kp}P}{1+A_4\frac{J}{m_{tot}l^2}+A_5\frac{(m_p+m_{f3})a}{m_{tot}l}}}\,, \tag{6.38}$$

where,

$A_1 = 5.650,\ \ A_2 = 0.10,\ \ A_4 = 3.193,$ and $A_5 = 2.656.$

As derived in Chapter 3, equation (3.57),

$$m_{tot} = 4\pi R_m\left(\frac{h}{p}+0.285\right)t\rho_b + \left[\pi\left(R_m-\frac{h}{2}+\frac{2hR_2}{p}\right)^2 + \alpha_{f21}\,\mu R_m^3\right]\rho_f.$$

α_{f21} was calculated using formula (3.26):

$$\alpha_{f2k} = 0.066\,\frac{\int_0^l \left(\frac{d^2X_k}{dx^2}\right)^2 dx}{\int_0^l X_k^2(x)\,dx}\left(R_m-\frac{h}{2}\right)^2 p.$$

Taking $\frac{x}{l} = \xi$, both integrals in the above formula for the first mode can be rewritten as

$$\int_0^l \left(\frac{d^2X_1}{dx^2}\right)^2 dx = \frac{1}{l^3}\int_0^1 \left(\frac{d^2X_1}{d\xi^2}\right)^2 d\xi$$

and

$$\int_0^l X_1^2(x)\,dx = l\int_0^1 X_1^2(\xi)\,d\xi.$$

Substitution of these replacements into the formula for α_{f2k} leads to:

$$\alpha_{f21} = \frac{0.066}{l^4} \frac{\int_0^1 \left(\frac{d^2 X_1}{d\xi^2}\right)^2 d\xi}{\int_0^1 X_1^2(\xi)\, d\xi} \left(R_m - \frac{h}{2}\right)^2 p .$$

Since, according to (6.30),

$$\sqrt{\frac{\int_0^1 \left(\frac{d^2 X_1}{d\xi^2}\right)^2 d\xi}{\int_0^1 X_1^2(\xi)\, d\xi}} = A_1 ,$$

the final expression for α_{f21} becomes

$$\alpha_{f21} = 0.066 \frac{A_1^2}{l^4} \left(R_m - \frac{h}{2}\right)^2 p . \qquad (6.39)$$

Using in the this formula either of the mode functions, (6.34) or (6.36), gives almost identical results:

$$\alpha_{f21} = 2.101 \left(R_m - \frac{h}{2}\right)^2 \frac{p}{l^4} .$$

The total moment of inertia of the cross-section of bellows is given by (3.67):

$$J = \pi R_m^3 \left[\left(2\frac{h}{p} + 0.571 \right) t \rho_b + \frac{h}{p} (2R_2 - t) \rho_f \right] .$$

6.6. Second and Third Lateral Modes Natural Frequencies of Universal Expansion Joint without Lateral Supports

As in the case of the first mode, the frequency equation remains the same (6.32),

$$\cosh kl \, \sin kl + \sinh kl \, \cos kl - \frac{a\left(m_p + m_{f3}\right)}{l m_{tot}} kl \left(1 - \cosh kl \, \cos kl\right) = 0 . \qquad (6.40)$$

For moderate convolution depth,

$$m_p + m_{f3} = 0.66666 \, m_{tot} .$$

The frequency equation (6.40) was solved for three different connecting pipe lengths, $a = l$, $a = 1.5\,l$, $a = 2\,l$. The second mode solutions were obtained as follows:

$$k_2\, l_l = 4.951418, \quad k_2\, l_{1.5l} = 4.89277, \quad k_2\, l_{2l} = 4.858652.$$

Now, substitution of the values of k_{2l} into expression (6.27) for D/C and subsequent use of (6.33) gives three slightly different approximate second mode functions for the universal expansion joint. These three mode functions, normalized to unity, are:

$$X_2 = \frac{1}{1.5570}\left[\cosh c\xi - \cos c\xi - 0.9894701\left(\sinh c\xi - \sin c\xi\right)\right],$$

$$X_2 = \frac{1}{1.5644}\left[\cosh c\xi - \cos c\xi - 0.9877887\left(\sinh c\xi - \sin c\xi\right)\right],$$

$$X_2 = \frac{1}{1.5690}\left[\cosh c\xi - \cos c\xi - 0.9867564\left(\sinh c\xi - \sin c\xi\right)\right],$$

where $c = kl$ and $\xi = \dfrac{x}{l}$.

Substitution of these three mode functions and their derivatives into expressions (6.30) gives the three sets of coefficients, A_1, A_2, A_4, A_5 for three different lengths of a, as shown in Table 6.1.

Table 6.1. Comparison of coefficients A_i for the second mode

a	l	$1.5\,l$	$2\,l$
A_1	26.267	25.316	24.267
A_2	0.025	0.02485	0.0248
A_4	17.27	15.93	15.15
A_5	0.222	0.118	0.073

It can be concluded on the basis of the data in Table 6.1 that the second mode coefficient, A_2, is practically independent of the connecting pipe length, a. Therefore, A_2 can be considered as a constant, approximately equal to 0.0249. The values of the other three coefficients are plotted as functions of a/l in the Fig.6.3.

The final expression for the second lateral mode without lateral supports can be rewritten from (6.31) just taking $M_h = 0$ and $k_h = 0$. Actually, it is the same as (6.38):

$$f_2 = \frac{1}{4\pi}\frac{A_1 R_m}{l^2}\sqrt{\frac{kp}{m_{tot}}}\sqrt{\frac{1-4\pi A_2 \frac{l^2}{kp}P}{1+A_4\frac{J}{m_{tot}l^2}+A_5\frac{(m_p+m_{f3})a}{m_{tot}l}}}, \qquad (6.41)$$

where

$$m_{tot} = 4\pi R_m\left(\frac{h}{p}+0.285\right)t\rho_b + \left[\pi\left(R_m-\frac{h}{2}+\frac{2hR_2}{p}\right)^2 + \alpha_{f22}\,\mu R_m^3\right]\rho_f.$$

α_{f22} can be calculated using formula (6.39), already derived for the first lateral mode:

$$\alpha_{f22} = 0.066\frac{A_1^2}{l^4}\left(R_m-\frac{h}{2}\right)^2 p.$$

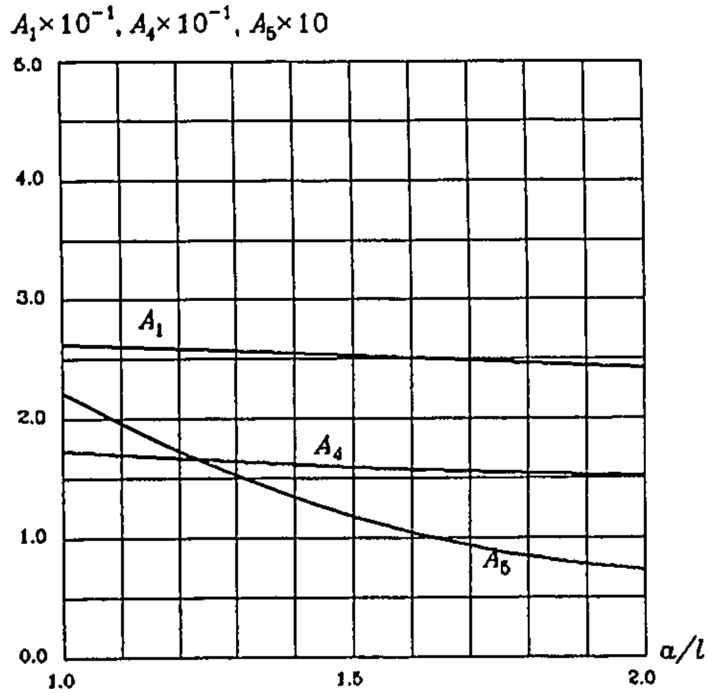

Fig.6.3. Coefficients A_1, A_4, A_5 for second lateral mode natural frequency formula (6.41)

The three sets of coefficients, A_1, A_2, A_4, A_5 for the three different lengths of, a, were obtained in a similar way for the third mode as shown in Table 6.2.

Table 6.2. Comparison of coefficients A_i for the third mode

a	l	$1.5\,l$	$2\,l$
A_1	66.309	65.033	64.306
A_2	0.0118	0.0119	0.0119
A_4	52.16	50.41	49.44
A_5	0.1022	0.0511	0.0305

Table 6.2 shows that the coefficient A_2 can be considered to be independent of a, as in the case of the second mode, and approximately equal to 0.0119. The rest of the coefficients, A, were plotted as functions a/l in Fig.6.4.

The second mode frequency formula (6.41) and subsequent formulas for m_{tot} and α_{f22} can be used for third mode frequency calculation.

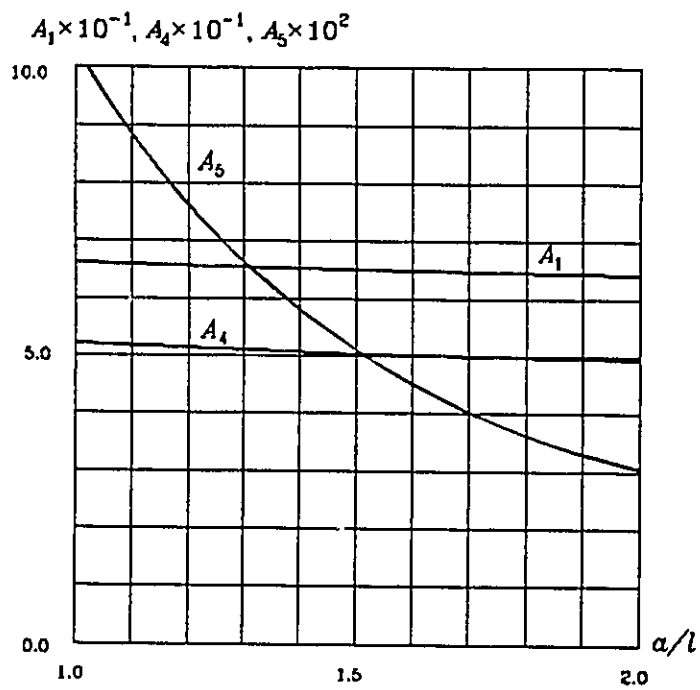

Fig.6.4. Coefficients A_1, A_4, A_5 for third lateral mode natural frequency formula (6.41)

6.7. First Lateral Mode Natural Frequency of Universal Expansion Joint with Lateral Supports

In this case it is necessary to take into account the transverse stiffness of the supports, k_h, and their equivalent mass, M_h. In practice, the transverse stiffness of lateral supports, k_h, varies over the range

$$k_b < k_h < 3k_b \,,$$

where k_b is the fixed-fixed bellows transverse stiffness.

Consider the case when

$$k_h = k_b \,.$$

Let $a = 2\,l$. Then,approximately, the ratio residing in the frequency equation (6.28),

$$\frac{M_h + a\left(m_p + m_{f3}\right)}{l m_{tot}} \cong 2 \,,$$

and this frequency equation simplifies to

$$\cosh kl \,\sin kl \,+\, \sinh kl \,\cos kl \,-\, \left[2kl \,-\, \frac{12}{(kl)^3}\right]\left(1 - \cosh kl \,\cos kl\right) \,=\, 0 \,.$$

The computerized solution of the equation above for the first mode frequency gives $k_1\,l = 1.7829$. From (6.26) we obtain:

$$X \,=\, U(x) \,+\, \frac{D}{C}\, V(x)$$

Substitution of the above value $k_1 l$ into equation (6.27) gives the ratio

$$\frac{D}{C} = -\,1.18326 \,.$$

Substitution of the expressions for $U(x)$ and $V(x)$ from (6.25) and this numerical value of ratio D/C into the general expression for the mode function above gives the exact function for the differential equation (6.14) which can be used as the approximate mode function for calculation of the coefficients A in (6.30). Normalized to unity, this mode function becomes:

$$X = \frac{1}{1.0059}\left[\cosh c\frac{x}{l} - \cos c\frac{x}{l} - 1.18326\left(\sinh c\frac{x}{l} - \sin c\frac{x}{l}\right)\right],$$

where $c = 1.7829$.

Let $\frac{x}{l} = \xi$. Then the mode function can be rewritten as

$$X = \frac{1}{1.0059}\left[\cosh c\xi - \cos c\xi - 1.18326\left(\sinh c\xi - \sin c\xi\right)\right], \tag{6.42}$$

the first and second derivatives of which are

$$\frac{dX}{dx} = \frac{c}{1.0059}\left[\sinh c\xi + \sin c\xi - 1.18326\left(\cosh c\xi - \cos c\xi\right)\right],$$

and

$$\frac{d^2X}{dx^2} = \frac{c^2}{1.0059}\left[\cosh c\xi + \cos c\xi - 1.18326\left(\sinh c\xi + \sin c\xi\right)\right].$$

Now values of the integrals in (6.30) can be obtained integrating them as before. The value of $X(\xi)$ at $\xi = 1$ was calculated from (6.42) and is $X(1) = 1$. Substitution of these integral values into the expressions for A (6.30) gives:

$A_1 = 5.636$, $A_2 = 0.10$, $A_3 = 0.0831$,

$A_4 = 3.177$, $A_5 = 2.638$.

Substitution of these coefficients into (6.29) finally gives the frequency expression:

$$f_1 = \frac{1}{2\pi}\frac{5.636}{l^2}\sqrt{\frac{EI}{m_{tot}}}\sqrt{\frac{1 - 0.1000\dfrac{l^2}{EI}P\pi R_m^2 + 0.0831\dfrac{k_h l^3}{EI}}{1 + \dfrac{3.177\,J}{l^2 m_{tot}} + 2.638\,\dfrac{M_h + \left(m_p + m_{f3}\right)a}{m_{tot} l}}}\,. \qquad (6.43)$$

Let us find now the analogous frequency expression for the case when

$$k_h = 3k_b$$

and, as before, $a = 2l$. Then the frequency equation (6.28) becomes

$$\cosh kl\ \sin kl + \sinh kl\ \cos kl - \left[2kl - \frac{36}{(kl)^3}\right]\left(1 - \cosh kl\ \cos kl\right) = 0\,.$$

The first frequency solved from this equation is $k_1 l = 2.119375$ and the mode function obtained as in the previous section is:

$$X = \frac{1}{1.3499}\left[\cosh c\frac{x}{l} - \cos c\frac{x}{l} - 1.04462\left(\sinh c\frac{x}{l} - \sin c\frac{x}{l}\right)\right], \qquad (6.44)$$

where $c = 2.119375$. Calculation of coefficients, A, (6.30) and substitution of their values into (6.29) gives the frequency expression based on the mode function (6.44), which, according to the comparison of numerical coefficients, gives a slightly different frequency than the frequency given by (6.43):

$$f_1 = \frac{1}{2\pi}\frac{5.605}{l^2}\sqrt{\frac{EI}{m_{tot}}}\sqrt{\frac{1 - 0.0995\,\dfrac{l^2}{EI}P\pi R_m^2 + 0.0822\,\dfrac{k_h l^3}{EI}}{1 + \dfrac{3.126\,J}{l^2 m_{tot}} + 2.584\,\dfrac{M_h + \left(m_p + m_{f3}\right)a}{m_{tot} l}}}\,. \qquad (6.45)$$

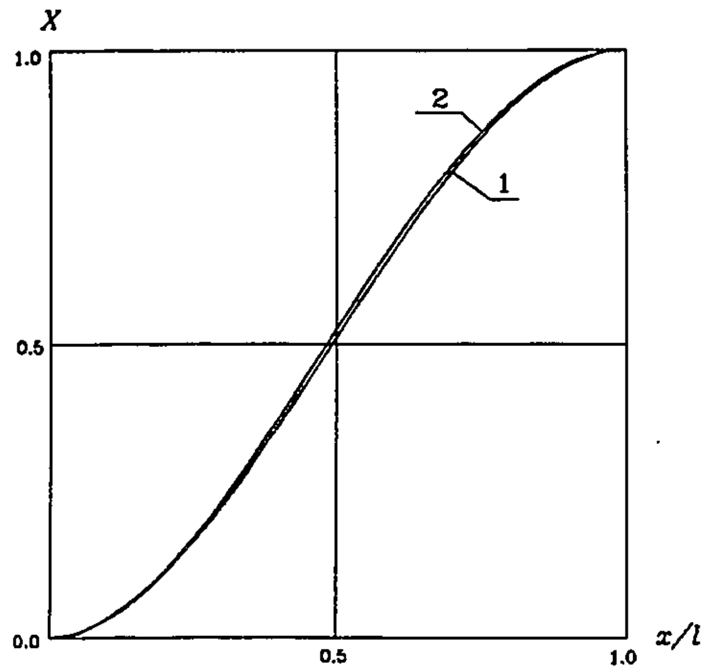

Fig.6.5. The mode shapes: **1**, for $k_h = k_b$, **2**, for $k_h = 3k_b$.

The mode shapes for $k_h = k_b$ and $k_h = 3k_b$ are compared in Fig.6.3. As seen from the figure, the difference between these two modes is quite small. Let us compare the two frequency expressions (6.43), (6.45) derived using these slightly different mode functions. For this we take the typical bellows with the same dimensions as in the previous section, for which $EI = 5.0$ Nm^2 , $J = 11.5\times10^{-4}$ kgm, $P\pi R_m^2 = 6000$ N, $m_{tot} = m_p + m_{f3} = 5.0$ kg/m, but $a = 2l = 0.15$ m, $k_h = k_b$, and $M_h = 0$. Substitution of these values into equations (6.43) and (6.45) gives $f = 72.44$ Hz and $f = 72.48$ Hz accordingly. The frequencies for same data as above except that $k_h = 3k_b$ were $f = 114.73$ Hz and $f = 114.66$ Hz. The comparison of these two pairs of frequencies shows that the differences between them are less than 0.1%. Therefore, in the practical range of the connecting pipe lengths, a, and the support stiffness, k_h , either of the two frequency formulas derived above are equally good, or, even better, a new formula with numerical coefficients obtained as the mean values of corresponding numerical coefficients in formulas (6.43) and (6.45) can be used:

$$f_1 = \frac{1}{2\pi}\frac{5.620}{l^2}\sqrt{\frac{EI}{m_{tot}}}\sqrt{\frac{1 - 0.0998\frac{l^2}{EI}P\pi R_m^2 + 0.0826\frac{k_h l^3}{EI}}{1 + \frac{3.152\,J}{l^2 m_{tot}} + 2.611\frac{M_h + (m_p + m_{f3})a}{m_{tot} l}}}. \tag{6.46}$$

The final expression for the natural frequency of the transverse vibration of a universal expansion joint according to the first lateral mode with lateral supports becomes:

$$f_1 = \frac{1}{2\pi}\frac{5.620}{l^2}\sqrt{\frac{kpR_m^2}{m_{tot}}}\sqrt{\frac{1 - 0.399\pi\frac{l^2}{kp}P + 0.330\frac{k_h l^3}{kpR_m^2}}{1 + \frac{3.152\,J}{m_{tot}l^2} + 2.611\frac{M_h + (m_p + m_{f3})a}{m_{tot} l}}},$$

or, following (6.31) notations,

$$f_1 = \frac{1}{4\pi}\frac{A_1 R_m}{l^2}\sqrt{\frac{kp}{m_{tot}}}\sqrt{\frac{1 - 4\pi A_2\frac{l^2}{kp}P + 4A_3\frac{k_h l^3}{kpR_m^2}}{1 + A_4\frac{J}{m_{tot}l^2} + A_5\frac{M_h + (m_p + m_{f3})a}{m_{tot} l}}}, \tag{6.47}$$

where

$A_1 = 5.62$, $A_2 = 0.0998$, $A_3 = 0.0826$,

$A_4 = 3.152$, $A_5 = 2.611$.

As in the previous section,

$$m_{tot} = 4\pi R_m\left(\frac{h}{p} + 0.285\right)t\rho_b + \left[\pi\left(R_m - \frac{h}{2} + \frac{2hR_2}{p}\right)^2 + \alpha_{f21}\,\mu R_m^3\right]\rho_f\,.$$

α_{f21} can be calculated using formula (6.39):

$$\alpha_{f21} = 0.066\,\frac{A_1^2}{l^4}\left(R_m - \frac{h}{2}\right)^2 p\,.$$

Using in the above formula mode functions (6.41) and (6.44) gave slightly different α_{f21} results:

$$\alpha_{f21} = 2.096\left(R_m - \frac{h}{2}\right)^2 \frac{p}{l^4}$$

and

$$\alpha_{f21} = 2.074\left(R_m - \frac{h}{2}\right)^2 \frac{p}{l^4}.$$

Since the numerical coefficients in the expressions above are very close, the mean value can be used to calculate α_{f21}:

$$\alpha_{f21} = 2.085\left(R_m - \frac{h}{2}\right)^2 \frac{p}{l^4}.$$

The total moment of inertia of the cross-section of the bellows is given by (3.67):

$$J = \pi R_m^3 \left[\left(2\frac{h}{p} + 0.571\right) t\rho_b + \frac{h}{p}\left(2R_2 - t\right)\rho_f\right].$$

It should be noted, that formula (6.47) can be used for calculation of the natural frequencies of universal expansion joints without supports, almost with the same degree of precision as in formula (6.38). In this case k_h and M_h must be taken equal to zero.

6.8. The Exact Solution of Universal Expansion Joint Lateral Mode Natural Frequency and Its Comparison with the Rayleigh Quotient Solution

The lateral mode natural frequency formula for universal expansion joints was derived in the previous section using the Rayleigh method. This was the approximate solution, of course. Now, in order to determine the error inherent in the derived frequency formula (6.47), the same problem will be solved exactly.

Consider the governing differential equation (6.8), derived in Section 6.2:

$$EI\frac{d^4X}{dx^4} + P\pi R_m^2\frac{d^2X}{dx^2} + J\omega^2\frac{d^2X}{dx^2} - \omega^2 m_{tot}X = 0,$$

From here,

$$\frac{d^4X}{dx^4} + \frac{P\pi R_m^2 + J\omega^2}{EI}\frac{d^2X}{dx^2} - \omega^2\frac{m_{tot}}{EI}X = 0. \tag{6.48}$$

If

$$c = \sqrt{\frac{P\pi R_m^2 + J\omega^2}{2EI}} \tag{6.49}$$

and

$$\lambda = \sqrt{\frac{m_{tot}\omega^2}{EI}} \ . \tag{6.50}$$

Then equation (6.48) becomes

$$\frac{dX^4}{dx^4} + 2c^2\frac{dX^2}{dx^2} - \lambda^4 X = 0.$$

This is the same equation as (4.22) in Section 4.3. As derived there, the general solution of this equation is

$$X = A\sinh\alpha x + B\cosh\alpha x + C\sin\beta x + D\cos\beta x, \tag{6.51}$$

the first and the third derivatives of which are

$$\frac{dX}{dx} = A\alpha\cosh\alpha x + B\alpha\sinh\alpha x + C\beta\cos\beta x - D\beta\sin\beta x,$$

$$\frac{d^3X}{dx^3} = A\alpha^3\cosh\alpha x + B\alpha^3\sinh\alpha x - C\beta^3\cos\beta x + D\beta^3\sin\beta x,$$

where

$$\alpha = \sqrt{-c^2 + \sqrt{c^4 + \lambda^4}}\ , \tag{6.52}$$

$$\beta = \sqrt{c^2 + \sqrt{c^4 + \lambda^4}}\,, \tag{6.53}$$

and A, B, C, D are the arbitrary constants.

The boundary conditions remain the same as in previous sections of this chapter,

$$\frac{d^3X(l)}{dx^3} = -\frac{\omega^2\left[M_h + \left(m_p + m_{f3}\right)a\right]}{EI}X(l) + \frac{k_h}{EI}X(l),$$

or

$$\frac{d^3X(l)}{dx^3} = -\,bX(l), \tag{6.54}$$

if

$$b = \frac{\omega^2\left[M_h + \left(m_p + m_{f3}\right)a\right]}{EI} - \frac{k_h}{EI}. \tag{6.55}$$

The rest of the boundary conditions are the same as given by (6.9) and (6.10):

$$\frac{dX(l)}{dx} = 0, \tag{6.56}$$

$$X(0) = \frac{dX(0)}{dx} = 0. \tag{6.57}$$

Substitution of the general solution (6.51) and its derivatives into boundary condition expressions (6.54), (6.56), and (6.57) gives us the set of linear equations with respect to A, B, C, and D:

$$B + D = 0,$$

$$\alpha A + \beta C = 0,$$

$$A\alpha\cosh\alpha l + B\alpha\sinh\alpha l + C\beta\cos\beta l - D\beta\sin\beta l = 0,$$

$$[\alpha^3\cosh\alpha l + b\sinh\alpha l]\,A + [\alpha^3\sinh\alpha l + b\cosh\alpha l]\,B$$
$$-\,[\beta^3\cos\beta l - b\sin\beta l]\,C + [\beta^3\sin\beta l + b\cos\beta l]\,D = 0.$$

For a nontrivial solution the determinant formed by the coefficients of this system of algebraic equations must be equal to zero:

$$\begin{vmatrix} 0 & 1 & 0 & 1 \\ \alpha & 0 & \beta & 0 \\ \alpha\cosh\alpha l & \alpha\sin\alpha l & \beta\cos\beta l & -\beta\sin\beta l \\ c_1 & c_2 & -c_3 & c_4 \end{vmatrix} = 0,$$

where,

$$c_1 = \alpha^3\cosh\alpha l + b\sinh\alpha l,$$
$$c_2 = \alpha^3\sinh\alpha l + b\cosh\alpha l,$$
$$c_3 = \beta^3\cos\beta l - b\sin\beta l,$$
$$c_4 = \beta^3\sin\beta l + b\cos\beta l.$$

The expansion of the above determinant results in the frequency equation for the system shown in Fig.6.1:

$$\begin{aligned} & b[2\alpha\beta + \alpha^2\sin\beta l\sinh\alpha l - \beta^2\sin\beta l\sinh\alpha l - 2\alpha\beta\cos\beta l\cosh\alpha l] \\ & - \alpha\beta^4\sin\beta l\cosh\alpha l - \alpha^4\beta\cos\beta l\sinh\alpha l - \alpha^2\beta^3\cos\beta l\sinh\alpha l \\ & \qquad - \alpha^3\beta^2\sin\beta l\cosh\alpha l = 0, \end{aligned} \tag{6.58}$$

where b, α, and β are given by (6.55), (6.52), and (6.53). It should be noted that when $c = 0$, then $\alpha = \beta = \lambda$. Here, as must be the case, the frequency equation (6.58) simplifies to the frequency equation (6.28) as derived in Section 6.3.

Let us take the universal expansion joint with defined geometrical and physical parameters: bellows length, $l = 0.0693$ m, mass moment of inertia per unit length, $J = 0.001153$ kgm, $EI = 5.078$ Nm^2, total bellows mass, $m_{tot} = 5.138$ kg/m, total connecting pipe mass, $m_p + m_{\beta} = 5.0$ kg/m, $a = 1.5l$, and no lateral supports. According to (4.31), the maximum allowable pressure in bellows is,

$$P_{max} = \frac{\pi k p}{6.6661^2}. \tag{6.59}$$

According to (3.1),

$$EI = \frac{1}{4} k p R_m^2. \tag{6.60}$$

Substitution of (6.59), (6.60) and the numerical values given above into (6.49) and (6.50) leads to

$$c = \sqrt{616.49 + 0.0001135\,\omega^2}. \tag{6.61}$$

and

$$\lambda = \sqrt{1.0029\,\omega}. \tag{6.62}$$

From (6.55),

$$b = 0.10235\omega^2. \tag{6.63}$$

Now, using expressions (6.61), (6.62), (6.63), (6.52) and (6.53), the frequency equation (6.58) can be solved at the computer precision level. The first natural frequency obtained from a computerized solution of (6.58) is given in Table 6.3.

The same frequency was calculated for the same bellows data using frequency formula (6.47) derived in the previous section from the Rayleigh quotient. Both results are compared in Table 6.3.

Table 6.3. Comparison of the exact and approximate frequency solutions for the universal expansion joint first lateral mode

Mode #	Exact ω	Rayleigh ω	Error
	(rad/s)	(rad/s)	(%)
1	331.167	333.17	0.60
2	3500.822		

As seen from the comparison in Table 6.1, the error of the first frequency obtained from the Rayleigh quotient is comparatively small. Therefore, formula (6.47) is adequate for estimating the first lateral natural frequency of a universal expansion joint.

6.7. Instability Condition for Universal Expansion Joint Lateral Mode

It may be seen from equation (6.47) that using the particular combination of parameters P, p, k, and l, the numerator of the expression under the last root becomes equal to zero:

$$1 - 0.399\,\pi \frac{l^2}{kp} P + 0.33 \frac{k_h l^3}{kpR^2} = 0 .$$

From here the critical pressure is,

$$P_{cr} = 0.798 \frac{kp}{l^2} + 0.263 k_h \frac{l^3}{R_m^2} .$$

For bellows without lateral supports $k_h = 0$, and the above expression simplifies to

$$P_{cr} = 0.798 \frac{kp}{l^2} . \qquad (6.54)$$

It should be noted that formula (6.54) gives the same result as formula (5.20) derived for a single bellows, provided that in (5.20) the bellows length is taken as $2l$. This occurs because the presence of the connecting pipe doesn't play any role in the stability of the first lateral mode.

CHAPTER 7

THEORETICAL INVESTIGATION OF NATURAL VIBRATIONS OF UNIVERSAL EXPANSION JOINT ROCKING MODE

7.1. Derivation of Boundary Conditions for Vibration of Universal Expansion Joint Rocking Mode

It is easily seen that, in the case of the vibration of the bellows in any rocking mode, (Fig. 4.3) the middle point of the connecting pipe does not translate because of the geometrical and physical symmetry of the system (Fig. 4.1) with respect to the imaginary middle vertical axis, provided the Coriolis forces acting on the bellows from the fluid flowing inside are neglected. Therefore, as a mathematical approximation, one half of the physical system can be taken with its left end fixed and right end simply supported in the middle of the connecting pipe, as shown in Fig.7.1. Since at the end A the bellows is fixed, the boundary conditions at this end are simply geometrical, i.e.,

$$w(0,t) = \frac{\partial w(0,t)}{\partial x} = 0. \tag{7.1}$$

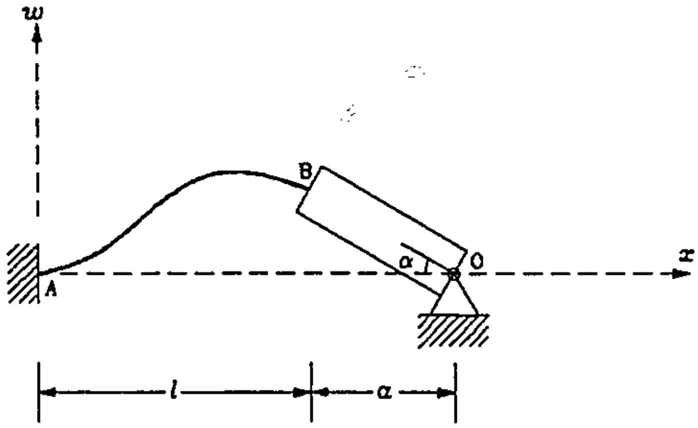

a) First mode shape

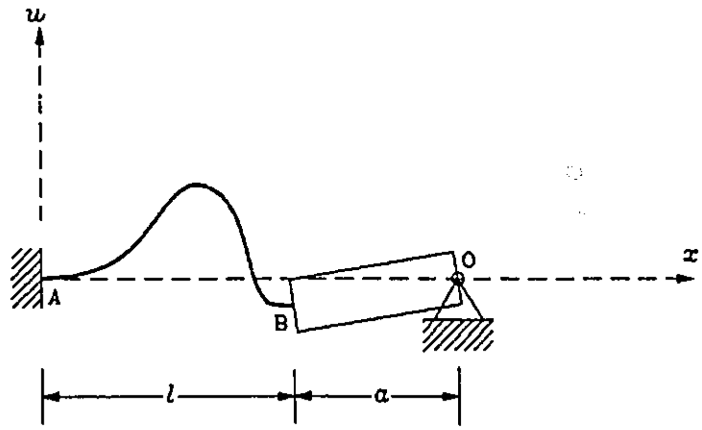

b) Second mode shape

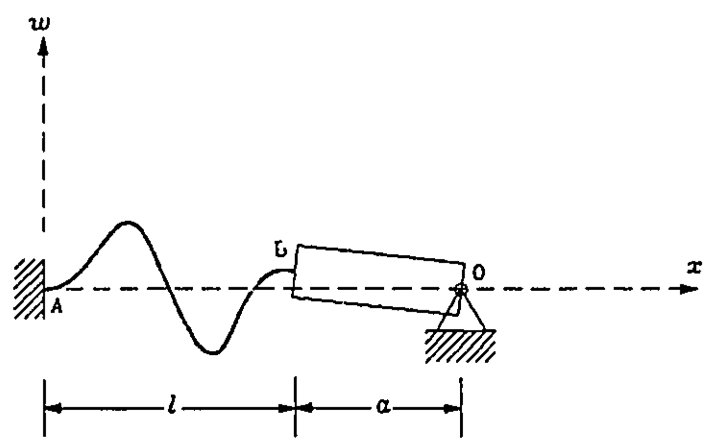

c) Third mode shape

Fig.7.1. Mathematical models for the rocking modes

It is not difficult to derive the geometrical boundary condition at the end B. As seen from the Fig.7.1,

$$\sin\alpha = -\frac{w(l,t)}{a}.$$

On the other hand,

$$\alpha = \frac{\partial w(l,t)}{\partial x}.$$

From here,

$$\sin\frac{\partial w(l,t)}{\partial x} = -\frac{w(l,t)}{a}. \tag{7.2}$$

For small α,

$$\sin\frac{\partial w(l,t)}{\partial x} \cong \frac{\partial w(l,t)}{\partial x}.$$

Substitution of the last approximation into (7.2) gives the third boundary condition:

$$\frac{\partial w(l,t)}{\partial x} = -\frac{1}{a}w(l,t). \tag{7.3}$$

The minus sign is conventional in expression (7.3). Expressions (7.1) and (7.3) are three of the four necessary boundary conditions. The fourth boundary condition can be derived from the rotation differential equation written for the connecting pipe OA (Fig.7.1):

$$J_{tot}\varepsilon = M(l,t) + Q(l,t)a + F_{sp}a \tag{7.4}$$

where

J_{tot} is the mass moment of inertia with respect to O of the connecting pipe, including the fluid inside,

ε is the angular acceleration of the connecting pipe,

$M(l,t)$ and $Q(l,t)$ are the moment and the shear force at the end A of the bellows,

F_{sp} is the spring force.

The total mass moment of inertia, according to (3.68), is

$$J_{tot} = \frac{(m_p + m_{f3})a^3}{3} + \frac{(2m_p + m_{f3})aR^2}{4} + M_h a^2, \tag{7.5}$$

where

m_p is the connecting pipe mass,

m_{f3} is the fluid mass contained in the connecting pipe,

M_h is the mass of the lateral support,

R is the mean radius of the connecting pipe,

$$\varepsilon = \frac{\partial^2 w(l,t)}{\partial t^2}\,\frac{1}{a}, \tag{7.6}$$

and

$$F_{sp} = -k_h\, w(l,t), \tag{7.7}$$

where

k_h is the spring stiffness of the lateral support.

Since

$$M = EI\,\frac{\partial^2 w}{\partial x^2}, \tag{7.8}$$

substitution of expressions (4.33), (7.5), (7.6), (7.7) and (7.8) into (7.4) gives:

$$\frac{J_{tot}}{a}\,\frac{\partial^2 w(l,t)}{\partial t^2} = EI\,\frac{\partial^2 w(l,t)}{\partial x^2} + EI\,\frac{\partial^3 w(l,t)}{\partial x^3}\,a$$

$$+ P\pi R_m^2 a\,\frac{\partial w(l,t)}{\partial x} - Ja\,\frac{\partial^3 w(l,t)}{\partial x\,\partial t^2} - k_h\, w(l,t)\, a\,.$$

From this the fourth boundary condition becomes:

$$\begin{aligned}\frac{\partial^3 w(l,t)}{\partial x^3} = &-\frac{\partial^2 w(l,t)}{\partial x^2}\,\frac{1}{a} - \frac{P\pi R_m^2}{EI}\,\frac{\partial w(l,t)}{\partial x} \\ &+\frac{k_h}{EI}\,w(l,t) + \frac{J}{EI}\,\frac{\partial^3 w(l,t)}{\partial x\,\partial t^2} + \frac{J_{tot}}{EIa^2}\,\frac{\partial^2 w(l,t)}{\partial t^2}.\end{aligned} \tag{7.9}$$

7.2. Derivation of Differential Equation and Boundary Conditions Using Hamilton's Principle

Since the rocking mode of bellows vibration is rather complex, the differential equation derived in Chapter 4 and the boundary conditions obtained above using the Newtonian approach will be checked in this section by deriving them using Hamilton's principle. The most convenient form of this principle for a tube conveying fluid is the so called Extended Hamilton's principle which was derived by Benjamin (1961), McIver (1973), and Laithier and Paidoussis (1981). Since we disregard the Coriolis and centrifugal forces acting on the tube for reasons explained in Chapter 4, we will use here the Hamilton's principle written in its usual form, given, for example, in Humar (1990):

$$\partial \int_{t_1}^{t_2} (T - V)\, dt = 0 \tag{7.10}$$

where,

T is the kinetic energy of the pipe plus the fluid therein,

V is the potential energy of the pipe (fluid is considered incompressible).

The kinetic energy of the system shown in Fig.7.1 including the fluid flowing inside can be expressed as follows:

$$T = T_1 + T_2 \,,$$

where

T_1 is the kinetic energy of the bellows with fluid inside,

T_2 is the kinetic energy of the connecting pipe with the fluid inside, including lateral supports.

Since

$$T_1 = \int_0^l \left[\frac{1}{2} m_{tot} \left(\frac{\partial w}{\partial t} \right)^2 + \frac{1}{2} J \left(\frac{\partial^2 w}{\partial x \partial t^2} \right)^2 \right] dx \,,$$

where, according to (3.57),

$$m_{tot} = 4\pi R_m\left(\frac{h}{p}+0.285\right)t\rho_b+\left[\pi\left(R_m-\frac{h}{2}+\frac{2hR_2}{p}\right)^2+\alpha_{f2k}\,\mu\,R_m^3\right]\rho_f\,.$$

Since the connecting pipe rotates, the kinetic energy, including lateral supports, is:

$$T_2 = \frac{J_{tot}\,\omega^2}{2},$$

where

J_{tot} is given by (7.5),

ω is the angular velocity of the connecting pipe.

Since

$$\omega = \left.\frac{\partial w}{\partial t}\right|_{x=l}\frac{1}{a},$$

the kinetic energy T_2 becomes:

$$T_2 = \frac{1}{2}J_{tot}\left(\left.\frac{\partial w}{\partial t}\right|_{x=l}\frac{1}{a}\right)^2.$$

The total kinetic energy of the whole system:

$$T = \int_0^l\left[\frac{1}{2}m_{tot}\left(\frac{\partial w}{\partial t}\right)^2+\frac{1}{2}J\left(\frac{\partial^2 w}{\partial x\,\partial t}\right)^2\right]dx+\frac{1}{2}J_{tot}\left(\left.\frac{\partial w}{\partial t}\right|_{x=l}\frac{1}{a}\right)^2. \qquad (7.11)$$

Potential energy of the system is

$$V = V_1+V_2+V_3,$$

where

V_1 is the bending strain energy of the bellows,

V_2 is the buckling strain energy in the bellows caused by the pressure inside,

V_3 is the lateral support stiffness energy.

It is well known that

$$V_1 = \int_0^l \frac{1}{2} EI \left(\frac{\partial^2 w}{\partial x^2}\right)^2 dx\,,$$

$$V_2 = \int_0^l \frac{1}{2} P\pi R_m^2 \left(\frac{\partial w}{\partial x}\right)^2 dx\,,$$

and

$$V_3 = \frac{1}{2} k_h\, w^2(l).$$

Therefore, the potential energy is:

$$V = \int_0^l \frac{1}{2} EI \left(\frac{\partial^2 w}{\partial x^2}\right)^2 dx - \int_0^l \frac{1}{2} P\pi R_m^2 \left(\frac{\partial w}{\partial x}\right)^2 dx + \frac{1}{2} k_h\, w^2(l)\,, \qquad (7.12)$$

where

P is the inside pressure,

R_m is the mean radius of the bellows.

Substitution of (7.11) and (7.12) into (7.10) gives:

$$\delta \int_{t_1}^{t_2} \int_0^l \left[\frac{1}{2} m_{tot} \left(\frac{\partial w}{\partial t}\right)^2 + \frac{1}{2} J \left(\frac{\partial^2 w}{\partial x \partial t}\right)^2\right] dx\,dt + \delta \int_{t_1}^{t_2} \frac{1}{2} J_{tot} \left(\left.\frac{\partial w}{\partial t}\right|_{x=l} \frac{1}{a}\right)^2 dt$$

$$- \delta \int_{t_1}^{t_2} \int_0^l \left[\frac{1}{2} EI \left(\frac{\partial^2 w}{\partial x^2}\right)^2 - \frac{1}{2} P\pi R_m^2 \left(\frac{\partial w}{\partial x}\right)^2\right] dx\,dt - \delta \int_{t_1}^{t_2} \frac{1}{2} k_h w^2(l)\, dt = 0\,.$$

Variation of this leads to the following expression:

$$\int_{t_1}^{t_2}\int_0^l\left(m_{tot}\frac{\partial w}{\partial t}\,\delta\frac{\partial w}{\partial t}+J\frac{\partial^2 w}{\partial x\partial t}\,\delta\frac{\partial^2 w}{\partial x\partial t}\right)dx\,dt+\int_{t_1}^{t_2}\frac{J_{tot}}{a^2}\left.\frac{\partial w}{\partial t}\right|_{x=l}\delta\left.\frac{\partial w}{\partial t}\right|_{x=l}dt$$

$$-\int_{t_1}^{t_2}\int_0^l EI\frac{\partial^2 w}{\partial x^2}\,\delta\frac{\partial^2 w}{\partial x^2}\,dx\,dt+\int_{t_1}^{t_2}\int_0^l P\pi R_m^2\frac{\partial w}{\partial x}\,\delta\frac{\partial w}{\partial x}\,dx\,dt-\int_{t_1}^{t_2}k_h w(l)\,\delta\,w(l)\,dt\;=\;0,$$

or

$$\int_{t_1}^{t_2}\int_0^l m_{tot}\frac{\partial w}{\partial t}\,\frac{\partial\delta w}{\partial t}\,dx\,dt+\int_{t_1}^{t_2}\int_0^l J\frac{\partial^2 w}{\partial x\partial t}\,\frac{\partial^2\delta w}{\partial x\partial t}\,dx\,dt+\int_{t_1}^{t_2}\frac{J_{tot}}{a^2}\frac{\partial w(l)}{\partial t}\,\frac{\partial\delta w(l)}{\partial t}\,dt$$

$$-\int_{t_1}^{t_2}\int_0^l EI\frac{\partial^2 w}{\partial x^2}\,\frac{\partial^2\delta w}{\partial x^2}\,dx\,dt+\int_{t_1}^{t_2}\int_0^l P\pi R_m^2\frac{\partial w}{\partial x}\,\frac{\partial\delta w}{\partial x}\,dx\,dt-\int_{t_1}^{t_2}k_h w(l)\,\delta w(l)\,dt\;=\;0.$$

Integrating by parts the 1st and 3rd terms with respect to time, the 5th term with respect to coordinate x, the 2nd term with respect to time and coordinate x, the 4th term with respect to the coordinate x twice, we obtain:

$$m_{tot}\int_0^l\left(\frac{\partial w}{\partial t}\,\delta w\Big|_{t_1}^{t_2}-\int_{t_1}^{t_2}\frac{\partial^2 w}{\partial t^2}\,\delta w\,dt\right)dx$$

$$+J\left[\int_0^l\frac{\partial^2 w}{\partial x\partial t}\,\delta\left(\frac{\partial w}{\partial x}\right)\Big|_{t_1}^{t_2}dx-\int_{t_1}^{t_2}\frac{\partial^3 w}{\partial x\partial t^2}\,\delta w\Big|_0^l\,dt+\int_{t_1}^{t_2}\int_0^l\frac{\partial^4 w}{\partial x^2\partial t^2}\,\delta w\,dx\,dt\right]$$

$$+\frac{J_{tot}}{a^2}\left[\frac{\partial w(l)}{\partial t}\,\delta w(l)\Big|_{t_1}^{t_2}-\int_{t_1}^{t_2}\frac{\partial^2 w(l)}{\partial t^2}\,\delta w(l)\,dt\right]$$

$$+EI\left[\int_{t_1}^{t_2}\frac{\partial^2 w}{\partial x^2}\,\delta\left(\frac{\partial w}{\partial x}\right)\Big|_0^l\,dt-\int_{t_1}^{t_2}\frac{\partial^3 w}{\partial x^3}\,\delta w\Big|_0^l\,dt+\int_{t_1}^{t_2}\int_0^l\frac{\partial^4 w}{\partial x^4}\,\delta w\,dx\,dt\right]$$

$$+ \; P\pi R_m^2 \int_{t_1}^{t_2} \left(\frac{\partial w}{\partial x} \delta w \Big|_0^l - \int_0^l \frac{\partial^2 w}{\partial x^2} \delta w \, dx \right) dt \; - \; k_h \int_{t_1}^{t_2} w(l) \, \delta w(l) \; dt \; = \; 0.$$

Noting that $\delta w = \delta \left(\frac{\partial w}{\partial x} \right) = 0$ at times t_1 and t_2, we then obtain on regrouping terms and substituting bounds in the above equation:

$$- \int_{t_1}^{t_2} \int_0^l \left(EI \frac{\partial^4 w}{\partial x^4} + P\pi R_m^2 \frac{\partial^2 w}{\partial x^2} - J \frac{\partial^4 w}{\partial x^2 \partial t^2} + m_{tot} \frac{\partial^2 w}{\partial t^2} \right) \delta w \, dx \, dt$$

$$+ \int_{t_1}^{t_2} \left[EI \frac{\partial^3 w(l)}{\partial x^3} \delta w(l) - EI \frac{\partial^2 w(l)}{\partial x^2} \delta \left[\frac{\partial w(l)}{\partial x} \right] + P\pi R_m^2 \frac{\partial w(l)}{\partial x} \delta w(l) - k_h \, w(l) \, \delta w(l) \right.$$

$$\left. - \; J \frac{\partial^3 w(l)}{\partial x \, \partial t^2} \delta w(l) - \frac{J_{tot}}{a^2} \frac{\partial^2 w(l)}{\partial t^2} \delta w(l) \right] dt$$

$$- \int_{t_1}^{t_2} \left[EI \frac{\partial^3 w(0)}{\partial x^3} \delta w(0) - EI \frac{\partial^2 w(0)}{\partial x^2} \delta \left[\frac{\partial w(0)}{\partial x} \right] + P\pi R_m^2 \frac{\partial w(0)}{\partial x} \delta w(0) \right.$$

$$\left. - \; J \frac{\partial^3 w(0)}{\partial x \, \partial t^2} \delta w(0) \right] dt \; = \; 0.$$

Taking into account the relationship (7.3), the last equation can be rewritten as follows:

$$- \int_{t_1}^{t_2} \int_0^l \left(EI \frac{\partial^4 w}{\partial x^4} + P\pi R_m^2 \frac{\partial^2 w}{\partial x^2} - J \frac{\partial^4 w}{\partial x^2 \partial t^2} + m_{tot} \frac{\partial^2 w}{\partial t^2} \right) \delta w \, dx \, dt$$

$$+ \int_{t_1}^{t_2} \left\{ EI \frac{\partial^3 w(l)}{\partial x^3} + EI \frac{\partial^2 w(l)}{\partial x^2} \frac{1}{a} + P\pi R_m^2 \frac{\partial w(l)}{\partial x} - k_h \, w(l) - J \frac{\partial^3 w(l)}{\partial x \, \partial t^2} \right.$$

$$\left. - \; \frac{J_{tot}}{a^2} \frac{\partial^2 w(l)}{\partial t^2} \right\} \delta w(l) \, dt$$

$$-\int_{t_1}^{t_2}\left[EI\frac{\partial^3 w(0)}{\partial x^3} + P\pi R_m^2\frac{\partial w(0)}{\partial x} - J\frac{\partial^3 w(0)}{\partial x\,\partial t^2}\right]\delta w(0)\,dt$$

$$+\int_{t_1}^{t_2} EI\frac{\partial^2 w(0)}{\partial x^2}\,\delta\left[\frac{\partial w(0)}{\partial x}\right]dt = 0.$$

According to boundary conditions (7.1), the above functional is equal to zero if

$$EI\frac{\partial^4 w}{\partial x^4} + P\pi R_m^2\frac{\partial^2 w}{\partial x^2} - J\frac{\partial^4 w}{\partial x^2\partial t^2} + m_{tot}\frac{\partial^2 w}{\partial t^2} = 0 \qquad (7.13)$$

and

$$EI\frac{\partial^3 w(l)}{\partial x^3} + EI\frac{\partial^2 w(l)}{\partial x^2}\frac{1}{a} + P\pi R_m^2\frac{\partial w(l)}{\partial x} - k_h w(l) - J\frac{\partial^3 w(l)}{\partial x\,\partial t^2} - \frac{J_{tot}}{a^2}\frac{\partial^2 w(l)}{\partial t^2} = 0,$$

or

$$\frac{\partial^3 w(l)}{\partial x^3} = -\frac{\partial^2 w(l)}{\partial x^2}\frac{1}{a} - \frac{P\pi R_m^2}{EI}\frac{\partial w(l)}{\partial x} + \frac{k_h}{EI}w(l) + \frac{J}{EI}\frac{\partial^3 w(l)}{\partial x\,\partial t^2} - \frac{J_{tot}}{EIa^2}\frac{\partial^2 w(l)}{\partial t^2} = 0.$$

(7.14)

Eq.(7.13) and (7.14) are the differential equation and the fourth boundary condition which are the same as those derived in the previous section.

7.3. Solution of the Differential Equation

We employ a separation of variables approach by expressing w as the product of a function $X(x)$ and some harmonic function, $T(t)$. Thus

$$w = X(x)\,T(t). \qquad (7.15)$$

Substitution of (7.15) into (7.13), (7.1), (7.3), (7.14) and following division by $T(t)$ leads to the ordinary differential equation

$$EI\frac{d^4X}{dx^4} + P\pi R_m^2\frac{d^2X}{dx^2} + J\omega^2\frac{d^2X}{dx^2} - \omega^2 m_{tot}X = 0 \tag{7.16}$$

and boundary conditions

$$X(0) = \frac{dX(0)}{dx} = 0, \tag{7.17}$$

$$\frac{dX(l)}{dx} = -\frac{X(l)}{a}, \tag{7.18}$$

$$\frac{d^3X(l)}{dx^3} = -\frac{d^2X(l)}{dx^2}\frac{1}{a} - \frac{P\pi R_m^2}{EI}\frac{dX(l)}{dx} - \frac{J\omega^2}{EI}\frac{dX(l)}{dx}$$
$$- \omega^2\frac{J_{tot}}{EIa^2}X(l) + \frac{k_h}{EI}X(l). \tag{7.19}$$

Now we multiply both sides of the differential equation (7.16) by X and integrate over the domain of the bellows, Voltera and Zachmanoglou (1965):

$$EI\int_0^l \frac{d^4X}{dx^4}X\,dx + P\pi R_m^2\int_0^l \frac{d^2X}{dx^2}X\,dx + J\omega^2\int_0^l \frac{d^2X}{dx^2}X\,dx - \omega^2 m_{tot}\int_0^l X^2\,dx = 0.$$

Integrating by parts the first integral with respect to the coordinate twice, and the second and third just once, we obtain:

$$EI\left[\frac{d^3X}{dx^3}X\Big|_0^l - \frac{d^2X}{dx^2}\frac{dX}{dx}\Big|_0^l + \int_0^l\left(\frac{d^2X}{dx^2}\right)^2 dx\right] + P\pi R_m^2\left[\frac{dX}{dx}X\Big|_0^l - \int_0^l\left(\frac{dX}{dx}\right)^2 dx\right]$$
$$+ J\omega^2\left[\frac{dX}{dx}X\Big|_0^l - \int_0^l\left(\frac{dX}{dx}\right)^2 dx\right] - \omega^2 m_{tot}\int_0^l X^2 dx = 0,$$

or, after substitution of bounds,

$$EI\left[\frac{d^3X(l)}{dx^3}X(l) - \frac{d^3X(0)}{dx^3}X(0) - \frac{d^2X(l)}{dx^2}\frac{dX(l)}{dx} + \frac{d^2X(0)}{dx^2}\frac{dX(0)}{dx}\right.$$

$$\left. + \int_0^l \left(\frac{d^2X}{dx^2}\right)^2 dx\right] + P\pi R_m^2\left[\frac{dX(l)}{dx}X(l) - \frac{dX(0)}{dx}X(0)\right.$$

$$\left. - \int_0^l \left(\frac{dX}{dx}\right)^2 dx\right] + J\omega^2\left[\frac{dX(l)}{dx}X(l) - \frac{dX(0)}{dx}X(0)\right.$$

$$\left. - \int_0^l \left(\frac{dX}{dx}\right)^2 dx\right] - \omega^2 m_{tot}\int_0^l X^2 dx = 0.$$

Substituting boundary conditions (7.17), (7.18), and (7.19) into the above expression gives:

$$- EI\frac{d^2X(l)}{dx^2}\frac{1}{a}X(l) - P\pi R_m^2\frac{dX(l)}{dx}X(l) - J\omega^2\frac{dX(l)}{dx}X(l)$$

$$-\omega^2\frac{J_{tot}}{a^2} + k_h X(l) + X^2(l) + EI\frac{d^2X(l)}{dx^2}\frac{1}{a}X(l) + EI\int_0^l\left(\frac{d^2X}{dx^2}\right)^2 dx$$

$$- P\pi R_m^2 a\left[\frac{dX(l)}{dx}\right]^2 - P\pi R_m^2\int_0^l\left(\frac{dX}{dx}\right)^2 dx$$

$$+ J\omega^2\frac{dX(l)}{dx}X(l) - J\omega^2\int_0^l\left(\frac{dX}{dx}\right)^2 dx - \omega^2 m_{tot}\int_0^l X^2 dx = 0.$$

After cancellation of similar terms in the expression above, the squared natural frequency for the universal expansion joint rocking mode can be expressed as follows:

$$\omega^2 = \frac{EI\int\limits_0^l \left(\frac{d^2X}{dx^2}\right)^2 dx - P\pi R_m^2 \int\limits_0^l \left(\frac{dX}{dx}\right)^2 dx + k_h X^2(l)}{m_{tot}\int\limits_0^l X^2 dx + J\int\limits_0^l \left(\frac{dX}{dx}\right)^2 dx + \frac{J_{tot}}{a^2} X^2(l)} . \tag{7.20}$$

The expression (7.20) is the same as found in previous chapters – the Rayleigh quotient derived from differential equation (7.13) and the associated boundary conditions to it. Now the expressed frequency is:

$$f_k = \frac{1}{2\pi}\sqrt{\frac{EI\int\limits_0^l \left(\frac{d^2X}{dx^2}\right)^2 dx - P\pi R_m^2 \int\limits_0^l \left(\frac{dX}{dx}\right)^2 dx + k_h X^2(l)}{m_{tot}\int\limits_0^l X^2 dx + J\int\limits_0^l \left(\frac{dX}{dx}\right)^2 dx + \frac{J_{tot}}{a^2} X^2(l)}} . \tag{7.21}$$

7.4. Solution of the Bernoulli-Euler Equation

Equation (7.13) and the boundary condition (7.14) simplified to the Bernoulli-Euler conditions for the same system shown in Fig.7.1 become:

$$EI\frac{\partial^4 w}{\partial x^4} + m_{tot}\frac{\partial^2 w}{\partial t^2} = 0, \tag{7.22}$$

$$\frac{\partial^3 w(l)}{\partial x^3} = -\frac{\partial^2 w(l)}{\partial x^2}\frac{1}{a} + \frac{1}{EI}\frac{J_{tot}}{a^2}\frac{\partial^2 w(l)}{\partial t^2} + \frac{k_h}{EI}w(l) . \tag{7.23}$$

The kinematic boundary conditions remain the same as before:

$$\frac{\partial w(l)}{\partial x} = -\frac{w(l)}{a}, \tag{7.24}$$

$$w(0) = \frac{\partial w(0)}{\partial x} = 0. \tag{7.25}$$

As in the previous section, taking $w = X(x)\,T(t)$, provided $T(t)$ is a harmonic function, the above differential equation becomes

$$EI\frac{d^4X}{dx^4} - \omega^2 m_{tot} X = 0,$$

or

$$\frac{d^4X}{dx^4} - k^4 X = 0, \tag{7.26}$$

if

$$k^4 = \frac{\omega^2 m_{tot}}{EI}. \tag{7.27}$$

Boundary condition (7.23) becomes

$$\frac{d^3X(l)}{dx^3} = -\frac{d^2X(l)}{dx^2}\frac{1}{a} - \frac{\omega^2}{EI}\frac{J_{tot}}{a^2}X(l) + \frac{k_h}{EI}X(l)$$

or

$$a\frac{d^3X(l)}{dx^3} = -\frac{d^2X(l)}{dx^2} - b\,X(l) \tag{7.28}$$

if

$$b = \frac{\omega^2 a}{EI}\frac{J_{tot}}{a^2} - \frac{k_h a}{EI}. \tag{7.29}$$

The rest of the boundary conditions are

$$\frac{dX(l)}{dx} = -\frac{X(l)}{a}, \tag{7.30}$$

$$X(0) = \frac{dX(0)}{dx} = 0. \tag{7.31}$$

For the case where EI, m_{tot} and $m_p + m_{f3}$ are constants, the general solution of the equation (7.26), according to Babakov (1989), is provided as follows:

$$X = AS(x) + BT(x) + CU(x) + DV(x), \tag{7.32}$$

where

A, B, C, D are integration constants,

$$S = \frac{1}{2}(\cosh kx + \cos kx), \tag{7.33}$$

$$T = \frac{1}{2}(\sinh kx + \sin kx),$$

$$U = \frac{1}{2}(\cosh kx - \cos kx),$$

$$V = \frac{1}{2}(\sinh kx - \sin kx).$$

Taking into account the boundary conditions (7.31), the general solution (7.32) may be simplified to

$$X = CU(x) + DV(x), \tag{7.34}$$

the first three derivatives of which are:

$$\frac{dX}{dx} = Ck\,T(x) + Dk\,U(x),$$

$$\frac{d^2X}{dx^2} = Ck^2\,S(x) + Dk^2\,T(x),$$

$$\frac{d^3X}{dx^3} = Ck^3V(x) + Dk^3S(x).$$

Substitution of (7.34) and its derivatives into (7.28) and (7.30) leads to the system of linear equations with respect to constants C and D:

$$C\left[k^2S(l) + ak^3V(l) + bU(l)\right] + D\left[k^2T(l) + ak^3S(l) + bV(l)\right] = 0,$$

$$C\left[U(l) + akT(l)\right] + D\left[V(l) + akU(l)\right] = 0. \tag{7.35}$$

For a nontrivial solution, the determinant formed by the coefficients C and D in the above equations must be equal to zero:

$$\begin{vmatrix} k^2S(l) + ak^3V(l) + bU(l) & k^2T(l) + ak^3V(l) + bV(l) \\ U(l) + akT(l) & V(l) + akU(l) \end{vmatrix} = 0.$$

The expansion of the above determinant gives

$$kS(l)V(l) - kU(l)T(l) - ak^2T^2(l) + ak^2V^2(l) - a^2k^3S(l)T(l)$$
$$+ a^2k^3U(l)V(l) + abU^2(l) - abV(l)T(l) = 0.$$

Substitution of the expressions for S, T, U, V given by (7.33) results in the frequency equation

$$\left[1 + (ak)^2\right]\cosh kl \ \sin kl - \left[1 - (ak)^2\right]\sinh kl \ \cos kl$$
$$+ 2ak \sinh kl \ \sin kl - \frac{ab}{k}\left(1 - \cosh kl \ \cos kl\right) = 0,$$

or, after substitution of b from (7.29), the frequency equation becomes

$$\left[1+\left(\frac{a}{l}\right)^2(kl)^2\right]\cosh kl\ \sin kl - \left[1-\left(\frac{a}{l}\right)^2(kl)^2\right]\sinh kl\ \cos kl$$

$$+\ 2\frac{a}{l}kl\sinh kl\ \sin kl$$

$$-\left[\frac{J_{tot}}{m_{tot}la^2}\left(\frac{a}{l}\right)^2(kl)^3 - \frac{k_h}{\frac{EI}{l^3}}\left(\frac{a}{l}\right)^2\frac{1}{kl}\right](1-\cosh kl\ \cos kl) = 0.$$

Since the transverse stiffness of a fixed-fixed bellows as a beam according to Frocht (1951) is

$$k_b = \frac{12\,EI}{l^3},$$

and J_{tot} is given by (7.5), the frequency equation can be rewritten as

$$\begin{aligned}
&\left[1+\left(\frac{a}{l}\right)^2(kl)^2\right]\cosh kl\ \sin kl - \left[1-\left(\frac{a}{l}\right)^2(kl)^2\right]\sinh kl\ \cos kl \\
&+\ 2\frac{a}{l}kl\sinh kl\ \sin kl \\
&-\left\{\left[\frac{(m_p+m_{f3})^2}{3m_{tot}l}+\frac{2m_p+m_{f3}}{4m_{tot}l}\frac{R^2}{a}+\frac{M_h}{m_{tot}l}\right]\left(\frac{a}{l}\right)^2(kl)^3\right. \\
&\left.-\frac{12k_h}{k_b}\left(\frac{a}{l}\right)^2\frac{1}{kl}\right\}(1-\cosh kl\ \cos kl) = 0.
\end{aligned} \tag{7.36}$$

This is the final expression of the frequency equation for the system shown in Fig.7.1. In the following two sections this frequency equation will be applied to find the mode functions of the Bernoulli-Euler equation (7.22) as the approximate mode functions for the Rayleigh quotient (7.21).

7.5. General Expression for Universal Expansion Joint Rocking Modes Natural Frequencies

The natural frequency formula for a universal expansion joint without lateral supports can now be easily derived from the frequency expression (7.21), derived in Section 7.3. From there the frequency is,

$$f_k = \frac{1}{2\pi}\sqrt{\frac{\dfrac{EI}{l^3}\displaystyle\int_0^1\left(\frac{d^2X}{d\xi^2}\right)^2 d\xi - \frac{P\pi R_m^2}{l}\int_0^1\left(\frac{dX}{d\xi}\right)^2 d\xi + k_h X^2(1)}{l\,m_{tot}\displaystyle\int_0^1 X^2 d\xi + \frac{J}{l}\int_0^1\left(\frac{dX}{d\xi}\right)^2 d\xi + \frac{J_{tot}}{a^2}X^2(1)}}\,,$$

or

$$f_1 = \frac{1}{2\pi}\frac{A_1}{l^2}\sqrt{\frac{EI}{m_{tot}}}\sqrt{\frac{1 - A_2\dfrac{l^2}{EI}P\pi R_m^2 + A_3\dfrac{k_h^2 l^3}{EI}}{1 + A_4\dfrac{J}{m_{tot}l^2} + A_5\dfrac{J_{tot}}{m_{tot}la^2}}}\,, \qquad (7.37)$$

where

$$A_1 = \sqrt{\frac{\displaystyle\int_0^l\left(\frac{d^2X}{d\xi^2}\right)^2 d\xi}{\displaystyle\int_0^l X^2 d\xi}}\,, \qquad A_2 = \frac{\displaystyle\int_0^l\left(\frac{dX}{d\xi}\right)^2 d\xi}{\displaystyle\int_0^l\left(\frac{d^2X}{d\xi^2}\right)^2 d\xi}\,, \qquad A_3 = \frac{X^2(1)}{\displaystyle\int_0^l\left(\frac{d^2X}{d\xi^2}\right)^2 d\xi}\,,$$

$$A_4 = \frac{\displaystyle\int_0^l\left(\frac{dX}{d\xi}\right)^2 d\xi}{\displaystyle\int_0^l X^2 d\xi}\,, \qquad A_5 = \frac{X^2(1)}{\displaystyle\int_0^l X^2 d\xi}\,. \qquad (7.38)$$

Since, according to (3.1),

$$EI_{eq} = \frac{1}{4} kpR_m^2 ,$$

the final expression for the natural frequency of transverse rocking mode vibration of a universal expansion joint, similar to the case of lateral modes described in Chapter 6, becomes:

$$f_1 = \frac{1}{4\pi} \frac{A_1 R_m}{l^2} \sqrt{\frac{kp}{m_{tot}}} \sqrt{\frac{1 - 4\pi A_2 \dfrac{l^2}{kp} P + 4A_3 \dfrac{k_h l^3}{kpR_m^2}}{1 + A_4 \dfrac{J}{m_{tot} l^2} + A_5 \dfrac{J_{tot}}{m_{tot} l a^2}}} . \tag{7.39}$$

As seen from (7.39), in order to obtain the final expression for the frequency, f, it is necessary to calculate the integrals, residing in (7.38), in which the mode function, X, and its first and second derivatives are involved.

7.6. First Rocking Mode Natural Frequency of Universal Expansion Joint without Lateral Supports

Now the approximate mode function for the first rocking mode of the universal expansion joint will be derived. If there are no lateral supports, then k_h and M_h are equal to zero and the general frequency equation (7.36) becomes

$$\left[1 + \left(\frac{a}{l}\right)^2 (kl)^2\right] \cosh kl \ \sin kl - \left[1 - \left(\frac{a}{l}\right)^2 (kl)^2\right] \sinh kl \ \cos kl$$

$$+ 2\frac{a}{l} k l \sinh kl \ \sin kl - \frac{(m_p + m_{f3})}{3m_{tot}} \left(\frac{a}{l}\right)^3 (kl)^3 \left(1 - \cosh kl \ \cos kl\right) = 0. \tag{7.40}$$

It can be seen from the Fig.2.1 that for the moderate convolution depth,

$$m_p + m_{f3} \cong m_{tot}.$$

Assume to begin with that $a = l$. Then the frequency equation (7.40) simplifies to

$$\left[1 + (kl)^2\right]\cosh kl \ \sin kl - \left[1 - (kl)^2\right]\sinh kl \ \cos kl$$

$$+ \ 2kl \sinh kl \ \sin kl - \frac{1}{3}(kl)^3 \ (1 - \cosh kl \ \cos kl) = 0.$$

The computerized solution of the above frequency equation for the first mode gives $k_1 l = 2.404155$. From (7.34) we get:

$$X = U(x) + \frac{D}{C} V(x). \tag{7.41}$$

From equation (7.35) the ratio D/C is

$$\frac{D}{C} = -\frac{U(l) + akT(l)}{V(l) + akU(l)} = -\frac{\cosh kl - \cos kl + \frac{a}{l}kl(\sinh kl + \sin kl)}{\sinh kl - \sin kl + \frac{a}{l}kl(\cosh kl - \cos kl)} = -1.056106,$$

for $kl = k_1 l = 2.404155$. Substitution of expressions for $U(x)$ and $V(x)$ and the value of the ratio D/C into (7.41) gives the exact mode function for differential equation (7.22) which can be used as the approximate mode function for calculation of the coefficients, A, in (7.38). This mode function, normalized to unity, becomes:

$$X = \frac{1}{1.3135}\left[\cosh c\frac{x}{l} - \cos c\frac{x}{l} - 1.0561\left(\sinh c\frac{x}{l} - \sin c\frac{x}{l}\right)\right], \tag{7.42}$$

where c=2.404155.

Let

$$\frac{x}{l} = \xi.$$

Then the mode function (7.42) can be rewritten as

$$X = \frac{1}{1.3135}\left[\cosh c\xi - \cos c\xi - 1.05611\left(\sinh c\xi - \sin c\xi\right)\right], \tag{7.43}$$

the first and the second derivatives of which are:

$$\frac{dX}{dx} = \frac{c}{1.3135}\left[\sinh c\xi + \sin c\xi - 1.05611\left(\cosh c\xi - \cos c\xi\right)\right],$$

and

$$\frac{d^2X}{dx^2} = \frac{c^2}{1.3135}\left[\cosh c\xi + \cos c\xi - 1.05611\left(\sinh c\xi + \sin c\xi\right)\right].$$

Now values of the integrals in (7.38) can be obtained by numerical integration. Substitution of these values into expressions (7.38) gives:

$A_1 = 7.390$, $A_2 = 0.0568$, $A_4 = 3.0994$, $A_5 = 1.904$.

The value of $X(\xi)$ at $\xi = 1$ was calculated from (7.43) and is $X(1) = 0.9384624$. Substitution of all these numerical values into (7.37) gives

$$f_1 = \frac{1}{2\pi}\,\frac{7.390}{l^2}\sqrt{\frac{EI}{m_{tot}}}\sqrt{\frac{1 - 0.0568\dfrac{l^2}{EI}P\pi R_m^2}{1 + \dfrac{3.0994\,J}{l^2 m_{tot}} + 1.904\dfrac{J_{tot}}{m_{tot} l a^2}}}\,. \tag{7.44}$$

Let us now determine how the mass ratio, residing in the frequency equation (7.40), affects the mode function and subsequently the frequency expression. To do this, we take, for example,

$$m_p + m_{f3} = \frac{1}{2}m_{tot}\,.$$

Now the frequency equation (7.40) becomes

$$\left[1 + (kl)^2\right]\cosh kl\ \sin kl - \left[1 - (kl)^2\right]\sinh kl\ \cos kl$$

$$+ 2kl\sinh kl\ \sin kl - \frac{1}{6}(kl)^3\ (1-\cosh kl\ \cos kl) = 0,$$

the first solution of which, $k_1l = 2.536511$, and the mode function, obtained in the same way as above, is

$$X = \frac{1}{1.4125}\left[\cosh c\frac{x}{l} - \cos c\frac{x}{l} - 1.02618\left(\sinh c\frac{x}{l} - \sin c\frac{x}{l}\right)\right], \tag{7.45}$$

where $c = 2.536511$. Calculation of coefficients (7.38) and substitution of their values into (7.37) gives the familiar frequency expression,

$$f_1 = \frac{1}{2\pi}\frac{7.370}{l^2}\sqrt{\frac{EI}{m_{tot}}}\sqrt{\frac{1 - 0.0570\dfrac{l^2}{EI}P\pi R_m^2}{1 + \dfrac{3.0934\,J}{l^2 m_{tot}} + 1.866\dfrac{J_{tot}}{m_{tot} l a^2}}}. \tag{7.46}$$

Let us compare the two frequency expressions (7.44) and (7.46) using numerical values of a typical bellows, $EI = 5.0$ Nm^2 , $J = 11.5\times10$ kgm, $P\pi R_m^2 = 6000$ N, $m_p + m_{f3} = m_{tot} = 5.0$ kg/m, and $a = l = 0.075$ m. Substitution of these values into equations (7.44) and (7.46) gives accordingly, 123.71 Hz and 123.69 Hz.

As is seen, the difference is very small. Even the mode shapes on which the derivation of the formulas (7.44) and (7.46) was based show a very small difference (see Fig.7.2). Therefore, we can conclude that the ratio of the connecting pipe mass to the bellows mass, as in the case of the first lateral vibration mode of the universal expansion joint, plays an insignificant role in the derivation of the approximate mode shape as well as in the subsequent derivation of the frequency expression of the first rocking mode.

Let us now consider the case when the connecting pipe is much longer, $a = 2l$, and, as before,

$$m_p + m_{f3} = m_{tot}.$$

In this case the frequency equation (7.41) becomes

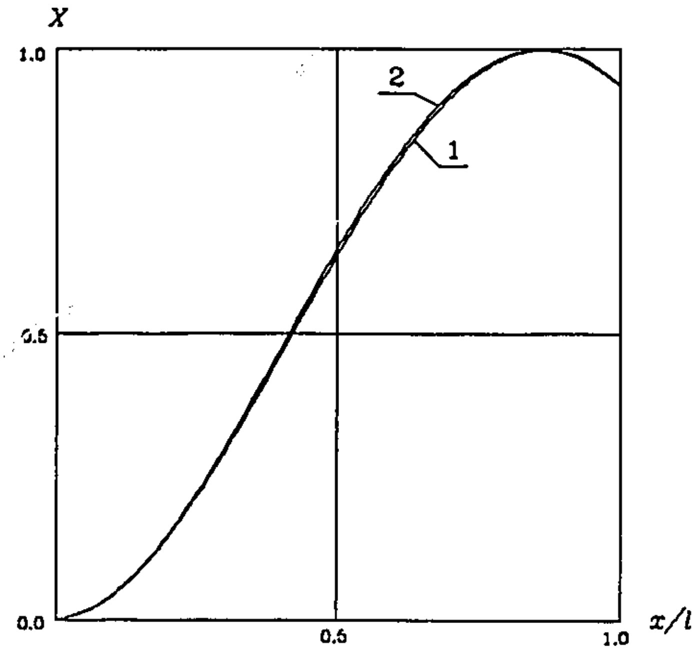

Fig.7.2. Mode shapes: 1 → eq.(7.43), 2 → eq.(7.45)

$$\left[1+4(kl)^2\right]\cosh kl \sin kl - \left[1-4(kl)^2\right]\sinh kl \cos kl$$

$$+ 2kl \sinh kl \sin kl - \frac{8}{3}(kl)^3 \left(1-\cosh kl \cos kl\right) = 0,$$

the first solution of which is $k_1 l = 2.038264$, and the mode function obtained in same way as above is

$$X = \frac{1}{1.1104}\left[\cosh c\frac{x}{l} - \cos c\frac{x}{l} - 1.13304\left(\sinh c\frac{x}{l} - \sin c\frac{x}{l}\right)\right], \tag{7.47}$$

where $c = 2.038264$. Calculation of coefficients (7.38) and substitution of their values into (7.37) gives the frequency expression, similar to (7.46),

$$f_1 = \frac{1}{2\pi}\frac{6.578}{l^2}\sqrt{\frac{EI}{m_{tot}}}\sqrt{\frac{1 - 0.0709\dfrac{l^2}{EI}P\pi R_m^2}{1 + \dfrac{3.0693J}{l^2 m_{tot}} + 2.260\dfrac{J_{tot}}{m_{tot} l a^2}}}. \tag{7.48}$$

Comparison of formulas (7.44) and (7.48) shows that the corresponding numerical coefficients in these formulas differ noticeably. This occurs because, for the rocking mode of bellows vibrations, unlike for the lateral mode described in previous chapter, the mode function depends significantly on the length of the connecting pipe, a, which resides in the boundary condition (7.18). The mode shapes are compared in Fig.7.3. It wouldn't be reasonable in this case to take the mean values of these coefficients for the whole range of connecting pipe lengths, as was done in Chapter 6. Therefore, these coefficients were calculated for the set of values of connecting pipe lengths in the range

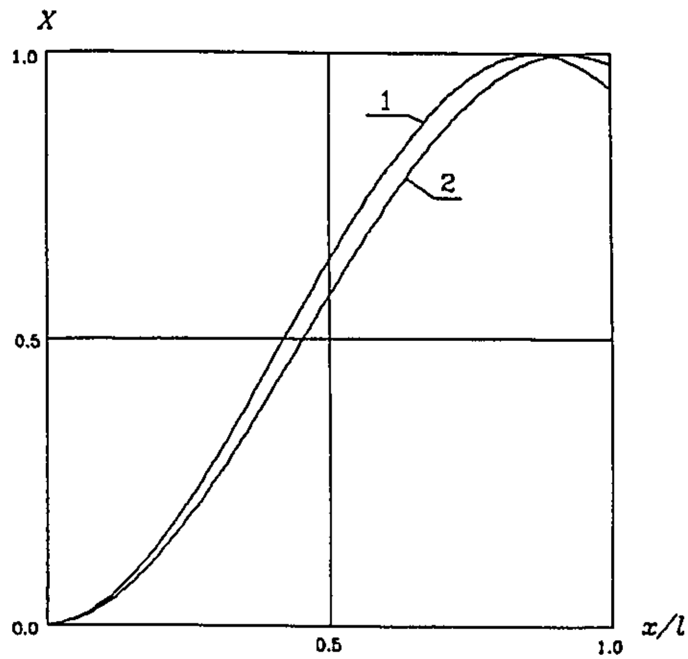

Fig. 7.3. Mode shapes: 1 → eq. (7.43), 2 → eq. (7.44)

$l < a < 2l$ and plotted in the graphs in Fig.7.4 except coefficient A_4, which appeared to be practically independent of a and equal to 3.08. Finally, the frequency expression (7.39), applied to the first rocking mode without lateral supports, becomes:

$$f_1 = \frac{1}{4\pi}\,\frac{A_1 R_m}{l^2}\sqrt{\frac{kp}{m_{tot}}}\;\sqrt{\frac{1 - 4\pi A_2 \dfrac{l^2}{kp} P}{1 + \dfrac{3.08 J}{l^2 m_{tot}} + A_5 \dfrac{J_{tot}}{m_{tot} l a^2}}}\,, \tag{7.49}$$

where, as it was derived in Chapter 3, eq.(3.57),

$$m_{tot} = \frac{4\pi R_m}{p}\left(h + 0.285\,p\right) t\rho_b + \left[\pi\left(R_m - \frac{h}{2} + \frac{2hR_2}{p}\right)^2 + \alpha_{f2k}\,\mu R_m^3\right]\rho_f.$$

As in previous chapters, α_{f2k} was calculated using formula (3.26):

$$\alpha_{f21} = 0.066\,\frac{\int_0^l \left(\frac{d^2X_k}{dx^2}\right)^2 dx}{\int_0^l X_k^2(x)\,dx}\left(R_m - \frac{h}{2}\right)^2 p.$$

Taking $\frac{x}{l} = \xi$, both integrals in the above formula can be rewritten as

$$\int_0^l \left(\frac{d^2X_1}{dx^2}\right)^2 dx = \frac{1}{l^3}\int_0^1 \left(\frac{d^2X_1}{d\xi^2}\right)^2 d\xi$$

and

$$\int_0^l X_1^2(x)\,dx = l\int_0^1 X_1^2(\xi)\,d\xi.$$

Substitution of these replacements into the formula for α_{f21} leads to:

$$\alpha_{f21} = \frac{0.066}{l^4}\,\frac{\int_0^l \left(\frac{d^2X_1}{d\xi^2}\right)^2 d\xi}{\int_0^1 X_1^2(\xi)\,d\xi}\left(R_m - \frac{h}{2}\right)^2 p.$$

Since, according to (7.37),

$$\sqrt{\frac{\int_0^l \left(\frac{d^2 X_1}{d\xi^2}\right)^2 d\xi}{\int_0^l X_1^2\, d\xi}} = A_1 ,$$

the final expression for α_{f21} becomes

$$\alpha_{f21} = 0.066\, \frac{A_1^2}{l^4} \left(R_m - \frac{h}{2}\right)^2 p , \tag{7.50}$$

where A_1 can be taken from the graph in Fig.7.4.

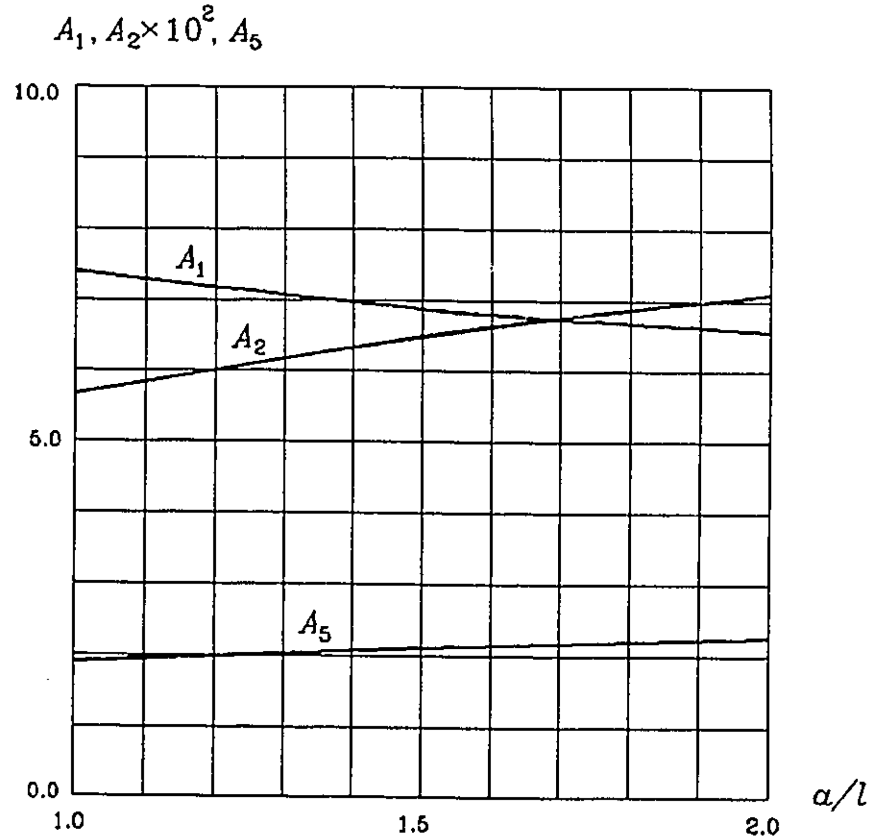

Fig.7.4. Coefficients A_1, A_2, and A_5 for the first rocking mode without lateral supports

The total moment of inertia of the cross-section of bellows is given by (3.67):

$$J = \pi R_m^3 \left[\left(2\frac{h}{p} + 0.571 \right) t\rho_b + \frac{h}{p}\left(2R_2 - t\right)\rho_f \right].$$

Provided M_h is equal to zero, the second moment of inertia of the connecting pipe, J_{tot}, given by (3.68), becomes:

$$J_{tot} = \frac{\left(m_p + m_{f3}\right)a^3}{3} + \frac{2m_p + m_{f3}}{4} a R^2 .$$

7.7. Second and Third Rocking Mode Natural Frequency of Universal Expansion Joint without Lateral Supports

For the second mode, the frequency equation remains the same as for the first rocking mode, (7.40),

$$\left[1 + \left(\frac{a}{l}\right)^2 (kl)^2\right] \cosh kl \ \sin kl - \left[1 - \left(\frac{a}{l}\right)^2 (kl)^2\right] \sinh kl \ \cos kl$$

$$+ 2\frac{a}{l} kl \sinh kl \ \sin kl - \frac{\left(m_p + m_{f3}\right)}{3m_{tot}} \left(\frac{a}{l}\right)^3 (kl)^3 \left(1 - \cosh kl \ \cos kl\right) = 0. \qquad (7.51)$$

It can be seen from Fig.2.1 that for the moderate convolution depth,

$$m_p + m_{f3} \cong 0.66666\, m_{tot} .$$

The frequency equation (7.51) was solved for three different connecting pipe lengths, $a = l$, $a = 1.5l$, $a = 2l$. The second solution of (7.51) for these three different a values gave:

$$k_2 l_l = 5.300058, \ \ k_2 l_{1.5l} = 5.159754, \ \ k_2 l_{2l} = 5.076394 .$$

Substitution of these three values into expression (7.35) for D/C and subsequent use of (7.34) gives three slightly different approximate second rocking mode functions for the universal expansion joint. These three mode functions, normalized to unity, are:

$$X_2 = \frac{1}{1.5314}\left[\cosh c\xi - \cos c\xi - 0.99542\left(\sinh c\xi - \sin c\xi\right)\right],$$

$$X_2 = \frac{1}{1.5400}\left[\cosh c\xi - \cos c\xi - 0.99340\left(\sinh c\xi - \sin c\xi\right)\right],$$

$$X_2 = \frac{1}{1.5465}\left[\cosh c\xi - \cos c\xi - 0.99189\left(\sinh c\xi - \sin c\xi\right)\right], \qquad (7.52)$$

where

$$c = kl \quad \text{and} \quad \xi = \frac{x}{l}.$$

Substitution of these three mode functions and their derivatives into expressions (7.38) gives the three sets of coefficients, A_1 , A_2 , A_4 , A_5 for three different lengths of a as shown in Table 7.1.

Table 7.1. Comparison of coefficients A for the second rocking mode

a	l	$1.5l$	$2l$
A_1	30.910	29.320	28.200
A_2	0.0237	0.0243	0.0245
A_4	22.63	20.85	19.48
A_5	0.9499	0.6377	0.4469

Since these coefficients vary noticeably with respect to a, they are plotted in Fig.7.5. The frequency expression remains the same as in (7.39):

$$f_1 = \frac{1}{4\pi}\,\frac{A_1 R_m}{l^2}\sqrt{\frac{kp}{m_{tot}}}\sqrt{\frac{1 - 4\pi A_2 \dfrac{l^2}{kp} P}{1 + A_4 \dfrac{J}{m_{tot} l^2} + A_5 \dfrac{J_{tot}}{m_{tot} l a^2}}}, \qquad (7.53)$$

where, as derived in Chapter 3, eq.(3.57),

$$m_{tot} = \frac{4\pi R_m}{p}(h + 0.285\,p)\,t\rho_b + \left[\pi\left(R_m - \frac{h}{2} + \frac{2hR_2}{p}\right)^2 + \alpha_{f22}\mu_{1/2}R_m^3\right]\rho_f .$$

α_{f22} can be calculated using formula (7.50) for the first rocking mode:

$$\alpha_{f22} = 0.066\,\frac{A_1^2}{l^4}\left(R_m - \frac{h}{2}\right)^2 p .$$

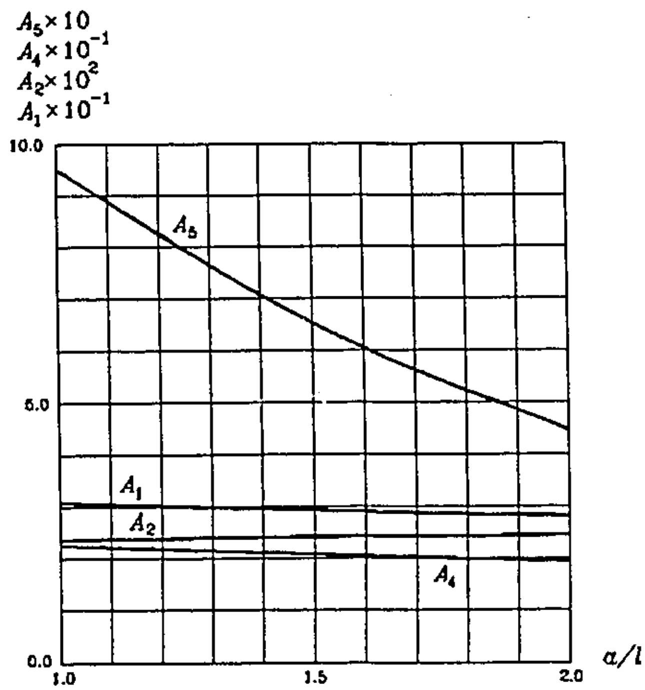

Fig.7.5. Coefficients A_1, A_2, A_4, A_5 for the second rocking mode without lateral supports

The total moment of inertia of the cross-section of bellows is given by (3.67):

$$J = \pi R_m^3\left[\left(2\frac{h}{p} + 0.571\right)t\rho_b + \frac{h}{p}(2R_2 - t)\,\rho_f\right].$$

Provided M_h is equal to zero, the second moment of inertia of the connecting pipe, J_{tot}, given by (3.68) in Chapter 3, becomes:

$$J_{tot} = \frac{(m_p + m_{f3})a^3}{3} + \frac{2m_p + m_{f3}}{4} a R^2.$$

The second mode frequency formula (7.53) and subsequent formulas for m_{tot} and α_{f22} can be used for third mode frequency calculation. The coefficients A_1, A_2, A_4, A_5 must be taken from Fig.7.6.

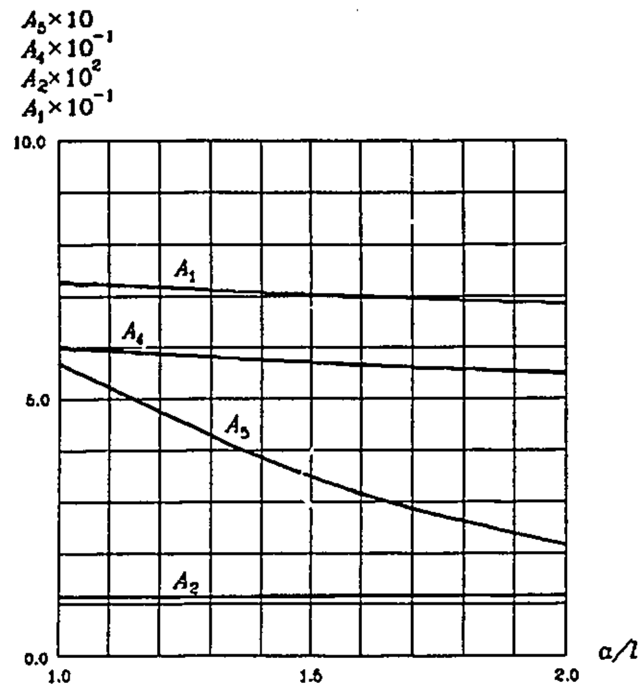

Fig.7.6. Coefficients A_1, A_2, A_4, A_5 for the third rocking mode without lateral supports

7.8. First Rocking Mode Natural Frequency of Universal Expansion Joint with Lateral Supports

It is necessary in this case to take into account the transverse stiffness of the lateral supports, k_h, and their equivalent mass, M_h. In practice the transverse stiffness of lateral supports, k_h, varies over the range:

$$k_b < k_h < 3k_b.$$

Since the transverse stiffness of lateral supports in the given range doesn't affect the mode shape of the bellows appreciably, an average value is taken

$$k_h = 1.5k_b\,,$$

where k_b is the fixed-fixed bellows transverse stiffness.

Approximately,

$$M_h \cong \frac{a}{3}\left(m_p + m_{f3}\right),$$

and

$$m_p + m_{f3} \cong m_{tot}\,.$$

For the first case, assume

$$a = l.$$

Since the radius of the connecting pipe, R, is significantly smaller than pipe length, a, a simple analysis of the ratio, residing in the brackets of the frequency equation (7.36) shows, that

$$\left[\frac{\left(m_p + m_{f3}\right)}{3m_{tot}}\frac{a}{l} + \frac{\left(2m_p + m_{f3}\right)}{4m_{tot}}\frac{R^2}{a\,l}\right]\left(\frac{a}{l}\right)^2 (k\,l)^3 \cong \frac{2}{3},$$

and the frequency equation (7.36) simplifies to

$$\left[1 + (kl)^2\right]\cosh kl\ \sin kl\ - \left[1 - (kl)^2\right]\sinh kl\ \cos kl$$

$$+\ 2\,kl\sinh kl\ \sin kl\ - \left[\frac{2}{3}(kl)^3 - \frac{18}{kl}\right]\left(1 - \cosh kl\ \cos kl\right) = 0\,.$$

A computerized solution of the equation above for the first mode frequency gives $k_1 l = 2.50138$.

From (7.34) we obtain the general expression of the mode function:

$$X = U(x) + \frac{D}{C}V(x)\,.$$

Substitution of the obtained value $k_1 l$ into (7.35) produces the ratio

$$\frac{D}{C} = -1.03349.$$

Substitution of expressions for $U(x)$ and $V(x)$ from (7.33) and the above numerical value of D/C into the general expression of the mode function above gives the exact solution for differential equation (7.22) which can be used as the approximate mode function for the calculation of coefficients A in (7.38). Normalized to unity, this mode function becomes:

$$X = \frac{1}{1.3870}\left[\cosh c\frac{x}{l} - \cos c\frac{x}{l} - 1.03349\left(\sinh c\frac{x}{l} - \sin c\frac{x}{l}\right)\right]. \qquad (7.51)$$

Let $\frac{x}{l} = \xi$. Then the mode function (7.42) can be rewritten as

$$X = \frac{1}{1.387}\left[\cosh c\xi - \cos c\xi - 1.03349\left(\sinh c\xi - \sin c\xi\right)\right],$$

the first and the second derivatives of which are:

$$\frac{dX}{dx} = \frac{c}{1.387}\left[\sinh c\xi + \sin c\xi - 1.03349\left(\cosh c\xi - \cos c\xi\right)\right],$$

and

$$\frac{d^2X}{dx^2} = \frac{c^2}{1.387}\left[\cosh c\xi + \cos c\xi - 1.03349\left(\sinh c\xi + \sin c\xi\right)\right].$$

Now values of the integrals in (7.38) can be obtained by numerical integration. Substitution of these values into expressions (7.38) gives:

$A_1 = 7.372,\quad A_2 = 0.0569,\quad A_3 = 0.0345,\quad A_4 = 3.094,\quad A_5 = 1.877.$

The value $X(1) = 0.9361$ was calculated from the mode function expression $X(\xi)$ given above.

Substitution of all these numerical values into (7.37) gives the frequency expression,

$$f_1 = \frac{1}{2\pi}\frac{7.372}{l^2}\sqrt{\frac{EI}{m_{tot}}}\sqrt{\frac{1-0.0569\dfrac{l^2}{EI}P\pi R_m^2 + 0.0345\dfrac{k_h^2 l^3}{EI}}{1+3.094\dfrac{J}{m_{tot}l^2} + 1.877\dfrac{J_{tot}}{m_{tot}la^2}}}\,. \tag{7.52}$$

Let us now take

$$a = 2l$$

while the rest of the parameters remain the same. Then the frequency equation (7.36) becomes

$$\left[1+4(kl)^2\right]\cosh kl\ \sin kl - \left[1-4(kl)^2\right]\sinh kl\ \cos kl$$

$$+\ 4kl\sinh kl\ \sin kl - \left[\frac{16}{3}(kl)^3 - \frac{72}{kl}\right]\left(1-\cosh kl\ \cos kl\right) = 0.$$

A computerized solution of the equation above for the first mode frequency gives $k_1 l = 2.1385$. Normalized to unity the mode function, obtained as in the previous section, is:

$$X = \frac{1}{1.2012}\left[\cosh c\frac{x}{l} - \cos c\frac{x}{l} - 1.09572\left(\sinh c\frac{x}{l} - \sin c\frac{x}{l}\right)\right], \tag{7.53}$$

where $c = 2.1385$. Calculation of coefficients (7.38) using the mode function (7.53) with its first and second derivatives and substituting their values into (7.37) gives the frequency expression:

$$f_1 = \frac{1}{2\pi}\frac{6.563}{l^2}\sqrt{\frac{EI}{m_{tot}}}\sqrt{\frac{1-0.0710\dfrac{l^2}{EI}P\pi R_m^2 + 0.0521\dfrac{k_h^2 l^3}{EI}}{1+3.058\dfrac{J}{m_{tot}l^2} + 2.242\dfrac{J_{tot}}{m_{tot}la^2}}}\,. \tag{7.54}$$

Comparison of formulas (7.52) and (7.54) shows that the corresponding numerical coefficients, as in the previous section, are appreciably different. This occurs because, for the rocking mode of bellows vibrations, unlike the lateral mode described in the previous chapter, the mode function depends significantly on the length of the connecting pipe, a, which resides in the boundary condition (7.18). The mode shapes are compared in Fig.7.7. It wouldn't be reasonable in this case to take the mean values of these coefficients for the whole range of connecting pipe lengths, as was done in Chapter 6, except A_4, which appeared to be practically independent of a and equal to ~3.073.

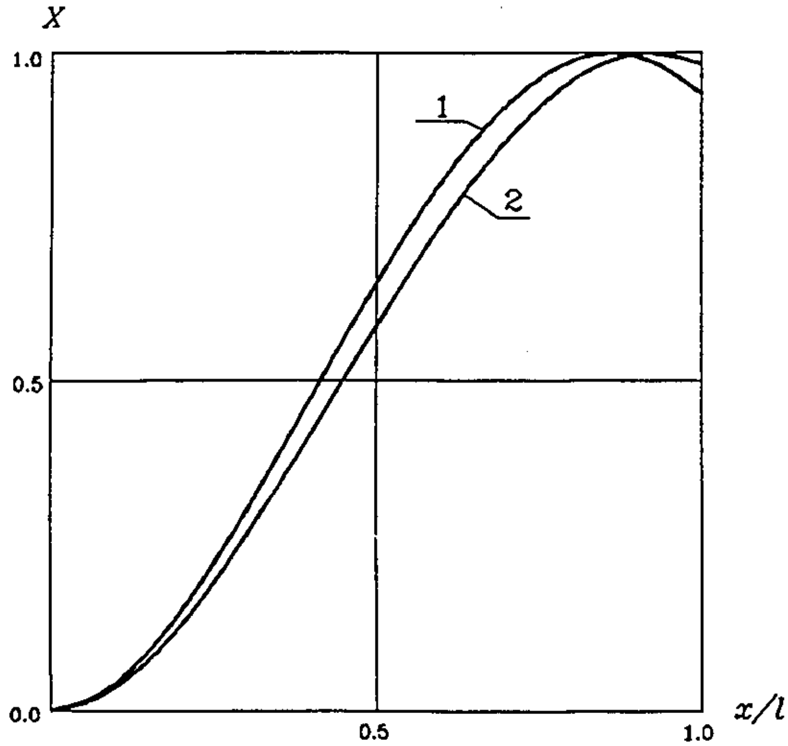

Fig.7.7. The mode shapes: 1 → for $a = l$, 2 → for $a = 2l$

Therefore, these coefficients were calculated for the set of values of connecting pipe lengths in the range $l < a < 2l$ and plotted in Fig.7.8 as functions of the connecting pipe length, a.

The final expression for the natural frequency of the transverse vibration of a universal expansion joint in its rocking mode with lateral supports becomes, using (7.39):

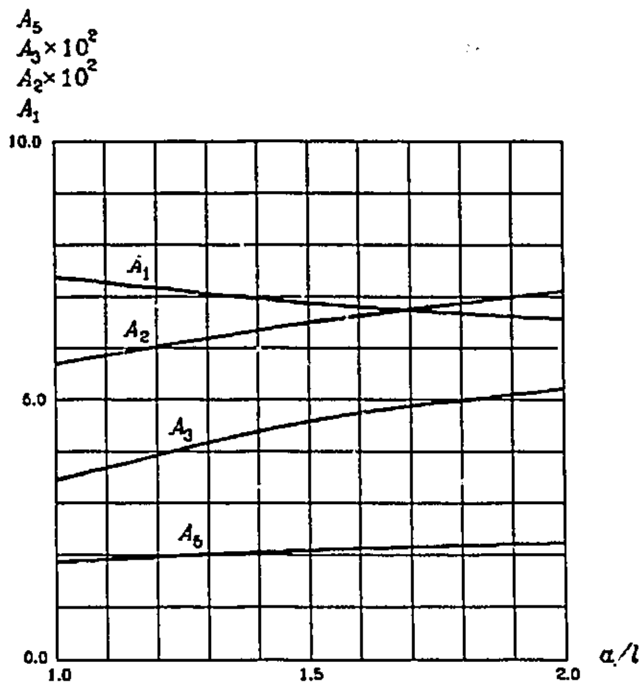

Fig.7.8. Coefficients A_1 , A_2 , A_3 , and A_5 for the rocking mode with lateral supports

$$f_1 = \frac{1}{4\pi}\,\frac{A_1 R_m}{l^2}\,\sqrt{\frac{kp}{m_{tot}}}\,\sqrt{\frac{1 - 4\pi A_2 \dfrac{l^2}{kp} P + 4A_3 \dfrac{k_h l^3}{kpR_m^2}}{1 + 3.073 \dfrac{J}{m_{tot} l^2} + A_5 \dfrac{J_{tot}}{m_{tot} l a^2}}}\,, \qquad (7.56)$$

where, as it was derived in Chapter 3, equation (3.57),

$$m_{tot} = 4\pi R_m \left(\frac{h}{p} + 0.285\right) t\rho_b + \left[\pi\left(R_m - \frac{h}{2} + \frac{2hR_2}{p}\right)^2 + \alpha_{f21}\,\mu_{1/2}\,R_m^3\right]\rho_f\,.$$

As in previous sections, α_{f21} can be calculated using formula (7.50), derived earlier in this chapter:

$$\alpha_{f21} = 0.066\,\frac{A_1^2}{l^4}\left(R_m - \frac{h}{2}\right)^2 p\,.$$

The total moment of inertia of the cross-section of bellows is given by (3.67):

$$J = \pi R_m^3 \left[\left(2\frac{h}{p} + 0.571 \right) t\rho_b + \frac{h}{p}\left(2R_2 - t\right)\rho_f \right].$$

According to (3.68),

$$J_{tot} = \frac{\left(m_p + m_{f3}\right)a^3}{3} + \frac{2m_p + m_{f3}}{4} a R^2 + M_h a^2.$$

7.9. The Exact Solution of Universal Expansion Joint Rocking Mode Natural Frequency and Its Comparison with Rayleigh Quotient Solution

The rocking mode natural frequency formulae for universal expansion joints were derived in previous sections using the Rayleigh method. These were approximate solutions, of course. Here, as in Chapter 6, we will solve the same problem exactly, in order to define the error inherent in the approximate frequency formula (7.49).

Let's take the differential equation (7.16) already given in Section 7.3,

$$EI\frac{d^4X}{dx^4} + P\pi R_m^2 \frac{d^2X}{dx^2} + J\omega^2 \frac{d^2X}{dx^2} - \omega^2 m_{tot} X = 0 \qquad (7.57)$$

From here,

$$\frac{d^4X}{dx^4} + \frac{P\pi R_m^2 + J\omega^2}{EI}\frac{d^2X}{dx^2} - \omega^2 \frac{m_{tot}}{EI} X = 0.$$

If

$$c = \sqrt{\frac{P\pi R_m^2 + J\omega^2}{2EI}} \qquad (7.58)$$

and

$$\lambda = \sqrt{\frac{m_{tot}\omega^2}{EI}}, \qquad (7.59)$$

then equation (7.57) becomes

$$\frac{d^4X}{dx^4} + 2c^2\frac{d^2X}{dx^2} - \lambda^4 X = 0.$$

This is the same equation as (4.22) in Section 4.3. As was derived there, the general solution of this equation is

$$X = A\sinh\alpha x + B\cosh\alpha x + C\sin\beta x + D\cos\beta x, \qquad (7.60)$$

first, second and third derivatives of which are

$$\frac{dX}{dx} = A\alpha\cosh\alpha x + B\alpha\sinh\alpha x + C\beta\cos\beta x - D\beta\sin\beta x,$$

$$\frac{d^2X}{dx^2} = A\alpha^2\sinh\alpha x + B\alpha^2\cosh\alpha x - C\beta^2\sin\beta x - D\beta^2\cos\beta x,$$

$$\frac{d^3X}{dx^3} = A\alpha^3\cosh\alpha x + B\alpha^3\sinh\alpha x - C\beta^3\cos\beta x + D\beta^3\sin\beta x,$$

where

$$\alpha = \sqrt{-c^2 + \sqrt{c^4 + \lambda^4}}, \qquad (7.61)$$

$$\beta = \sqrt{c^2 + \sqrt{c^4 + \lambda^4}}. \qquad (7.62)$$

and A, B, C, D are the arbitrary constants.

The boundary conditions are the same as in previous sections of this chapter,

$$\frac{d^3X(l)}{dx^3} = -\frac{d^2X(l)}{dx^2}\frac{1}{a} - \frac{P\pi R_m^2}{EI}\frac{dX(l)}{dx} - \frac{J\omega^2}{EI}\frac{dX(l)}{dx}$$
$$- \omega^2\frac{J_{tot}}{EIa^2}X(l) + \frac{k_h}{EI}X(l). \qquad (7.19)$$

or

$$\frac{d^3X(l)}{dx^3} = -\frac{1}{a}\frac{d^2X(l)}{dx^2} - 2c^2\frac{dX(l)}{dx} - bX(l) \tag{7.63}$$

if

$$b = \omega^2\frac{J_{tot}}{EIa^2} - \frac{k_h}{EI} \tag{7.64}$$

and c is given by (7.58).

The rest of the boundary conditions are the same as given by (7.18) and (7.17):

$$\frac{dX(l)}{dx} = -\frac{X(l)}{a}, \tag{7.65}$$

$$X(0) = \frac{dX(0)}{dx} = 0, \tag{7.66}$$

Substitution of the general solution (7.60) and its derivatives into boundary condition expressions (7.63), (7.65), and (7.66) gives the set of linear equations with respect to A, B, C, and D:

$$B + D = 0,$$

$$\alpha A + \beta C = 0,$$

$$\begin{aligned}&(\alpha a\cosh\alpha l + \sinh\alpha l)A + (\alpha a\sinh\alpha l + \cosh\alpha l)B \\ &+ (\beta a\cos\beta l + \sin\beta l)C - (\beta a\sin\beta l - \cos\beta l)D = 0,\end{aligned}$$

$$\begin{aligned}&\left(\alpha^3\cosh\alpha l + \frac{\alpha^2}{a}\sinh\alpha l + 2c^2\alpha\cosh\alpha l + b\sinh\alpha l\right)A \\ &+\left(\alpha^3\sinh\alpha l + \frac{\alpha^2}{a}\cosh\alpha l + 2c^2\alpha\sinh\alpha l + b\cosh\alpha l\right)B \\ &-\left(\beta^3\cos\beta l + \frac{\beta^2}{a}\sin\beta\alpha l - 2c^2\beta\cos\beta l - b\sin\beta l\right)C \\ &+\left(\beta^3\sin\beta l - \frac{\beta^2}{a}\cos\beta\alpha l - 2c^2\beta\sin\beta l + b\cos\beta l\right)D = 0.\end{aligned}$$

For a nontrivial solution, the determinant formed by the coefficients of this system of algebraic equations must be equal to zero:

$$\begin{vmatrix} 0 & 1 & 0 & 1 \\ \alpha & 0 & \beta & 0 \\ \begin{matrix}\alpha a \cosh \alpha l \\ + \sinh \alpha l\end{matrix} & \begin{matrix}\alpha a \sinh \alpha l \\ + \cosh \alpha l\end{matrix} & \begin{matrix}\beta a \cosh \beta l \\ + \sinh \beta l\end{matrix} & \begin{matrix}-(\beta a \sin \beta l \\ - \cos \beta l)\end{matrix} \\ c_1 & c_2 & -c_3 & c_4 \end{vmatrix} = 0,$$

where,

$$c_1 = \alpha^3 \cosh \alpha l + \frac{\alpha^2}{a} \sinh \alpha l + 2c^2 \alpha \cosh \alpha l + b \sinh \alpha l,$$

$$c_2 = \alpha^3 \sinh \alpha l + \frac{\alpha^2}{a} \cosh \alpha l + 2c^2 \alpha \sinh \alpha l + b \cosh \alpha l,$$

$$c_3 = \beta^3 \cos \beta l + \frac{\beta^2}{a} \sin \beta a l - 2c^2 \beta \cos \beta l - b \sin \beta l,$$

$$c_4 = \beta^3 \sin \beta l - \frac{\beta^2}{a} \cos \beta a l - 2c^2 \beta \sin \beta l + b \cos \beta l.$$

Expansion of the above determinant results in the frequency equation for the system shown in Fig.7.1:

$$\begin{aligned} &(\alpha b_2 - \beta a_2 - \alpha\beta a b_1 + \alpha\beta a a_1)(1 - \cos\beta l \cosh\alpha l) \\ &- (\alpha a_2 - \beta b_2 - \beta^2 a a_1 + \alpha^2 a b_1) \sin\beta l \sinh\alpha l \\ &- (\alpha b_1 + \alpha a_1 + \beta^2 a a_2 + \alpha\beta a b_2) \sin\beta l \cosh\alpha l \\ &+ (\beta a_1 + \beta b_1 - \alpha^2 a b_2 - \alpha\beta a a_2) \cos\beta l \sinh\alpha l = 0, \end{aligned} \tag{7.67}$$

where:

α and β are given by (7.61) and (7.62),

$$a_1 = \frac{\alpha^2}{a} + b,$$

$$a_2 = \alpha^3 + 2c^2\alpha,$$

$$b_1 = \frac{\beta^2}{a} - b,$$

$$b_2 = \beta^3 - 2c^2\beta.$$

It should be noted that when $c = 0$, $\alpha = \beta = \lambda$. Here, as must be the case, the frequency equation (7.67) simplifies to the frequency equation (7.36) derived in Section 7.4.

Let us take the universal expansion joint with the following geometrical and physical parameters: bellows length, $l = 0.0693$ m, mass moment of inertia per unit length, $J = 0.001153$ kgm, $EI = 5.078\ \mathrm{Nm}^2$, total bellows mass, $m_{tot} = 5.138$ kg/m, total connecting pipe mass, $m_p + m_\beta = 5.0$ kg/m, $a = l$, and no lateral supports. According to (4.31), the maximum allowable pressure in bellows is,

$$P_{max} = \frac{\pi k p}{6.666 l^2}. \tag{7.68}$$

According to (3.1),

$$EI = \frac{1}{4} k p R_m^2. \tag{7.69}$$

Substitution of (7.68), (7.69) and the numerical values given above into (7.58) and (7.59) leads to

$$c = \sqrt{616.49 + 0.0001135\omega^2} \tag{7.70}$$

and

$$\lambda = 1.0029\sqrt{\omega}. \tag{7.71}$$

From (7.64), providing $k_h = 0$,

$$b = 0.0227\,\omega^2. \tag{7.72}$$

Now, using expressions (7.76), (7.71), (7.72), (7.61) and (7.62), the frequency equation (7.67) can be solved at the computer precision level. The first and the second natural frequency obtained from computerized solution of (7.67) are given in Table 7.2.

The same frequency was calculated for the same bellows data using frequency formula (7.49) derived in the previous section from the Rayleigh quotient. Both results are compared in Table 7.2.

Table 7.2. Comparison of the exact and approximate frequency solutions for the universal expansion joint first rocking mode

Mode #	Exact ω	Rayleigh ω	Error
	(rad/s)	(rad/s)	(%)
1	935.686	938.93	0.35
2	3855.928		

As seen from the comparison in Table 7.2, the error of the frequency obtained from the Rayleigh quotient is comparatively small. Therefore, formula (7.49) is sufficiently accurate for estimation of the first rocking mode frequency of a universal expansion joint.

7.10. Instability Condition for Universal Expansion Joint Rocking Mode

It may be seen from equation (7.56) that with the particular combination of the parameters P, p, k, and l the numerator of the expression under the last root can become equal to zero:

$$1 - 4\pi A_2 \frac{l^2}{kp} P + 4A_4 \frac{k_h l^3}{kpR_m^2} = 0 .$$

From here the critical pressure is,

$$P_{cr} = \frac{kp}{4\pi l^2 A_2} + \frac{k_h l A_4}{\pi R_m^2 A_2} .$$

The last equation shows that the presence of lateral supports increases the critical pressure, P_{cr} , and makes an expansion joint less susceptable to buckling. For the expansion joint without lateral supports, $k_h = 0$, and the above expression simplifies to

$$P_{cr} = \frac{kp}{4\pi l^2 A_2}.$$

All parameters residing in the above formulas were listed earlier in this Chapter.

CHAPTER 8

EXPERIMENTAL INVESTIGATION OF NATURAL TRANSVERSE VIBRATIONS OF BELLOWS EXPANSION JOINT

8.1. Apparatus for Investigation of Natural Transverse Vibrations of Fixed-Fixed Bellows

An experimental investigation of the frequencies of natural transverse vibrations of bellows was conducted using the apparatus shown in Fig.8.1. The apparatus is made up of the left and right flanges **1** and **3** rigidly fixed to each other by four bolts **4**. To maintain the appropriate distance between the two flanges, spacers, **2**, were used around the bolts, **4**. The length of the spacers was chosen such that the test piece of the bellows, **9**, was almost in a strain free state. Bellows flanges were fixed to the frame flanges **1** and **3** using eight bolts, **6**. Later experiments showed that the frequency results didn't depend on the degree of tightening of the bolts, **6**, exept in the case where they were almost loose. The pressure inside the bellows was controlled by means of the valves, **5**, **8** and the pressure gauge , 7.

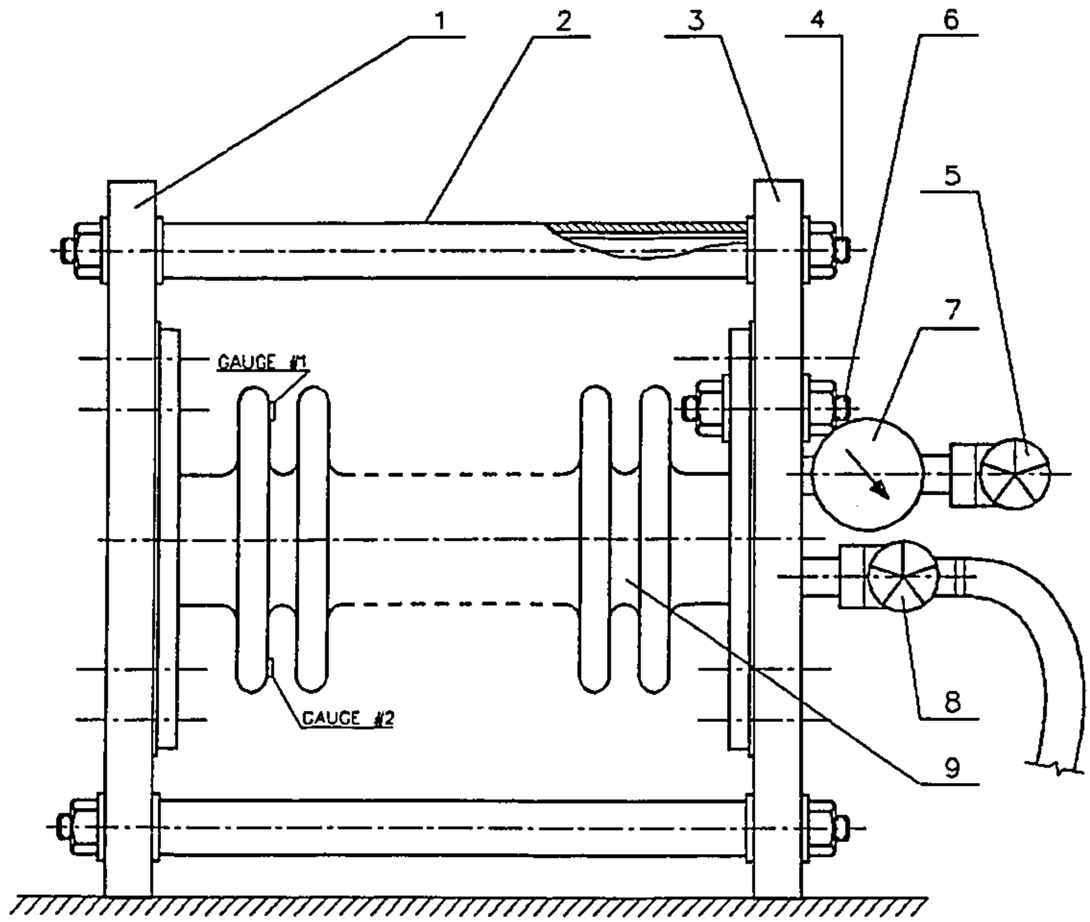

Fig.8.1. The principle scheme of the test apparatus
for investigation of natural transverse vibration of bellows expansion joint

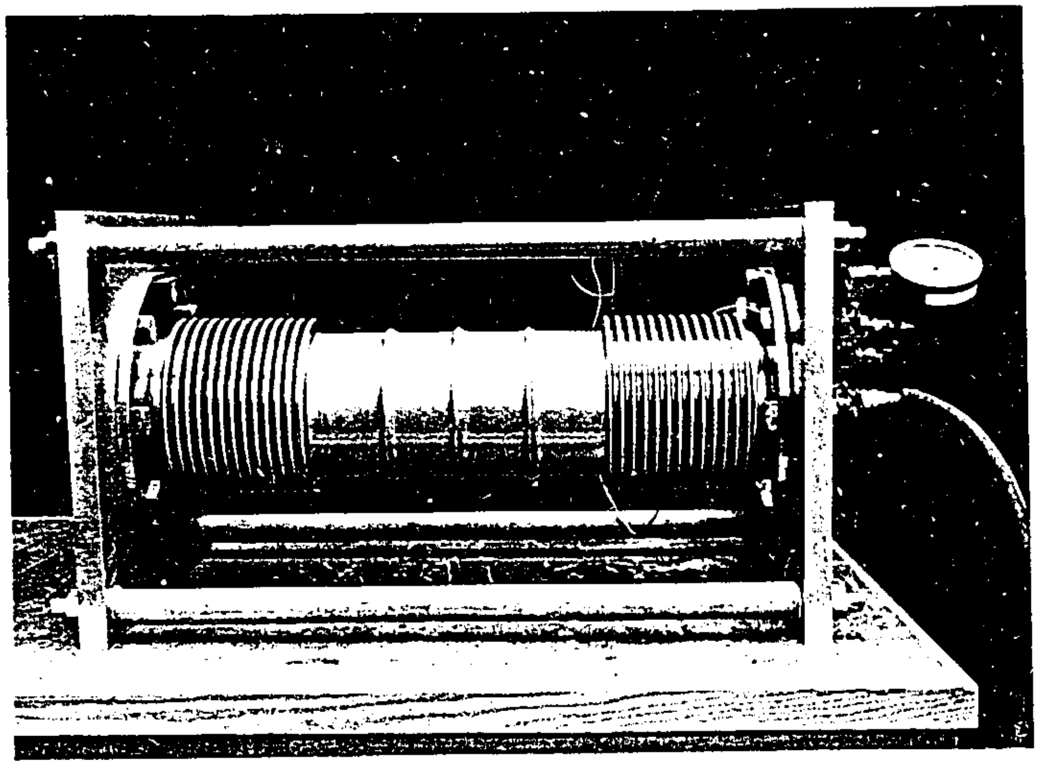

Fig.8.2. General view of mounted bellows

It is comparatively difficult to assure a perfectly fixed boundary condition because any body to which an experimental specimen is fixed is not absolutely rigid. It was especially important in this case that both flanges of the frame be fixed with respect to each other. Therefore, the frame was designed to have its first axial natural frequency as high as possible in comparison with the first transverse natural frequency of the bellows expansion joint to be mounted inside of it. For this purpose, the end flanges of the frame were made of comparatively light aluminum while the bolts and spacers were made from more rigid steel.

This structure, from the point of view of axial vibrations, was treated as a rod (four bolts with spacers) carrying two concentrated masses at the ends (flanges).The first natural frequency was calculated using a formula taken from Voltera, Zachmanoglou (1965):

$$f_1 = \frac{1}{2\pi}\sqrt{\frac{EQ}{L(m+\rho LQ/3)}}$$

$$= \frac{1}{2\pi}\sqrt{\frac{2.07\times10^{11}\times0.002556}{0.112\times(17.50+7860.0\times0.112\times0.002556/3.0)}} = 2561 \text{ Hz},$$

where

E is the modulus of elasticity of bolts in Pa,

Q is the cross-sectional area of the bolts in m^2,

L is one half the distance between the centroidal planes of flanges in m,

ρ is the density of the bolt material in kg/m^3,

m is the mass of a flange, kg.

The above calculated first frequency of the frame (2561 Hz) is more than 20 times higher than the first natural frequency of the fixed-fixed single bellows expansion joint (124 Hz). Such a large difference between the natural frequencies of the bellows and the frame permits the neglect of any dynamical interaction between them till at least 800 Hz, i.e., up to the fourth natural frequency of the specimen of an expansion joint used. For a double bellows expansion joint test or for experiments with water inside, the natural frequences of the bellows were even lower. Therefore, the frame described above was considered as a reliable apparatus for the implementation of the "fixed-fixed" boundary condition for testing the bellows.

According to beam bending theory, the deformation of a beam is proportional to the second derivative of the mode function. The analysis of the mode functions of the single and double bellows expansion joints demonstrated that the extreme values of the second derivatives are at the fixed ends of a bellows. Furthermore, as it was shown by Jakubauskas (1991), the most flexible areas of a convolution are the very outermost and the very innermost zones of the flat surface of a convolution. Therefore, strain gauges were glued in the outermost zone of a flat surface of one of the end convolutions (Figure 8.1). Because of the small geometry of a convolution, the strain gauges used were as small as possible, type MM EA-06-031EG-350.

8.2. The Method and Results of Experimental Investigation of Natural Vibrations of Bellows Expansion Joint

Three broadly different test procedures are currently used for the experimental investigation of vibrations. These techniques are called swept sine, random and impulsive excitation procedures. Each of them has certain inherent advantages and disadvantages. Two types of excitation may be used for all three above mentioned test procedures: base excitation and direct excitation of the vibrating body itself. The excitation can be implemented as a concentrated force applied at one or a few stations or as a distributed force using, for example, magnetic or acoustic excitation. Which kind of test procedures or excitation type is to be used, depends on the instrumentation available and on the nature of the test body itself.

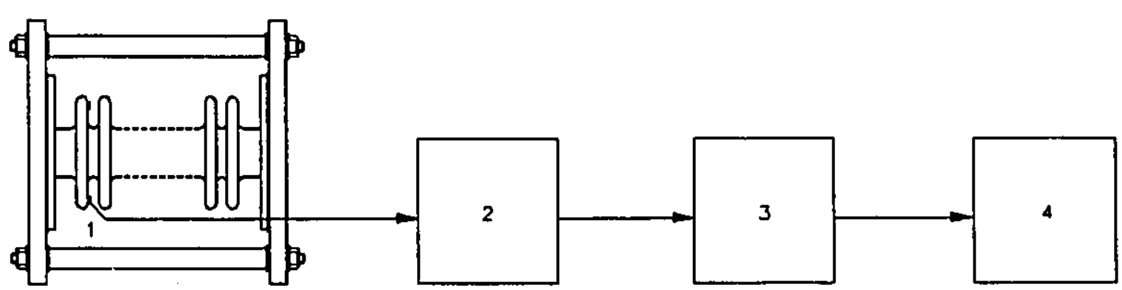

Fig.8.3. Shock excitation diagram

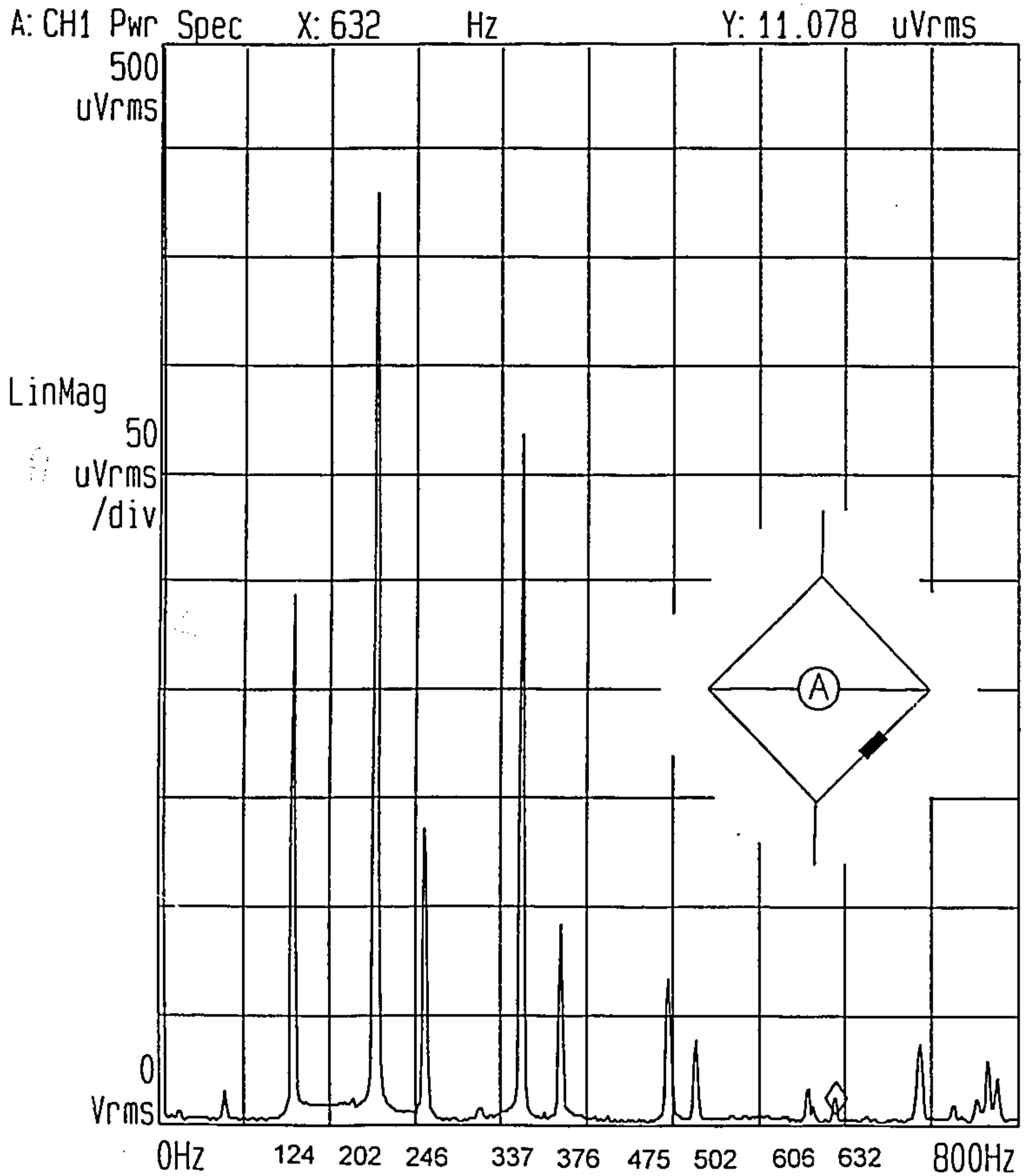

Fig.8.4. General frequency spectrum for 13 convolution single bellows expansion joint (air, P=0)

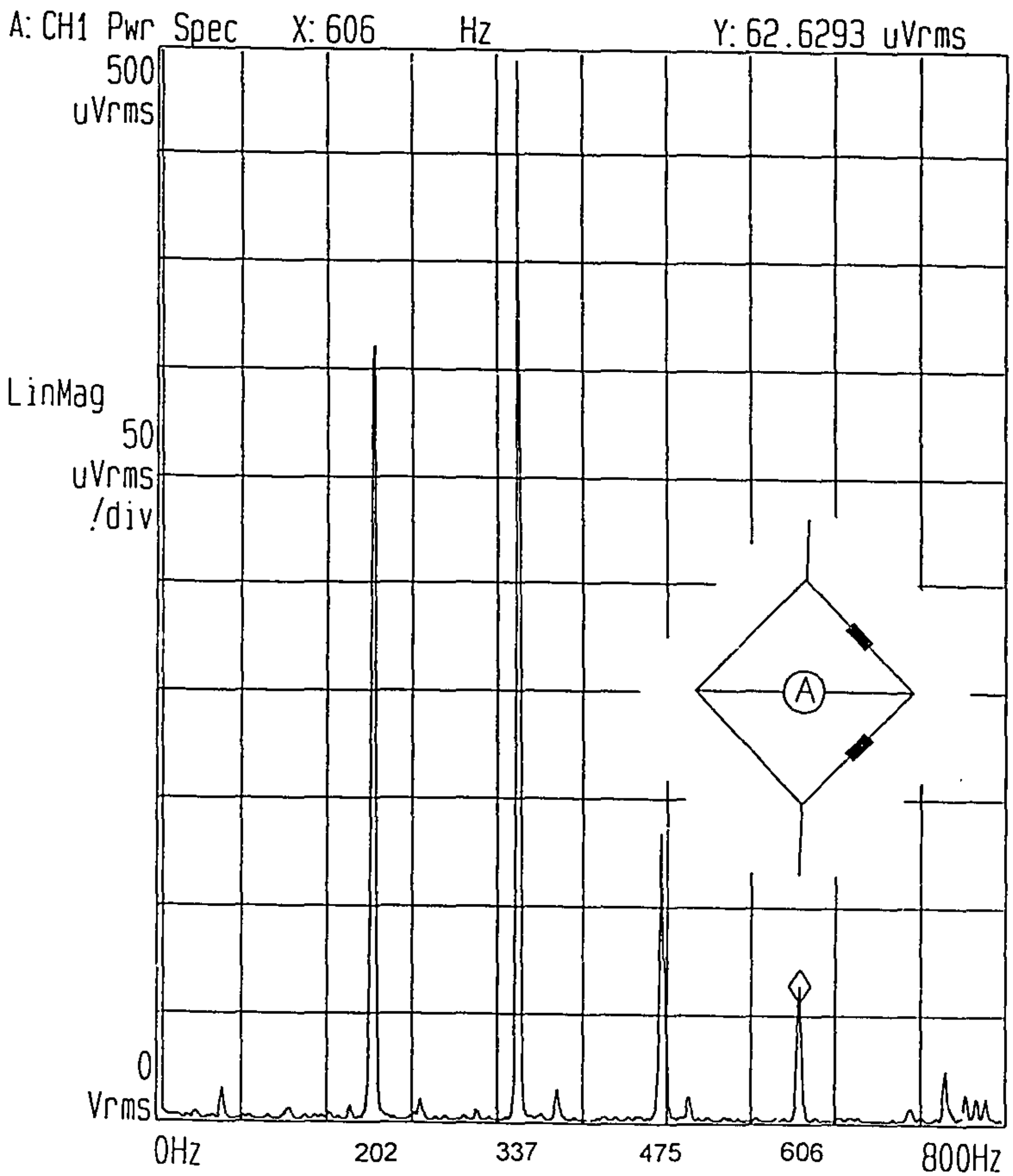

Fig.8.5. Transverse vibration frequency spectrum for 13 convolution single bellows expansion joint (air, P=0)

Since the shock excitation technique is the most simple, and is both fast and accurate enough in determining the natural frequencies, it was decided to use this method for the investigation of the natural frequencies of the transverse vibration of the expansion joints. A schematic diagram of the experiment is shown in Fig.8.3. The signal from the strain gauge, 1, glued on the surface of the bellows was transmitted through the bridge, 2, to the amplifier, 3, and then to the FFT analyzer 4. Each time the bellows frame was impacted with the same body,the signal was captured by the FFT analyzer.

Naturally, the one gauge experiment registers the natural frequencies of all possible mode shapes, Jakubauskas (1991). Therefore, when using just one gauge, the frequency spectra obtained from the FFT analyzer is very dense (see Fig.8.4), and identification of the resonant frequencies of the bending modes by comparison with the calculated frequencies using the derived formulas becomes unreliable. In order to eliminate the unwanted axisymmetric frequencies, a system of two gauges was used, glued on opposite sides of the bellows (Figure 8.1) and connected in the two arms of a bridge as shown in Fig.8.5. The same polarity signals from the axisymmetric modes cancelled each other, at least in the lower frequency band, while the opposite polarity signals from the bending modes were additive and provided a signal of double strength. The frequency spectra obtained in this way for the first four bending modes of single and double bellows expansion joints are shown in Fig.8.5 and Fig.8.8.

Fig.8.6 shows the frequency spectra for the same bellows in the case of its axial vibration. It is easy to notice that the general frequency spectra shown in Fig.8.4 can be obtained by simple summation of the transverse (Fig.8.5) and axial (Fig.8.6) frequency spectra.

In principle, it is possible to extend the frequency spectra range by using the four or even eight strain gauges technique. This would strengthen the useful signal of the bending modes and help to eliminate the frequency peaks of the axisymmetric modes as well.

The transverse vibration frequency spectra with water inside the bellows is shown in Fig.8.7. It is readily noticeable that the same resonant peaks moved significantly towards the lower frequency range.

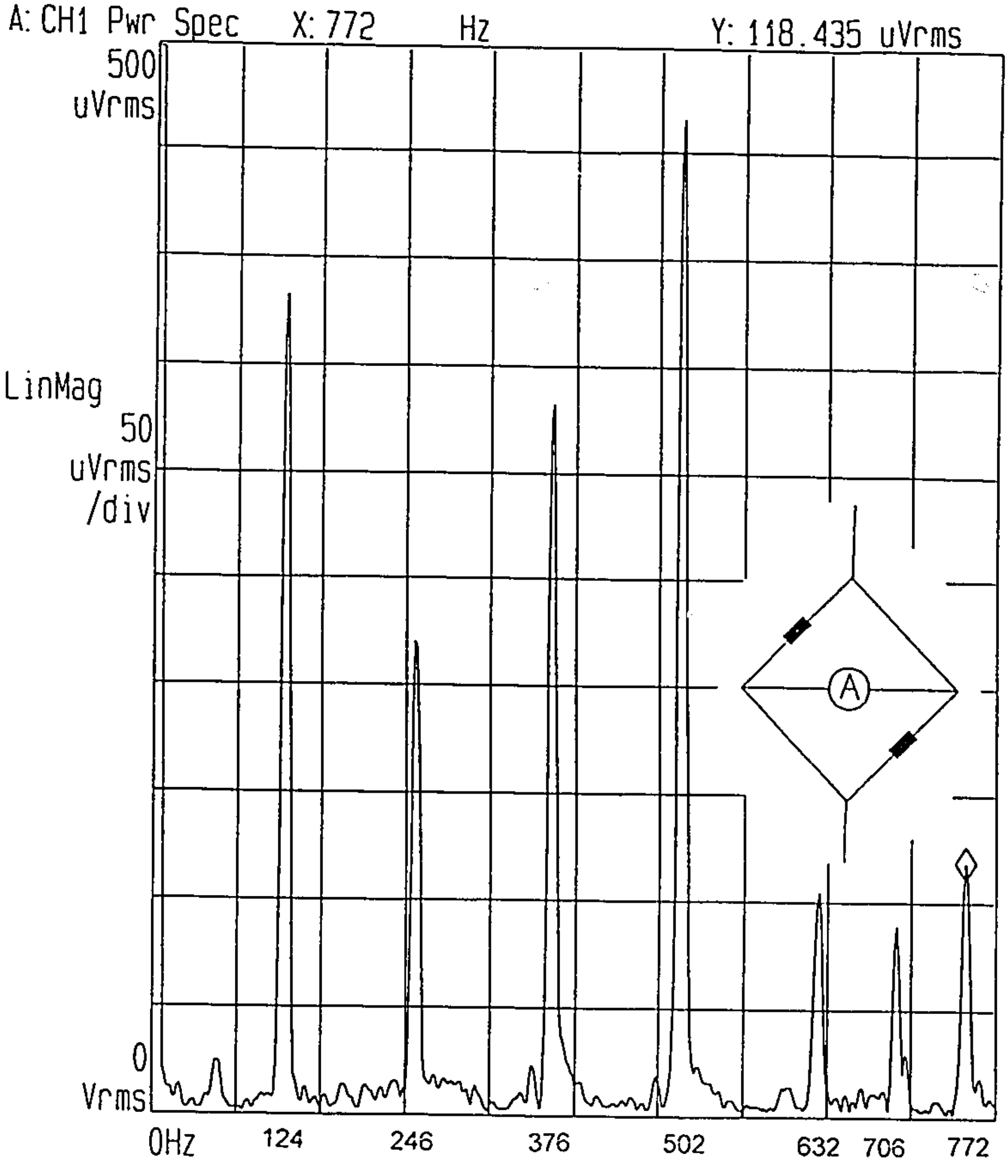

Fig.8.6. Axial vibration frequency spectrum for
13 convolution single bellows expansion joint (air, P=0)

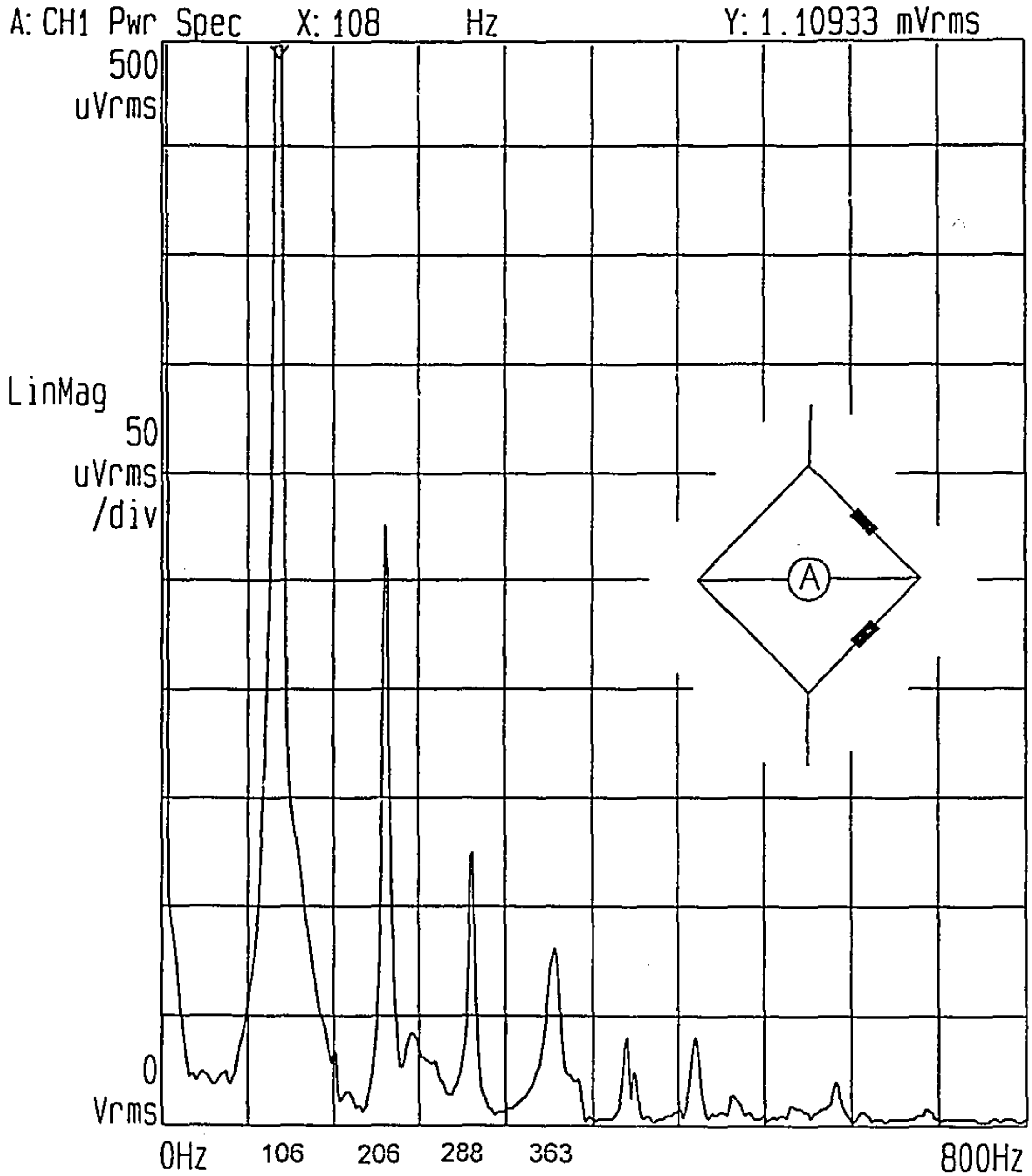

Fig.8.7. Transverse vibration frequency spectrum for single bellows expansion joint (water, P=200 kPa)

Similar frequency spectra were obtained at the pressure $P = 200$ kPa with the frequency peaks slightly moved to the lower frequency side.

Fig.8.8 shows the transverse frequency spectrum for a double bellows expansion joint at $P = 0$ kPa. One can see the pairs of the lateral and rocking modes frequency peaks in this picture. In Fig.8.9 the general frequency spectra is shown for the same double bellows expansion joint specimen obtained from the single gauge experiment. The comparison of these graphs shows the axial frequency peaks in Fig.8.9 in addition to the transverse ones shown in Fig.8.8. Fig.8.10 shows the transverse frequency spectrum with water inside at $P = 0$ kPa. As in the case of a single bellows expansion joint, here all the peaks are considerably moved towards the lower frequency range, as well. Similar frequency spectra were obtained at the pressure $P = 200$ kPa.

It was important for the impulsive testing to match the duration of the impulsive force input to the band of the frequencies to be analyzed. This requires proper selection of the nature of the materials of both colliding bodies, the hammer and the structure. The exciting shock was applied directly to the bellows. Different materials were used as a hammer: pieces of wood, small aluminum or steel bars. The application of the impulse using different materials resulted in different durations of shock. The duration of the shock may also be shortened using low level energy impacts. However, low energy impacts excited vibrations with amplitudes too small to be registered by the instrumentation, especially for the higher modes. Even more important for the impulsive testing is the selection of the location of the application of the impulsive force. The shocks applied in the middle of the bellows, because of its higher flexibility, caused longer shock durations and, subsequently, the very first lowest vibration modes were excited. On the other hand, the application of the shocks close to the fixed end of bellows, because of its lower flexibility, caused shorter duration impacts and, therefore, higher frequency modes to be excited. So, control of the shock duration allowed different natural frequencies to be excited, which can be seen from the heights of the peaks in Fig.8.4-8.10.

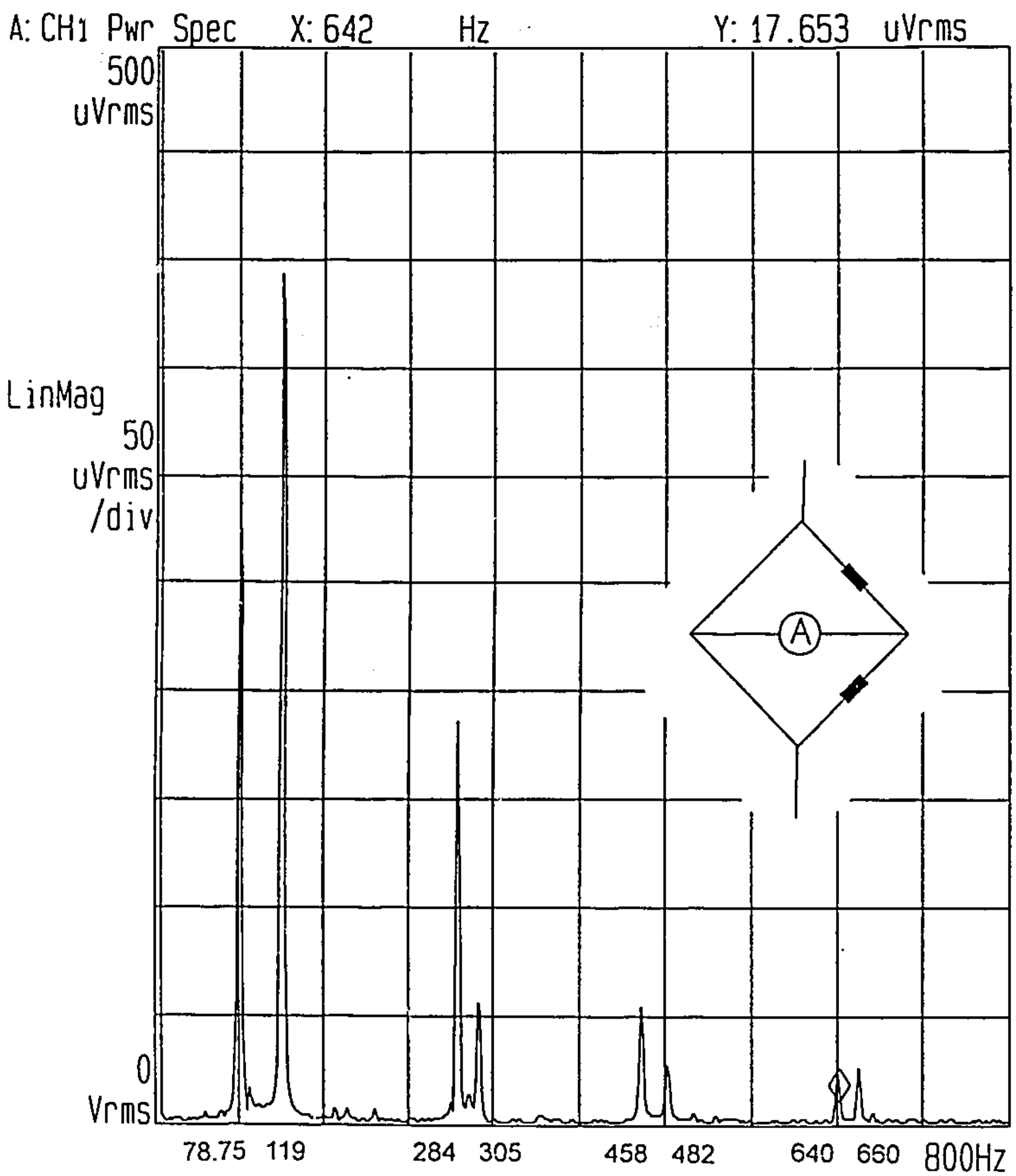

Fig.8.8. Transverse vibration frequency spectrum for
13 convolution double bellows expansion joint (air, P=0)

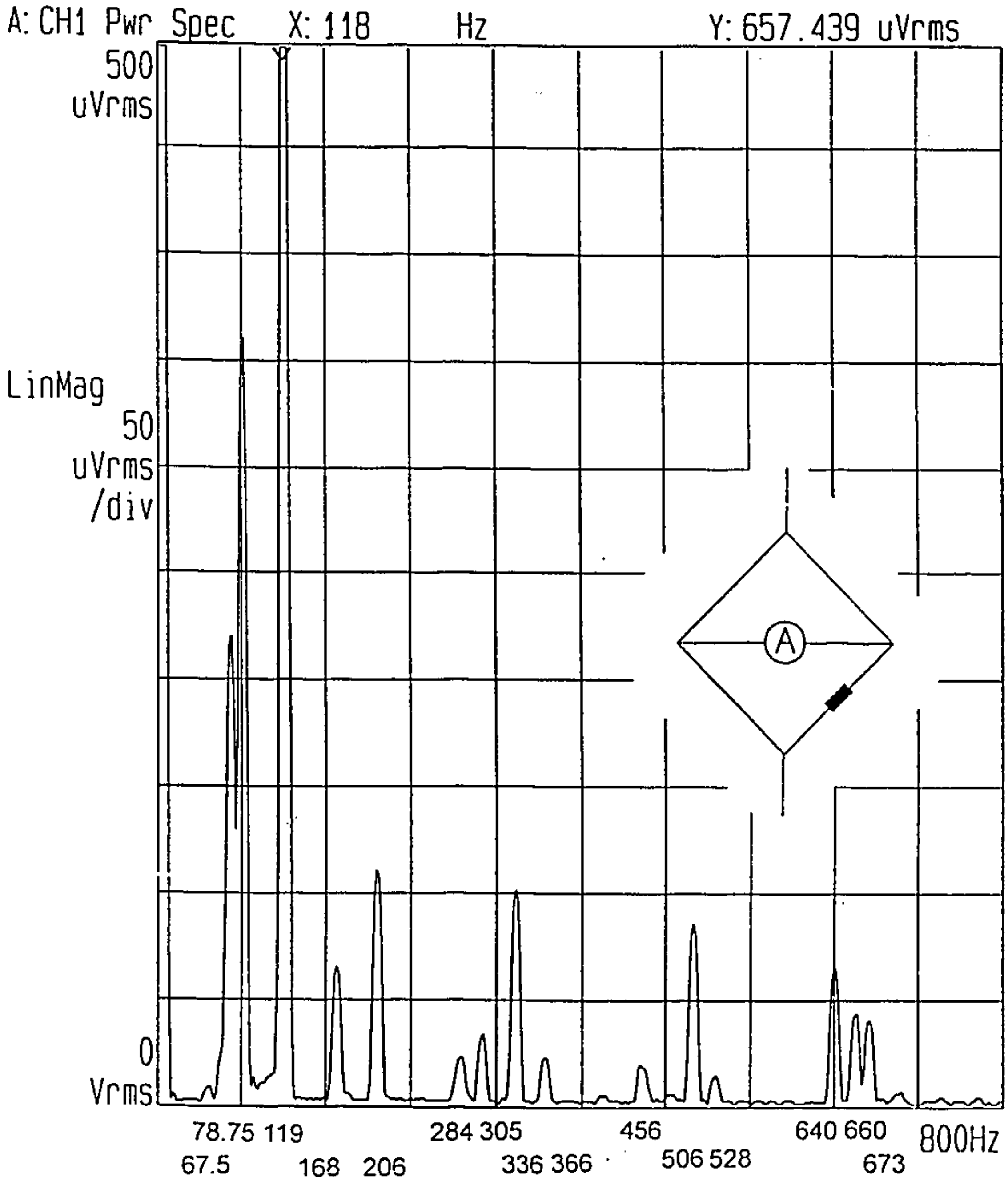

Fig.8.9. General frequency spectrum for 13 convolution double bellows expansion joint (air, P=0)

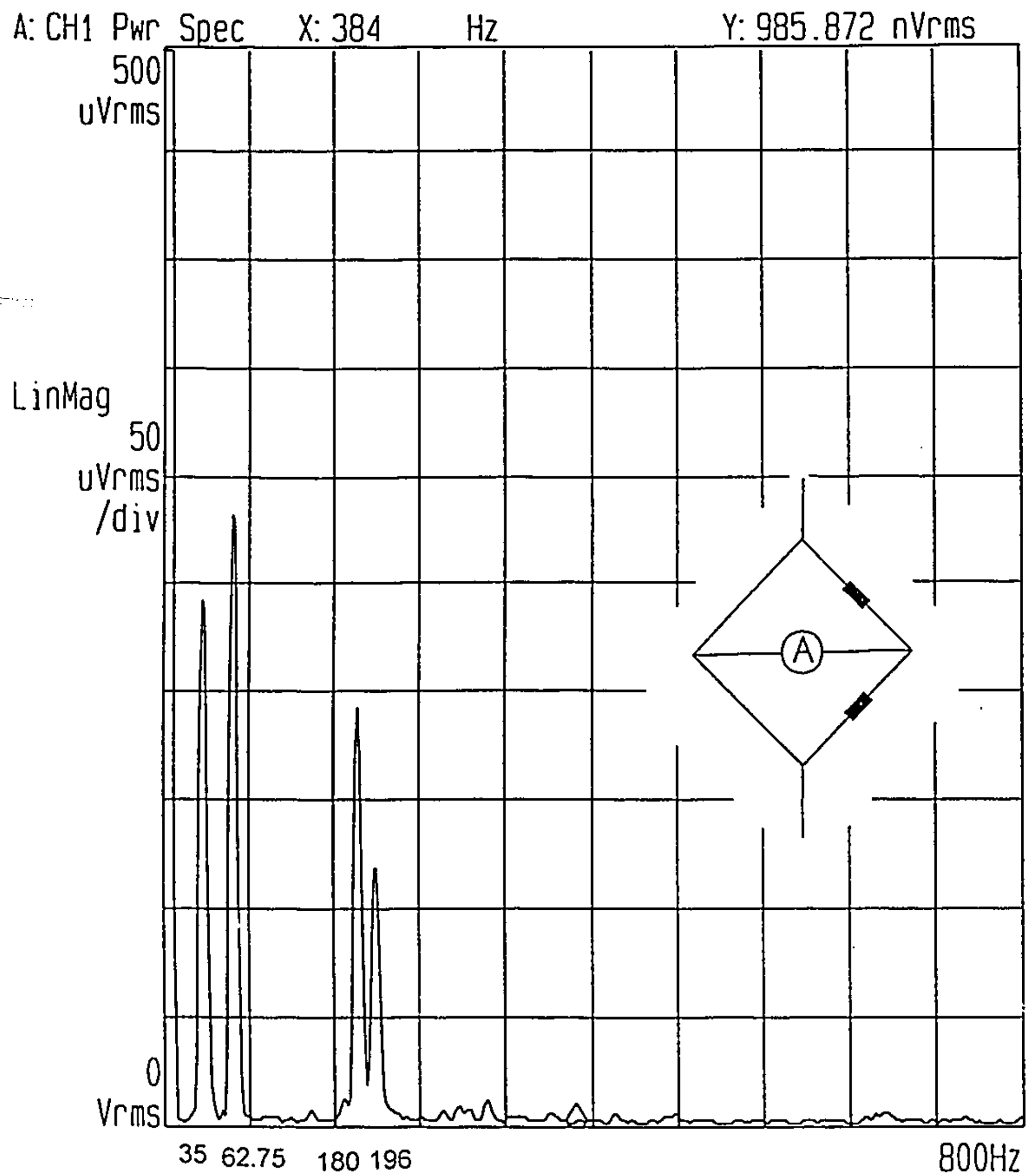

Fig.8.10. Transverse vibration frequency spectrum for double bellows expansion joint (water, P=0)

Figures 8.4 - 8.10 show the frequency spectra for tests of the single and double bellows expansion joints with the following data: $R_m = 0.0842$ m, $h = 0.0157$ m, $R_1 = 0.00353$ m, $R_2 = 0.00248$ m, $l = 0.1555$ m, t = 0.0004 m for single bellows and $R_m = 0.0844$ m, $h = 0.0158$ m, $R_1 = 0.00308$ m, $R_2 = 0.00268$ m, $l = 0.1517$ m, t = 0.0006 m, a = 0.1502 m for double bellows expansion joints.

As mentioned in previous chapters, the theoretical investigations of bellows expansion joint natural frequencies were based on many assumptions and simplifications. Shear and damping were neglected. Perfectly fixed bellows end boundary conditions were assumed.

Table 8.1. Comparison of experimental and theoretical solution results for single bellows expansion joint at $P = 0$ kPa

Mode shape #	with air		Error	with water		Error
	Experimental	Theoretical		Experimental	Theoretical	
	Hz	Hz	%	Hz	Hz	%
1	202	199	-1.6	112	111	-0.6
2	336	329	-2.2	210	208	-0.9
3	476	455	-4.3	289	286	-1.1
4	606	579	-4.4	363	345	-4.9

Table 8.2. Comparison of experimental and theoretical solution results for single bellows expansion joint at $P = 200$ kPa

Mode shape #	with air		Error	with water		Error
	Experimental	Theoretical		Experimental	Theoretical	
	Hz	Hz	%	Hz	Hz	%
1	188	187	-0.3	106	105	-0.9
2	328	320	-2.6	206	202	-1.8
3	466	449	-3.7	287	282	-1.7
4	596	574	-3.7	360	342	-5.0

Table 8.3. Comparison of experimental and theoretical solution results for double bellows expansion joint at $P = 0$ kPa

Mode shape #	with air		Error	with water		Error
	Experimental	Theoretical		Experimental	Theoretical	
	Hz	Hz	%	Hz	Hz	%
lat_1	78.8	81.2	3.1	34.8	36.0	3.6
roc_1	119	121	1.8	62.7	62.3	-0.7
lat_2	284	294	3.4	181	194	7.2
roc_2	305	311	1.8	196	208	6.3
lat_3	458	475	3.8	–	343	–
roc_3	482	487	1.1	–	352	–

Table 8.4. Comparison of experimental and theoretical solution results for double bellows expansion joint at $P = 200$ kPa

Mode shape #	with air		Error	with water		Error
	Experimental	Theoretical		Experimental	Theoretical	
	Hz	Hz	%	Hz	Hz	%
lat_1	72.5	75.5	4.1	32.3	33.5	3.8
roc_1	111	116	5.3	59.0	59.9	1.5
lat_2	278	289	3.8	180	191	6.0
roc_2	296	306	3.2	197	205	4.1
lat_3	456	471	3.4	–	340	–
roc_3	480	484	0.8	–	349	–

The mode shapes of the bellows with and without fluid were assumed to be identical. Furthermore, the boundary condition for calculation of the half-convolution added mass caused by convolution deformation, λ, was derived from the axial static deformation of bellows, although static and dynamic deformations of bellows convolution may differ slightly. Moreover, this boundary condition was considered to be the same for all of the bellows convolutions which in reality may not be exactly true. The bellows was assumed to behave like a beam rather than a shell. Additionaly, the Young's modulus value used in calculations was a nominal value for stainless steel, T-321 S/S, from which the expansion joint specimens were made, although it is known that Young's modulus can vary slightly from one steel shipment to another.

Finally, the geometry of bellows specimens wasn't perfect. The gradual increase of the inside pressure from 0 to 200 kPa caused a somewhat nonlinear decrease in the natural frequency of the bellows. This might be explained by the somewhat imperfect geometry, which could cause a nonlinear shape change of the bellows under increasing pressure.

Any of the these assumptions, simplifications, and imperfections or some combination of them could be the cause of the differences between the frequencies obtained theoretically and from the experiments, as shown in Tables 8.1 - 8.2. However, it must be said that the agreement between theory and experiment is generaly excellent, especially for the lowest few modes. This agreement justifies the various assumptions and simplifications made in both the modeling of the bellows and the determination of the added mass. It also suggests that the lowest natural frequencies of bellows, at best, are rather insensitive to geometric imperfections in the manufacturing of bellows expansion joints.

The small negative error obtained for single bellows expansion joint with respect to the experimental results suggests that the actual stiffness may be slightly greater than that calculated. The analysis apparently begins to deteriorate by about the fourth mode. On the other hand, the positive error for the double bellows expansion joint, evidenced throughout Tables 8.3 - 8.4, may reflect the effect of the bending flexibility of the connecting pipe between the sets of convolutions. The theoretical calculations assumed

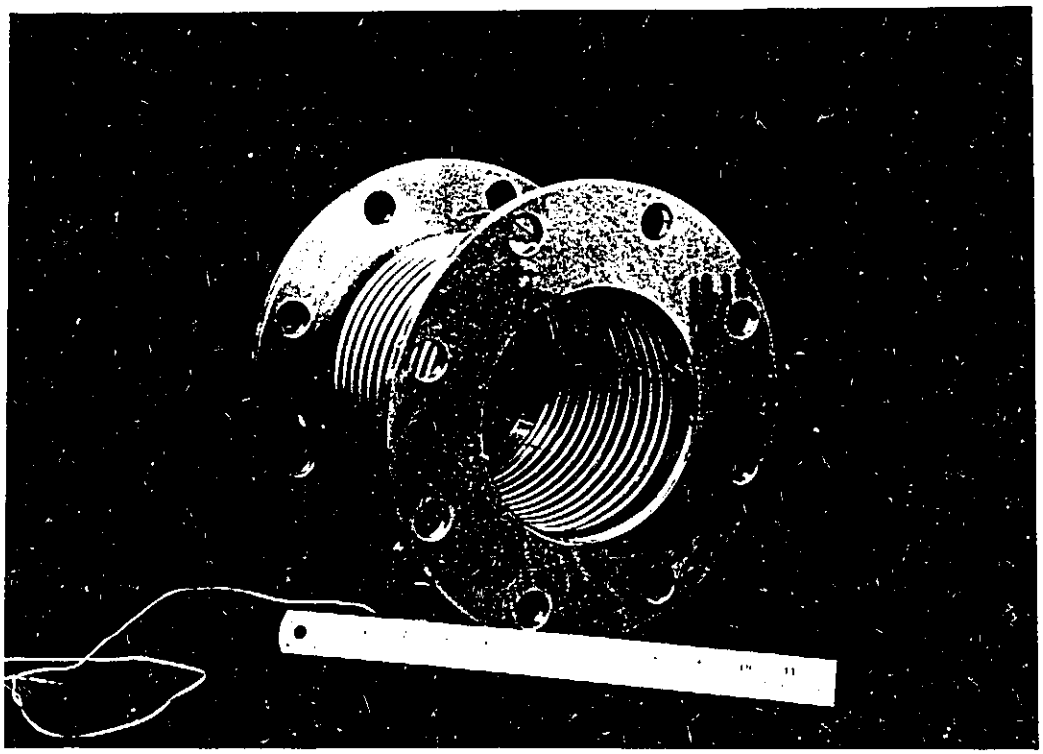

Fig.8.11. The single bellows expansion joint specimen

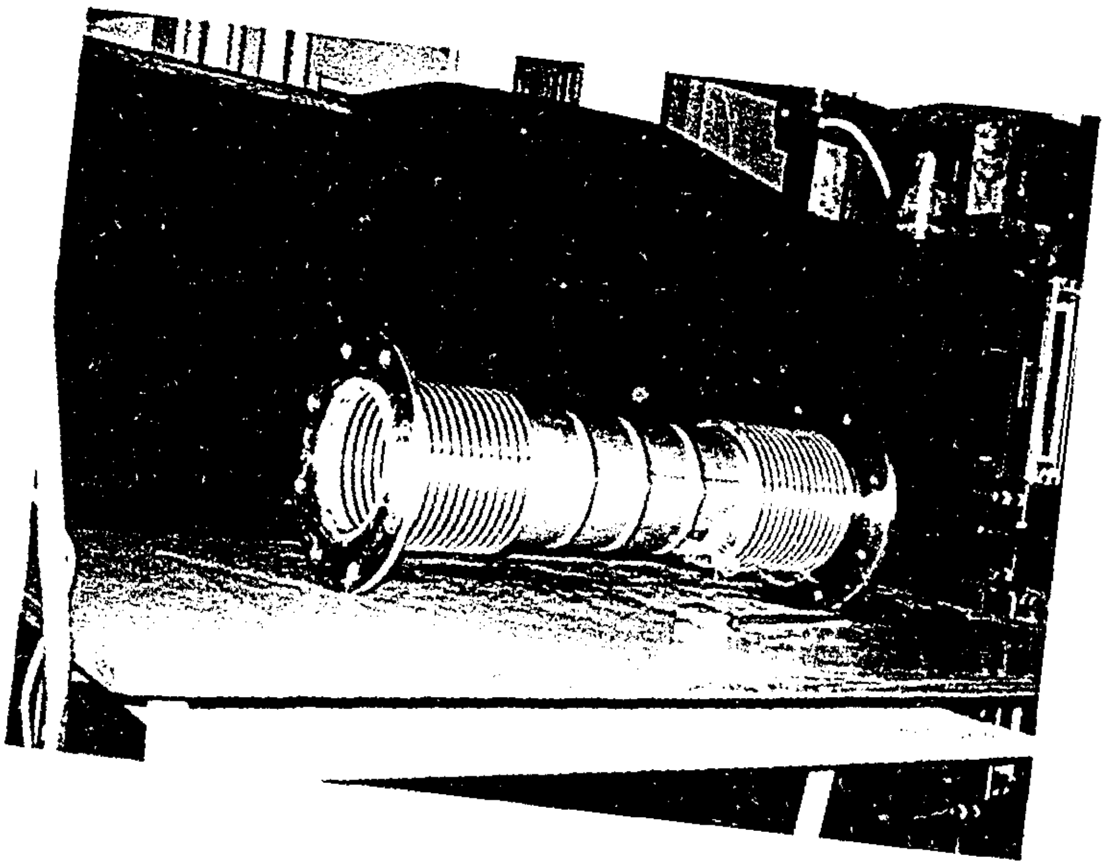

Fig.8.12. The double bellows expansion joint specimen

flexibility is expected to be less. In the case of the lateral modes, the bending moment throughout the length of the connecting pipe is relatively high (see Fig.6.1). In the case of the rocking modes, the connecting pipe freely rotates about its centre (Fig.7.1). Therefore, the bending moment acting on the rotating pipe becomes less significant and the assumption of its being rigid produces less error in the theoretical predictions.

In Tables 8.5 - 8.8 the experimental natural frequency results for a single bellows expansion joint specimen are compared with theoretical predictions obtained in four different ways: (1) the current method using differential equation (4.36),

$$EI\frac{\partial^4 w}{\partial x^4} + P\pi R_m^2\frac{\partial^2 w}{\partial x^2} - J\frac{\partial^4 w}{\partial x^2\,\partial t^2} + m_{tot}\frac{\partial^2 w}{\partial t^2} = 0,$$

(2) from the Bernoulli-Euler differential equation with added mass, m_{f2}, (3) without m_{f2},

$$EI\frac{\partial^4 w}{\partial x^4} + m_{tot}\frac{\partial^2 w}{\partial t^2} = 0,$$

and (4) using the method given in the EJMA Standard (1980). One can notice comparatively good agreement between the experimental and the present theoretical results. The EJMA results, especially for higher modes, are significantly higher than the experimental ones. The agreement between the EJMA method results and Bernoulli-Euler approach is reasonably good. This suggests that the EJMA Std. method is based on Bernoulli-Euler approach which is clearly not adequate for precise frequency calculations. The comparison of the two Bernoulli-Euler solution results, with and without added mass, m_{f2} , demonstrates the great influence of this type of added mass, especially for higher modes.

Similar relationships between frequencies calculated using different methods can also be seen for a double bellows expansion joint specimen in Tables 8.9 - 8.12. The influence of m_{f2} is lower because the double bellows expansion joint specimen live length was twice as long as the single bellows specimen length, and the added mass m_{f2} is the reciprocal of the fourth degree of the live bellows length.

Table 8.5. Comparison of frequency calculation results (Hz) for single bellows expansion joint without fluid at $P = 0$ kPa

Mode #	Experimental	Theoretical	Bernoulli-Euler	EJMA Standard
1	202	199	344	345
2	337	329	919	923
3	475	455	1792	1810
4	606	579	2977	2992

Table 8.6. Comparison of frequency calculation results (Hz) for single bellows expansion joint with water at $P = 0$ kPa

Mode #	Experimental	Theoretical	Bernoulli-Euler (with m_{f2})	Bernoulli-Euler (without m_{f2})	EJMA Standard
1	112	111	137	141	140
2	210	208	323	388	386
3	289	286	461	761	753
4	363	345	515	1258	1252

Table 8.7. Comparison of frequency calculation results (Hz) for single bellows expansion joint without fluid at $P = 200$ kPa

Mode #	Experimental	Theoretical	Bernoulli-Euler	EJMA Standard
1	188	187	334	345
2	328	320	919	923
3	466	449	1792	1810
4	596	574	2977	2992

Table 8.8. Comparison of frequency calculation results (Hz) for single bellows expansion joint with water at $P = 200$ kPa

Mode #	Experimental	Theoretical	Bernoulli-Euler (with m_{f2})	Bernoulli-Euler (without m_{f2})	EJMA Standard
1	106	105	137	141	141
2	206	202	323	388	386
3	287	282	461	761	753
4	360	342	515	1258	1252

Table 8.9. Comparison of frequency calculation results (Hz) for double bellows expansion joint without fluid at $P = 0$ kPa

Mode #	Experimental	Theoretical	Bernoulli-Euler	EJMA Standard
lat_1	78.8	81.2	91.8	91.8
roc_1	119	121	143	158
lat_2	284	294	550	–
roc_2	305	311	629	–
lat_3	458	475	1411	–
roc_3	482	488	1512	–

Table 8.10. Comparison of frequency calculation results (Hz) for double bellows expansion joint with water at $P = 0$ kPa

Mode #	Experimental	Theoretical	Bernoulli-Euler (with m_{f2})	Bernoulli-Euler (without m_{f2})	EJMA Standard
lat_1	34.8	36.0	37.2	37.2	51.0
roc_1	62.7	62.3	65.9	66.0	89.1
lat_2	181	194	262	270	–
roc_2	196	208	293	304	–
lat_3	–	343	581	707	–
roc_3	–	352	617	745	–

Table 8.11. Comparison of frequency calculation results (Hz) for double bellows expansion joint without fluid at $P = 200$ kPa

Mode #	Experimental	Theoretical	Bernoulli-Euler	EJMA Standard
lat_1	72.5	75.5	91.8	91.6
roc_1	111	116	143	158
lat_2	278	289	550	–
roc_2	296	306	629	–
lat_3	456	471	1411	–
roc_3	480	484	1512	–

Table 8.12. Comparison of frequency calculation results (Hz) for double bellows expansion joint with water at $P = 200$ kPa

Mode #	Experimental	Theoretical	Bernoulli-Euler (with m_{f2})	Bernoulli-Euler (without m_{f2})	EJMA Standard
lat_1	32.3	33.5	37.2	37.2	51.0
roc_1	59.0	59.9	65.9	66.0	89.1
lat_2	180	191	262	270	–
roc_2	197	205	293	304	–
lat_3	–	340	581	707	–
roc_3	–	349	617	745	–

CHAPTER 9

INVESTIGATION OF FLOW INDUCED VIBRATIONS IN BELLOWS EXPANSION JOINTS

9.1. General Information about Water/Wind Tunnels

A water/wind tunnel is a device designed for passing a stream of fluid with prescribed spatial and temporal variations over a model or full-size structure which is placed in its working section. The rest of the components are used to generate this stream. Tunnels are conventionally divided into low-speed and high-speed tunnels. In low-speed tunnels the predominant factors are inertia and viscosity while the influence of compressibility is negligible. This type of tunnel usually provides good Reynolds number similarity. In high-speed tunnels the forces due to inertia and compressibility are of major importance and usually provide good Mach number similarity. Two different types of tunnels are generally used:

a) the closed-circuit tunnel, in which the same fluid is recirculated and,

b) the open-circuit tunnel in which all the working fluid is discharged to the atmosphere at the one end, while fresh fluid is drawn in at the other end.

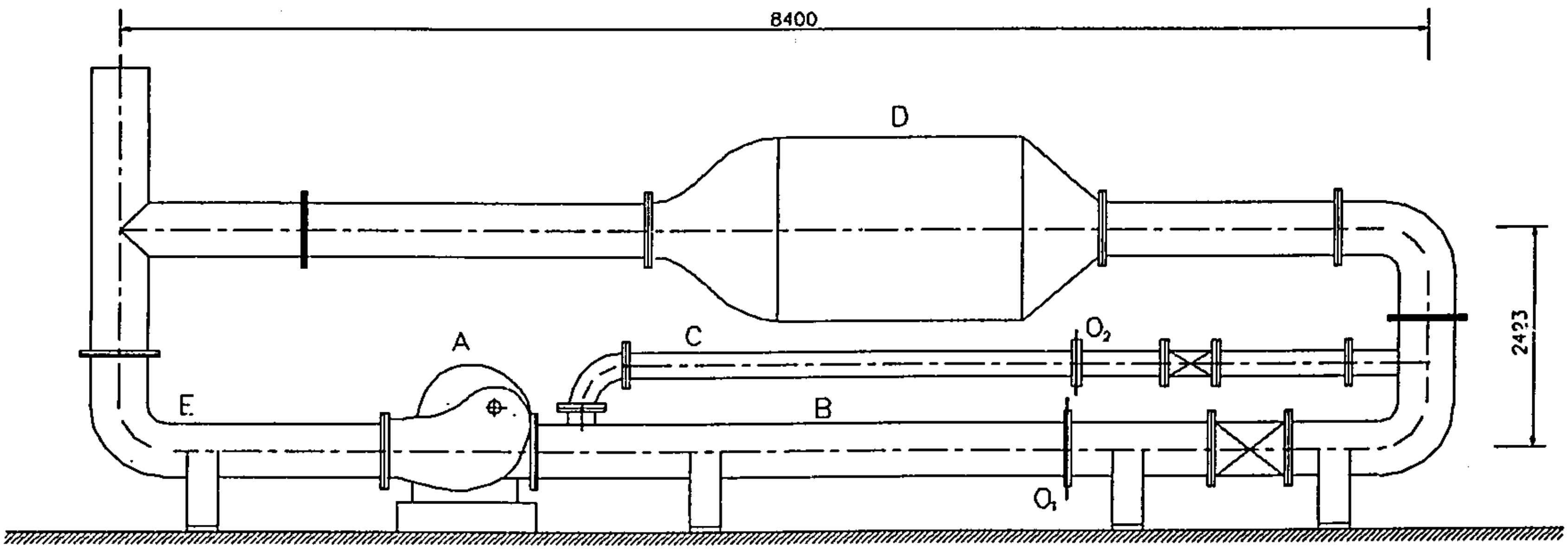

NOTE: ALL DIMENSIONS ARE IN MILLIMETRES.

Fig.9.1. Existing water loop

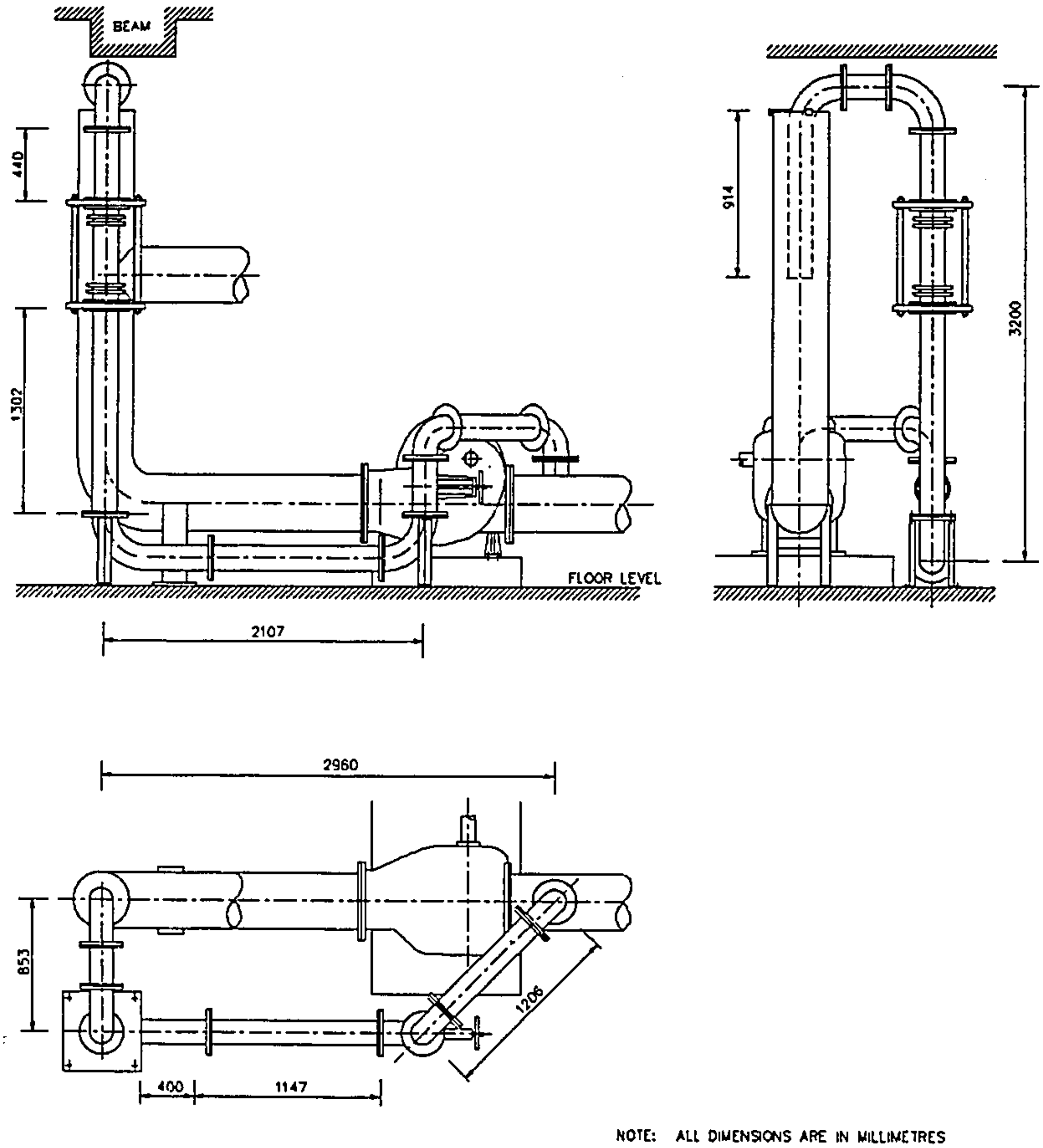

Fig.9.2. Assembly drawing of new design

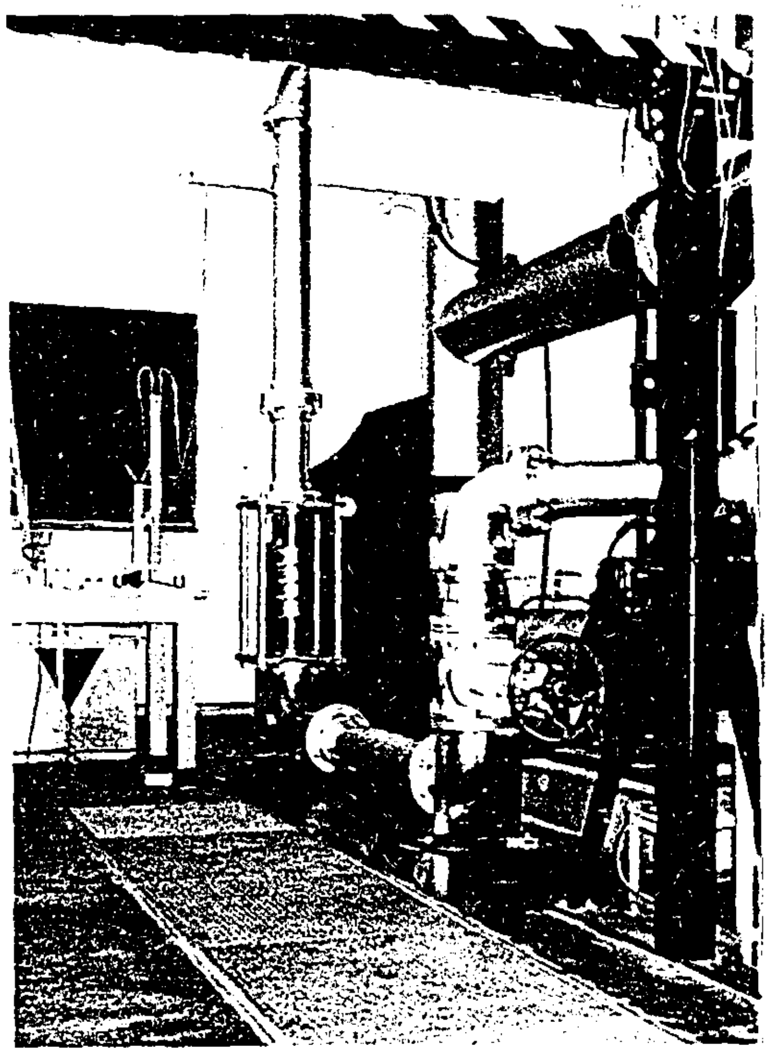

Fig.9.3. Assembled loop

Since it was desired to design a general purpose low-speed tunnel using water as the working fluid, the first approach was selected. The design principles, limitations, and description of the experimental facility are given below.

9.2. Water Tunnel Design

The existing water loop is shown in Fig.9.1. The loop is equipped with the horizontal 6" by-pass line, which could be the ideal place for installing of 6" bellows expansion joint specimen. It was soon realised that the expansion joint installed in the horizontal position would create a serious convolution deaeration problem, since there would be nc way either to check the presence of air or to remove it from the upper sections of the bellows convolutions. The presence of air in the bellows could significantly impair the entire experiment. On the other hand, as is seen from Fig.9.1, there was not enough space in the plane of the loop to install the bellows expansion joint vertically. Therefore, it was decided to design an additional 6" loop driven by the same pump an branching from the beginning of the 6" by-pass line of the existing loop, as shown in Fig.9.1. The assembly drawing of the new design is presented in Fig.9.2. It is geometrically more complex since it is out of the plane of the existing loop. It also has a comparatively long vertical span, which gives more freedom to manipulate the flow excitation force by installing the bellows either closer to or further from the adjacent upstream elbow. As seen from Fig.9.2, the expansion joint specimen was installed in the loop together with the frame, which was used in the free vibration experiments. This frame provided alignment of the pipes upstream and downstream of the bellows and essentially decoupled the bellows vibrations from relative pipe movement. The assembled loop is shown in the photo in Fig. 9.3.

The pumping system consists of the motor, the clutch, the brake, and the pump. The motor is a three-phase 200 hp motor running at constant speed. The clutch is hydraulic and provides the mechanical coupling between the motor and the pump through the friction force produced by water between the two concentric cylinders. The gap between cylinders is controlled by a magnetic field generated by an electric current. To dissipate the heat produced by the friction, the clutch has a water cooling system. The pump is a double suction Babcock & Wilcox centrifugal pump with a maximum capacity of 22.7 m^3 /min (20.79 m/s through 6" diameter pipe) at 33.5 m of head. Since the motor is able to produce high power, flow stabilization becomes difficult to achieve when the loop is running at low speeds. The motor can transmit power to the pump even when the clutch is completely disengaged. To cope with this problem, the drive system was connected to an elecrically controlled brake, which was installed between the pump and the clutch. The brake absorbs power from the shaft and can be set in a range of 0% to 100%. With this device, better control of the pump speed can be obtained , especially at low speeds.

The 6" diameter piping system shown in Fig.9.2 consists of a 6.03 m straight pipe, six 90^0 elbows of mean radius 0.236 m, one gate valve, and one T junction. Simple hydraulic calculations, Simon (1981), showed that the total head loss in the 6" portion of the loop at 10 m/s mean flow velocity was 20.22 m. A comparison of the pump capacity data with this head loss in the 6" piping system demonstrated that there was adequate power to run the flow at velocities even greater than 10 m/s. Let us now look at the flow velocity requirements necessary to generate the resonant vibrations according to the measured natural frequencies of the single and double bellows expansion joints already described in Chapter 8. Tables 8.1-4 show that all the measured natural frequencies, of the water filled expansion joint, are within the range of 30 to 360 Hz. The required experimental velocity, V , which will excite resonance at a frequency, f, can be obtained according to Weaver and Ainsworth (1989) by using a Strouhal number value

$$S = \frac{f\,l}{V_p} = 0.45, \qquad (9.1)$$

where,

l is the convolution pitch,

f is the resonant response frequency,

V_p is the mean flow velocity through the bellows at the peak resonant response amplitude.

This velocity range corresponding to the natural frequency range was calculated to be between 0.77 and 9.56 m/s. Here the maximum velocity roughly corresponds to the maximum design loop velocity mentioned earlier – more than 10 m/s. It should be noted that Strouhal number value, 0.45, was obtained by Weaver and Ainsworth (1989) for axial vibrations of bellows.

The flow velocity was measured using a Pitot-static probe, ASME(1971), connected to a differential manometer filled with mercury as the working fluid. The velocity profile was determined upstream of the bellows by two orthogonal traverses of the probe at the same cross-section. The static pressure in the bellows was measured using a low range pressure gauge. The vibration response was measured using the strain gauge system described in Chapter 8 amplified and fed into an FFT analyser. The amplitudes were averaged from 60 measurements. The frequency and averaged amplitude were then recorded and the velocity incremented. The average velocity, V_{av}, was calculated from the measured maximum velocity at the centreline of the pipe, V_{max}, using the empirical formula taken from Fox and McDonald (1985):

$$\frac{V_{av}}{V_{max}} = \frac{2n^2}{(n+1)(2n+1)},$$

where n depends on the Reynolds number of flow.

9.3 Experimental Results

The first tests on the bellows in the loop were conducted with nearly ideal upstream flow conditions, so that the flow in the bellows was fully developed and the velocity profile was relatively flat. The Reynolds number based on convolution pitch at maximum flow rates was of the order of 10^6.

The pump was started with the gate valve closed, so the flow rate at these conditions remained equal to zero and the bellows response observed. Then the gate valve was gradually opened to increment the flow from zero and the response measurements repeated. When the gate valve was fully opened and the flow could no longer be controled in this way, the hydraulic clutch was engaged to continue the increments of the flow. The maximum bulk flow velocity was reached approximately at 8 m/s. It was found that the maximum bulk flow velocity depended slightly on expansion joint type (single or double bellows) and on the location of the installation of the joint in the loop.

Installation of the joint in the vicinity of the upstream elbow, lowered the maximum flow velocity by ~ 8% in comparison with the case when the joint was installed in a more distant location downstream of the elbow. This can be explained by the increased loss of the pressure head in the joint due to velocity profile distortion by the elbow. On the other hand, the effect on maximum bulk flow velocity of the type of the joint (single or double) was insignificant.

It should be noted that the flow rate increment sequence from zero to about 8 m/s, took approximately one hour time during which the temperature of the water in the loop increased above the ambient temperature by ~ 7^0 C. However, no significant Strouhal number changes related to this temperature rise were observed. This means that the influence of the viscosity on the Strouhal number is negligibly small, at least over the range of parameters in these experiments.

Two types of excitation of the bellows were found. First, structural excitation was encountered after starting the pump with the gate valve closed, when flow velocity was equal to zero (see Fig. 9.4). This type of excitation continued throughout the entire range of flow velocities, up to 8 m/s, and appeared to be random in character. This broad band excitation is considered to be generated by the hydraulic clutch and pump, modified and transmitted through the piping system of the loop, and by the turbulence of the flow. Small frequency peaks due to this excitation can be seen throughout the entire velocity range, (see Fig.9.4 through 9.14). According to the widely accepted classification of the flow induced vibration types, Weaver (1989), these are forced vibrations.

Second, and most important, another type of vibration was observed in the bellows, very distinct from those considered above. This type of vibration appeared very suddenly, and was very strong, reaching maximum amplitudes 40 - 60 times higher than the amplitudes of the forced vibrations(compare small and high peaks in Fig.9.4 through 9.14). These vibrations were so strong that they ,excited the entire piping system of the

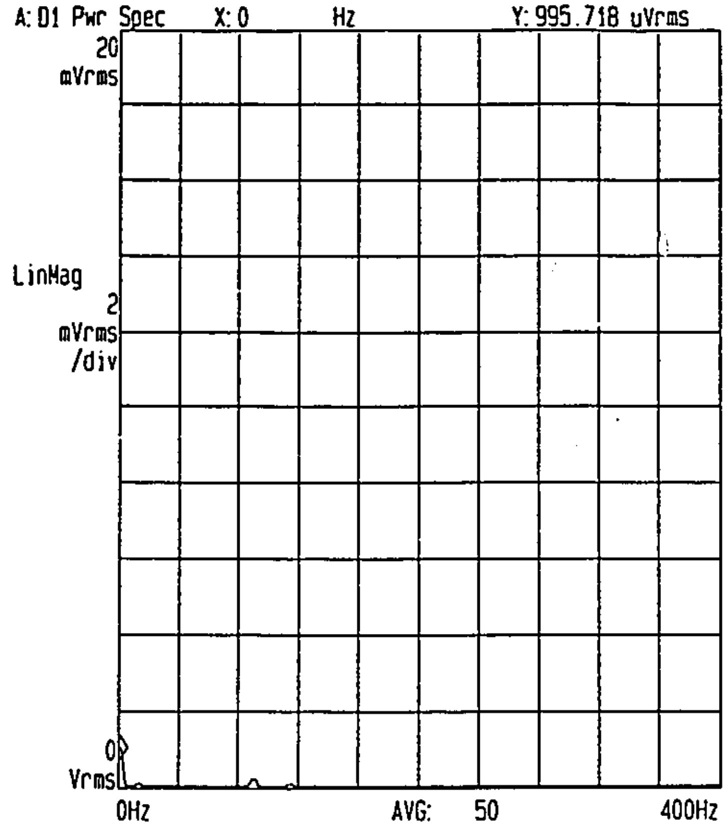

Fig.9.4. Single bellows expansion joint frequency spectrum generated by flow at $V_{av} = 0$

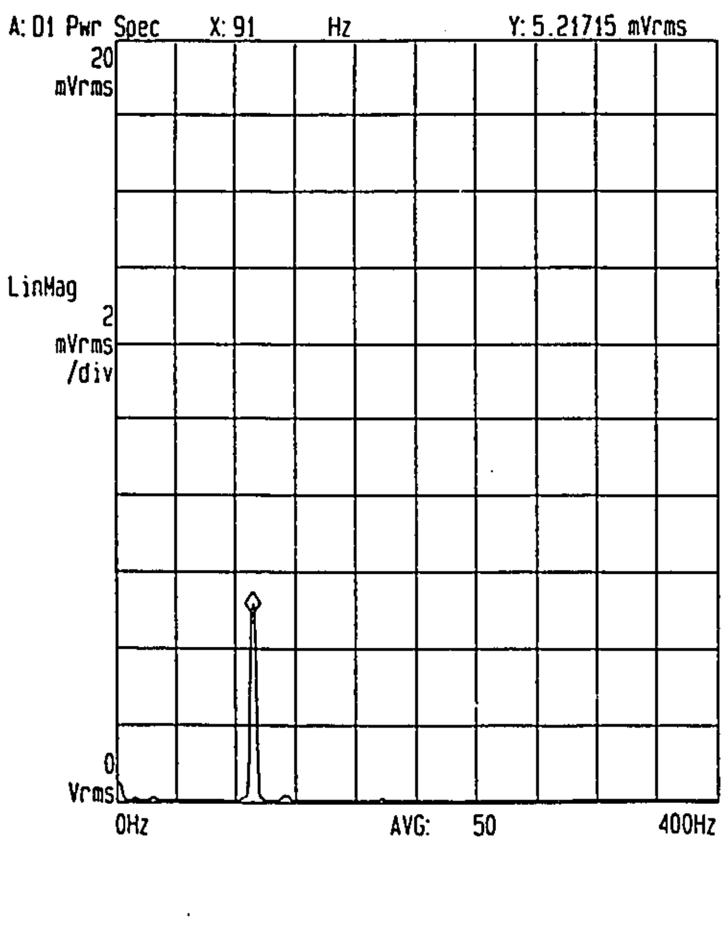

Fig.9.5. Single bellows expansion joint frequency spectrum generated by flow at $V_{av} = 1.83$ m/s

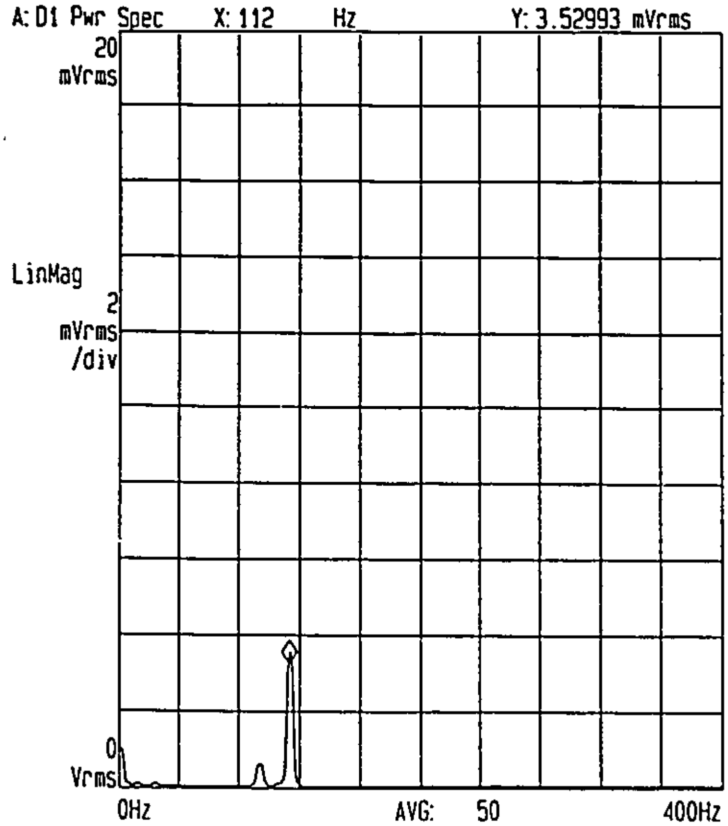

Fig.9.6. Single bellows expansion joint frequency spectrum generated by flow at V = 2.25 m/s

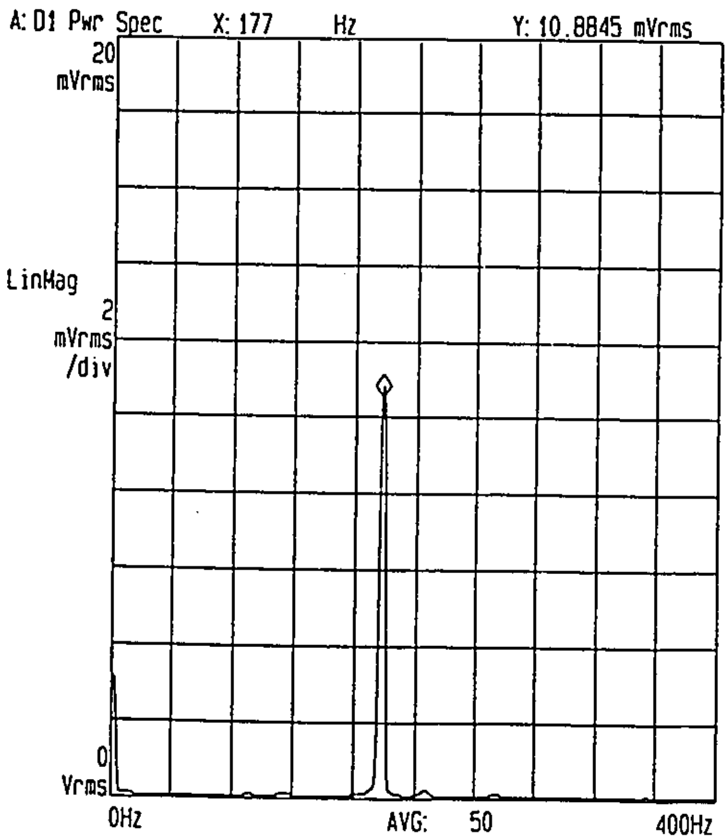

Fig.9.7. Single bellows expansion joint frequency spectrum generated by flow at V =3.83 m/s

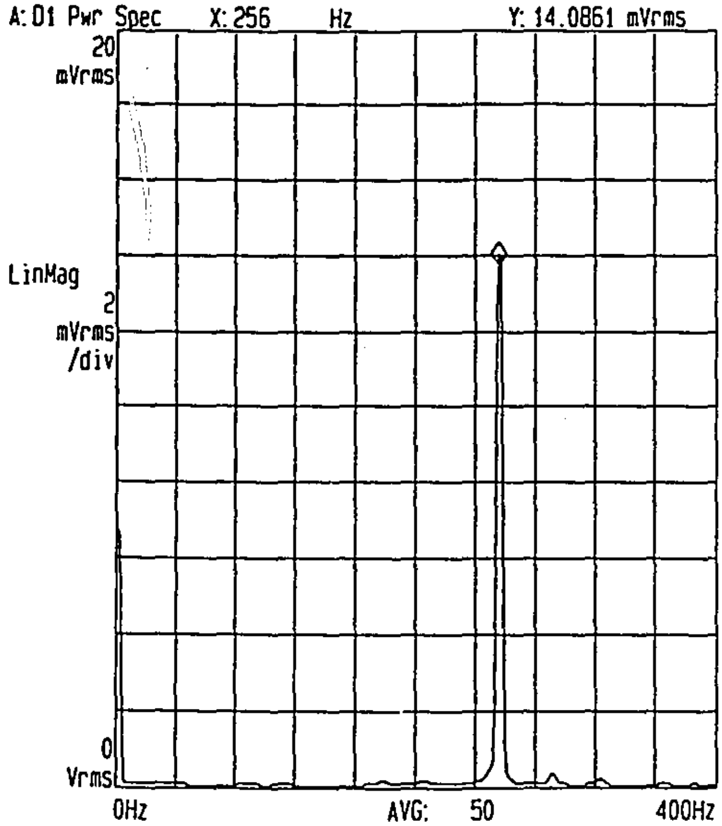

Fig.9.8. Single bellows expansion joint frequency spectrum generated by flow at V =5.71 m/s

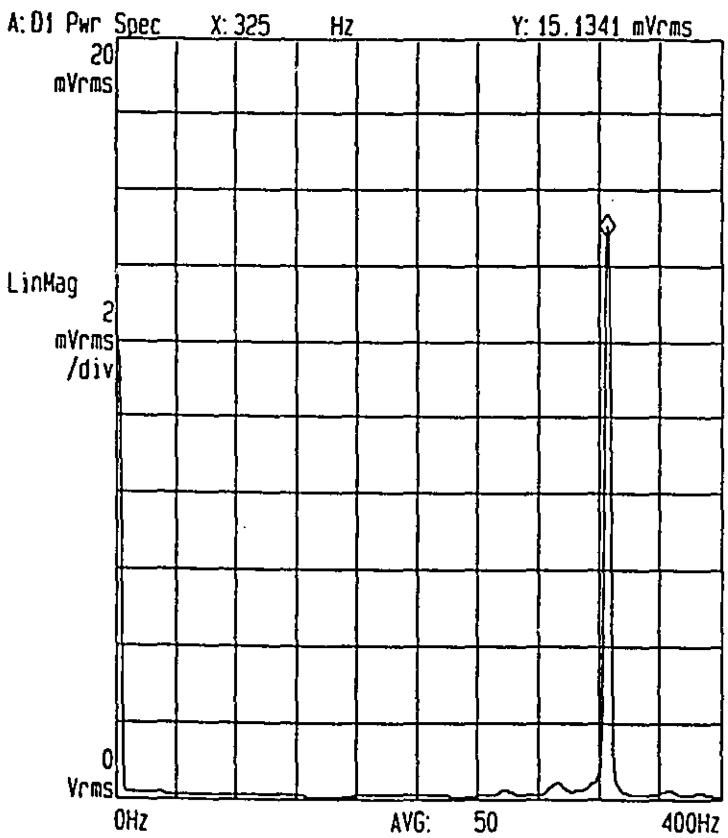

Fig.9.9. Single bellows expansion joint frequency spectrum generated by flow at V =7.59 m/s

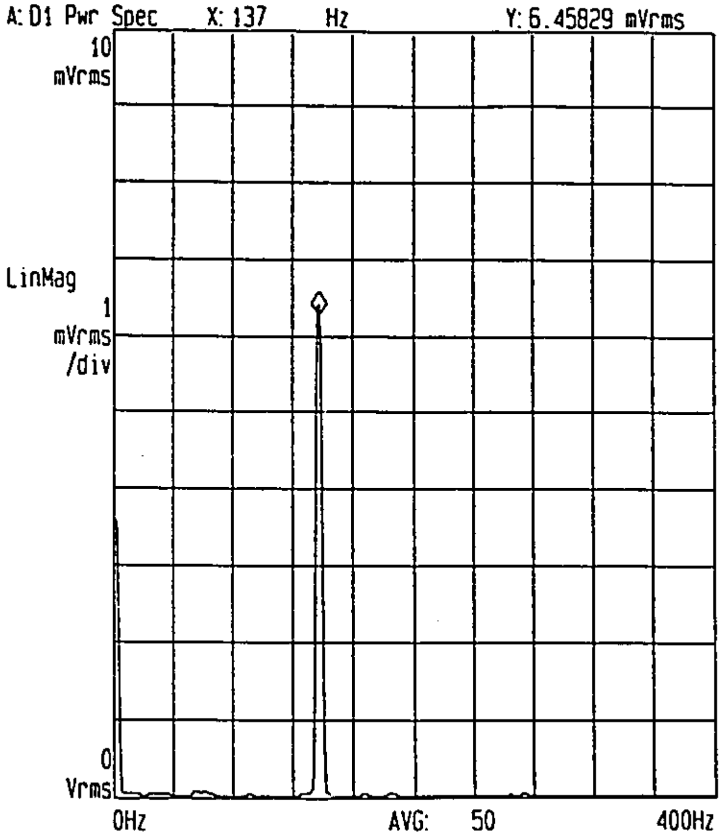

Fig.9.10. Double bellows expansion joint frequency spectrum generated by flow at V = 2.8 m/s

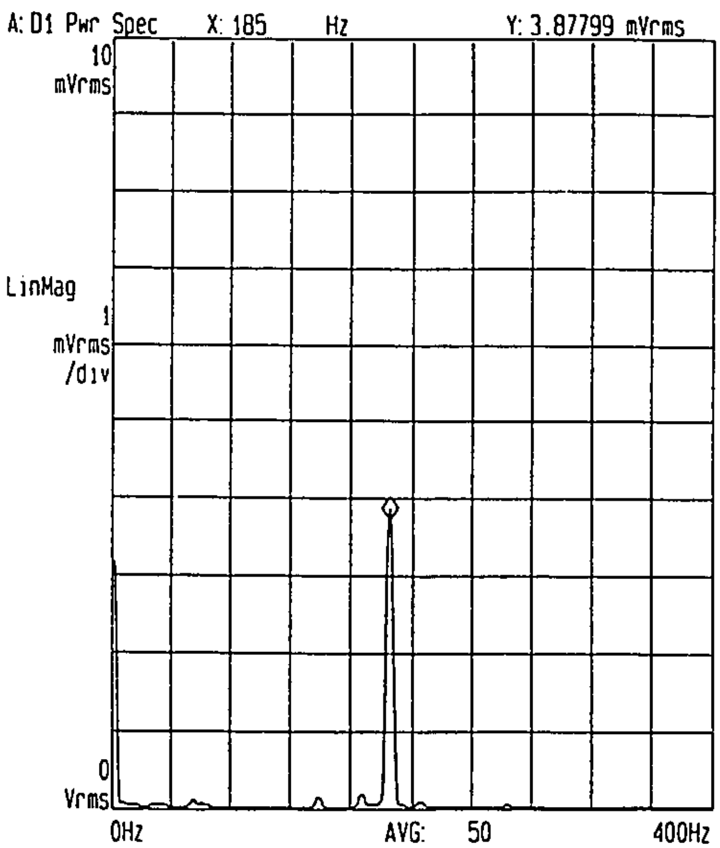

Fig.9.11. Double bellows expansion joint frequency spectrum generated by flow at V = 3.39 m/s

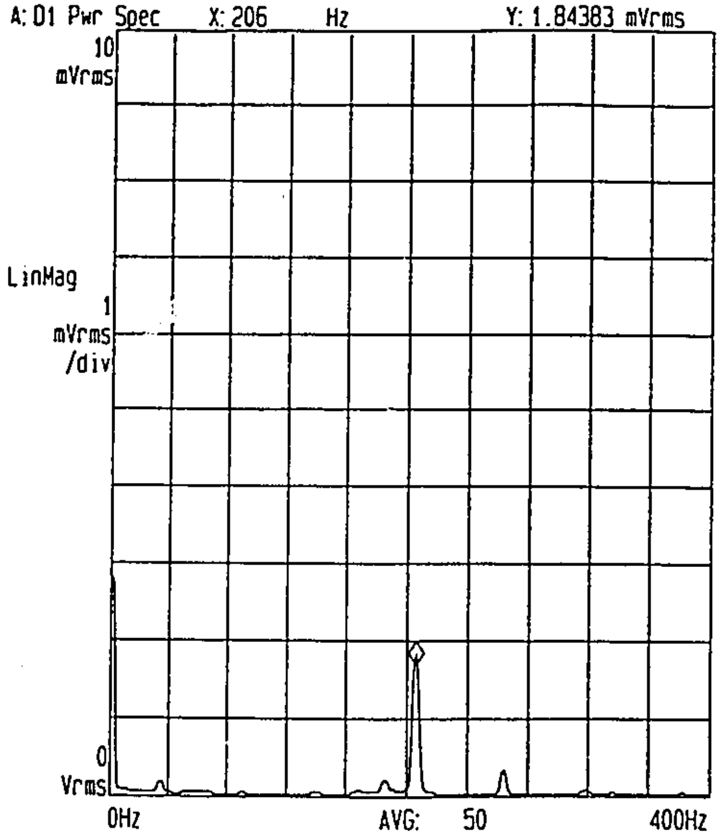

Fig.9.12. Double bellows expansion joint frequency spectrum generated by flow at V = 4.42 m/s

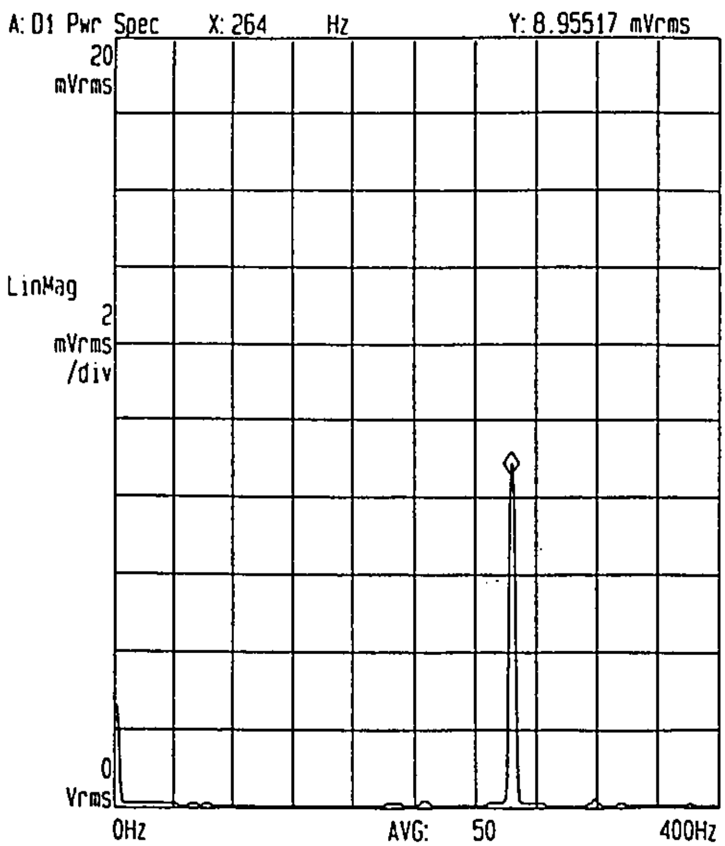

Fig.9.13. Double bellows expansion joint frequency spectrum generated by flow at V = 5.04 m/s

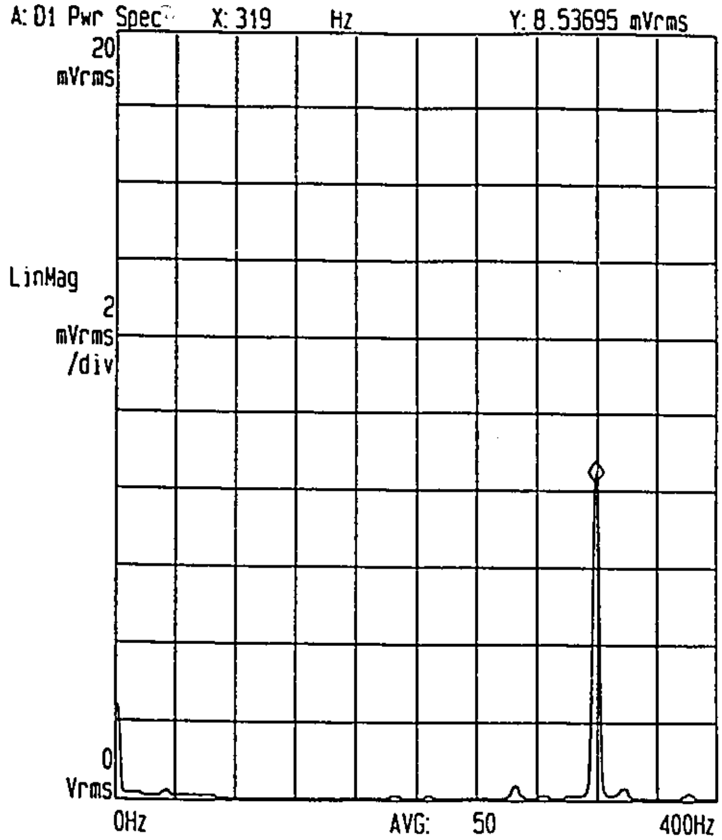

Fig.9.14. Double bellows expansion joint frequency spectrum generated by flow at V = 6.05 m/s

loop. The vibration amplitudes were sufficiently large that it was possible, for the lower vibration modes, to see the nodes and the maximum amplitude locations (antinodes) on the bellows with the naked eye. Indeed, there was a real danger that the bellows could fail by fatigue before the end of the experiments, as happened in the experiments conducted by Weaver and Ainsworth (1989). It was obvious that these were neither structurally excited bellows vibrations nor dynamic response due to turbulent flow excitation. Rather, the bellows vibrations coupled with the flow over a particular flow velocity range, through a "feed-back" mechanism. The existence of a "lock-in" flow velocity region indicates that these bellows vibrations can be classified as self controlled vibrations.

The peak outputs of the strain gauges on the bellows convolutions are plotted against the bulk flow velocity through the bellows, Fig.9.15 through 9.18. A comparison of these outputs for single and double bellows expansion joints with frequency spectra obtained using shock excitation (Fig.9.19 through 9.22) shows that some natural frquencies were not excited by flow. This can be explaned by the fact that, at the low na-

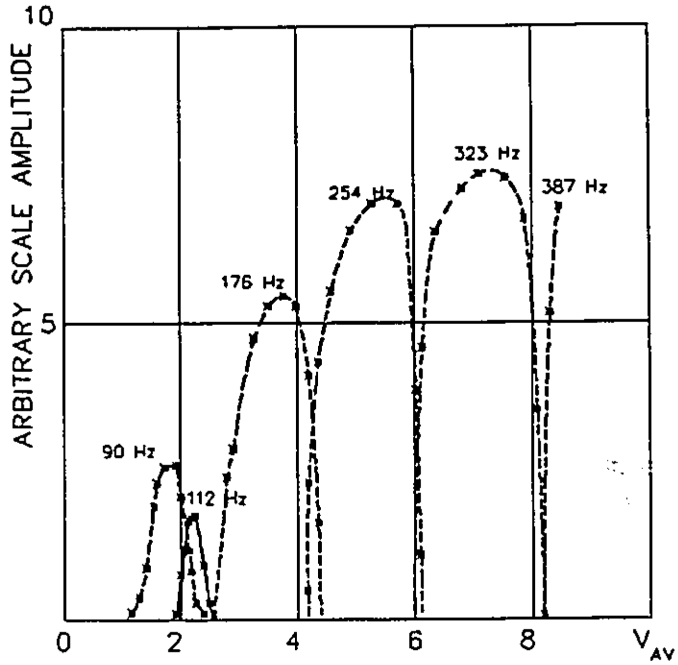

Fig.9.15. Amplitude response of a single bellows expansion joint as a function of mean flow velocity (at the upstream elbow) (----- axial modes, —— transverse modes)

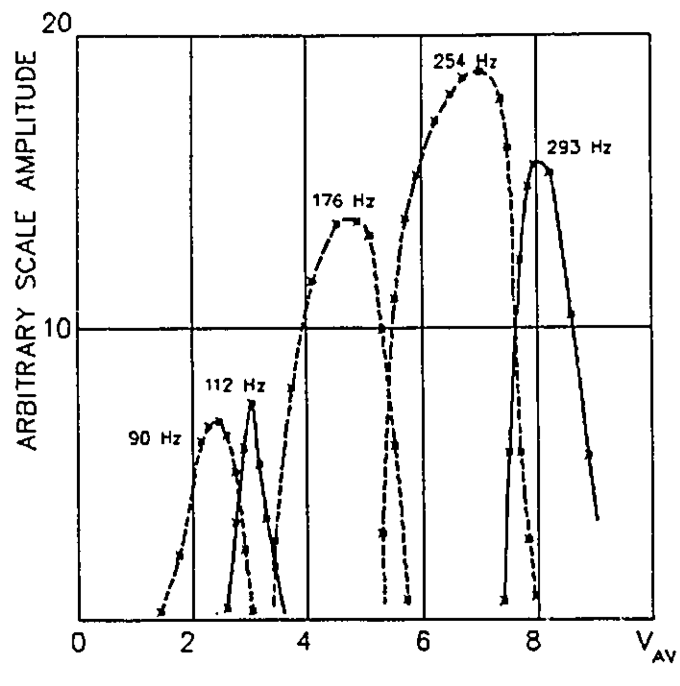

Fig.9.16. Amplitude response of a single bellows expansion joint as a function of mean flow velocity (away from the elbow) (----- axial modes, —— transverse modes)

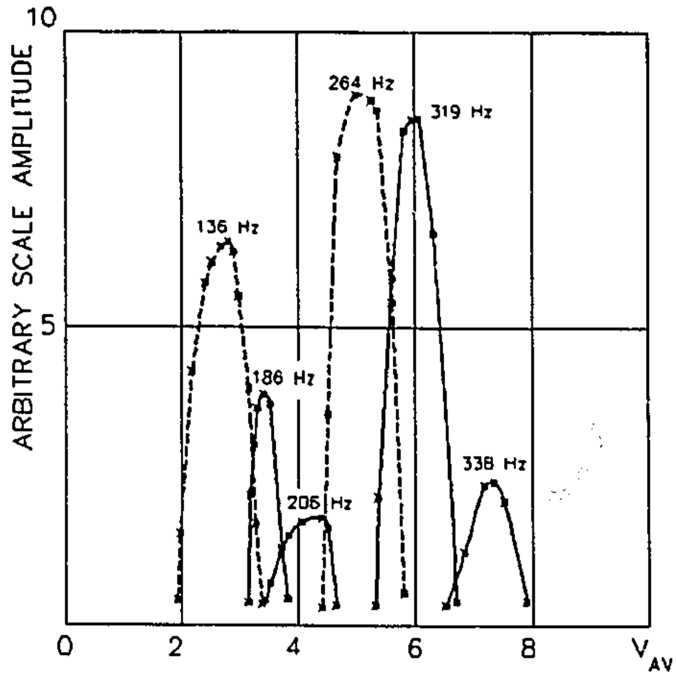

Fig.9.17.Amplitude response of a double bellows expansion joint as a function of mean flow velocity (at the upstream elbow) (----- axial modes, —— transverse modes)

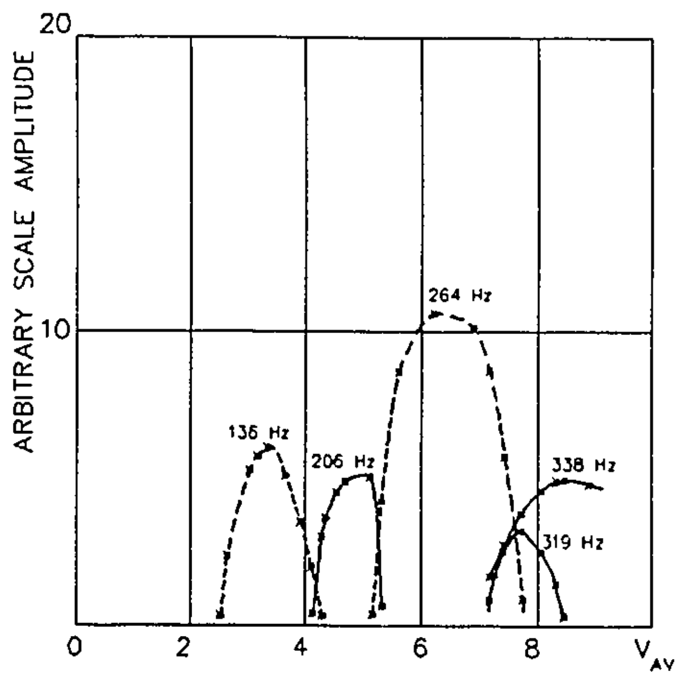

Fig.9.18. Amplitude response of a double bellows expansion joint as a function of mean flow velocity (away from the elbow) (----- axial modes, —— transverse modes)

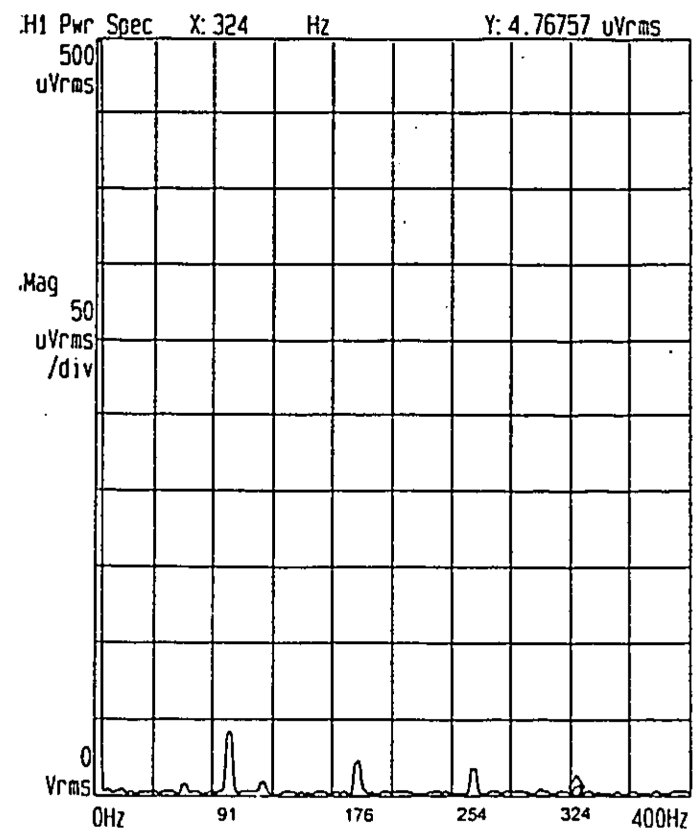

Fig.9.19. Axial vibration frequency spectrum for single bellows expansion joint specimen

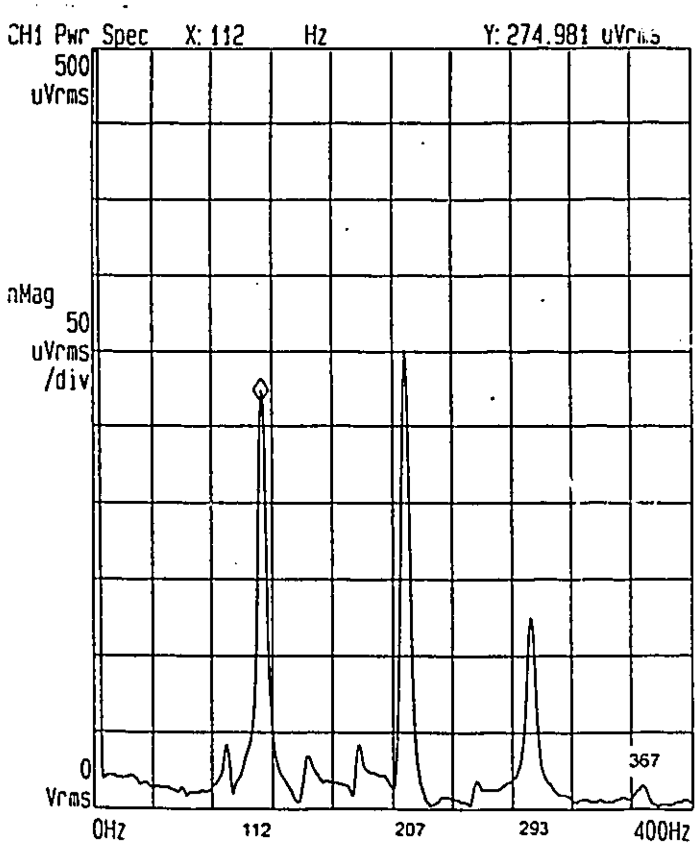

Fig.9.20. Transverse vibration frequency spectrum for single bellows expansion joint specimen

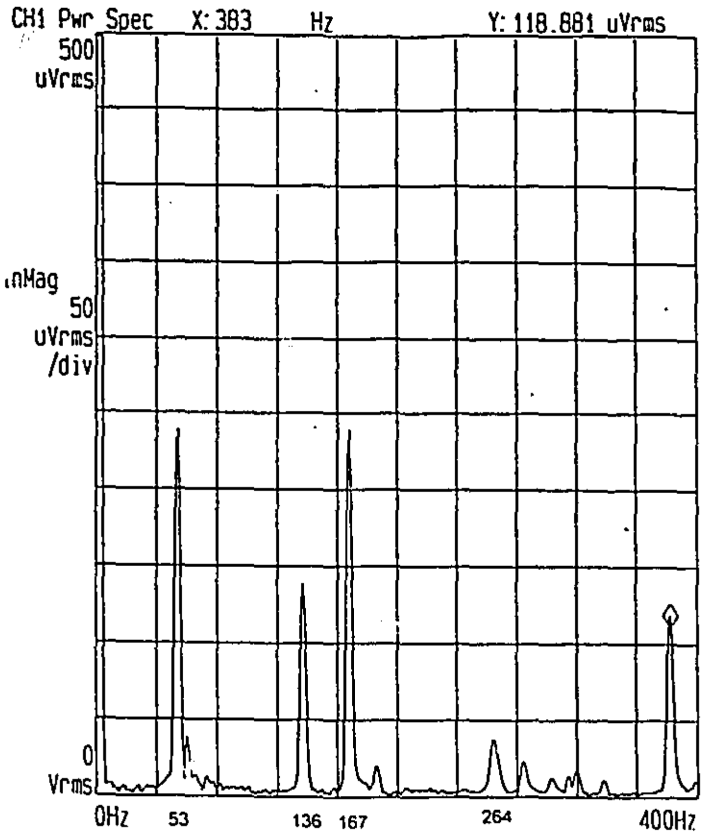

Fig.9.21. Axial vibration frequency spectrum for double bellows expansion joint specimen

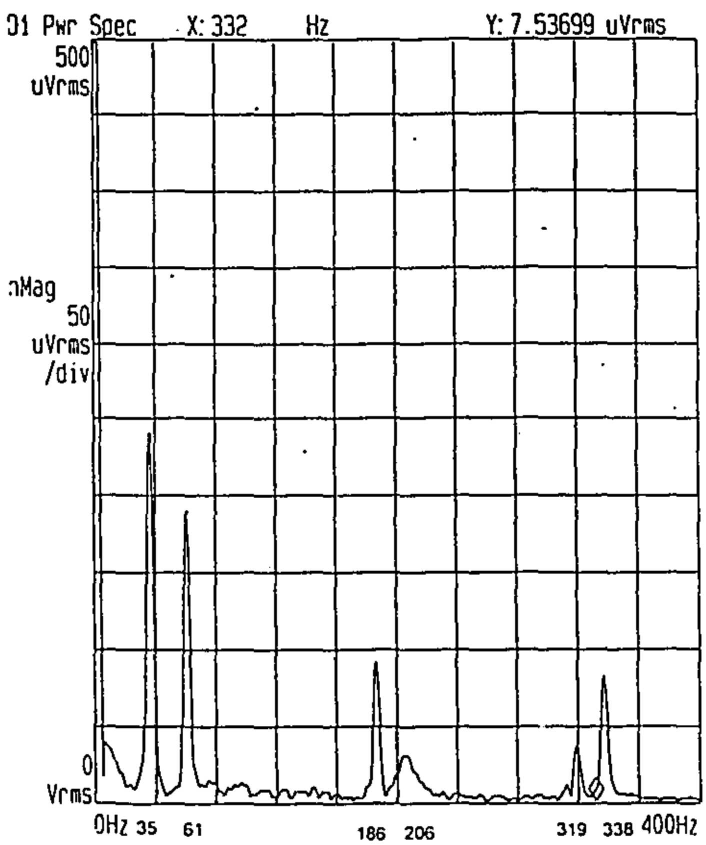

Fig.9.22. Transverse vibration frequency spectrum for double bellows expansion joint specimen

tural frequencies (for example, 35, 53, and 61 Hz for double bellows joint) the corresponding resonant flow velocities do not have sufficient energy to ovecome the system damping. As a result, no self-excitation mechanism develops. In the case of the single bellows expansion joint, some higher frquency transverse vibrations were not observed, for example, 207 Hz. Possibly because they were overwhelmed by the strong coupling two adjacent axial frequencies 176 and 254 Hz (see Fig.9.15 and 9.16).

Flow induced vibration responses for single bellows are shown in Fig.9.15 and 9.16. These two graphs are identical with respect to generated frequencies, but noticeably differ with respect to calculated Strouhal numbers according to formula (9.1). Another difference in these graphs is that the peeks in Fig.9.16 are shifted towards higher velocities with respect to the same frequency peeks shown in Fig.9.15, when the expansion joint was placed at the elbow. The same phenomenon was encountered in the experiments by Weaver and Ainsworth (1989) when they installed flow distribution distorting elements upstream of the bellows. Generally, similar remarks can be made for the response peaks of double bellows expansion joint shown in Fig.9.17 and 9.18. The calculated Strouhal numbers for each peek are shown in Tables 9.1. and 9.2. It is seen from these tables that, in the case of nearly ideal upstream flow conditions (expansion joint installed away from the upstream elbow) the Strouhal numbers agree well with those obtained by Weaver and Ainsworth (1989), $S \cong 0.45$, but they noticeably disagree when the expansion joint is installed right at the upstream elbow. This can be explained by the flow velocity profile distortion caused by the upstream elbow. A much higher velocity exists at the outside of the elbow then at the inside on the downstream end.

Table 9.1. Strouhal numbers for single bellows expansion joint

f (Hz) / Location	91	112	176	254	323
At elbow	0.59	0.59	0.55	0.63	0.51
Away from elbow	0.46	0.44	0.43	0.44	0.45

Table 9.2. Strouhal numbers for double bellows expansion joint

Location \ f (Hz)	136	186	206	264	319	338
At elbow	0.56	0.63	0.54	0.60	0.61	0.53
Away from elbow	0.46	–	0.46	0.44	0.47	0.46

The excelent agreement between the frequency values generated by shock and those produced by flow shows that no significant non-linearity in frequency exists, even at the extremely large vibration amplitudes generated by the flow. This means that the natural frequencies calculated using the approach developed for still fluid in this thesis can be used with confidence to predict the flow-induced vibrations of bellows expansion joints.

CHAPTER 10

SUMMARY AND CONCLUSIONS

It is very important to know the natural frequencies for predicting the dynamical response of a system. In the framework of this thesis the system under consideration were bellows expansion joints. Several types of bellows expansion joints are used in practice: single, double, or multiple. Theoretical models for the investigation of the transverse vibration in single and double bellows were developed in this thesis. The differential equation with necessary boundary conditions was derived and solved exactly. The effects of liquid added mass were determined using a finite element analysis and established in the form of added mass coefficients for use in the dynamic analysis of the bellows. Approximate solutions in the form of the explicit frequency formulas were also obtained using the Rayleigh quotient method for quick use by means of the scientific calculator during the expansion joint design process.The approximate solutions were compared quantitatively with the exact solution to verify their accuracy. In order to simplify the double bellows expansion joint problem it was devided into two separate problems for lateral and rocking modes. These two problems were governed by the same differential equation, but with two different boundary condition sets.

For the comprehensive evaluation of the theoretical frequency formulas, free vibration experiments with and without fluid and under static pressure were conducted. The existence of transverse vibrations in bellows was shown by means of flow induced bellows vibration experiments.

The flow-induced vibration experiments exibited the vibrations of bellows expansion joints in some of the transverse vibration modes, even for nearly ideal upstream flow conditions. The presence of the transverse vibrations, which were as strong as the axial ones, suggests that they are excited by a similar fluid-structure feed-back mechanism as previously studied for axial vibrations. Thus, this flow excitation mechanism is even more complex than previously thought.

The investigations reported in this thesis demonstrate that the formulas currently used for the calculation of natural frequencies of transverse vibrations in bellows expansion joints are not adequate for reasonable predictions in design practice. Comparison of these calculated natural frequencies with experiments showed very significant differences, especially for the higher vibration modes. This can be explained by the simplistic approach, based on the Bernoulli-Euler differential equation, used throughout all previous investigations of the natural transverse vibrations of bellows expansion joints.

The analysis provided in this thesis demonstrated that, even for as short and stubby a "beam" as a bellows expansion joint, the shear influence is negligible because of the transverse flexibility of a bellows. On the other hand, the inertia of rotation of the bellows cross-section including the fluid trapped in the convolutions, remains an important factor for the natural transverse frequencies of bellows, as does the internal pressure.

It was found that the added fluid mass, caused by convolution deformation during bellows bending, which has been ignored by previous authors, varies inversely as the fourth power of the bellows live length. In addition, this type of added mass depends very strongly on the vibration mode of bellows. Therefore, for typical bellows, this type of the added mass is very significant , especially for the higher vibration modes.

On the other hand, some simple calculations demonstrated that the Coriolis forces exerted by the flow inside bellows has a negligible effect on the natural frequencies of bellows, less than ~ 0.5% for the highest practical fluid velocities. Therefore, the influence of the Coriolis forces in the theoretical investigations of the natural transverse vibrations in bellows was ignored. It was also found that the influence of the centrifugal forces of the flowing fluid was negligible and, therefore, assumed equal to zero in the analysis.

Based on these assumptions, a reasonable model for transverse vibrations of bellows was shown to be the Bernoulli-Euler differential equation for an appropriate beam with additional terms to account for internal pressure and the inertia of rotation of a cross-section including added mass.

The bellows transverse natural frequencies calculated using the formulas derived from the Rayleigh quotient and from the frequency equations derived from the differential equation agreed very well. This indicated that the mode shape functions solved from the Bernoulli-Euler differential equation were precise enough to use as the approximate mode shape functions in the Rayleigh quotient expression obtained from the derived differential equation. The natural frequency results determined from the experiments compared with those obtained from the formulas derived in this work exhibited an error of less than 2% for the lower vibration modes. For higher modes calculated, this error was within 5%.

The excelent agreement between the natural frequencies of the bellows obtained from the still fluid experiments using the shock excitation and the resonant frequencies obtained from the flow induced vibration experiments showed that, despite the very large amplitudes, the bellows response remained linear. Also, the agreement of these two frequencies indicated that the effect of energy dissipation of energy on the natural frequencies of bellows is negligible and can be ignored. Additionaly, this agreement of the two frequencies confirmed the preliminary theoretical conclusions regarding the negligibility of the Coriolis and the centrifugal forces of the inside flow exerted on bellows. Therefore, bellows expansion joint frequency calculations using the formulas derived in this work, provide much more accurate prediction formulas than formulas already available in the current literature.

It should be noted that all the formulas available in the literature for calculation of axial bellows spring rate are not sufficiently accurate for precise calculations of natural frequencies. Therefore, a finite element analysis is recommended for calculation of the bellows axial spring rate used for the calculation of transverse natural frequencies.

The comparison of the results obtained from the free and flow-induced vibration experiments demonstrated that the lowest modes are not always the first modes to be excited by the flow. It appears that, in certain cases for which the lowest mode frequencies are quite low, the available dynamic head is not sufficient to overcome the system damping. Thus, the first mode to develop self-controled, potentially damaging, vibrations cannot be confidently predicted using current knowledge. The determination of the criterion for the excitation of the particular frequencies by the inside flow goes beyond of the scope of this thesis. Therefore, for the establishment of such a criterion as well as for a better understanding of self-controled bellows vibrations, further studies on the vibration excitation mechanism are recommended. Practicaly useful would be research on the effects of non-uniform velocity distribution.

REFERENCES

Andreeva, L.E., (1975) "Bellows", Mashinostroienie, Moscow, (in Russian).

Axelrad, E.L., (1986) "Theory of Flexible Shells", North-Holland.

Babakov, I.M., (1968) "Theory of Vibrations", Publishers Nauka, Moscow (in Russian).

Bass, R.L., and **Holster, J.L.**, (1972) "Bellows Vibration with Internal Cryogenic Flows", ASME, Journal of Engineering for Industry, Vol.94, 1972, pp.70-75.

Beards, C.F., (1983) "Structural Vibration Analysis", Ellis Horwood Ltd., West Sussex, England.

Beer, F.P., Johnston, E.R., (1981) "Vector Mechanics for Engineers", McGraw-Hill Ryerson Ltd.

Benjamin, T.B., (1961) "Dynamics of a System of Articulated Pipes Conveying Fluid. 1. Theory", Proceedings of the Royal Society (London) 261(A), 457-486.

Broyles, R.K., (1989) "Bellows Instability", Metalic Bellows and Expansion Joints, PVP-Vol. 168, 1989, pp.67-72.

Broyles, R.K., (1994) "EJMA Design Equations", PVP-Vol.279, Developments in a Progressing Technology, ASME.

Chen, W.F., Lui, E.M., (1987) "Structural Stability", Elsvier Science Publishing Co., Inc..

Daniels, V.R., (1966) "Dynamic Aspects of Metal Bellows", The Shock and Vibration Bulletin, No.35,Part 3, Jan., pp. 107-124.

EJMA Standard, (1980) Expansion Joint Manufacturers Association, Inc., 5th Ed..

Filipov, P., (1965) "Vibrations of Mechanical Systems", Naukova Dumka, Kiev (in Russian).

Flanders, H., (1985) "Calculus", W. H. Freeman and Co., New York.

Fluege, W., (1973) "Stress in Shells, 2nd ed., Springer-Verlag.

Fox, R.W., and **McDonald, A.T.**, (1985) "ntroduction to Fluid Mechanics" John Willey and Sons, Inc.

Franke, M.E., and **Carr, D.L.**, (1975) "Effect of Geometry on Open Cavity Flow-Induced Pressure Oscilations", AIAA Paper 75-492, AIAA 2nd Aeroacustic Conference, Va., USA, March 24-26, 1975.

Frocht, M.M., (1951) "Strength of Materials", The Ronald Press Co., USA.

Gerlach, C.R., (1969) "Flow Induced Vibrations of Metal Bellows", ASME, Journal of Engineering for Industry, Vol. 91, 1969, pp.1196-1202.

Gerlach, C.R., (1972) "Vortex Excitation of Metal Bellows", ASME, Journal of Engineering for Industry, Vol.94, pp.87-94.

Gerlach C.R., and **Schroeder, E., C.**, "Study of Minimum Pressure Loss in High Velocity Duct Systems", Interim Technical Report No. 1, Contract NAS8-21133, Southwest Research Institute, July 1969.

Gidi, A., (1993) "An Experimental Study of Flow Induced Bellows Vibrations", M. Eng. Thesis, McMaster University.

Green, G., (1833) "On the Vibration of Pendulums in Fluid Media", Edin., Trans., 1833, Papers, pp.315.

Haringx, J.A., (1952) "Instability of Bellows Subjected to Internal Pressure", Philips Res. Rep. 7, pp. 189-196.

Housner, G.W., (1952) "Bending Vibrations of a Pipe Line Containing Flowing Fluid", Journal of Applied Mechanics, 19, pp. 205-208.

Humar, J.L., (1990) "Dynamics of Structures", Prentice Hall, Englewood Cliffs, New Jersey.

International Symposium on Vibration Problems in Industry (1973), UK Atomic Energy Authority at Windscale, N.P.L., Keswick, England.

Irons, B.M., (1965) "Structural Eigenvalue Problems; Elimination of Unwanted Variables", J.A.I.A.A.,3, 961.

IUTAM/IAHR, (1974) Proc. of Symposium on Flow-Induced Structural Vibrations, Karlsruhe, Germany. Springer Verlag, Berlin.

Jakubauskas, V.F., (1991) "Investigations of Natural Vibrations of Bellows", M. Eng. Thesis, McMaster University.

Jakubauskas, V.F., Weaver D.S., (1992) "Natural Vibrations of Fluid Filled Bellows", PVP-Vol.244, Axial and Annular Flow-Induced Vibration and Instabilities, pp 145-158.

Koch, S.S., (1933) "Eine eksperimentelle Methode zur Beschtimmung der reduzierten Masse des mitschwingenden Wassers bei Schifs Schwingungen", Ing.- Archiv, Bd.4, Nr.2.

Laithier, B.E., Paidoussis, M.P., (1981) "The Equations of Motion of Initially Stressed Timoshenko Tubular Beams Conveying Fluid", Journal of Sound and Vibration, 79(2), 1981, pp. 175-195.

Lewis, F.M., (1929) "The Inertia of the Water Surrounding a Vibrating Ship", Trans. Soc. Naval. Arch., Marine Eng..

Li Ting-Xin, Li Tian-Xiang and **Guo Bing-Liang**, (1986) "Research on Axial and Lateral Natural Frequencies of Bellows with Different End Conditions", 86-PVP-14, ASME.

Long, R.H., (1955) "Experimental and Theoretical Study of Transverse Vibration of a Tube Containing Flowing Fluid", Journal of Applied Mechanics, 22, pp. 65-68.

Lyte, A.D., (1968) "Dynamics of Bellows Filled with an Incompressible Liquid", Journal of Spacecraft and Rockets, Vol. 5, No.1, pp.9-13.

McIver, D.B., (1973) "Hamilton's Principle for Systems of Changing Mass", Journal of Engineering Mathematics 7, 249-261.

Milne-Thompson, C.B.E., (1968) "Theoretical Hydrodynamics", 5th Ed., MacMillan and Co. Ltd..

Morishita, M., Ikahata, N., and **Kitamura, S.**, (1989) "Dynamic Analysis Methods of Bellows Including Fluid-Structure Interaction", Metalic Bellows and Expansion Joints, PVP-Vol.168, 1989, pp.149-157.

Naudascher, E., (1967) "From Flow Instability to Flow-Induced Excitation", ASCE, J. of Div. HY4.

Oldaker, I.E., et al., (1973) "An Overview of the Canadian Program to Investigate Vibration and Freeting in Nuclear Fuel Assemblies", CSME paper No.73-CSME-89.

Osweiller, F., (1989) "Design of an expansion joint by finite element program - comparison with the EJMA Standards", Metalic Bellows and Expansion Joints, PVP-Vol.168, 1989, pp. 87 -94.

Paidoussis, M.P., Laithier, B.E., (1976) "Dynamics of Timoshenko Beams Conveying Fluid", Journal of Mechanical Engineering Science, Vol. 18, No 4, pp. 210-219.

Paidoussis, M.P., Luu, T.P., and **Laithier, B.E.**, (1986) "Dynamics of Finite-Length Tubular Beams Conveying Fluid", Journal of Sound and Vibration, 106(2), pp.311-331.

Paidoussis, M.P., (1979) "Flow-induced Vibrations in Nuclear Reactors and Heat Exchangers, Practical Experience and State of Knowledge", Symposium on Practical Experiences with Flow-Induced Vibrations, Karlsruhe, Germany,September 3-6, 1969.

Paliūnas, V., (1982) "Teorinė mechanika", Mokslas Publishers, Vilnius, Lithuania.

Paliūnas, V., and **Paliūnienė, A.**, (1978) "Free Vibrations Bars in Liquid", Mokslas Publishers, Vilnius, Lithuania.

Pramila, A., Laukkanen, J., and **Liukkonen, S.**, (1991) "Dynamics and Stability of Short Fluid-Conveying Timoshenko Element Pipes", Journal of Sound and Vibration, 144, pp.421-425.

Rockwell, D., and **Naudascher, E.**, (1978) "Review-Self-Sustaining Oscilations of Flow Past Cavities", ASME, Journal of Fluids Engineering, Vol.100, pp.152-165.

Ross, C.T.F., (1983) "Finite Element Problems for Axisymmetric Problems in Engineering", Ellis Horwood Ltd..

Sainsbury,R.N., King, D., (1971) "The Flow-Induced Oscillation of Marine Structures", Proc. Inst. Civil Eng., pp. 269-299.

Samuel, K.C., (1972) "Dynamics of Continuous Elements, Prentice-Hall Inc., Englewood Cliffs.

Sheinin, I.S., (1967) "Vibrations of Structures in Fluid", Energia, Leningrad, (in Russian).

Shin, Y.S., Wambsganss, M.W., (1973) "Flow-Induced Vibration in L.M.F.B.R. Steam Generators: A State-of-the Art Review", A.N.L. Report 75-16, May 1973.

Simon, A.L., (1981) "Basic Hydraulics", John Wiley & Sons, Inc..

Smith, I.M., and **Griffiths, D.V.**, (1988) "Programming the Finite Element Method", Second Ed., John Wiley and Sons Ltd..

Symposium on "Fluid-solid Interaction", (1963) ASME Winter Annual Meeting, Pittsburgh.

The American Society of Mechanical Engineers (ASME), (1971) "Fluid Meters", United Engineering Centre, New York.

Toebes, G.H., (1965) "Flow-Induced Structural Vibrations", J. of Eng. Mechanics Div., ASCE, EMG, pp.39-65.

Tong, P.J. Rossetos, J., (1977) "Finite Element Method, Basic Technique and Implementation", Massachusetts Institute of Technology.

Tsukimori, K., Iwata, K., Matsunaga, M., and **Imazu, A.** (1989) "Buckling of Bellows Subjected to Pressure Loadings", Metalic Bellows and Expansion Joints, PVP-Vol.168, 1989, pp.133-139.

Voltera, E., Zachmanoglou, E.C., (1965) "Dynamics of Vibrations", Charles E. Merill Books Inc., Columbus, Ohio.

Vrillon, B., Jeanpierre, F., Copin, A., Gregoire, J.P., (1975) "Theoretical and Experimental Studies on Behaviour of Chinon 3 Primary Coolant System", F6/6, 3rd SMiRT.

Warburton, G.B., (1976) "The Dynamical Behaviour of Structures", Pergamon Press Ltd., England.

Weaver, D.S., Myklatun, B., (1973) "On the Stability of Thin Pipes with an Internal Flow", Journal of Sound and Vibration, 31, pp.399-410.

Weaver, D.S., (1977) "On Collapse and Flutter Phenomena of Thin Tubes Conveying Fluid", Journal of Sound and Vibration", 50, pp.117-132.

Weaver, D.S., and **Ainsworth, P.**, (1989) "Flow-Induced Vibrations in Bellows", Transactions of the ASME, Vol.111, November 1989, pp.402-406.

Weaver, D.S., (1989) "Flow Induced Vibrations and Stability of Bellows", Proc. I Conf. Eng. Aero-Hydroelasticity, Prague, Dec. 1989, Vol.I, pp.37-46.

Weaver, D.S., (1976) "On Flow-induced Vibrations in Hydraulic Structures and their Alleviation", Canadian J. of Civil Eng., Vol.3, No.1.

Weaver, D.S., (1989) "An Introduction to Flow-Induced Vibrations", Notes, Department of Mechanical Eng., McMaster Un., Hamilton, Ont., Canada.

Westergaard, H.M., (1932) "Water Pressure on Dams During Earthquakes", Proc., ASCE, Vol.58, 2.

Zienkiewicz, O.C., (1971) "Finite Element Method in Engineering Science", Mc Graw-Hill.